REPORT DOCUMENTATION PAGE

Form Approved OMB NO. 0704-0188

1. AGENCY USE ONLY (Leave Blank)	2. REPORT DATE:	3. REPORT TYPE AND DATES COVERED Final Report 1-Apr-2002 - 30-Jun-2005

4. TITLE AND SUBTITLE

Experiments in Quantum Coherence and Computation with Single Cooper-Pair Electronics

5. FUNDING NUMBERS

DAAD190210045

6. AUTHORS

Robert J Schoelkopf, Steven M Girvin

8. PERFORMING ORGANIZATION REPORT NUMBER

7. PERFORMING ORGANIZATION NAMES AND ADDRESSES

Yale University
P.O. Box 208337

New Haven, CT 06520 -

9. SPONSORING/MONITORING AGENCY NAME(S) AND ADDRESS(ES)

U.S. Army Research Office
P.O. Box 12211
Research Triangle Park, NC 27709-2211

10. SPONSORING / MONITORING AGENCY REPORT NUMBER

43387-PH-QC.10

11. SUPPLEMENTARY NOTES

The views, opinions and/or findings contained in this report are those of the author(s) and should not contrued as an official Department of the Army position, policy or decision, unless so designated by other documentation.

12. DISTRIBUTION AVAILIBILITY STATEMENT

Approved for Public Release; Distribution Unlimited

12b. DISTRIBUTION CODE

13. ABSTRACT (Maximum 200 words)

The abstract is below since many authors do not follow the 200 word limit

14. SUBJECT TERMS

quantum computing, superconductors, Cooper-pair box, single electron transistor

15. NUMBER OF PAGES

Unknown due to possible attachments

16. PRICE CODE

17. SECURITY CLASSIFICATION OF REPORT	18. SECURITY CLASSIFICATION ON THIS PAGE	19. SECURITY CLASSIFICATION OF ABSTRACT	20. LIMITATION OF ABSTRACT
UNCLASSIFIED	UNCLASSIFIED	UNCLASSIFIED	UL

Report Title

Quantum Computing with Single Cooper-Pair Electronics

ABSTRACT

This project is for experimental and theoretical investigations on quantum computation using the single Cooper-pair electronics. We integrate a Cooper-pair box qubit with a high-speed, time-gated quantum readout amplifier, namely the Radio-Frequency Single-Electron Transistor. The physics of single qubits is being studied, in order to identify and reduce the mechanisms of decoherence. We are developing techniques for state manipulation and single-shot readout of qubits, with the goal of demonstrating >1,000 coherent single-bit operations, and to separate errors in control, or measurement-induced dephasing. Another area of investigation is the integration of Cooper-pair boxes with high-Q superconducting microwave resonators, to realize a solid-state version of cavity QED. These resonators are used for engineering coherence times, as a means of entangling charge states, as a mechanism for storing quantum coherence, and as a new type of QND measurement. Devices are fabricated at Yale, and were previously also made under a subcontract to Chalmers University. A closely-coupled theoretical effort, headed by Prof. Steven Girvin at Yale, is examining the phenomenology of dephasing in the Cooper-pair box due to 1/f noise and other mechanisms, calculating dephasing and mixing rates for qubits due to the backaction of an RF-SET, developing the circuit QED approach to quantum computing, and comparing architectures for realizing entanglement and quantum logic gates with the Cooper-pair box.

List of papers submitted or published that acknowledge ARO support during this reporting period. List the papers, including journal references, in the following categories:

(a) Papers published in peer-reviewed journals (N/A for none)

1) "Measurement of the Excited-state Lifetime of a Microelectronic Circuit"K. W. Lehnert, K. Bladh, L.F. Spietz, D. Gunnarsson, D.I. Schuster, P. Delsing, and R.J. Schoelkopf, Phys. Rev. Lett. 90, 027002 (2003).
2) "Quantum Fluctuations of Charge and the Polarizability of the Single-Electron Box," K. W. Lehnert, B.A. Turek, K. Bladh, D. Gunnarsson, P. Delsing, and R.J. Schoelkopf, Phys. Rev. Lett 91, 106801 (2003).
3) "Single-Electron Transistor Backaction on the Single-Electron Box," B.A. Turek, K. W. Lehnert, D. Gunnarsson, K. Bladh, P. Delsing, and R.J. Schoelkopf,
Phys. Rev. B. 71, 193304 (2005).
4) "Cavity Quantum Electrodynamics for Superconducting Electrical Circuits: an Architecture for Quantum Computation," Alexandre Blais, Ren-Shou Huang, Andreas Wallraff, S.M. Girvin, and R.J. Schoelkopf, Phys. Rev. A 69, 062320 (2004).
5) "Coherent Coupling of a Single Photon to a Superconducting Qubit Using Circuit Quantum Electrodynamics," A. Wallraff, D. Schuster, Alexandre Blais, L. Frunzio, Ren-Shou Huang, J. Majer, S. Kumar, S.M. Girvin, and R.J. Schoelkopf, Nature 431, 162 (2004).
6) "AC Stark Shift and Dephasing in a Superconducting Qubit Strongly Coupled to a Cavity Field," D.I. Schuster, A. Wallraff, Alexandre Blais, L. Frunzio, Ren-Shou Huang, J. Majer, S.M. Girvin, and R.J. Schoelkopf, Phys. Rev. Lett. 94, 123602 (2005).
7) "Approaching Unit Visibility for Control of a Superconducting Qubit with Dispersive Readout," A. Wallraff, D.I. Schuster, A. Blais, L. Frunzio, J. Majer, M.H. Devoret, S.M. Girvin, and R.J. Schoelkopf, Phys. Rev. Lett. 95, 060501 (2005).
8) "Backaction Effects of an SSET Measuring a Qubit: Spectroscopy and Ground State Measurements," B. Turek, H. Majer, A. Clerk, S.M. Girvin, A. Wallraff, K. Bladh, D. Gunnarson, T. Duty, P. Delsing, and R.J. Schoelkopf, IEEE Trans. on Appl. Superconductivity 15, 880 (2005).
9) "Fabrication and Characterization of Superconducting Circuit QED Devices for Quantum Computation," L. Frunzio, A. Wallraff, D. Schuster, J. Majer, and R.J. Schoelkopf, IEEE Trans. on Applied Superconductivity 15, 860 (2005).
10) "Theory of Microwave Parametric Down Conversion and Squeezing Using Circuit QED," K. Moon and S.M. Girvin, Phys. Rev. Lett. 95, 140504 (2005).
11) "Resonant Cooper-Pair Tunneling: Quantum Noise and Measurement Characteristics," A.A. Clerk, S.M. Girvin, A.K. Nguyen, and A.D. Stone, Phys. Rev. Letters 89, 176804 (2002).
12) "Quantum-Limited Measurement and Information in Mesoscopic Detectors," A.A. Clerk, S.M. Girvin, and A.D. Stone, Phys. Rev B 67, 165324 (2003).

Number of Papers published in peer-reviewed journals: 12.00

(b) Papers published in non-peer-reviewed journals or in conference proceedings (N/A for none)

1) "Qubits as Spectrometers of Quantum Noise," R.J. Schoelkopf, A.A. Clerk, S.M. Girvin, K.W. Lehnert, and M.H. Devoret in "Quantum Noise in Mesoscopic Systems," Y.V. Nazarov (ed.), Kluwer Academic Publishers, Dordrecht, ISBN#1-4020-1239-X, April 2003.
2) "Prospects for Cavity QED with Superconducting Circuits: an Architecture for Solid-State Quantum Computing," S.M. Girvin, A. Blais, R. Huang, A. Wallraff, and R.J. Schoelkopf, Proceedings of the LXXIX Les Houches Summer School on Quantum Entanglement and Information Processing.
3) "Noise and Measurement Backaction in Superconducting Circuits: Qubits as Spectrometers of Quantum Noise," R.J. Schoelkopf, A.A. Clerk, K.W. Lehnert, and M.H. Devoret, Proceedings of the SPIE:Noise and Information in Nanoelectronics, Sensors, and Standards 5115, pp. 356-376 (2003).

Number of Papers published in non peer-reviewed journals: 3.00

(c) Papers presented at meetings, but not published in conference proceedings (N/A for none)

Number of Papers not Published: 0.00

(d) Manuscripts

1) "Qubit-Photon Interactions in a Cavity: Measurement Dephasing and Number Splitting,"
Jay Gambetta, Alexandre Blais, D. I. Schuster, A. Wallraff, L. Frunzio, J. Majer, S. M. Girvin, and R. J. Schoelkopf, submitted to Phys. Rev. A (2006).

Number of Manuscripts: 1.00

Number of Inventions:

Graduate Students

NAME	PERCENT_SUPPORTED	
Lafe Spietz	0.20	No
Joseph Schreier	0.10	No
FTE Equivalent:	**0.30**	
Total Number:	**2**	

Names of Post Doctorates

NAME	PERCENT_SUPPORTED	
Konrad Lehnert	1.00	No
Johannes Majer	1.00	No
Andreas Wallraff	0.10	No
Krishendu Sengupta	1.00	No
Jay Gambetta	1.00	No
FTE Equivalent:	**4.10**	
Total Number:	**5**	

Names of Faculty Supported

NAME	PERCENT_SUPPORTED	National Academy Member
Robert Schoelkopf	1.00	No
Steven Girvin	1.00	No
FTE Equivalent:	**2.00**	
Total Number:	**2**	

Names of Under Graduate students supported

NAME	PERCENT_SUPPORTED	
Sameer Kumar	1.00	No
William Braff	1.00	No
FTE Equivalent:	**2.00**	
Total Number:	**2**	

Names of Personnel receiving masters degrees

NAME
Total Number:

Names of personnel receiving PHDs

NAME
Total Number:

Names of other research staff

NAME	PERCENT_SUPPORTED	
Luigi Frunzio	1.00	No
FTE Equivalent:	**1.00**	
Total Number:	**1**	

Sub Contractors (DD882)

Inventions (DD882)

REPORT DOCUMENTATION PAGE

Form Approved
OMB NO. 0704-0188

1. AGENCY USE ONLY (Leave Blank)	2. REPORT DATE	3. REPORT TYPE AND DATES COVERED
	1/22/06	Final 4/1/02-8/31/05

4. TITLE AND SUBTITLE
Quantum Computing with Single Cooper-Pair Electronics

5. FUNDING NUMBERS
DAAD19-02-1-0045

6. AUTHOR(S)
R.J. Schoelkopf and S.M. Girvin

7. PERFORMING ORGANIZATION NAME(S) AND ADDRESS(ES)
Yale University, Department of Applied Physics
PO Box 208284, New Haven CT 06520-8284

8. PERFORMING ORGANIZATION REPORT NUMBER

9. SPONSORING / MONITORING AGENCY NAME(S) AND ADDRESS(ES)
U. S. Army Research Office
P.O. Box 12211
Research Triangle Park, NC 27709-2211

10. SPONSORING / MONITORING AGENCY REPORT NUMBER
43387-PH-QC

11. SUPPLEMENTARY NOTES
The views, opinions and/or findings contained in this report are those of the author(s) and should not be construed as an official Department of the Army position, policy or decision, unless so designated by other documentation.

12 a. DISTRIBUTION / AVAILABILITY STATEMENT
Approved for public release; distribution unlimited.

12 b. DISTRIBUTION CODE

13. ABSTRACT (Maximum 200 words)

This project is for experimental and theoretical investigations on quantum computation using the single Cooper-pair electronics. We integrate a Cooper-pair box qubit with a high-speed, time-gated quantum readout amplifier, namely the Radio-Frequency Single-Electron Transistor. The physics of single qubits is being studied, in order to identify and reduce the mechanisms of decoherence. We are developing techniques for state manipulation and single-shot readout of qubits, with the goal of demonstrating >1,000 coherent single-bit operations, and to separate errors in control, or measurement-induced dephasing. Another area of investigation is the integration of Cooper-pair boxes with high-Q superconducting microwave resonators, to realize a solid-state version of cavity QED. These resonators are used for engineering coherence times, as a means of entangling charge states, as a mechanism for storing quantum coherence, and as a new type of QND measurement. Devices are fabricated at Yale, and were previously also made under a subcontract to Chalmers University. A closely-coupled theoretical effort, headed by Prof. Steven Girvin at Yale, is examining the phenomenology of dephasing in the Cooper-pair box due to 1/f noise and other mechanisms, calculating dephasing and mixing rates for qubits due to the backaction of an RF-SET, developing the circuit QED approach to quantum computing, and comparing architectures for realizing entanglement and quantum logic gates with the Cooper-pair box.

14. SUBJECT TERMS	15. NUMBER OF PAGES
	16. PRICE CODE

17. SECURITY CLASSIFICATION OR REPORT	18. SECURITY CLASSIFICATION ON THIS PAGE	19. SECURITY CLASSIFICATION OF ABSTRACT	20. LIMITATION OF ABSTRACT
UNCLASSIFIED	**UNCLASSIFIED**	**UNCLASSIFIED**	**UL**

GENERAL INSTRUCTIONS FOR COMPLETING SF 298

The Report Documentation Page (RDP) is used for announcing and cataloging reports. It is important that this information be consistent with the rest of the report, particularly the cover and title page. Instructions for filling in each block of the form follow. It is important to ***stay within the lines*** to meet ***optical scanning requirements.***

Block 1. Agency Use Only (Leave blank)

Block 2. Report Date. Full publication date including day, month, and year, if available (e.g. 1 Jan 88). Must cite at least year.

Block 3. Type of Report and Dates Covered. State whether report is interim, final, etc. If applicable enter inclusive report dates (e.g. 10 Jun 87 - 30 Jun 88).

Block 4. Title and Subtitle. A title is taken from the part of the report that provides the most meaningful and complete information. When a report is prepared in more than one volume, repeat the primary title, and volume number, and include subtitle for the specific volume. On classified documents enter the title classification in parentheses.

Block 5. Funding Numbers. To include contract and grant numbers; may include program element number(s) project number(s), task number(s), and work unit number(s). Use the following labels:

C - Contract	**PR** - Project
G - Grant	**TA** - Task
PE - Program Element	**WU** - Work Unit Accession No.

Block 6. Author(s). Name(s) of person(s) responsible for writing the report, performing the research, or credited with the content of the report. If editor or compiler, this should follow the name(s).

Block 7. Performing Organization Name(s) and Address(es). Self-explanatory.

Block 8. Performing Organization Report Number. Enter the unique alphanumeric report number(s) assigned by the organization performing the report.

Block 9. Sponsoring/Monitoring Agency Name(s) and Address(es) Self-explanatory.

Block 10. Sponsoring/Monitoring Agency Report Number. (*if known)*

Block 11. Supplementary Notes. Enter information not included elsewhere such as; prepared in cooperation with....; Trans. of...; To be published in.... When a report is revised, include a statement whether the new report supersedes or supplements the older report.

Block 12a. Distribution/Availability Statement. Denotes public availability or limitations. Cite any availability to the public. Enter additional limitations or special markings in all capitals (e.g. NORFORN, REL, ITAR).

- **DOD** - See DoDD 4230.25, "Distribution Statements on Technical Documents."
- **DOE** - See authorities.
- **NASA** - See Handbook NHB 2200.2.
- **NTIS** - Leave blank.

Block 12b. Distribution Code.

- **DOD** - Leave Blank
- **DOE** - Enter DOE distribution categories from the Standard Distribution for unclassified Scientific and Technical Reports
- **NASA** - Leave Blank.
- **NTIS** - Leave Blank.

Block 13. Abstract. Include a brief (*Maximum 200 words)* factual summary of the most significant information contained in the report.

Block 14. Subject Terms. Keywords or phrases identifying major subject in the report.

Block 15. Number of Pages. Enter the total number of pages.

Block 16. Price Code. Enter appropriate price code (NTIS *only*).

Block 17. - 19. Security Classifications. Self-explanatory. Enter U.S. Security Regulations (i.e., UNCLASSIFIED). If form contains classified information, stamp classification on the top and bottom of the page.

Block 20. Limitation of Abstract. This block must be completed to assign a limitation to the abstract. Enter either UL (Unlimited) or SAR (same as report). An entry in this block is necessary if the abstract is to be limited. If blank, the abstract is assumed to be unlimited.

REPORT DOCUMENTATION PAGE (SF298)
(Continuation Sheet)

Final Project Report (04/01/02-8/31/05):
Experiments in Quantum Coherence and Computation with Single Cooper-Pair Electronics, (DAAD-19-02-1-0045)
PIs: R.J. Schoelkopf and S.M. Girvin

This is the final report on a grant, started in April 2002, for quantum computing with single Cooper-pair electronics. The grant is a combined effort consisting of theoretical investigations (under Co-PI Prof. Steve Girvin of Yale), fabrication of superconducting qubits, and the experimental implementation and testing of qubits and gates. Two different experimental approaches to implementing a quantum computer using single Cooper-pair box (CPB) superconducting charge qubits are being pursued. The first, a continuation of a previous effort, employs high-speed radio-frequency single-electron transistor (RF-SET) electrometers to measure the charge state of the qubit. The second approach, following the ideas described in our proposal, integrates CPB charge qubits with high quality-factor superconducting resonators to realize an analog of cavity quantum electrodynamics (cQED) in the solid state. This new approach (called circuit QED) was developed by the theoretical/experimental partnership during the first months of the current project, and has resulted in several breakthroughs for superconducting computing during the first experiments from February 2004 to the present.

This report will consist of several sections detailing the work in chronological order. Each period of performance is further subdivided , into categories describing the development of superconducting qubit fabrication at Yale, experiments on superconducting qubits coupled to microwave resonant cavities in the circuit QED architecture, experiments on RF-SET readouts of CPB qubits and measurements of the backaction and fidelity of such readouts, and the collaborative theoretical work done by co-invesitgator Steve Girvin's group.

Section A: Results from the period 4/1/02-12/31/02

A summary of achievements in this period:

- Our paper, describing the measurement of T2* and T1 in a Cooper-pair box (CPB) qubit, appeared in Physical Review Letters. (K.W. Lehnert et al., Phys. Rev. Lett. **90**, 027002 (2003). (reference #1)
- A manuscript, describing the first observation of quantum charge fluctuations in the single-electron box, was submitted to Physical Review Letters. (reference #2)
- Made first quantitative observations of the backaction of an SET, observed in the normal state during measurements of an electron box. A manuscript describing these experiments is in preparation for Physical Review Letters. (ref #3)
- Developed theoretical treatment of SSET operated in mode used in experiments, including predictions of backaction and signal to noise ratio in single-shot readouts of CPB. Work published in Physical Review Letters, A.A. Clerk et al., Phys. Rev. Lett. **89**, 176804 (2002). (ref #4)
- With Co-I Steve Girvin and student Ren-Shou Huang, devised new architecture for quantum entanglement and readout of qubits relying on high-Q superconducting resonators. A manuscript is in preparation.
- Published an extensive review article, "Qubits as Spectrometers of Quantum Noise," R.J. Schoelkopf et al. (cond-mat/0210247) on state mixing and transition rate calculations for superconducting qubits (ref #5).
- The PI and postdoc Dr. Konrad Lehnert delivered over 20 lectures and seminars on the observations of coherence and a long relaxation time in the Cooper-pair box, including 4 invited presentations at international conferences.
- Refined techniques for precision charge measurements, resulting in our ability to measure single charges with signal to noise of greater than 1,000.
- Developed software for complete computer automation of experiment box plus SET electrometer experiments, including ability to carry out various protocols for coherent state control.
- Separated electric and magnetic components of relaxation rate (T1) of CPB.
- Attempted single-shot readout of CPB, yielded signal to noise of approximately one. Improvements in sensitivity are underway.
- Found backaction of superconducting SET could be reduced sufficiently to observe 2e periodic Cooper-pair staircase.
- Performed spectroscopy of CPB in region approaching the charge degeneracy point where 1/f noise effects minimized.
- Attempted Rabi and Ramsey experiments with CPB at degeneracy point, unsucessfully, perhaps due to short T1 during measurement/readout phase.
- Observed extremely low offset charge (1/f) noise drift under certain circumstances in normal state of ~ ½ millielectron per hour.
- Designed improved CPB qubits with different parameters, redesigned mask.
- New devices with these parameters fabricated under subcontract to Chalmers, testing of these devices beginning.
- Co-I Girvin and coworkers began analysis of new readout schemes for CPB qubits based on RF manipulations of large Josephson junction, as being experimentally developed in group of Michel Devoret at Yale.
- Designed two qubit gates based on cavity-QED entanglement using a transmission line resonator.
- Fabrication of CPB qubits and readout SETs underway in Yale fabrication lab.
- Began fabrication of resonators for cavity-QED experiments.

As listed above, we have had significant progress on the theory, fabrication, and experimental aspects of our project on quantum computation with single Cooper-pair electronics. Several major publications have appeared and been submitted during this period. Funds have been used for partial summer salary for PI Schoelkopf and Co-I Girvin, and for postdoctoral associates Dr. Konrad Lehnert, Dr. Andreas Wallraff. Two graduate students, Ben Turek and David Schuster, have participated in the project with support from supplementary ARO student grants associated with this contract. Postdoctoral associate Konrad Lehnert left the project in Dec 2002, he is now a junior faculty member at Colorado University/ the Joint Institute for Laboratory Astrophysics (JILA). Some funds were employed for partial payment on a new dilution refrigerator from Cryoconcept, (Grenoble, France), which is due for delivery in May 2003 and will double our experimental capability.

In addition to the publication of our earlier results measuring the T1 and T2* of the Cooper-pair box under continuous measurement with the SET, we have made steady progress on perfecting quantum state control with this system and attempting to understand the mechanisms of relaxation and decoherence in these singe qubits. We found that the backaction of the continuous measurement, which can induce a "short step" feature, probably by inducing out of equilibrium quasiparticles in the box, could be reduced to a level that allows an observation of the nominally unperturbed, 2e periodic Cooper-pair staircase. This allowed us to measure much closer to the desired operation point of the box, near the degeneracy of the charge states. At this point, the CPB becomes first-order insensitive to 1/f charge offset noise, and recent results from Devoret and coworkers at Saclay have shown that this point can yield coherence times approaching the inelastic relaxation time of a microsecond. We were able to perform CW spectroscopy down to this degeneracy point, obtaining results in good agreement with our earlier work using two-photon transitions, farther away from degeneracy. We were also able to extract some evidence of the relative importance of electric and magnetic relaxation mechanisms in their contribution to T1. Operation at the degerenacy point requires an adiabatic movement away from this point during the readout phase. Our measurements appear to indicate that the T1 time at the degeneracy point may be less than 200 nanoseconds, which makes this readout phase highly inefficient. We attempted both Rabi and Ramsey experiments at the degeneracy point, but without success, probably because of the fast relaxation. The origin of the relaxation is not clear, but would be expected in this sample due to its strong coupling to the microwave control lines. In our next designs, the box will have a smaller charging energy, and also weaker capacitive coupling to the environment, hopefully improving the relaxation time.

We have also refined our charge measurement techniques, both to improve the accuracy and sensitivity of the measurement, and to make the experiment easier to control and more flexible. We invested in a complete computerized control of the experiment, with all gates controlled by programmable arbitrary waveform generators. This allows one to rapidly switch between different types of measurements and protocols, with rapid (80 MHz) control of gates and automatic cancellation of cross capacitances. This also allows

the experimenter to think and control the experiment in the relevant units and to explore the behavior on the many adjustable parameters. We have also perfected the method of calibration and data acquisition, allowing us to measure Coulomb staircases in the box (i.e the individual charge states) with both a signal to noise and a fidelity of 1 part in a thousand.

We employed these improved techniques to study a well-characterized box plus SET in the normal state, where we observed several interesting phenomena which add to our understanding of the system and its behavior as a qubit. First, we could observe a renormalization of the capacitance, or charging energy of the box, due to quantum fluctuations of the charge across the box junctions. This is the first experimental observation of this phenomenon in a box, though the problem has been extensively treated in the theoretical literature. The comparison of our observations with the theory of the box could be made with no adjustable parameters, since we had determined the capacitance and resistance of the box to high accuracy via the spectroscopy of the qubit in the superconducting state. The results are displayed in Figure 1, and a manuscript describing the results has been submitted to Physical Review Letters (ref. 2). These measurements point out that the charging energy of the box in the superconducting state can be significantly renormalized compared to the geometric capacitance, and that the charging energy in the normal state can be significantly reduced (in this case, by 20%) compared to that inferred from the superconducting state. The excellent agreement of the quantum fluctuations and the exact shape of the Coulomb staircase also implies that the calibration and fidelity of the SET charge measurement are now understood.

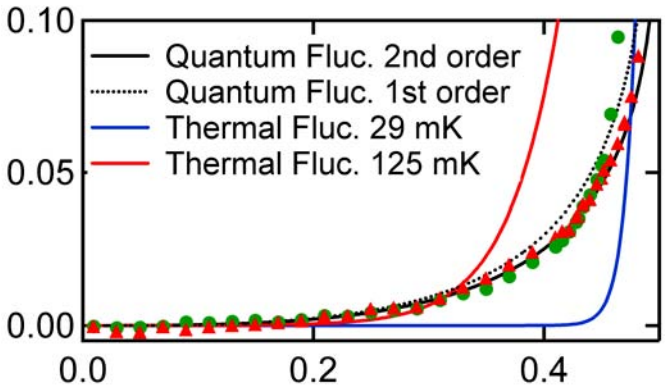

Figure 1: Detail of the coulomb staircase of box in normal state, and comparison with theory of quantum charge fluctuations. The vertical axis is charge on the box, and the horizontal axis is the gate charge, $Q=C_gV_g$, in units of the electron's charge. The agreement with the theory is excellent, both verifying our model of the box, and the calibration of the SET charge measurement.

Another phenomenon which we observed for the first time in these experiments is the backaction of the SET in its normal state. We were able to observe the influence of the SET's operating point on the shape, position, and symmetry of the Coulomb staircase. Graduate student Ben Turek (supported under a supplementary grant) performed these measurements, as well as developing the computer control software. In collaboration with Dr. Aash Clerk and Co-I Steve Girvin, a simple model for this backaction was constructed, which compares well with the observations, again with no adjustable parameters. These observation mark the first quantitative study of backaction in an SET system, and prove that the dominant influence on the measured system can arise from the intrinsic noise of the SET, which is coupled to the box via the measurement system. A manuscript describing these results is in preparation (Turek et al., Ref 3) for Physical Review Letters. Mr. Turek will next extend these measurements into the superconducting state, where the coherence of the box is important, and one can measure both dephasing due to low frequency backaction, as well as the positive and negative frequency components of the SET's noise spectrum. An analysis of this case, and the physics of mixing in qubits due to backaction or the coupling to a nonequilibrium environment is presented in the review article by Schoelkopf et al. (reference 5). In order to carry out these measurements of the backaction, Mr. Turek introduced an automatic proceedure by which the computer could null slow (20 minute) drifts in the offset charges of the box and electrometer. Interestingly, we found that the 1/f noise in the normal state could be substantially smaller than in the superconducting state, where it limited our qubit coherence time. Specifically, we found that by reducing the voltages and power dissipated in the measurement, the 1/f was substantially reduced to less than 1 millielectron of drift per hour, as compared to approximately 10 millielectrons in 5 minutes in the superconducting state. We intend to follow up on these observations with further studies of the 1/f noise and its dependence on power, temperature and past history of the control voltages. These lessons may imply a method for further improvement of the coherence in superconducting qubits, by reducing the 1/f noise.

Based on our earlier experiments, and on an understanding of the Hamiltonian of the CPB qubit, graduate student David Schuster (supported by a supplementary student grant) has undertaken a study of the optimal parameter choices for a Cooper-pair box charge qubit. These calculations include the effects of relaxation due to the electromagnetic environment, dephasing due to low frequency noise, and the signal to noise ratio in a single-shot measurement of the qubit using a superconducting SET. The latter calculation takes advantage of the theoretical work by Dr. Aash Clerk, a postdoc in our collaborator Steven Girvin's group at Yale. David's computer code can also include the effects of higher charge states when the charging energy becomes comparable to the Josephson energy, and can determine all the matrix elements for transistions between states. As we expected, we find that optimal behavior of the box is obtained for substantially lower ratios of charging to Josephson energy. This change both increases the expected lifetime of the qubits, for a fixed capacitive coupling to the environment, and reduces the curvature of the energy bands near the charge degeneracy point, thus reducing the effects of the 1/f charge noise. David has most recently begun extending these calculations to calculate the coupling energy and gate operation time for boxes coupled to transmission line resonators. In addition, these calculations can be employed to estimate the efficiency of our new proposed readout using a dispersive QND measurement of the qubit via a resonator.

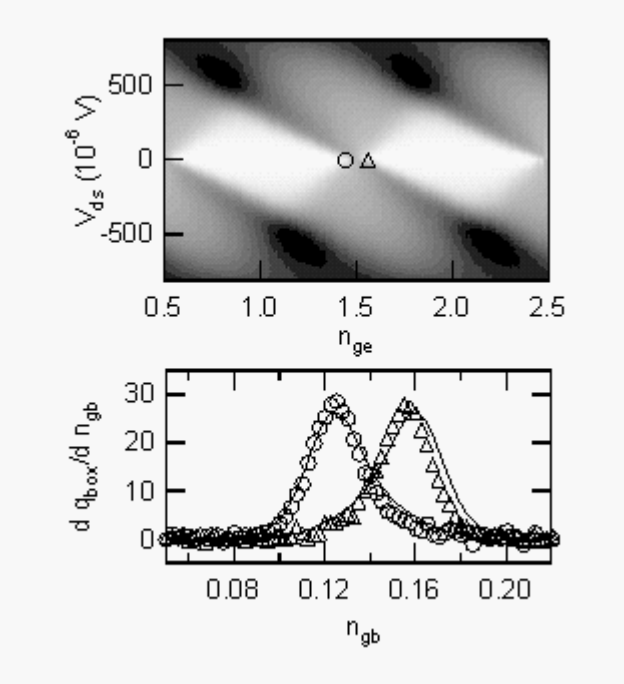

Figure 2: Top: measured RF conductance of a normal SET, as a function of electrometer gate and drain bias. Bottom: Measured derivative of the "Coulomb staircase" of a normal electron box measured at two different operating points (denoted by the corresponding symbols in the top panel) (B. Turek et al., ref. 3, compared to theory (solid curves). The effect of the detector back action causes a shift, a broadening, and an asymmetry of the curves which cannot arise due to thermal rounding and which systematically depends on the operating point of the SET.

Using the results of these calculations, we have designed a new set of CPB qubits. These designs have been sent to our collaborators at Chalmers University in Sweden. The first set of devices following these designs have recently been received, and testing will begin soon. We have also made progress in refining our fabrication techniques at Yale. Mr. Schuster has learned an electron-beam fabrication process for producing SETs and Cooper-pair box qubits. He has trained in cleanroom techniques and safety, passed the cleanroom qualification exam, and become a skilled operator of our electron microscope and the pattern generation software. Some delays were related to a defective beam-blanking assembly in our microscope, and to the failure of the cryopumping system in the system used for the double-angle evaporation of junctions. David assisted in repairs of the SEM, and an overhaul of our evaporation system, including the installation of new pumping system. These facilities are now significantly improved in their performance and functioning properly. David has produced several initial devices with sub 100 nm features, and is currently fabricating SETs and boxes for our project. He is now beginning to integrate boxes with the high-Q resonators for our new applications of cavity-QED techniques to these solid-state qubits.

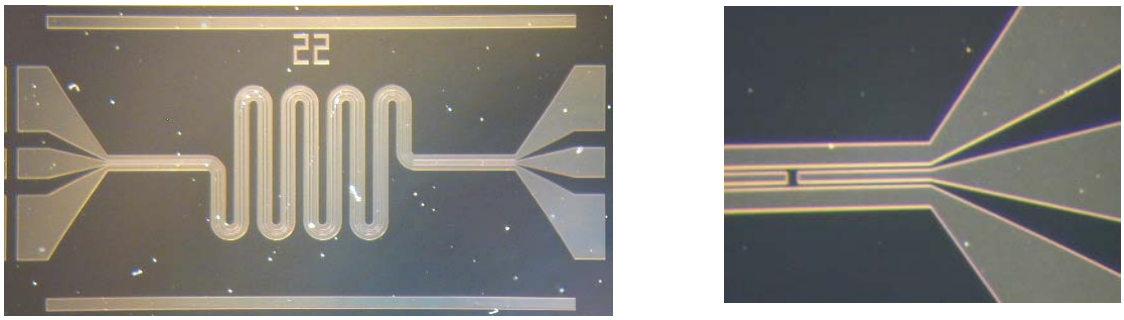

Figure 3: Optical micrographs of superconducting coplanar waveguide resonator for 10 GHz. Devices consist of aluminum films on oxidized silicon wafer. Left panel shows overall view of chip (5 x 10 mm), and right panel shows a detail near end, depicting the gap in center strip used to weakly couple in and out of the resonator.

Postdoctoral associate Andreas Wallraff designed a mask for the transmission line resonators, and these were fabricated in our Yale cleanroom using optical lithography. Images of these devices are shown in Figure 3. Dr. Wallraff has also redesigned a sample holder and microwave launchers. We have also purchased parts for a complete 10 GHz measurement system which will allow the testing of the resonators at millikelvin temperatures, and for us to measure qubit states via pulsed measurements of the cavity transmission. These devices can also allow us to entangle a CPB qubit with a single 10 GHz photon, as well as produce entanglement between CPB qubits that are separated by ~ a centimeter across a chip. Basic designs for two-qubit gates based on this approach are being analyzed, and show that gate operation times of 10-100 nanoseconds are possible. Though we must first study single qubits and their interaction with the resonators, and demonstrate our new readout scheme based on the frequency pulling of the resonant cavity by the qubit, this approach is scalable immediately to two qubits, and probably to 10's or 100's of qubits. It is in principle possible to readout multiple qubits via frequency multiplexing in this scheme, which would be another highly attractive feature. We hope to test single qubit devices in the next six months, and to fabricate two-qubit devices on the same timescale.

The theoretical program supported by the ARO consists of Steven Girvin (PI) and Krishnendu Sengupta (postdoc). Additional group members who are also contributing significantly to papers acknowledging ARO support are: Aashish Clerk (postdoc, primarily supported by the Keck Foundation), and Renshou Huang (graduate student, primarily supported by the NSF). We also collaborate with Yale theorist A. Douglas Stone.

Sengupta and Girvin are presently collaborating with Yale experimentalist Michel Devoret and University of Cambridge theorist Andrew Green on a quantum theory of two new readout schemes proposed by Devoret. Both readout schemes take advantage of the fact that a Josephson junction obeys the non-linear equations of motion of a physical pendulum in a gravitational field. In the first scheme, a microwave pulse drives the pendulum into the inverted state of maximum potential energy (phase $\theta = \pi$). Quantum mechanically, the pendulum then has equal probability amplitude to fall down both to the left and the right at the same time. A charge-phase qubit in parallel with this Josephson junction will bias the fall one way or the other depending on the state of the qubit. In the second proposed readout scheme, a microwave pulse does not invert the pendulum but drives it instead to the bifurcation point between large and small amplitude response due to the non-linearity. The precise amplitude at which the bifurcation occurs is modulated by the state of the qubit in parallel with the junction.

We have developed classical Langevin equations to simulate the effect of finite temperature in reducing the readout fidelity. We have implemented these numerically with a very fast solver which we developed that gives the probability distribution for the time evolution of the junction phase. We have also developed a quantum Langevin equation that relies on the assumption that quantum fluctuations are small. We are now in the process of refining our numerical solver for the quantum case so that we can study the crossover from thermal to quantum limited detection at low temperatures. In addition we are beginning to think seriously about how to go beyond the quantum Langevin approximation so that we can better describe the quantum tunneling of the junction phase between the two different readout states. We expect to have preprints completed on this project during the coming year.

In collaboration with Rob Schoelkopf at Yale, Huang and Girvin are studying charge qubits (Cooper boxes) coupled to high *Q* resonators. We have recently demonstrated theoretically that various interesting analogs of 'cavity QED' effects in atomic physics should be readily observable in superconducting co-planar wave guide resonators. In particular we have investigated the change in T_1 of the qubit due to the change in the spectrum of zero-point voltage fluctuations caused by imbedding the qubit in the resonator. On resonance T_1 is dramatically shortened while off-resonance (dimensionless detuning $\delta > \sqrt{Q}$), T_1 can be greatly enhanced. Experimental measurement of this effect will allow us to distinguish intrinsic decoherence due to spontaneous photon emission (fluorescence) from extrinsic effects (quasiparticle excitations, etc.). We have also predicted the existence of a fairly strong pulling of the cavity resonance frequency that depends on the state of the qubit and may offer a highly efficient, low dissipation readout scheme.

In collaboration with Aash Clerk and Douglas Stone at Yale, we have analyzed the superconducting single electron transistor (SSET) as a quantum detector. In particular we have studied the operation of the device on the double Josephson quasiparticle (DJQP) resonance feature that Schoelkopf's group has discovered is very desireable from an experimental point of view. We developed a new and relatively simple density matrix scheme to determine the measurement efficiency and the strength of the backaction of the detector. We do this by treating the qubit and the SSET on an equal footing and use the qubit as a spectrum analyzer for the backaction noise produced by the detector. This is a very physical approach that turns out to be computationally simple and efficient. It has allowed us to develop an understanding of the role of superconducting coherence in determining both the fano factor for the shot noise in the detector output and the backaction. We were able to show that operation of the SSET at the DJQP point is nearly ideal, approaching within a factor of 2 of the quantum limit. We also were able to obtain the full spectrum of the quantum backaction noise and showed that under some operating conditions, the superconducting coherence of the SSET leads to a novel effect of population inversion in the qubit. This arises under bias conditions where the work done by the power supply exceeds the charging energy for putting a Cooper pair in the SSET leads onto the island. In this case, tunneling can proceed only if the qubit absorbs the excess energy. Thus the spectral density of backaction noise is larger at negative frequencies than positive and leads to qubit population inversion. This work was published in *Physical Review Letters*. (Reference #4)

We then extended our results to a general theory of linear response detectors and developed a general information-theoretic description of the quantum measurement process (Reference # 6). For the special case of normal-state quantum point contact type of detectors, we were able to push the analysis quite far and give general expressions for the backaction in terms of the rate at which accessible information about the state of the qubit is obtained at the output of the detector. For the case where one of the contacts is superconducting, Aash Clerk has shown that the noise is substantially enhanced.

References/Publications During This Period:

1) 'Measurement of the Excited-State Lifetime of a Microelectronic Circuit,' K.W. Lehnert, K. Bladh, L.F. Spietz, D. Gunnarsson, D.I. Schuster, P. Delsing, and R.J. Schoelkopf, *Phys. Rev. Lett.* **90**, 027002 (2003)

2) 'Quantum Charge Fluctuations and the Polarizability of the Single-Electron Box,' K.W. Lehnert, B.A. Turek, K. Bladh, D. Gunnarsson, P. Delsing, and R.J. Schoelkopf, submitted to Phys. Rev. Lett. (2003).

3) 'Measuring the Backaction of a Single-Electron Transistor on the Single-Electron Box,' B.A. Turek, K.W. Lehnert, K. Bladh, D. Gunnarsson, P. Delsing, and R.J. Schoelkopf, in preparation.

4) 'Resonant Cooper Pair Tunneling: Quantum Noise and Measurement Characteristics,' A. A. Clerk, S. M. Girvin, A. K. Nguyen, A. D. Stone, *Phys. Rev. Lett*. **89**, 76804 (2002).

5) 'Qubits as Spectrometers of Quantum Noise,' R. J. Schoelkopf, A. A. Clerk, S. M. Girvin, K. W. Lehnert, M. H. Devoret, to appear in: *Quantum Noise* (ed. by Yu. V. Nazarov and Ya. M. Blanter) e-print: cond-mat/0210247

6) ‘Quantum-Limited Measurement and Information in Mesoscopic Detectors,’ A. A. Clerk, S. M. Girvin, A. D. Stone, submitted to *Physical Review B*, e-print: cond-mat/0211001.

7) A. A. Clerk, ‘Resonant Cooper-Pair Tunneling: Counting Statistics and Frequency-Dependent Current Noise,’ (Kluwer, Proceedings of 2002 Erice Conference) in preparation.

Section B: **Results from the period 1/03-12/03**

A summary of achievements in this period:

I. Fabrication:

- Commissioned new fabrication setup (with M. Devoret), students and postdocs have gained expertise in fabrication.
- Produced and tested single-electron transistors and CPB qubits at Yale.
- Characterized junction areas and energy scales, can now fabricate qubits with specified transition frequencies.
- Produced detailed mask design for coupled two-qubit gate using CPB and SET readouts.
- Demonstrated fabrication process for qubits and SETs with controlled high-frequency coupling, including chip level microwave design.
- Began fabrication development for qubits with higher transition temperatures and superconducting bandgap engineering.
- Developed fab process for high quality-factor superconducting cavities.
- Developed process and fabricated single and multiple qubits integrated to cavities, devices are under test.

II. SET Readout of Cooper-pair Box Qubits:

- Obtained and tested new set of qubits from Chalmers with decreased charging energy to eliminate parity problems/quasiparticle generation
- Observed full Cooper-pair staircase and performed spectroscopy down to 1/f insensitive charge degeneracy point of CPB.
- Demonstrated controlled tuning of tunnel coupling of qubit Hamiltonian
- Remeasured relaxation times (T1) of a Chalmers qubit, and found systematic variation due to SET readout.
- Found that cause of fast relaxation in Chalmers coherent oscillation experiments is the SET backaction.
- Confirmed theoretical description of qubit relaxation and SET backaction, and observed predicted population inversion due to measurement.
- Observed activation of 1/f noise by SET readout, and very low levels of 1/f charge noise on long timescales.
- Two Physical Review Letters on this work appeared this year, one on measurements of relaxation and decoherence time of CPB as measured by SET, the second on renormalization of charging energy in the box by quantum charge fluctuations.

III. Theory of Superconducting Qubits and Readouts:

- Proposed new architecture for solid-state quantum computing using CPB qubits and resonant cavities (scQED).
- A paper on superconducting cQED published on cond-mat archive and submitted to Phys Rev B.
- Calculated single-shot signal-to-noise ratios, backaction, and lifetimes for qubits using scQED control and readout, confirmed by numerical quantum simulations.
- Proposed extension scQED/qubit architecture for tagged single photon production.
- Published an article (Phys Rev. B) and submitted a second article on general theory of quantum noise and measurements.
- Our review article on quantum noise and its effects on qubits was invited for a Colloquium in Reviews of Modern Physics.
- Numerical calculations of new RF quantum tunneling (RF-MQT) readout used by M. Devoret group at Yale.

IV. Cavity QED Experiments with Cooper-pair Box Qubits:

- Tested quality factors of both Al and Nb transmission-line resonators, including temperature and magnetic field dependence.
- Obtained high quality factor resonators (Nb) with Q > 500,000 at 250 mK
- Assembled and tested 5-10 GHz microwave readout system for cavity-based QND measurement of qubits
- Designed both one qubit and two coupled qubit designs for scQED architecture.
- Tested signal-to-noise of pulsed cavity readout, found high-fidelity single-shot readout of qubits should be possible.
- Testing of single qubits in cavities underway.

As summarized above, there has been significant progress in all areas of fabrication (I), theory (III), and measurements of qubits using two types of readouts, the RF-SET (section II) and resonant cavities/scQED (section IV). These individual steps are detailed in separate sections below, and are followed by a discussion of future plans (V) and priorities for the coming year.

There are several landmarks in the progress. First, a state-of-the-art new fabrication facility (shared with Prof. M. Devoret, also at Yale) was commissioned, and several students and postdocs have been trained to use these facilities.

For the last approximately six months, this facility has worked very well, so that single-electron transistors and superconducting qubits are routinely produced, with a cycle time of a few days, rather than the timescale of order 6 months to a year when relying on overseas collaborations. In particular, this has allowed us to pursue a novel approach involving the coupling of CPB qubits to resonant cavities, as described in section IV.

Second, we have found that the relaxation time of the CPB qubit can be dramatically affected by the SET readout. This helps to explain the variability of the relaxation rates (T1 times) seen in our previous experiments, and seen by our collaborators at Chalmers. In fact, the variation in the relaxation time and in the ground and excited state populations of the qubit under measurement agrees qualitatively with the predictions made by our theory group for the double-Josephson quasiparticle (DJQP) process in the SSET. This is encouraging because it means that by properly choosing the parameters of the qubit and the SET, and by implementing the correct protocols for controlling the measurement and turning it on and off, we should be able to perform one qubit operations. The issue of understanding how to attain a reliably long (i.e. > 1 microsecond) relaxation time remains the dominant roadblock both for demonstrating coherent control and for realizing a good single-shot readout with the SET. It is interesting to note that the irreproducibility of the relaxation time has been observed and remains an incompletely mastered issue for all superconducting qubits, be they phase, flux and charge. Saclay has only just recently been able to repeat their long coherence time measurement for the CPB, for the past 1.5 years they have had an anomalously fast relaxation that has prevented coherence time investigations. Nakamura et al. (unpublished) have recently reported that they also suffer from fast relaxation (T1 < 10 ns at the degeneracy point!), and Chalmers has observed T1s in the range 10-100 ns in several devices. Trying to pin down the actual mechanisms of relaxation and dephasing (at least in the case where the dephasing is not limited by 1/f charge noise) remains a major hurdle for all superconducting qubits, and will be the focus of our investigations in the next year.

Third, we have proposed a new approach for solid-state quantum computation based on coupling, controlling, and measuring CPB qubits by embedding them in high-Q resonant cavities. A detailed and realistic engineering study indicates that it is possible to have strong coherent coupling between a qubit and a single microwave photon. This approach has several strengths, being able to entangle qubits which are separated, provide a high-fidelity single-shot readout of the qubit states, and do so within an electromagnetic environment that should strongly enhance the lifetimes of the qubit. It is also simpler to fabricate, less complex to operate, capable of measuring the qubit at its optimal point for decoherence, and produces no on-chip dissipation or quasiparticles.

Finally, we have made significant and rapid progress towards implementing this improved scQED architecture for superconducting qubits. We have mastered the design of the resonators, fabricated cavities in both aluminum and niobium, measured their losses and observed high quality factors two orders of magnitude better than that required for the first generation experiments, and built and tested the microwave electronics for the scQED single-shot readouts. Our tests indicate that the signal-to-noise for single-shot readouts should be easily achievable. We have also fabricated both single and multiple qubits into resonators, and the first tests are underway (Jan 2004).

A continuing frustration is that the two dilution refrigerators (one for Devoret group, one for the Schoelkopf group) have still not been delivered, despite being over a year beyond their delivery date. Our single fridge is presently set up to handle either SET or scQED types of experiments, but the necessity for sharing time on this single apparatus has already proven a bottleneck. Personnel working on this project include two QuaCGR students, Ben Turek (SETs and backaction) and David Schuster (fabrication and scQED), and a postdoc, Dr. Hannes Majer. Dr. Majer comes from the Mooij group at Delft, and has been leading the work on SET readouts and backaction. Other personnel working on this project, with their primary funding from other sources, include a postdoc, Dr. Andreas Wallraff, who leads the scQED experimental effort, and a senior research scientist, Dr. Luigi Frunzio. Dr. Frunzio has over a decade of experience in fabrication of superconducting devices, and leads the effort on fabrication and process development. Significant funds ($60k per calendar year, equivalent to support of a graduate student) have been used, as planned, in support of the fabrication collaboration with Prof. Per Delsing's group at Chalmers University in Sweden. This collaboration continues to provide CPB box/SET samples for our experiments, albeit with a long lead time.

I. Process Development and Fabrication of Superconducting Qubits at Yale University

This year has seen great progress in our fabrication capabilities at Yale. In collaboration with Michel Devoret's group, a robust process for Al/AlOx/Al shadow evaporated junctions has now been realized, so that single-electron transistors and CPB qubits can be produced, with a typical cycle time of one or two days. Steady progress has been made in reducing feature sizes to yield devices with appropriately large charging energies for sensitive SETs. An electron micrograph of such an SET is shown in Figure 1, along with an enlargement showing the actual junction region, consisting of crossed lines < 75 nanometers in width.

Typically the basic device testing is performed in a Helium-3 refrigerator down to 250 mK. Conventional dc transport measurements of approximately a dozen SETs and test qubits can be performed in a single cool-down, lasting a couple of days to a week. At least six such design/fabricate/test cycles have been carried out in the last few months. Charging energies of the SETs are extracted from I-V characteristic measurements, as well as measurements of the RF "charging diamonds" of an RF-SET. A typical sample consists of 10 to 20 SETs and a similar number of test CPB qubits, which are small area SQUIDs configured for I-V curve measurements, rather than being measured as a qubit using an SET. This allows measurements of the resistance, critical current, sub-gap I-V characteristics, and flux modulation patterns, each of which are useful for determining important qubit characteristics. Successive iterations of this processing

and testing has resulted in good control of the junction areas, current densities, and resistances, which can be reproduced to approximately 20% tolerances. This means that we can fabricate CPB qubits with good control over the energy spectrum of the qubit, in order to minimize problems with quasiparticles and parity, and to yield an optimal set of transition frequencies.

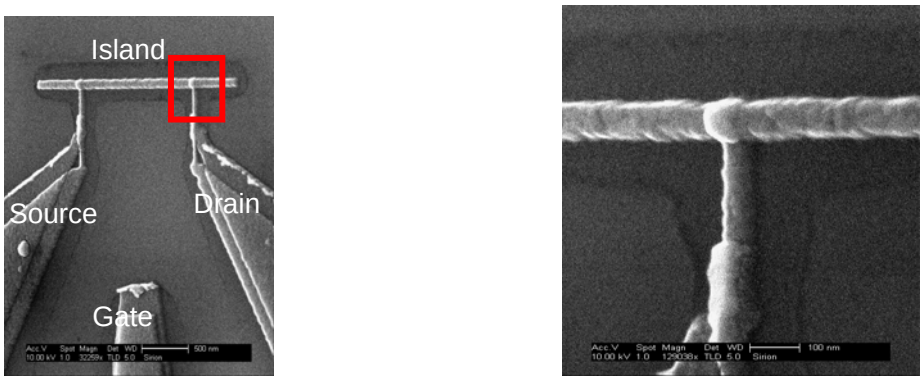

Figure 1: Electron micrograph of finished SET device fabricated at Yale (by D. Schuster and L. Frunzio). Left image shows overview of the SET, with the island, drain, source and gate labeled. Such a device has a charging energy E_C ~ 1-3 Kelvin. Right image shows a detail of one of the small junctions, with linewidths less than 75 nanometers.

We have also designed a new generation of sample holders with the goal of efficiently coupling microwave signals to qubits, and to present our qubits with a well-engineered, broad-band 50 Ohm electromagnetic environment. We have used custom-made microwave circuit boards with vias, and developed a coupling scheme using surface-mount SMP launchers, which can convert from a coaxial input to an on-board balanced transmission line, in a coplanar waveguide (CPW) geometry. This has the advantage that broadband interconnects to the chip can be made using conventional wire bonding, also available in our lab. In order to exploit the advantages of this design philosophy, the qubit and SET chip must also incorporate these CPW lines. These can then be fabricated to make a constant impedance, broadband taper from the millimeter scale to the micron scale of the qubits. This required a combination of the fine-line electron-beam lithography and large scale patterning with our e-beam lithography system. This process was developed, and a test sample using this design is shown in Figure 2. Fabrication of actual qubit/readout chips is underway, and first tests will measure the capacitive coupling and quality of the junctions configuring them as a pair of coupled SETs. This fabrication and testing is underway. The chip-level microwave engineering is important in allowing fast microwave pulses for qubit control, and in preventing anomalous relaxation due to environmental resonances, and has not so far proven feasible with samples fabricated at Chalmers.

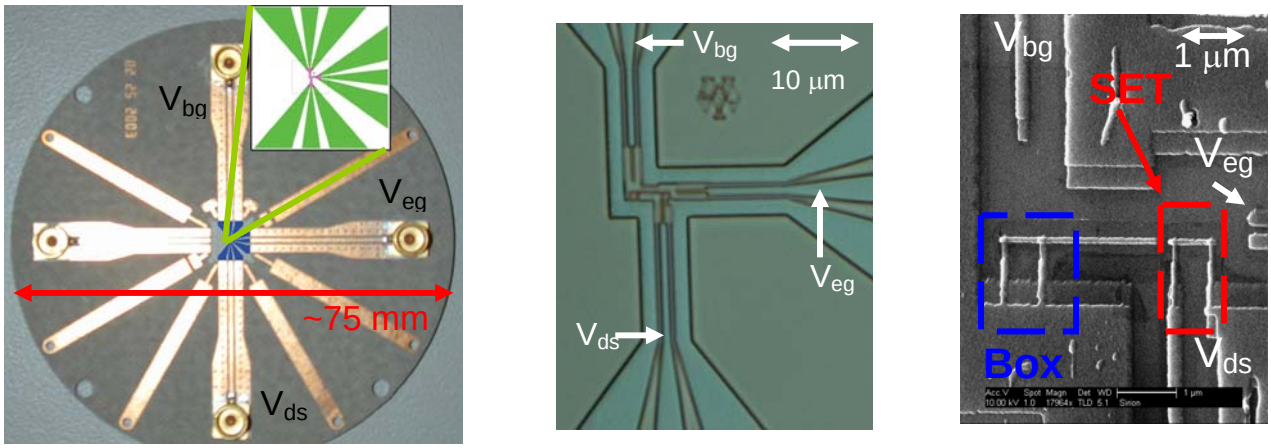

Figure 2: Pictures of Box+SET samples designed for efficient coupling of microwave pulses and control of the electrical environment to limit relaxation rates. A) Left panel shows a custom microwave circuit board, with 4 coplanar waveguide (CPW) lines for high frequency signals. The 5 x 5 mm chip containing SET and CPB qubit is placed in a machined recess at the center of the board. B) Optical micrograph of a test sample, fabricated at Yale, which incorporates CPW line tapers to match the device to circuit board. C) SEM image of a sample containing CPB box qubit, and readout SET in this optimized geometry.

Another effort in design has looked at extending this type of design to a coupled qubit system for demonstrating simple gates. This requires two CPB qubits with capacitive coupling, and two individual RF-SETs for readout of the qubit states. A mask design for such a circuit is shown in Figure 3, and is intended for use with the same sample holder and design philosophy as described above for single qubits. Schemes for two qubit control and gate operation with such a circuit have been investigated by our theory team, as described in section III below.

Other fabrication work has investigated a possible process for producing qubits with higher Tc superconductors, in order to reduce the importance of quasiparticle effects. We have invested in some techniques for etching tantalum islands (Tc = 4 K), and also experimented with oxygen-doped aluminum films, which can have Tc's up to 2 Kelvin.

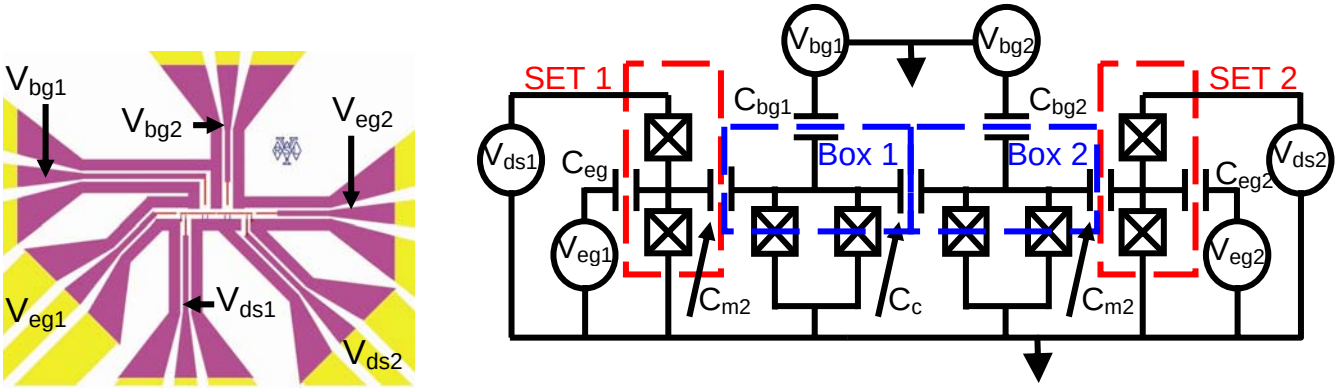

Figure 3: Left: Mask design for a two-qubit gate using CPB qubits and SET readouts. All lines are coupled to CPW transmission lines. Right: a circuit schematic of the two qubit-two SET readout circuit. The boxes have a fixed coupling by a capacitor. Operation protocols for such a gate have been theoretically investigated and described below.

The final area of work in fabrication has been in the production of high-Q resonant cavities for the scQED architecture (see description of the architecture below in Section III, and of recent experimental progress in Section IV). Optical lithography is used to produce approximately 30 resonators at a time on a two-inch silicon or sapphire wafer. Two different generations of optical masks have been designed and tested. Resonators with both aluminum and niobium superconducting films were made and tested down to 250 mK, showing more than adequate quality factors. We have also developed several techniques for integrating CPB qubits into the resonant cavities to achieve the scQED architecture. This uses the standard process for Al shadow-evaporated junctions, described above, and fabricated within the resonator by direct write, after aligning to the resonator structure to tolerances of about 150 nanometers. An example of both single and multiple qubits inside one of these resonators is shown in Figure 4. Testing of such qubits at 20 mK is underway.

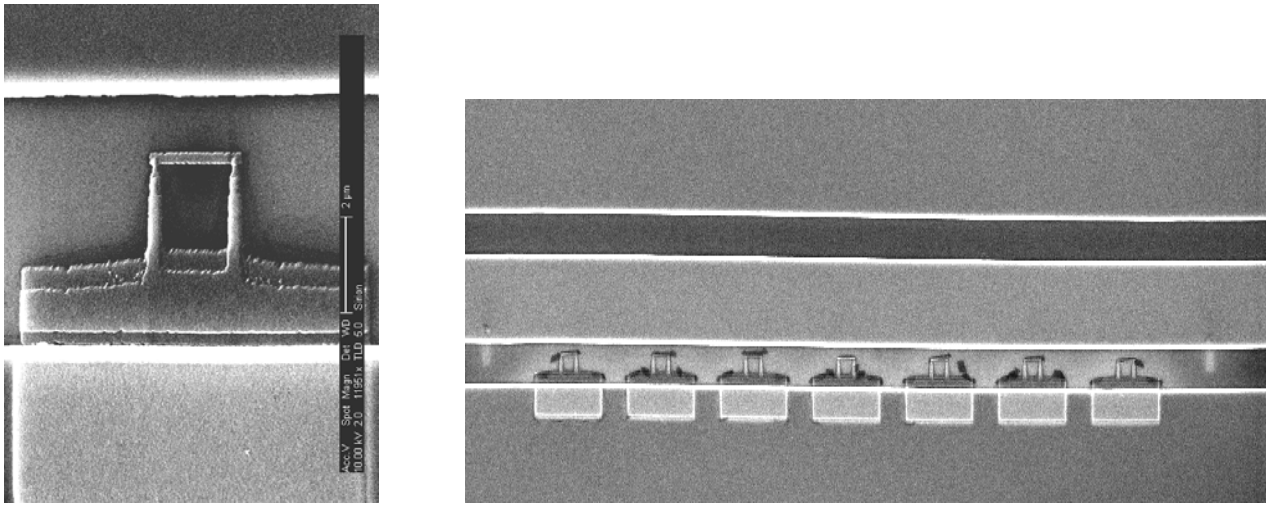

Figure 4: Electron micrograph of CPB qubits inside transmission line resonators. Shown are a single qubit, with an island, two junctions, and a small SQUID loop to allow tuning of the Josephson energy. On right is a test sample with seven qubits coupled to a single resonator.

II. SET Readout of Cooper-pair Box Qubits

As described above, we now have the capability to fabricate our own CPB qubits and SETs, but up until now we have been forced to rely on samples obtained through our collaboration with Chalmers University in Sweden. We found in our earlier experiments that it was detrimental to have too large a charging energy for the CPB, as this leads both to relatively strong dephasing due to 1/f noise, and creates problems with excess quasiparticles occupying the island, since the charging energy can be comparable with the superconducting gap. This second problem is particularly detrimental, since it means that the CPB cannot be operated near the charge degeneracy point in gate voltage, where the results of Saclay have shown that 1/f dephasing can be minimized, leading to coherence times approaching one microsecond. Finally, the large charging energy raises all the energy scales of the box, meaning that much higher frequency (and much more difficult to generate and couple) microwaves are required for control, and shortening the relaxation times available for the control and readout of the states. Our goal was therefore to investigate CPB qubits with a more optimal choice of energies, namely a lower charging energy so that charging energy is equal to the Josephson coupling energy, $E_C \sim E_J$.

We obtained such samples this summer from Chalmers University (a turn-around time of about one year). Most of our expectations for improvement have been borne out by measurements carried out in the fall and winter of 2003. First, the problem of excess quasiparticles ("poisoning") was reduced, allowing an observation of the fully two-electron periodic Cooper-pair staircase. We were also able to observe the modulation of the ground state of the box by tuning the flux through the SQUID loop, which modulates the Josephson coupling, or the tunnel splitting (sigma-x term) in the Hamiltonian. A comparison of the charge signals obtained with the previous samples and the improved devices this year is shown in Figure 5.

We have also performed microwave spectroscopy on these improved qubits, and studied the relaxation times. This spectroscopy confirmed that the design goal $E_C \sim E_J$ was achieved. Due to the improvements in the qubits, we could now study the transitions and energy spectrum of the box all the way down to the desired operation point, at the charge degeneracy point. This is the point where the qubit is minimally affected by 1/f noise. The data in Figure 6 requires approximately 8 hours to acquire, and indicates the excellent stability of the offset charge and the parity which was obtained. Because the microwave coupling at the chip level (see discussion in Section I on design of qubits with microwave coupling) is not possible so far with the Chalmers samples, the power coupled to the qubit, and its expected lifetime are not yet well controlled versus frequency. We were therefore not yet able to search for spurious resonances or interactions with impurities suggested by Martinis and co-workers.

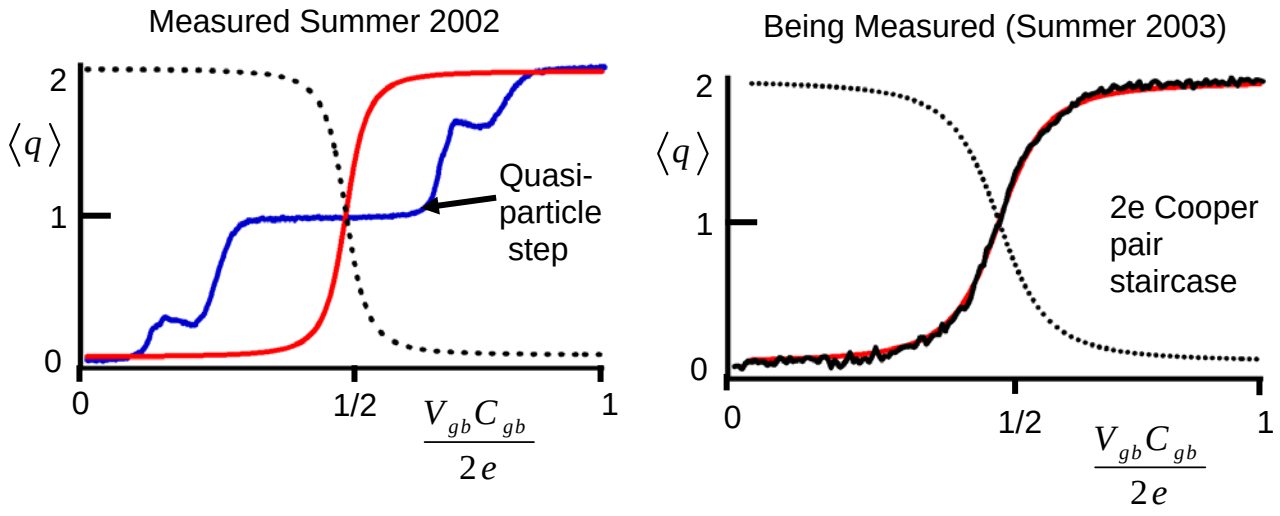

Figure 5: Comparison of charging staircases for two CPB qubits with different charging energies. On left is the old design with $E_C \sim \Delta$, causing non-equilibrium quasiparticles to be generated in the qubit, and obscuring the ground state of the qubit. On right is a recent measurement of a device with reduced charging energy, showing elimination of the quasiparticle feature, and a good measurement of the qubit, including at the charge degeneracy point (center of staircase) where 1/f noise effects are minimized.

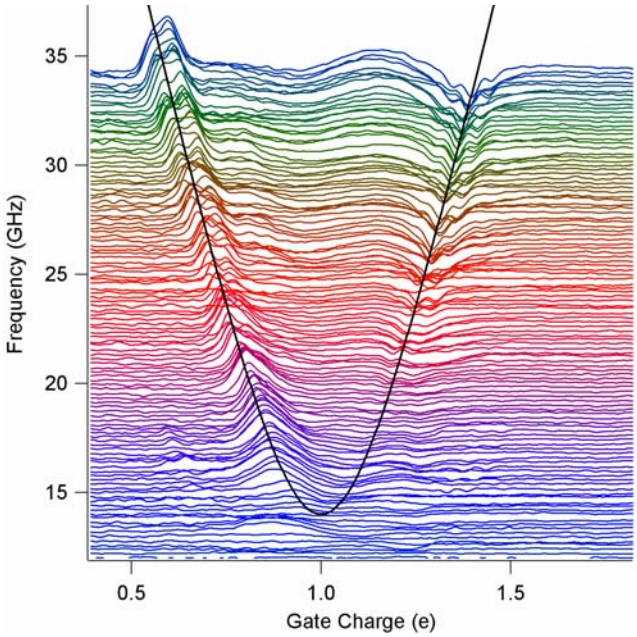

Figure 6: Spectroscopy of an improved CPB qubit as measured by an RF-SET. The photoresponse (i.e. the difference in the Cooper pair staircase with and without CW microwaves applied to the gate) is displayed as a function of both gate charge and microwave frequency. Shown is a fit to the simple hyperbolic energy spectrum of the box, which yields the energies of the qubit, E_C = 18.9 GHz and E_J = 14.9 GHz, and indicates that the design goal $E_C \sim E_J$ was achieved. Due to the improvement in the parity described above, the transition between the two lowest states can now be followed down to the degeneracy point, n_g=1, shown at the center of the plot. This is the point where the qubit is minimally affected by 1/f noise. This data requires approximately 8 hours to acquire, and indicates the excellent stability of the offset charge and the parity which was obtained.

Following our suggestions for improved qubit parameters, and also using our techniques and experience gained from extensive spectroscopy of CPB qubits using the SET, the Chalmers team sought to observe coherent oscillations and repeat the original observation of Nakamura and co-workers. Using one of the improved samples described above, and the expensive picosecond pulse generator used by Nakamura (not available in our lab) they succeeded in observing these oscillations. These measurements, however, still used a continuous measurement by the SET, and operated away from the charge degeneracy point, thus inducing maximal 1/f dephasing, so that the observed coherence times were only on the order of one nanosecond.

This fall we have made extensive studies of the relaxation times (T1) of the new Chalmers samples. We have found that the dominant effect on the qubit lifetime can be the backaction of the SSET, and shown that this time can sometimes be reduced by more than an order of magnitude by the SSET. This observation is very important for our goals of using the SET as a qubit readout, and also for the superconducting quantum computing community as a whole. Though not always emphasized, the problem of short and/or variable relaxation times has been observed to be a major challenge for all groups, working either with charge, flux, or phase qubits. An example of this variability of relaxation times in shown in Figure 7. The relaxation of two different spectroscopy peaks in the CPB qubit are acquired simultaneously, with the only difference being the precise biasing point of the electrometer. The transitions of the box which are measured with a higher current and higher conductance thru the SET are observed to have much faster relaxation, in qualitative agreement with our model of the backaction of the SET. We have again observed, for appropriate operating conditions, relaxation times in excess of 1.2 microseconds, which is consistent with our expectations for spontaneous emission of the box into its 50 Ohm electromagnetic environment (here there is no cavity to suppress this decay!). We find that there are many areas of operation of the electrometer which strongly damp the qubit and cause the state to reset" in times of less than 100 nanoseconds. The theory of the backaction of the SSET, developed by our collaborators Aash Clerk and Steve Girvin under this project earlier, suggests that this fast relaxation can even occur under conditions in which the SET is nominally "off," and very little current flows. It also suggests an explanation for the observation of uniformly fast relaxation in the experiments at Chalmers using fast pulse generators. Since the fast pulses couple strongly to their RF-SET, they sample many of the "forbidden" regions of bias where the SET gives fast relaxation. This suggest to us that fast pulses, though capable of showing basic coherence, are not desirable in the long run for quantum computation, and that one must carefully control the qubit in order not to perturb the SET too strongly, which will lead to excess dephasing and relaxation in the control phase before the measurement.

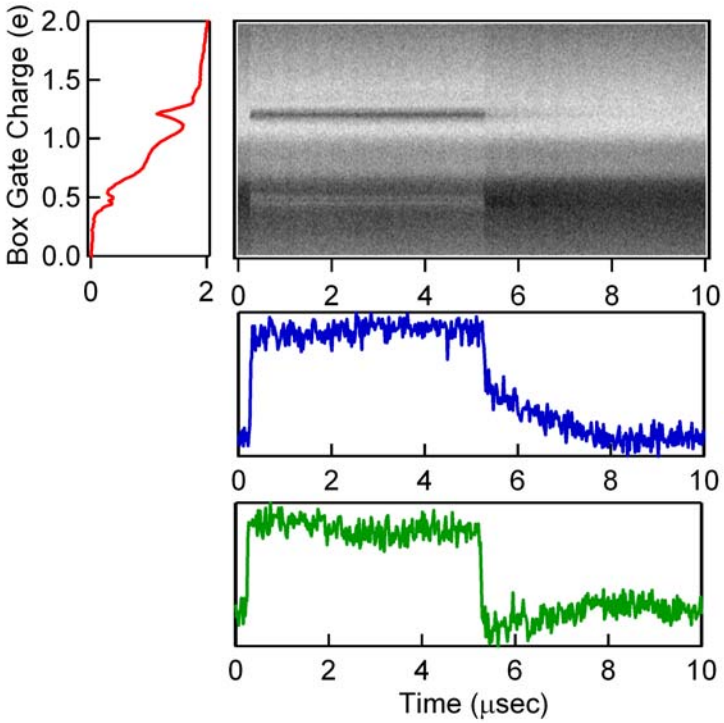

Figure 7: Measured dependence of relaxation time (T1) on the SET backaction. Top panel shows a grayscale image of the average charge on the CPB qubit as a function of time (horizontal axis) and gate charge (vertical axis). Each vertical slice of the image consists of a measurement of the Cooper-pair staircase, as shown by the line cut in upper left. In this measurement, a microwave pulse at 30 GHz is applied during the first 5 microseconds, and then switched off with a fall time of ~ 20 nanoseconds. The streaks in the greyscale image correspond resonant absorption of the microwaves by the qubit, i.e. the peaks shown in the line cut when the qubit transition frequency match the microwave stimulus. After the microwaves are switched off, the decay to the ground state of the box is measured using the RF-SET with a timing resolution of < 50 nanoseconds. The first of the lower linecuts shows the T1 decay of one of the peaks, with a slow component having a time constant of ~ 2 microseconds. The lower curve shows the second peak, which decays in a time less than the timing resolution of the experiment, i.e. over an order of magnitude faster. The only difference in the two decays is caused by the differing backaction of the readout SSET at the two points, in agreement with theoretical predictions.

Another observation which confirms the importance of the SET's backaction to the dephasing and relaxation of the CPB qubit is that the measurement can actually induce a population inversion in our qubits. This effect was again predicted by our theory collaborators. It comes from the fact that the SSET backaction represents a coupling to a non-equilibrium noise source, which can preferentially excite, rather than relax the qubit. The population inversion is manifested as the observation that the system is more likely to occupy the excited state in the presence of a continuous measurement, and of an average charge greater than electron. Such a measurement is shown in Figure 8. Again, the qualitative behavior of this effect is in good agreement with theory, and induced only for certain specific qubit parameters and SET bias conditions. It also gives direct evidence that the interaction with the measurement circuitry can dominate over the passive portions of the circuitry, and over the intrinsic losses in the qubit. In other words, it indicates that the qubit may be of high fidelity if the readout is properly operated and optimized.

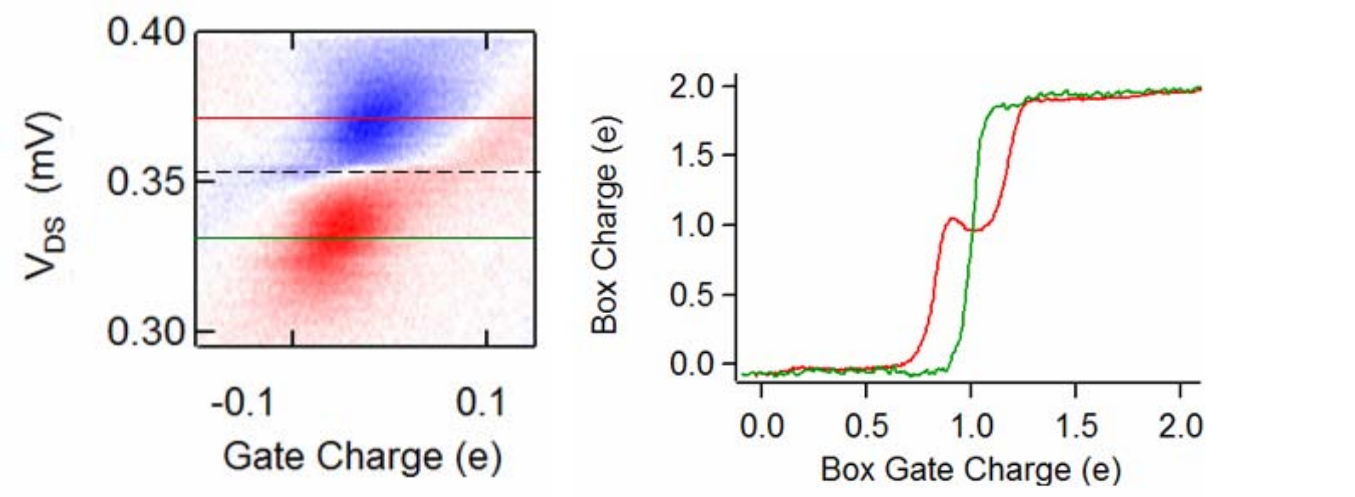

Figure 8: Observation of population inversion of the qubit due to SET backaction. Left panel shows the observed reflected RF power from the SSET within a narrow range of the DJQP resonance used for the measurement. The dashed line indicates the center of the DJQP resonance. The solid lines indicate the operating drain-source bias voltage used for two measurements of the Cooper-pair staircase of the box, shown in the right panel. These measurements are performed with the Josephson energy, E_J, tuned to a small value of about 5 GHz. Under these conditions, the ground state of the box is uniformly observed (in green, smooth step-like behavior) when the SET is biased below the DJQP resonance, and the SET tends to mostly absorb energy from the qubit. In contrast, the red trace, obtained with SSET biased above resonance, shows a prominent extra bump, with a charge greater than 1 electron, i.e. with a higher probability to be in the excited, rather than ground, state, which would correspond to a population inversion or a negative temperature of the qubit. This effect was independently predicted by earlier theory work under this project, and indicates that the SET is the dominant source of relaxation or excitation for the qubit.

We have therefore confirmed the detailed mechanism of the effect of the readout on the qubit, which was the next item on our flow chart for the SET/CPB project. This fact, and our detailed understanding, means that we can now design and fabricate (using device at Yale) a CPB qubit and SET readout which are optimized and capable of providing a single-shot readout and long coherence times. It emphasizes a continuing theme found in our experiments: one cannot simply design a qubit and expect to achieve long coherence times, without first understanding in detail the effects of the readout circuitry and how to operate it.

A final interesting observation regards the 1/f charge noise in our system. We often observe that the level of charge noise in the qubit seems much lower than that in the measuring SET. By controlling the bias on the SET, we studied how the low-frequency 1/f noise in the SET varied with the bias and power levels dissipated by the SET. We found a very striking effect, in which the 1/f noise could be dramatically increased when more power is dissipated. This suggests that the 1/f noise in superconducting qubits may be in part or in whole an “activated” process. By avoiding all dissipation on the chip, using for example the scQED measurement techniques described in Section IV, one may hope to reduce the 1/f noise and gain a corresponding increase in coherence times.

III. Theory of Superconducting Qubits and Readouts

III.A. Cavity QED

In a joint experiment/theory collaboration we have conceived a new architecture for quantum computation, adapting the idea of cavity QED (quantum electrodynamics) from atomic physics to superconducting electrical circuits, an idea that we refer to as scQED. The essential point of cavity QED is to make the mode frequencies of the electromagnetic field discrete by confining them inside a resonant cavity. The smaller the volume of the cavity, the more frequently the trapped photons will interact with atoms inserted into the cavity leading to strong coupling of the two. There are two interesting limits: First if the atomic transition matches the frequency of the cavity, then the excitation will flop back and forth between the photon field and the atom forming an entangled state of atom and photon. In the strong coupling limit where the Rabi flopping rate greatly exceeds the relaxation rates of the both the cavity and the atom, this entanglement is strong and robust. Second, if the atomic transition is strongly detuned from the cavity frequency, there is no mode into which the atom can decay. Thus, the spontaneous emission is strongly suppressed and the qubit lifetime greatly enhanced. A second advantageous feature of the strongly detuned case is that virtual excitations of the qubit by the cavity photons pulls the resonance frequency of the cavity up or down depending on the state of the qubit. Thus this effect can be used as a high fidelity quantum non-demolition readout.

The key feature of our proposal is that we use a quasi-one-dimensional 'cavity' formed from a coplanar wave guide resonator (see Fig. 9b), which has a very tiny total mode volume of order 10^{-5} cubic wavelengths. This, combined with the large transition dipole matrix element of the Cooper pair box 'atom', gives us a vacuum Rabi rate of order 100 MHz, some 2000 times stronger than can be achieved in the analogous atomic physics experiments which use three-dimensional microwave cavities. With this strong coupling, a qubit detuned 10% from a cavity with even a modest Q of only 10^4, still pulls the cavity several line widths, making detection of the qubit state very easy and efficient. We have performed stochastic wave function simulations of the homodyne detection process, and some sample results are illustrated in Fig. 10.

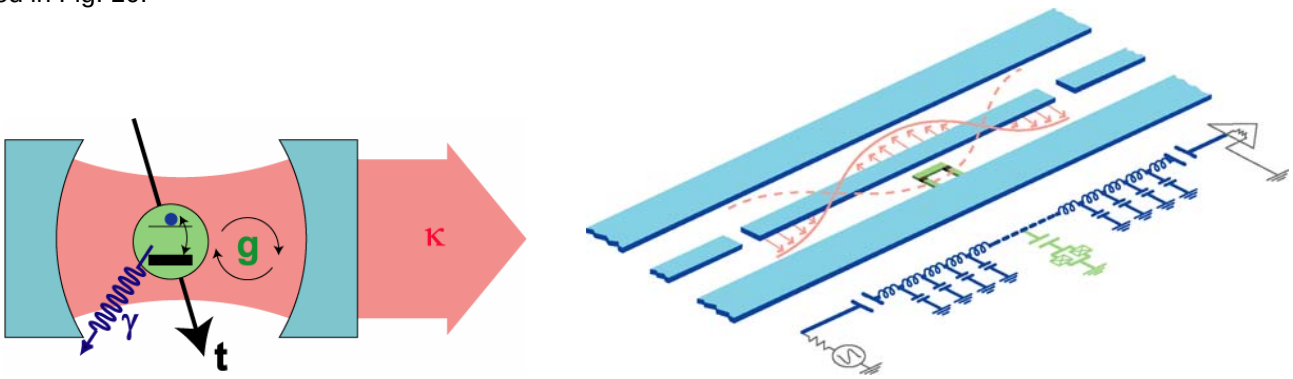

Figure 9 a) Standard representation of cavity quantum electrodynamic system, comprising a single mode of the electromagnetic field in a cavity with decay rate κ coupled with a coupling strength g to a two-level system with spontaneous decay rate γ and cavity transit time t_{transit}. b) Schematic layout and effective circuit of proposed implementation of cavity QED using superconducting circuits. The 1D transmission line resonator consists of a full-wave section of superconducting coplanar waveguide, which may be lithographically fabricated using conventional optical lithography. A Cooper-pair box qubit is placed between the superconducting lines, and is capacitively coupled to the center trace at a maximum of the voltage standing wave, yielding a strong electric dipole interaction between the qubit and a single photon in the cavity. The box consists of two small ($\sim 100\text{nm}\times 100\text{nm}$) Josephson junctions, configured in a $\sim 1\mu\text{m}$ loop to permit tuning of the effective Josephson energy by magnetic field. Input and output signals are coupled to the resonator, via the capacitive gaps in the center line, from 50Ω transmission lines which allow measurements of the amplitude and phase of the cavity transmission, and the introduction of dc and rf pulses to manipulate the qubit states. Multiple qubits (not shown) can be similarly placed at different antinodes of the standing wave to generate entanglement and two-bit quantum gates across distances of several millimeters.

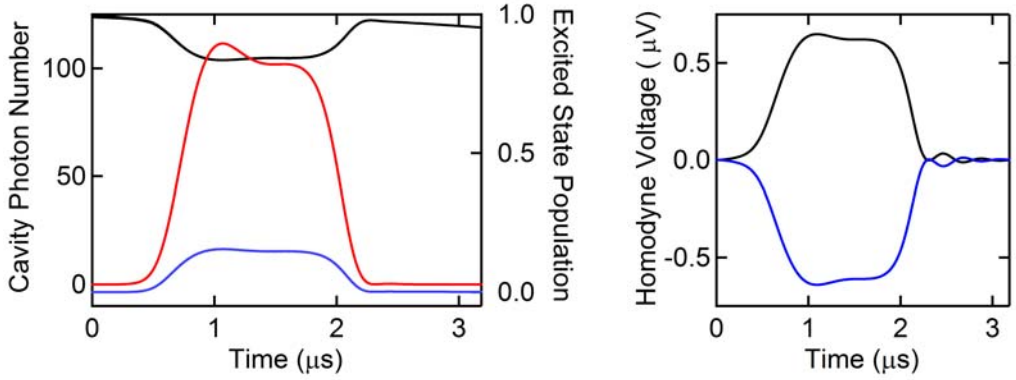

Figure 10: Use of the coupling between a Cooper-pair box qubit and a transmission-line resonator to perform a dispersive quantum non-demolition measurement. To perform a measurement of the qubit, a pulse of microwave photons, at a probe frequency $\omega_{\text{p}} = \omega_{\text{r}}$, is sent through the cavity. The qubit causes a state-dependent 'pulling' of the cavity frequency, and a phase shift of the transmission. a) (Left) Results of numerical simulations of this QND readout using the quantum state diffusion method. A microwave pulse with duration $\sim 1.5\mu\text{s}$ coherently excites the cavity to a photon number $\langle n\rangle \sim 100$. The intracavity photon number (left axis, in red), and occupation probability of the excited state, for the case in which the qubit is initially in the ground (blue) or excited (black) state, are shown as a function of time. Though the qubit states are coherently mixed during the pulse, the probability of real transitions is seen to be small.

Depending on the qubit's state, the pulse is either above or below the combined cavity-qubit resonance, and so is transmitted with a large relative phase shift that can be detected with homodyne detection. c) The real component of the cavity electric field amplitude (left axis), and the transmitted voltage phasor (right axis) in the output transmission line, for the two possible qubit states. The opposing phase shifts cause a change in sign of the output, which can be measured with high signal-to-noise to realize a single-shot, QND measurement of the qubit.

During the past year we have performed a detailed (and conservative) engineering analysis for this new architecture [1] and designed the first round of experiments that are about to begin. During the coming year, the theoretical effort will further develop our understanding of what to expect from these experiments and how to analyze them, as well as develop new ideas for the second round of experiments. In addition, we will build on the initial results we have for multi-qubit design in which the qubits are coupled via virtual photon exchange through the resonator. We have begun examining pulse sequence protocols to carry out one and two-bit gate operations.

We are also in the preliminary stages of development of an idea for electrically biasing the qubits in the resonator to turn on and off their mutual coupling without introducing extra dephasing. Another project now underway with graduate student Ren-Shou Huang and postdoc Alexandre Blais is the modeling of the effects of 1/f noise. Because dc bias modifies the high frequency polarizability of the qubit, the cavity pull and therefore the phase shift of the transmitted microwaves is a direct measure of the 1/f noise amplitude acting on the qubit. This will initially prove useful as a direct diagnostic of the noise and might ultimately permit feedback control to eliminate the low frequency part of the noise.

III.B Controlled Not Protocol for Capacitively Coupled Qubits

Devoret and Girvin jointly supervised the senior thesis of Yale undergraduate Kenneth Canfield who explored pulse sequence protocols to realize the cNOT operation for a pair of capacitively coupled superconducting qubits. Canfield learned how to using a doubly rotating reference frame for the two qubits, developed numerical routines to model the effects of different control pulse sequences. Girvin supervised two other senior theses in 2002-3: Aryesh Mukherjee (now a graduate student at Harvard) who studied cavity QED and Themis Athanassiadou (now a graduate student at Illinois) who studied the EPR pairs and the Bell inequality. The 2003-4 senior thesis of Clifford Cheung is on the production of tagged single photons and is described separately below.

III.C Tagged Single Photon Production

One offshoot of the scQED architecture we have developed is a theoretical proposal for a device for producing single microwave photons. Yale undergraduate Clifford Cheung is doing his senior thesis under the supervision of Professor Girvin analyzing a design consisting of a pair of coplanar wave guide resonators mutually coupled through a Cooper pair box qubit. The essential idea is that by choosing the frequency of the first resonator to be equal to the sum of the frequency of the second resonator plus the qubit transition frequency, one can cause creation of a single photon in the second resonator to be associated with a spin flip of the qubit. This spin flip will change the pull on the first cavity and be readily detectable by monitoring its output. This will automatically 'tag' the photon production event. Cliff Cheung started work on this last summer and has been doing an excellent job on the analysis. We anticipate being able to write the thesis up for publication this spring.

III.D Quantum Noise and Measurements

Mesoscopic electrical devices are commonly proposed and used as detectors. We published this year a detailed theoretical study of quantum-limited measurements and a general theory of flow of information in mesocopic detectors [2]. Our theory postdoc Aash Clerk (in work separately supported by the Keck Foundation) has recently extended this picture to provide a theory of how dephasing affects the approach to the quantum limit in mesoscopic detectors [3]. We also wrote last year a tutorial article [4] on the general theory of quantum noise and its detection which we will be extending and revising this year for publication as an invited Colloquium in *Reviews of Modern Physics*.

III.E RF-MQT Readout Scheme

Michel Devoret and his group have developed a remarkable qubit readout scheme based on the elastic scattering of a microwave pulse from a Josephson junction that acts as a non-linear inductor producing a bifurcation in the phase of the reflected wave as the drive amplitude is increased. Postdoc Krishnendu Sengupta is working on a quantum theory of this measurement to supplement the classical simulations performed by Devoret's group. We have so far obtained numerical results for the limit of nearly zero damping and but now need to develop new numerical techniques to allow solution of the equations of motion in the presence of finite damping and a very large number of states in the Hilbert space.

IV. Cavity QED Experiments with Cooper-pair Box Qubits:

A major part of our experimental effort has been directed to implementing the cavity QED architecture for quantum computing with superconductors described briefly above. The concept for this architecture, described above, has been presented at several international conferences and workshops, and submitted for publication to Physical Review B.

The technology for the design, fabrication, and measurement of these devices has been developed, initial devices have been fabricated, and the first measurements are now underway. Future plans for this approach are discussed in section V.

One of the first tasks for implementing the cQED experiments was to master the design and fabrication of the cavities themselves. These are fabricated in our cleanroom at Yale using optical lithography (see section I). We have designed and tested resonant cavities from two generations of optical masks, and tested the quality factors of several different designs in both Al and Nb at temperatures down to 250 mK. These results have been very encouraging, as high quality factors (in excess of 10^5) are routinely observed. Our present designs use Nb resonators, in which we have attained quality factors of nearly a million (>600,000) at 100 mK. Our proposal and first generation devices only require a quality factor of about 10,000, which we easily obtain by strongly coupling the resonator to its input and output. We also studied the temperature and magnetic field dependence of the cavity losses, and found that though affected by large magnetic fields, the cavities can retain their high Q's even for fields of 10-100 Gauss, which is large enough to allow the Josephson energy of the qubit to be widely tuned via the simple application of a global field.

In order to perform such tests, we designed and implemented a new sample holder which allows for good high-frequency coupling to the resonators, without exciting spurious resonances that can confuse the measurement of a weakly coupled resonator. A picture of such a sample holder, incorporating a custom microwave circuit board with vias, is shown in Figure 11, along with a representative measurement of a single resonator transmission spectrum. This setup has two coaxial inputs, allowing the measurement of the transmission, and also allowing for separate control and measurement of a two-qubit cQED gate, as described below.

A further advantage of this cQED architecture is that it is trivial to imagine multi-qubit couplings, as the resonator itself can be used as a quantum bus to make entanglement between different qubits. Since the size of the CPB qubit is small compared to the dimensions of the resonator a large number of qubits can easily be fabricated inside a single cavity (see Figure 4). In order to operate multiple qubits inside the cavity, however, their offset charge must be separately controlled and set to the optimum value at the charge degeneracy point of the box. For the initial step to two qubits, this can be done without any additional complexity in fabrication or wiring, by placing the qubits within the resonator, but close enough to opposite ends so that there is a selective coupling from the input and output coaxial port to the individual qubits. This is shown schematically in Figure 12 below, along with a detailed drawing of the geometry near the end and the results of a finite-element capacitance simulation for the box and control wiring.

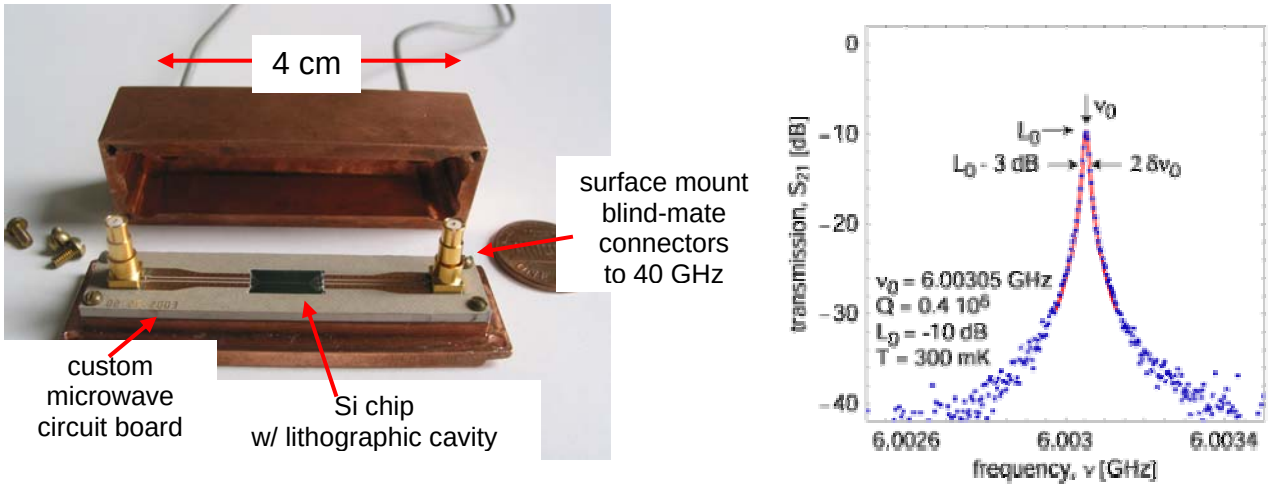

Figure 11: (left) Sample holder for high-frequency measurements of microwave transmission line resonators. (right) Measurement of a niobium coplanar-waveguide resonator at 250 mK, showing a quality factor in excess of 400,000, at a resonant frequency (full-wave resonator) of about 6 GHz.

In the last year we also built up a microwave test setup for measuring the transmission through the cavities and controlling the qubits within the cavities. A schematic of this apparatus, which includes the possibility to perform both single and two-qubit operations and measurements, is shown in Figure 13. The resonator has two equivalent ports, one of which is the transmit arm (on left), and the other the receive arm (right). Each arm has a bias-tee that allows the introduction of separate dc voltages to control the offset charge and tune the qubits separately into resonance with the cavity or with each other. The transmit arm connects to microwave generators at room temperature. Microwave pulses at different frequencies are used to perform one-bit rotations by irradiating at the transition frequencies of the two qubits. With our theory collaborators, we are also investigating ways in which a third microwave frequency can effective turn the two-qubit coupling on and off, to effect two-qubit operations and yield a CNOT. Finally, the readout is to be performed by irradiating on the transmit line near the cavity frequency (typically 6-10 GHz), and measuring the transmitted signal using a low noise cryogenic HEMT amplifier, located on the receive arm. The phase shift of the cavity is predicted to be as large

as 180 degrees for different states of a single qubit. In the case of a two-qubit sample, two pulses at slightly different frequencies can in principle yield two bits of classical information, allowing access to the states of both qubits, without introducing any additional wiring or channels for decoherence. We are optimistic that this minimal approach and relatively low complexity of this two-qubit setup make it a logical next step that can be attempted shortly after the characterization of single-qubit cQED samples.

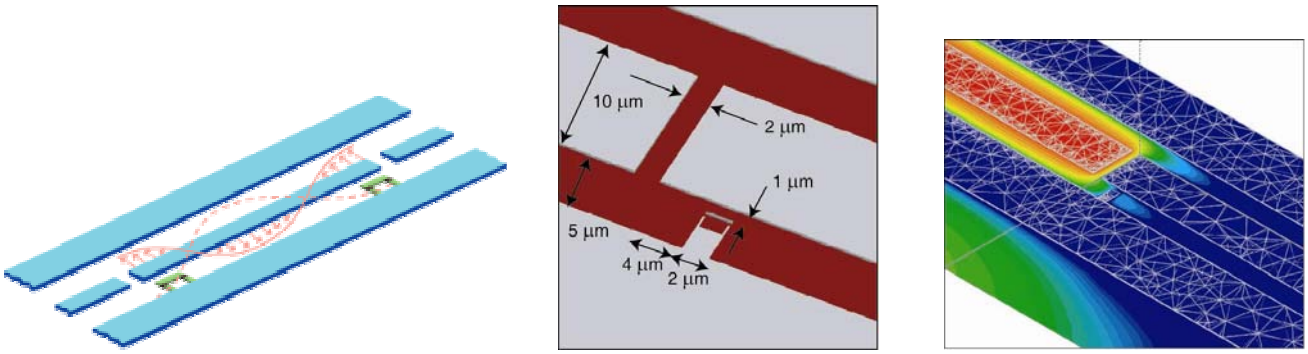

Figure 12: Design for a two-qubit gate in the superconducting cavity QED architecture. Two Cooper-pair boxes are placed near the ends of a transmission line resonator, so that they are coupled to the common electromagnetic mode. Two qubit interactions are effected by tuning the qubits into resonance with one another, via the combination of dc and ac signals on their gates. Center panel shows a detail of the physical layout of the CPB qubit near the end of the transmission line, and the right panel shows results of a finite-element electrostatic simulation of the geometry, from which the capacitances of the circuit are determined. This design shows that it will be possible to individually address two qubits from opposite ends of the resonator, without inducing a substantial channel for decay into the external electromagnetic environment.

The apparatus shown in Figure 13 has been tested in our ^{3}He refrigerator at 250 mK, and is presently installed in our dilution refrigerator and being used for tests of our first cQED samples with single qubits. In earlier tests on a cavity without a qubit, however, we performed several tests of the signal-to-noise expected for the cQED readout. First, we were able to show that even with the measurement and control lines in place, the photon occupancy of the cavity is small, less than a few photons, and probably in agreement with the number expected from thermal equilibrium at about 300 mK. Second, we were able to measure the noise temperature of the new HEMT amplifier, and found it to be as low as about 20 photons (6 K at 6 GHz), about five times better than our estimate used in the design study. To determine whether the phase shift through the cavity, and eventually the qubit state, can be detected in a single-shot measurement lasting less than a few microseconds, we made histograms of the measured transmission phase, and inserted a phase shift of pi at room temperature on the transmitting arm. Histograms showing the probability of occurrence for different measured phases are shown in Figure 14, for integration times of 300 nanoseconds and 1.5 microseconds, respectively. The fidelity for distinguishing between these two “classical” bits was greater than 90% and 99%, respectively. In a real experiment with a qubit, the maximum integration time, and thus the signal-to-noise and the fidelity, are entirely determined by the observed lifetime (T1) of the qubit. Using the cQED architecture, one may hope for this time to exceed 50 microseconds, and the readout to be very efficient. However, this lifetime can be limited by many so far unknown processes, and therefore the determination of the T1 lifetime limits for a box in the cavity remains one of our first priorities.

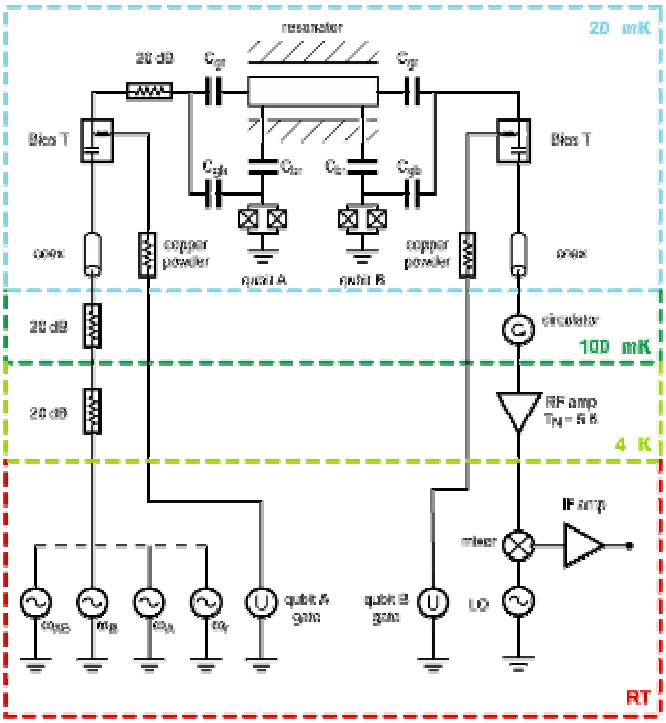

Figure 13: Schematic of the microwave apparatus for control and measurement of the cQED qubits. On left is the transmit arm, which connects the resonator to microwave sources at room temperature for generating one and two-qubit rotations. The selectivity is accomplished by using different frequencies, which are coupled to the qubits with some additional filtering by the resonator. Individual biasing of the gates of the two Cooper-pair boxes is provided by the lines coupled to the two arms via bias-tees. On the right is the receive arm, with cryogenic circulators and HEMT amplifier for performing readout via the phase of the cavity transmission.

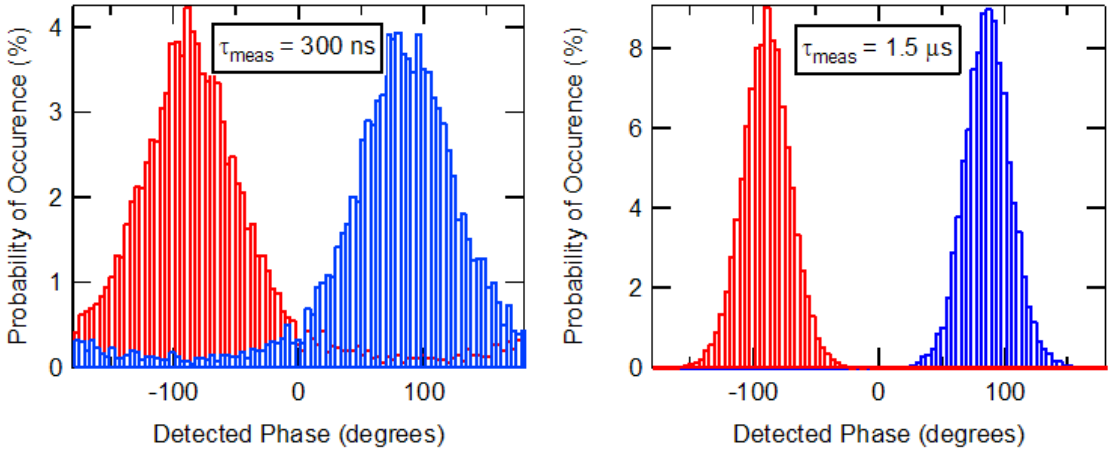

Figure 14: Test of the phase sensitive detection technique for the cQED resonators. A phase shift of 180 degrees was introduced on the transmit arm, and sent through an overcoupled resonator at 250 mK. The readout pulses had a magnitude of about 100 photons, and a duration of 300 ns and 1.5 microseconds, respectively. The fidelity for measurement of this classical bit was greater than 90% and 99% in the two cases, and was consistent with the noise expected from the first stage HEMT.

V. Plans for Future Work:

We conclude by briefly listing the priorities for the project in the next year. For the CPB box readout with an SET, the main obstacle remains the ability to obtain a reliably long (i.e. greater than 1 microsecond). We are optimistic that the recent results on the backaction of the SET indicate both that the intrinsic quality factor of the qubit itself is high, and that we will be able to design and make qubit/SET samples which can attain a high fidelity single-shot readout. We are presently calculating the optimum parameters for such a sample, based on the theory developed by Aash Clerk and Steve Girvin within our collaboration. These devices will include control of the RF environment, as described in Section I above. A major goal remains a careful study of the mechanisms of relaxation and decoherence in a single CPB qubit, as we view this as a necessary for determining the scalability and allowing a progression to multi-qubit devices and demonstration of

gates and algorithms. Though all of these may not be achievable in the next year, an ordering of the tasks we believe must be undertaken is given below.

Cooper-pair box with superconducting SET readout:

- Make CPB+SET at Yale with optimized parameters, coupling, and readout SET for long T1.
- Measure T1, T2 dependence on matrix elements and CPB parameters – determine mechanisms and limits of relaxation and decoherence.
- Perform single-shot measurements.
- Perform Rabi, Ramsey experiments by operating at charge degeneracy point.
- Design and make 2 qubit samples.
- Spectroscopy of coupled system, demonstration of CNOT operation.

For the theoretical portion of this project, work will continue on several new directions. First, there will be continued efforts in support of the experiments using SET readouts, as described above. Another area is investigations of various entanglement schemes, and techniques and pulse sequences for utilizing fixed two-qubit couplings, either due to direct capacitive coupling, as in the CPB/SET system, or due to qubit-cavity interactions in the cQED architecture. Investigations related to detection and generation of single microwave photons within the cQED devices is also continuing. Finally, we are beginning to investigate the detailed requirements, both in terms on necessary qubit coherence and control, and in terms of practical pulse sequences, for implementing simple gates or a Deutsch-Josza algorithm. For example, in the cQED experiments, it may be possible to perform Deutsch-Josza with a single qubit coupled to the cavity, in analogy to recent experiments by Blatt, Chuang, and coworkers with a single ion in a harmonic trap.

Theory of superconducting qubits and cavity QED:

- Further modeling of SET backaction and optimization of readout fidelity.
- Study schemes for single-photon generation and detection with cavities.
- Novel methods of generating entanglement, new pulse sequences for utilizing fixed qubit couplings.
- Feasibility studies and pulse sequencing for gate operation and simple (Deutsch-Josza) algorithms.

For the cavity QED implementation of the Cooper-pair box qubits, the first actual experiments are just now underway. Our first task will be to identify the qubit using the new readout mechanism, i.e. solely via its pulling of the cavity. Once the qubit can be found and characterized, there are several interesting experiments which can be performed. First, the basics of the qubit-cavity interaction must be verified, and spectroscopy of the qubit states performed to know its parameters and what pulse frequencies and sequences will be used to control it. Next, we will determine the decoherence (T2) and relaxation (T1) times of the qubit. By studying the enhancement of the T1 lifetime predicted in this setup, we hope to determine what the internal losses in the qubit are. This is a key measurement for CPB qubit designs, and perhaps for any future superconducting qubits.

Qubit experiments in superconducting cavities:

- Observe cavity pulling, tune box and verify basic physics of box-cavity interaction.
- Observe vacuum Rabi oscillations (resonant case).
- Develop fab process using SiN membranes for better control of capacitive coupling and to allow multiple qubit lines.
- Attempt single-shot QND measurement with cavity.
- Measure cavity-enhancement of T1 and intrinsic mechanism of T1 in box.
- Perform one-qubit operations, and Rabi and Ramsey experiments on qubit.
- Perform swap of qubit state with cavity mode.
- Measure two-qubit spectroscopy in cavity, attempt operation of a CNOT or Deutsch-Josza algorithm with two qubits.

VI. Publications Submitted or Appearing During This Period:

1) `Prospects for Strong-Coupling Cavity Quantum Electrodynamics with Electrical Circuits', S.M.Girvin,Ren-Shou Huang, Alexandre Blais, Andreas Wallraff, and R. J. Schoelkopf, cond-mat/0310670, and to appear in Proceedings of the LXXIX Les Houches Summer School on Quantum Entanglement and Information Processing.
2) `Quantum-Limited Measurement and Information in Mesoscopic Detectors', A.A. Clerk, S.M. Girvin, and A.D. Stone, *Phys. Rev. B* **67**, 165324 (2003).
3) 'Noise and Measurement Efficiency of a Partially Coherent Mesoscopic Detector', A.A. Clerk and A.D. Stone (submitted to Phys. Rev. B).
4) 'Qubits as Spectrometers of Quantum Noise,' R.J. Schoelkopf, A.A. Clerk, S.M. Girvin, K.W. Lehnert, and M.H. Devoret, "Quantum Noise in Mesoscopic Systems," Y.V. Nazarov (ed.), Kluwer Academic Publishers, Dordrecht, ISBN#1-4020-1239-X, April 2003.
5) 'Cavity Quantum Electrodynamics for Superconducting Electrical Circuits: An Architecture for Quantum Computation,' A. Blais, Ren-shou Huang, Andreas Wallraff, S.M. Girvin, and R.J. Schoelkopf, submitted to Phys. Rev A (2004).

6) ‘Measurement of the Excited-State Lifetime of a Microelectronic Circuit,’ K.W. Lehnert, K. Bladh, L.F. Spietz, D. Gunnarsson, D.I. Schuster, P. Delsing, and R.J. Schoelkopf, *Phys. Rev. Lett.* **90**, 027002 (2003).
7) ‘Quantum Charge Fluctuations and the Polarizability of the Single-Electron Box,’ K.W. Lehnert, B.A. Turek, K. Bladh, D. Gunnarsson, P. Delsing, and R.J. Schoelkopf, *Phys. Rev. Lett.* **91**, 106801 (2003).

Section C: **Results from the period 1/04-12/04**

A listing of milestones achieved in this period: (from August 2004 program review)

1) Observed SET backaction on qubit and effects on qubit relaxation
2) Demonstrated new type of dispersive qubit measurement with cavity QED
3) Tested superconducting charge qubits fabricated at Yale
4) Demonstrated long-lived (T2 > 200 ns) qubit with Q_ϕ ~ 10,000 at 1/f insensitive point
5) Coherently coupled superconducting qubit to a single microwave photon
6) Observed new source of qubit relaxation, mechanism still unknown
7) Fabricated two-qubit gates, testing can begin with new dilution fridge
8) Developed single photon production/detection schemes & quantum theory of RFMQT

During the period from the last program review (2003), we have therefore achieved all of our predicted milestones, as well as several of the long-term goals of our effort which we had not expected to reach so rapidly. Numerous publications (see below) were submitted and/or appeared in print, including a widely-publicized paper in Nature in which we reported the first coherent coupling of a solid-state qubit to a single photon.

I. RF Single-electron Transistor Readouts for Cooper-pair box Qubits

During the second half of the 2003 calendar year, we made several advances in our understanding of the SET as a measurement system for superconducting charge qubits. In particular, we observed that the backaction of the SET can have dramatic effects on both the polarization and relaxation time (T1) of the qubit during the measurement phase (**Milestone 1** above). We succeeded in measuring near-perfect 2e-periodic Cooper-pair staircases, indicating that the SET need not create quasiparticles in the qubit, and that the qubit can remain in the ground state, even in the presence of a continuous measurement. However, we also observed, under other conditions, that the SET can dramatically affect the steady-state population of the qubit, and can even create a measurement-induced population inversion in the qubit, as previously predicted by the theoretical part of our collaboration.

These results were extensively detailed in the 2003 calendar year interim progress report. During 2004, we have undertaken a detailed modeling effort in an attempt to determine the optimum parameters for an SSET readout of the CPB, based on the backaction model. A redesign of the SET-CPB samples was undertaken, and a process which allows a control of the electromagnetic environment for the qubit on chip was implemented at Yale. Samples for the next experiments along this approach have been fabricated. SETs with sufficiently large charging energies to realize the double Josephson quasiparticle feature (DJQP) used for the SET measurements have been made and tested at 250 mK. Several papers detailing the preliminary results on the SET backaction and its suitability as a quantum readout of CPB qubits have been submitted for publication (see papers 1 & 2 listed below)

II. Cavity QED with Superconducting Cooper-pair Box Qubits

In a joint experiment/theory collaboration we have conceived in the last two years a new architecture for quantum computation, adapting the idea of cavity QED (quantum electrodynamics) from atomic physics to superconducting electrical circuits, an idea that we refer to as cQED or 'circuit quantum electrodynamics' (see paper 3 below). During the past year we successfully implemented this new paradigm of 'quantum optics on a chip' and have two significant publications in *Nature* (Sept. 9, 2004, see paper 4 below) and *Phys. Rev. Lett.* (in press, see paper 5) which have confirmed the predictions in our proposal paper. This work was featured in the Search and Discovery section of the November issue of *Physics Today* and has attracted considerable interest within the atomic physics community and the superconducting qubit communities in the US and Europe. (see our website, www.eng.yale.edu/rslab for more info)

To achieve these cQED results, we employed devices fabricated in our nanofabrication facility at Yale, using a process for Nb transmission line resonators, patterned with optical lithography, combined with Cooper-pair box (CPB) qubits using submicron Al/AlOx/Al made with direct-write electron beam lithography. This process was developed during the previous year, and testing of the first devices began in January of 2004. An optical/SEM micrograph of such an integrated device, used for the work reported in Nature, is shown in Figure 1 below.

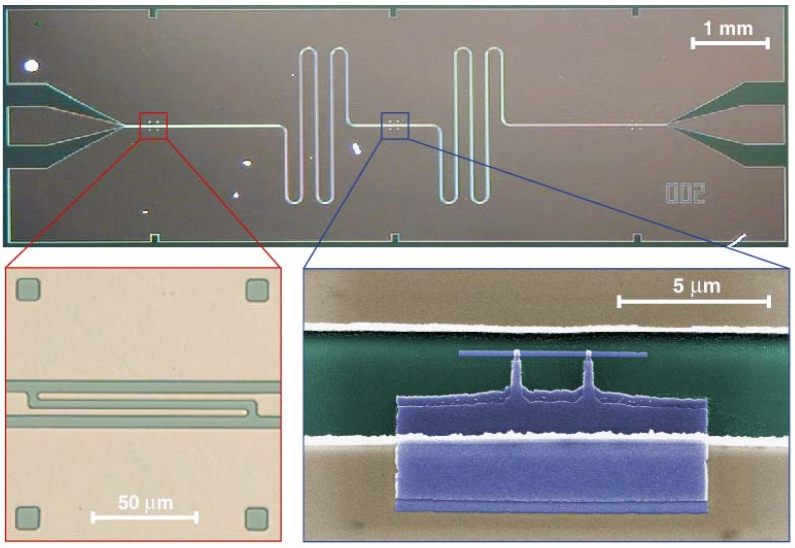

Figure 1: Micrograph of a superconducting integrated circuit for cavity QED experiments in control and measurement of a CPB qubit (adapted from paper 1). The Nb resonator (top), on a Si substrate, is patterned using optical lithography. An interdigitated capacitor (lower left) provides relatively strong coupling (Q ~ 10,000) of microwave signals in and out of the resonant cavity. A false color image (lower right) of the Al CPB qubit (blue), embedded at the center of the resonator. A loop allows control of the effective Josephson energy, and a dc voltage applied to the center conductor of the resonator provides the gate bias to control the Coulomb energy and allow operation at the charge degeneracy point.

We were then able to use the combined cavity-qubit system to perform a new type of dispersive measurement (**Milestone 2**) of the CPB qubit's ground and excited state properties. Microwave signals, with powers such that the cavity is typically occupied with 1 to 100 photons, were transmitted through the cavity. When the qubit is detuned in frequency from the cavity by several MHz to a GHz, these photons do not create any excitation or relaxation of the qubit. However, the qubit acts as an effective dielectric medium in the cavity, whose sign is positive or negative, depending on whether the qubit is in its ground or excited state. This creates a frequency shift of the cavity which can be an appreciable fraction of the cavity's linewidth, leading to an easily measurable phase shift of the transmitted signal. This measurement is unique so far amongst readouts for solid-state qubits in that it is a completely dissipation-free: it cannot excite the qubit, nor are any quasiparticles created or any photons absorbed within the chip. This technique appears to be a significant help in reducing the coupling to external degrees of freedom, and preserving the coherence and fidelity of the qubit itself.

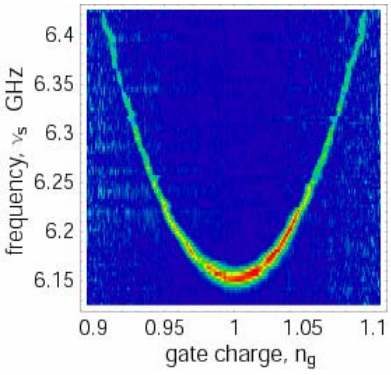

Figure 2: Spectroscopy of CPB qubit using cavity QED readout. The color scale shows the phase shift on a probe beam transmitted through the cavity at 6.0443 GHz, which is proportional to the excited state population. A continuous wave pump beam, whose frequency is varied from 6.1 to 6.5 GHz (vertical axis), excites the qubit when it matches the qubit transition frequency. The gate charge applied to the CPB is plotted on the horizontal axis, and the charge degeneracy point (gate charge of 1) is in the center of the plot, where the transition frequency is determined only by the Josephson energy, and the qubit is insensitive to 1/f charge noise.

We then performed spectroscopy on the qubit, by adding a second microwave tone which was tuned to the qubit transition frequency. Though this signal is attenuated by the cavity, it can nevertheless be made sufficiently strong to drive transitions in the qubit, and can further be pulse modulated to produce control of the qubit state. Measuring the change in the phase shift in response to this spectroscopic signal, we performed spectroscopy on the qubit as a function of frequency, shown in Figure 2. One notices that this spectrum is extremely clean, displaying none of the spurious junction resonances seen in larger junctions by Martinis and coworkers. Also, the transition can be followed smoothly down to the charge degeneracy point (center of Fig. 2), where the energy level separation of the qubit is an extremum, and the qubit is first-order insensitive to 1/f noise in the offset or gate charge. This point is found to give greatly enhanced coherence times for the CPB qubit. It can also be seen that the spectroscopic lines are sharp – one can use these linewidths to obtain a ***worst-case estimate*** of the coherence time (**Milestone 4**) indicating that T2 is greater than 200 ns. These times have since been confirmed in Ramsey and Rabi experiments, showing coherence times up to 800 ns, corresponding to a hase quality factor $Q_\phi = \omega_{01} T2 \sim 25{,}000$, allowing in principle thousands of one-bit operations. This spectroscopy constitutes the first coherence time measurements on a qubit fabricated at Yale (**Milestone 3**). Similarly encouraging results have been obtained by M. Devoret and co-workers, with devices measured at Saclay in France.

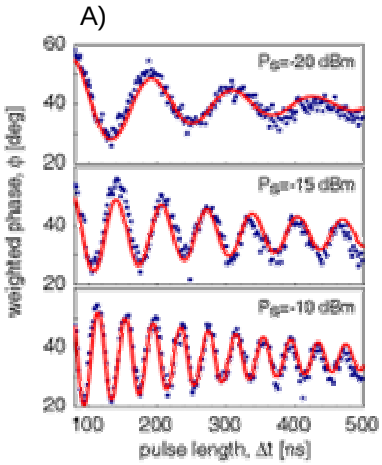

Figure 3: Rabi oscillations of a CPB qubit in a cavity. A) The phase shift, proportional to the excited state population, is plotted as a function of the length of the microwave pulse applied to the qubit. Increasing the power in the pulse (successive panels), increases the Rabi frequency. B) The response in time domain to a single Pi pulse, averaged over approximately 10,000 repetitions, with a weak continuous measurement. The phase shift returns to its ground state value as the excited-state population decays in the T1 time of approximately 0.7 microseconds. Red line shows predicted phase shift for a perfect Pi pulse, indicating that the fidelity of the oscillations is greater than 50%, and consistent with full contrast (100%).

To perform coherent control of the qubit in the cavity, we applied pulses of microwaves tuned to the qubit frequency. Since these are detuned from the cavity by 10 MHz to 1 GHz, their rise and fall times are simply limited to the inverse of this detuning, or about 1 to 100 nanoseconds. The response of the qubit to a pulse of microwaves, showing Rabi oscillations, is shown in Figure 3A. The Rabi frequency is observed to depend on the RF amplitude (not power), doubling for every 6 dB in microwave power, as expected. The fastest Rabi flops performed to date are about 30 ns, but this is still limited only by the microwave power applied and the pulse modulation electronics. An advantage of the cQED dispersive measurement, which is a quantum non-demolition (QND) measurement, is that it can be used either as a strong pulsed measurement, or as a weak continuous measurement, and it is particularly simple to understand. A time trace, showing the response of a weak continuous measurement (averaged over about 10,000 shots) with a Pi pulse is applied at ~ 4 microseconds, is shown in Figure 3B. The phase shift of the cavity should be equal and opposite between ground and excited state, so we know the degree of polarization change induced in the qubit. The decay of the phase back to the ground state value (-60 degrees), is a direct measurement of the energy relaxation, or T1, time of the qubit, here about 0.7 microseconds. The measurement rise time is simply determined by the photon lifetime in the cavity (i.e. the inverse of the cavity decay rate, $\kappa^{-1} = Q/\omega_{cavity}$). The observed phase shift indicates at least 50% fidelity for the Pi pulse, but because of the low-pass filtering effect of the cavity lifetime, the data are also consistent with fidelity of order 100%. More recent measurements have improved the T1 time of the qubit, and the separation between these two timescales, so that the fidelity can be more accurately determined.

The relaxation time of 0.7 microseconds observed in Fig 3, is similar to the best results observed with superconducting charge qubits, namely the earlier Yale/Schoelkopf measurements (Lehnert et al., 2003) using an RF-SET, and the results of Devoret and co-workers at Saclay. Because the detuning of the qubit from the cavity is predicted to reduce the spontaneous emission rate of qubit and enhance the T1 time, however, it these cQED measurements indicate (**Milestone 6**) that there is an intrinsic, or local, source of dissipation that can limit the ultimate coherence times of these devices. The cQED architecture is a ideal way to study these mechanisms, and improving the relaxation times, is a topic for future work in this project. We have already fabricated cQED samples on different dielectric substrates in order to determine if this affects the relaxation.

Taking advantage of the tunability of the CPB qubit, we were also able to investigate the resonant regime of cavity QED, where the qubit's transition matches the cavity frequency, and observe coherent superpositions between our qubit and a single microwave photon (**Milestone 5**). This required control of the CPB qubit Hamiltonian to a few parts in 10,000, so that the transition frequency at the degeneracy point is equal to the 6.044 GHz cavity frequency. In this case, the dipole coupling between the qubit and the cavity induces vacuum Rabi oscillations, at a rate 2g=12 MHz. This was observed spectroscopically by measuring the splitting of the cavity transmission into a doublet of peaks, separated by the splitting 2g, as shown in Figure 4 (adapted from Wallraff et al., Nature, paper 4). The two peaks correspond to excitation of the symmetric and anti-symmetric superpositions ($|\pm\rangle = |\downarrow, n=1\rangle \pm |\uparrow, n=0\rangle$) of the qubit in its ground (excited) state $|\downarrow\rangle (|\uparrow\rangle)$ and one (zero) photons in the cavity $|n=1\rangle (|n=0\rangle)$, and are expected to be entangled states, though that has not yet been demonstrated by correlation measurements. The width of these peaks is due to the combination of qubit and photon decay, since the states have a mixed qubit/photon character. The separation of the peaks by more than 10 linewidths indicates that our sample is clearly in the strong coupling limit of cavity QED, and that coherent exchange between qubit and cavity states is taking place. This also indicates that future experiments can use the cavity as an intermediary "bus" to transport entanglement across a chip to a different qubit, not necessarily a nearest-neighbor. Performing swap operations of the qubit and cavity, and between two qubits, is planned for the next year's work.

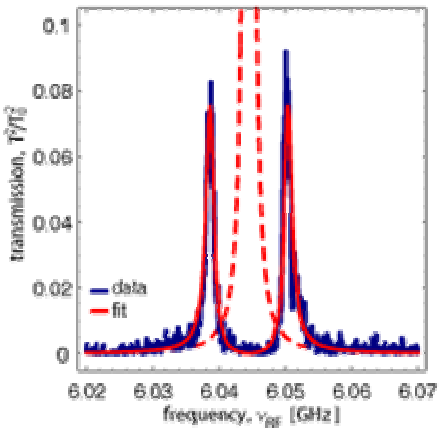

Figure 4: Vacuum Rabi splitting of the cavity mode due to coupling with a CPB qubit. The transmission through the cavity is plotted as a function of frequency, for a measurement probe beam of approximately -170 dBm, corresponding to 0.1 photons of excitation in the cavity. Dashed line shows the transmission through the bare resonator, when the qubit is strongly detuned, which has a Lorentzian shape with a Q of 10,000. Blue lines show the measured data when the qubit is tuned to resonance with the cavity frequency at the qubit charge degeneracy point. Solid red lines show a model prediction, based on the vacuum Rabi coupling strength 2g = 12 MHz extracted from measurements in the dispersive regime, the measured cavity quality factor, and a single fit parameter for the qubit transition linewidth, T2 = 200 ns. The clear separation of the peaks indicates that we are in the strong coupling limit of cavity QED, for the first time in a solid-state system. (Adapted from Wallraff et al., Nature 2004, paper 4)

Finally, we have fabricated cQED samples with multiple CPB qubits. Our second dilution refrigerator, already almost 1.5 years overdue, was further delayed and has only been commissioned in November 2004. We anticipate that testing of these multi-qubit devices will begin in 2005, when the new fridge has been instrumented and tested for microwave experiments. We have also observed the AC Stark shift of our qubits due to the measurement probe beam, and the dephasing that this induces in the qubit, which is described in the theory section below, and has been submitted to Physical Review Letters (Schuster et al., 2004, see paper 5 below). This means that we have a good understanding of the measurement–induced backaction of the cQED readout, when it is used as a weak continuous measurement. We have also performed pulsed measurement experiments with the cQED system, this work is in progress and will be described later. However, turning off the measurement is observed to enhance the coherence time of the CPB qubit in the cavity, leading to a record coherence time of 0.8 microseconds, as measured in a Ramsey experiment. The AC Stark shift can also be used in future as a mechanism for producing a single qubit phase gate, or to shift two qubits into resonance, as also described in the theory section below.

III.Theory

Cavity QED

We have continued our close cooperation of theory in Co-PI Steve Girvin's group and the experimental groups of Schoelkopf and Devoret. Particularly in the area of the cQED work with superconducting qubits, there has been an alternation of theoretical ideas and experimental results, leading for example to the theory of AC Stark shift and measurement dephasing, described below and in paper 5. In an effort to further develop theoretical ideas linking quantum optics to superconducting electrical circuits, we have recently hired with ARO support a new theory postdoctoral fellow, Jay Gambetta, who was trained in quantum optics and quantum measurement theory.

AC Stark Shift and Measurement Induced Dephasing

In a cavity QED system, the presence of the qubit in the cavity affects the cavity resonance frequency. Because the electrical polarizability of the qubit depends on the quantum state of the qubit, the cavity frequency is pulled one way if the qubit is in its ground state and in the opposite direction if the qubit is in its excited state. The result is a term in the Hamiltonian

$$H_1 = \left(\hbar\omega_R + \frac{g^2}{\Delta}\sigma^z \right)\hat{n} + \frac{\varepsilon_{01}}{2}\sigma^z \qquad (1)$$

where ω_R is the (bare) cavity frequency, ε_{01} is the bare qubit energy level difference, g is the coupling strength between the qubit and the cavity, Δ is the detuning of the qubit frequency from the cavity frequency, σ^z is the state of the qubit and $\hat{n}$ is the number of photons in the cavity. The cavity frequency is thus $\omega_R \pm \frac{g^2}{\hbar\Delta}$ depending on the state of the qubit. This frequency shift leads to a substantial shift in the phase of the transmitted microwaves which can be easily measured. Because the qubit is detuned from the cavity frequency, the measurement photons do not cause transitions in the qubit and the measurement is quantum non-demolition.

Because the qubit pulls the cavity frequency, it follows that the cavity pulls the qubit frequency. This effect, known in quantum optics as the 'light shift' or ac Stark effect can be easily understood by rearranging the terms in the Hamiltonian to read

$$H_1 = \hbar\omega_R \hat{n} + \frac{1}{2}\left(\varepsilon_{01} + 2\frac{g^2}{\Delta}\hat{n}\right)\sigma^z$$

This shows us that the qubit transition frequency is shifted by an amount $2\frac{g^2}{\Delta}$ for each measurement photon that is added to the cavity. The coupling is so strong in our system that this shift can easily exceed 0.6 MHz per photon which is comparable to the qubit transition linewidth. Fig. 5a shows data for the ac Stark shift from paper 5.

When the cavity is driven by a coherent microwave source, so that it has a definite phase (needed to determine the phase shift caused by the qubit), the cavity photon number is uncertain and has fluctuations on the scale of $\sqrt{\langle \hat{n} \rangle}$. These lead to an uncertainty in the qubit transition frequency and hence a broadening of the spectroscopic linewidth. We have developed a theory of this effect which is in excellent quantitative agreement with the experimental data, as can be seen in Fig. 5b.

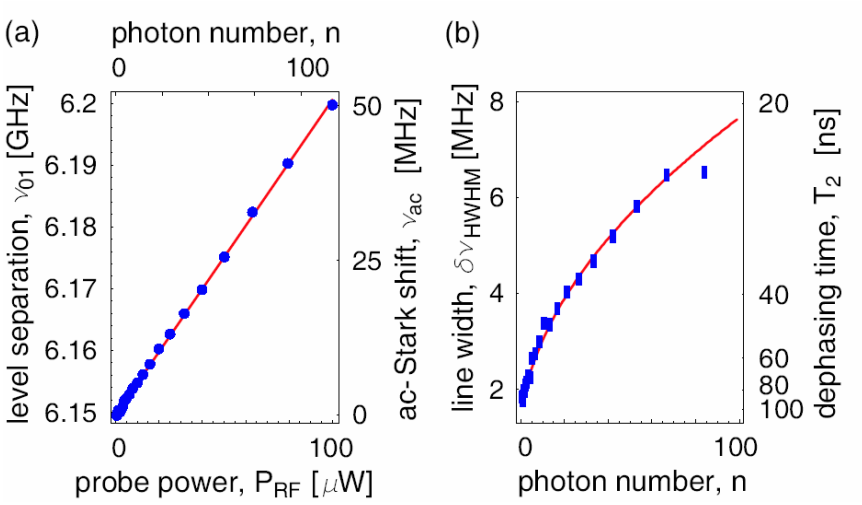

Figure 5: Measurement and theory of AC Stark shift and measurement induced dephasing for cQED readout of CPB qubit. (Adapted from Schuster et al., 2004, paper 5) a) The shift in the qubit frequency, as a function of the measurement probe beam power, which controllably populates the cavity with 1-100 photons, showing the linear Stark shift of ~ 0.6 MHz per photon. b) The linewidth of the qubit transition, also plotted as a function of the cavity photon number. The increase in linewidth is due to the shot noise on the number of photons in the cavity, and also causes a crossover in the lineshape from Lorentzian at low powers to Gaussian at high powers, in good agreement with theory.

The resulting random time-dependent fluctuations in the qubit splitting cause the relative phase in a superposition of ground and excited states to diffuse. This measurement induced dephasing by the quantum fluctuations in the light shift is precisely the measurement back action required by quantum mechanics. When information is gained about the state of the qubit, information about the phase of the qubit must be lost. We have shown that the cQED amplifier can in principle reach the quantum limit in which there is no extra dephasing beyond the minimum required by the Heisenberg uncertainty principle.

Single Qubit Gate Fidelity and Readout Fidelity

Photons applied to the cavity at the cavity frequency undergo a phase shift which depends on the state of the qubit. The entanglement of these photons with the qubit is the basis of our QND readout. Remarkably photons applied to the same input line but at the qubit frequency do not become entangled with the qubit, but rather cause coherent Rabi oscillations. (This is connected with the fact that most of the photons in the pulse at this non-resonant frequency are reflected from the cavity with a phase shift which is independent of the qubit state.) Thus by using frequency multiplexing, a single line serves as both measurement and control. Application of the pi pulse to the qubit flips its state and, according to Eq. 1 causes a sudden change in the resonant frequency of the cavity. We have performed detailed theoretical modeling and numerical simulations to compute the response of the cavity measurement photons to this transient. Because the quantum dynamics of our measurement process is so well understood, we should be able to do very accurate quantitative modeling of the measurement signal that results from a pi pulse as shown in Fig. 3b. Postdoc Alexandre Blais (supported on a different grant) had originally been doing rather expensive stochastic wave function simulations of this process, but recently has developed an extension of the cavity Bloch equations which yield very accurate results with very little numerical effort. Postdoc Jay Gambetta has developed a different approximation scheme and the two are in good agreement. We are currently in the process of using this to determine our state preparation (pi pulse) fidelity and our readout fidelity.

Theory of Single Qubit Phase Gate and RF Coupling for Two Qubit Gates

Charge based qubits are linearly sensitive to charge offset noise unless they are operated at a special symmetry point, the charge degeneracy ‘sweet spot’. Restriction to the sweet spot means that we cannot change the qubit

transition frequency by application of gate bias. This is a significant limitation because temporary controlled excursions in gate frequency are crucial for creation of single qubit phase gates, moving qubits into resonance with the cavity to entangle the qubit with a photon or moving two qubits into resonance with each other to perform entanglement gate operations. During the past year we have developed a theoretical protocol (**Milestone 8**) which overcomes all these difficulties without introducing extra dephasing. Rather than using a dc gate voltage to move away from the sweet spot, we apply a high frequency ac dither voltage. This shifts the qubit effective frequency upward but causes phase errors from low frequency 1/f noise to average out to zero. (Only the small charge offset noise at the high dither frequency contributes to dephasing.) During the coming year we plan to perform extensive numerical simulations to predict phase gate fidelity and the fidelity of two qubit coupling operations based on this protocol and design experiments to test these ideas.

The ac dither technique is complementary to a new RF controlled gate coupling scheme developed by Devoret in which each qubit is driven at its own transition frequency with a Rabi frequency which causes the Rabi sidebands of the two qubit dressed states to come into resonance with each other. We may eventually try to combine these techniques into a highly flexible RF gate coupling scheme.

Theory of Josephson Bifurcation Amplifier and Cavity Bifurcation Amplifier

During the past year, ARO supported postdoc Krishnendu Sengupta (now at U. Toronto), completed initial calculations on an approximate quantum theory of the Devoret's Josephson Bifurcation Amplifier (JBA). A rough draft of a paper has been prepared and we will be submitting it for publication early next year (**Milestone 8**). Devoret, Schoelkopf and Girvin have collaborated on the development of a new idea which combines the best features of the JBA amplifier and the cQED readout. The idea is to use a high Q CPW resonantor as in the present cQED set up, but load the cavity with a non-linear Josephson junction in such a way that the dispersive cQED read out scheme acquires the latching feature of the JBA. Theoretical work will be pursued in the coming year to develop a detailed engineering analysis of this proposed system.

Tagged Single Photon Production

One offshoot of the cQED architecture we have developed is a theoretical proposal for a device for producing single microwave photons. Yale undergraduate Clifford Cheung recently completed his senior thesis under the supervision of Professor Girvin analyzing a design consisting of a pair of coplanar wave guide resonators mutually coupled through a Cooper pair box qubit. The essential idea is that by choosing the frequency of the first resonator to be equal to the sum of the frequency of the second resonator plus the qubit transition frequency, one can cause creation of a single photon in the second resonator to be associated with a spin flip of the qubit. This spin flip will change the pull on the first cavity and be readily detectable by monitoring its output. This will automatically 'tag' the photon production event. Cliff Cheung, who is now a graduate student at Harvard, has written a paper on the subject which is in the final stages of editing.

Publications submitted or appearing during this period:

1) 'Backaction Effects of an SSET Measuring a Qubit: Spectroscopy and Ground State Measurements,' B. Turek, H. Majer, A. Clerk, S.M. Girvin, A. Wallraff, K. Bladh, D. Gunnarson, T. Duty, P. Delsing, and R.J. Schoelkopf, submitted to IEEE Trans. on Appl. Superconductivity (2004).

2) 'Measuring the Backaction of a Single-Electron Transistor on the Single-Electron Box,' B.A. Turek, K. W. Lehnert, K. Bladh, D. Gunnarsson, P. Delsing, and R.J. Schoelkopf, submitted to Phys. Rev. Lett. (2004).

3) 'Cavity quantum electrodynamics for superconducting electrical circuits: an architecture for quantum computation', Alexandre Blais, Ren-Shou Huang, Andreas Wallraff, S. M. Girvin, and R. J. Schoelkopf, *Phys. Rev. A* **69**, 062320 (2004).

4) 'Strong Coupling of a Single Photon to a Superconducting Qubit Using Circuit Quantum Electrodynamics', A. Wallraff, D. Schuster, A. Blais, L. Frunzio, R.-S. Huang, J. Majer, S. Kumar, S. M. Girvin, R. J. Schoelkopf, *Nature* **431**, 162-167 (Sept. 9, 2004).

5) 'AC-Stark Shift and Dephasing of a Superconducting Qubit Strongly Coupled to a Cavity Field', D. I. Schuster, A. Wallraff, A. Blais, L. Frunzio, R.-S. Huang, J. Majer, S. M. Girvin, R. J. Schoelkopf, *Phys. Rev. Lett.* (in press) [cond-mat/0408367].

6) 'Fabrication and Characterization of Superconducting Circuit QED Devices for Quantum Computation,' L. Frunzio, A. Wallraff, D. Schuster, J. Majer, and R.J. Schoelkopf, submitted to IEEE Trans. on Applied Superconductivity, 2004.

Section C: Results from the period 1/05-8/31/05

A summary of achievements in this period:

I. Single-electron Transistor Readouts of Cooper-Pair Box Qubits

During the Aug 2004-Aug 2005 period, we have continued with our efforts to measure the backaction of the RF-SET on the Cooper-pair box qubit, which is essentially to determining whether this is a viable method for performing single-shot readout of qubits. The present goal was to fabricate samples with a well-controlled electromagnetic environment, in order to study the effects of SET backaction on qubit lifetime. These devices turned out to be more challenging to fabricate than we had anticipated, but we have now been successful and final measurements are underway. A chip showing the Cooper-pair box qubit and RF-SET readout are shown in Figure 1, along with a measurement of the current-voltage characteristic of a qubit configured as a SQUID. The measurement of the IV curve displays resonances corresponding to points where the environment of the qubit changes abruptly, i.e. we are able to use the Josephson effect as a sort of "network analyzer" which probes the microwave engineering of the wiring. This confirms that we have succeeded in our goal of controlling the electromagnetic environment, at least up to ~ 30 GHz which is much higher than the transition frequency (about 6-8 GHz) planned for the qubits and recently measured. Characterization of a box has shown the desired energy level splittings in the qubit have been achieved, and that a working SET with proper characteristics to have a DJQP resonance used for readout is obtained. This work will conclude with a final set of measurements testing the backaction theory of the SET developed earlier in this project by our theory collaborators. A paper detailing preliminary measurements of the qubit ground state and showing full tunability of the qubit Hamiltonian have appeared this year in IEEE Transactions on Applied Superconductivity (Paper #1). An earlier paper quantitatively testing the backaction of the SET in the normal state also appeared in Physical Review B (Turek et al.; Paper #2).

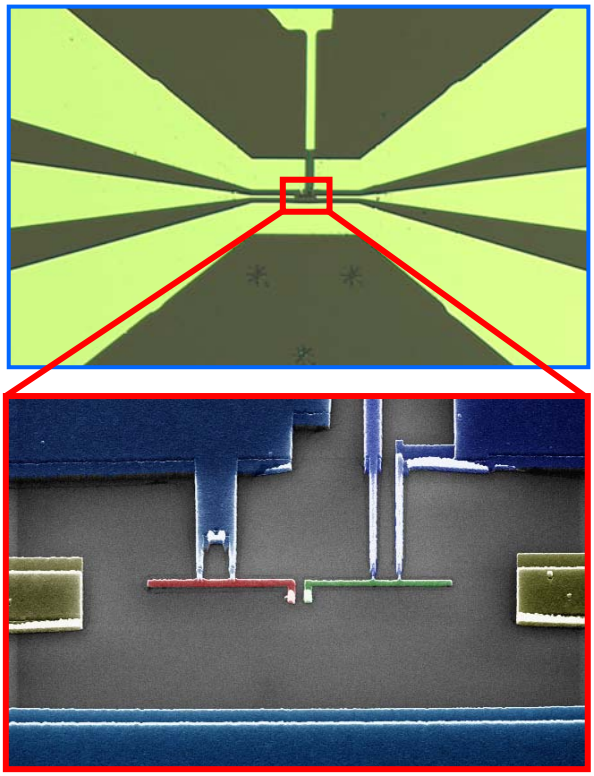

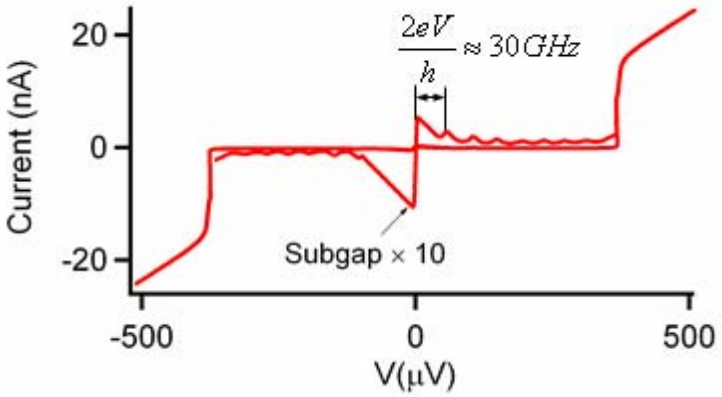

Figure 1: Left: Optical (top) and zoomed SEM micrographs of a completed CPB qubit –RF-SET readout chip with controlled electromagnetic environment. Right: Current-voltage characteristic of a "qubit" wired up as a SQUID for DC transport measurements, showing that, except for resonances seen by the qubit at relatively high frequencies of 30 and 50 GHz, the qubit should see a well controlled electromagnetic environment with 50 Ohm impedance. This sample is in use to test SET backaction limits on readout fidelity.

II. Cavity QED Experiments with Cooper-Pair Box Qubits

Achievements during this period:

1) Developed model and quantitative predictions for fidelity of continuous measurements.
2) Performed single-shot cavity QED readout with 40% fidelity.

3) Measured T2 > 500 ns and T1 > 7 μs for CPB qubit w/ cQED dispersive readout.
4) Observed Rabi oscillations with > 95% visibility.
5) Performed first experiments on two qubits in a cavity.

We have continued our very successful experiments on a new architecture for quantum computation, adapting the idea of cavity QED (quantum electrodynamics) from atomic physics to superconducting electrical circuits, an idea that we refer to as cQED or 'circuit quantum electrodynamics'. During the past year we have published our work on the AC Stark shift and the dephasing due to continuous measurements using the cavity as a quantum non-demolition probe of the state of the qubit (Schuster et al. PRL '05, Paper #3, below), and then concentrated on pulsed measurements and quantum control of the qubit. We were able to measure the fidelity of single-shot readouts for cQED measurement, perform Rabi and Ramsey experiments to obtain record values for coherence and excited state lifetimes of a superconducting qubit, perform the first high-fidelity control of the quantum state of a superconducting qubit as indicated by a visibility of Rabi flops which approaches unity (Wallraff et. al. PRL '05; Paper #4 below), and begin experiments on two remote qubits coupled via a single cavity.

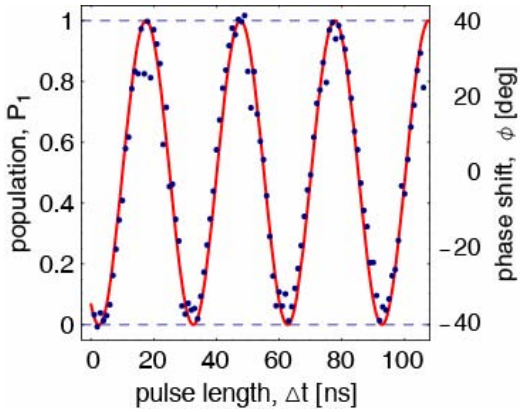

Figure 2: Rabi oscillations of a Cooper-pair box qubit in cQED architecture, using the cavity as a QND measurement of the qubit. The right axis shows the phase shift of the transmission thru the cavity, which can be directly converted into a qubit population in the excited state. Blue points are the data, and the red line is a sinusoidal oscillation (at the Rabi frequency) with unit amplitude. The data are consistent with a visibility of 95% +- 5%, marking the first demonstration of truly high-fidelity Note that there is no noticeable decay in the oscillation amplitude, consistent with the coherence time T2 = 500 nanoseconds measured in a Ramsey expt. (not shown).

The results of some of the time domain measurements on the qubit are shown in Figure 2. The advantage of the cQED measurement technique is that the interaction of qubit and measurement can be understood and tested in quantitative detail. In particular, our work on steady-state spectroscopy and backaction published in Paper 3 verify that we understand precisely how to convert the measured experimental quantity, the transmission phase shift through the cavity, directly into an excited state population of the qubit. This allows us to convert our measured Rabi oscillations into a quantitative qubit population, and to extract a precise measurement, for the first time, of the visibility of Rabi oscillations for a superconducting qubit. As seen in Figure 2, the Rabi oscillations are consistent with unit visibility, indicating that our qubit is not interacting strongly with spurious degrees of freedom in its environment, perhaps because it is protected by the cavity and the dispersive measurement which does not heat or excite quasiparticles or other modes. Using a pulsed measurement and two Pi/2 pulses on the qubit (i.e. a three-pulse experiment) we performed Ramsey experiments to measure the true coherence time of the qubit to be about 0.5 microseconds, essentially equaling the previous record achieved by Devoret and co-workers at Saclay. We also measured a relaxation (T1) time of the qubit of approximately 7 microseconds, which is also a record high value for such qubits, and again encouraging for future work.

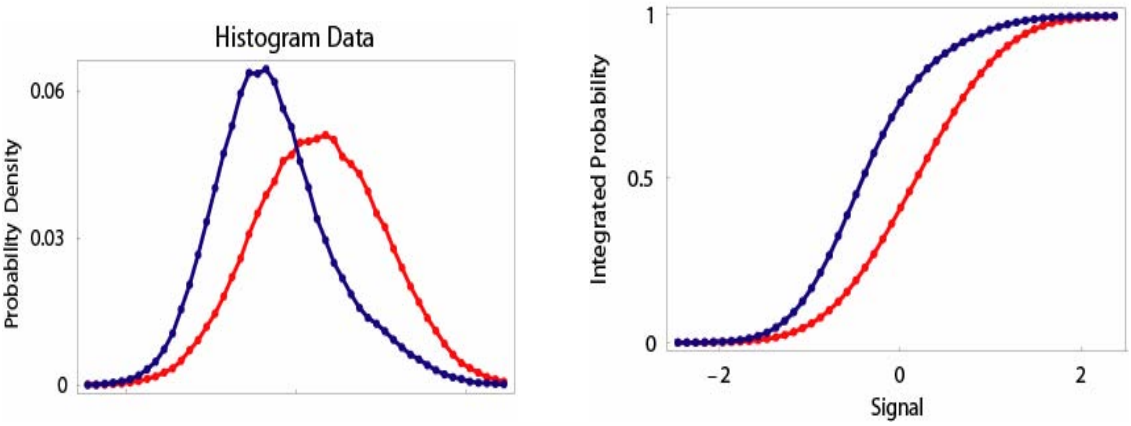

Figure 3: Fidelity of single-shot QND measurements of a qubit with the cavity. Left panel shows histogram of approximately 10^7 individual shots (about 5 minutes of data total) for measuring the qubit in the ground state (blue) or following a single Pi pulse to create the excited state (red). The probability (vertical axis) of obtaining a particular measurement value is plotted versus the total signal (horizontal axis, in arbitrary units). The right panel shows the

integrated probabilities for ground (blue) and excited state (red) as a function of the same signal. Around a threshold value of zero signal, the curves are separated by 30-40%, which indicates the fidelity for performing a single-shot measurement.

We have also studied the fidelity of single-shot measurements with the cQED dispersive measurement, as shown in Figure 3. This works well, and the measurement and data collection are rapid, making studies of qubit or readout behavior very efficient. The signal to noise is limited by a combination of the finite measurement time for a given shot (i.e. the T1 relaxation time of the qubit), the strength of the measurement probe signal (here about 10^{-16} Watts, corresponding to populating the cavity with about 10 photons at the 5 GHz cavity frequency), and the amplifier noise. The measured fidelity is about 30-40%, consistent with the expectations for these settings, but it should be possible to significantly improve this number either with increased qubit lifetime, lower amplifier noise, or stronger measurement signals. We have also undertaken a theoretical study of the measurement process and the readout fidelity (Braff et. al., in preparation; Paper 5), which explains both the observed histograms and the fidelity. This work was done by a Yale undergraduate, William Braff, as part of his senior thesis, and will be submitted to Phys. Rev. A.

Building on these results with the cavity QED architecture for the Cooper-pair box, we have begun experiments with two qubits coupled and readout via a single microwave cavity. A micrograph of such a sample is shown in Figure 4 below. Relatively simple measurements (see left grayscale plot) show the presence of the two qubits. By employing two gates and unequal SQUID loop areas for the qubits, the individual qubit properties can be found, and their energies can be controlled independently. This data also indicates that each qubit can be strongly coupled to the cavity mode. Using various RF methods (described in the theory section below), the coupling between the qubits via resonant or virtual exchange of a cavity photon could then be used to experiment with two-qubit gates.

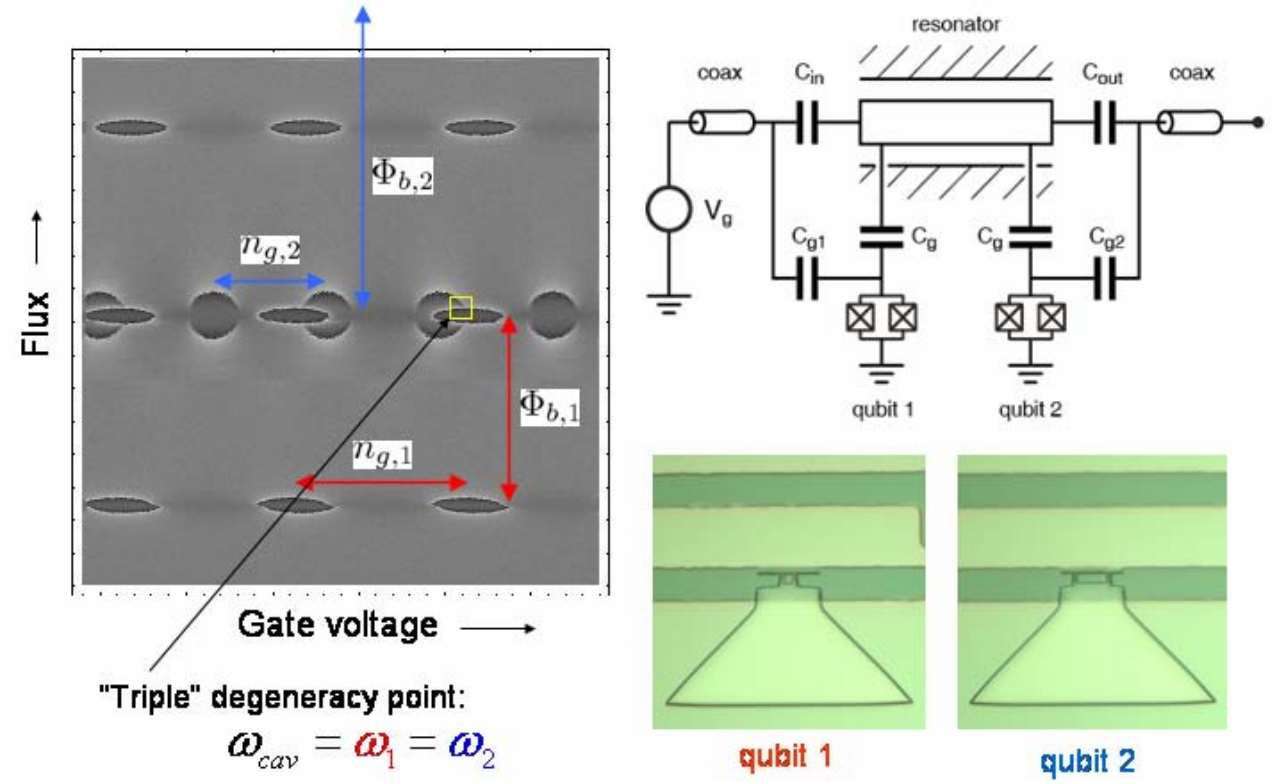

Figure 4: First experiments with two coupled qubits in a cavity. The schematic of the experiment is shown in the upper right. Two Cooper-pair box qubits are placed within a superconducting transmission-line resonant cavity, near the opposite ends, approximately 2 centimeters apart from one another. Gate voltages applied to the input and output ports of the resonator, respectively, control the gate charge of the two qubits independently. The qubits are fabricated with SQUID loops of different sizes (see optical micrographs in lower right), so that applying a global magnetic field tunes the Josephson energies, and thus the transition frequencies, of the two qubits with different periodicities. Measurements on this system are shown on the left. The gray scale indicates the phase shift through the cavity, which exhibits a sharp jump (boundaries of the dark ellipses) when one or the other of the qubits is tuned into resonance with the cavity. The figure shows tuning of the qubits with magnetic field (vertical axis) and one of the two gate voltages (horizontal). This type of figure allows both the determination of the Josephson and charging energies of the two qubits, and a determination of the setting which match qubit frequencies. An arrow indicates a point where both qubits may be tuned through resonance with the cavity (a triple degerneracy), where the qubits should be coupled to one another and entanglement and two-qubit

gates should be possible. Further experiments are in progress, including time-domain control of the individual qubits in this system.

III. Theory of Superconducting Qubits

During the past year the theory group of S. M. Girvin has continued to interact closely with the Schoelkopf and Devoret groups. We made significant advances in our understanding of the measurement process in the cavity QED archictecture, and of the on- and off-resonant ac stark shift for qubits in driven cavities. With visiting Professor Kyungsun Moon we developed a new proposal to use a qubit in a cavity to generate squeezed states of microwaves and our postdoc Alexandre Blais worked with Devoret's group to develop an analytically tractable approach for the FLICFORQ gate protocol. Blais and fellow postdoc Jay Gambetta also made considerable progress in developing and analyzing other two-qubit gates. Gambetta has also undertaken a new study of squeezing and parametric amplification that can be achieved using the Josephson Bifurcation Amplifier (JBA) and Cavity Bifurcation Amplifier developed by Devoret's group.

Quantum Control and Measurement of a Qubit in cQED
The cavity QED system can be used to detect the state of (one or more) qubits via the phase shift of probe microwaves transmitted through the cavity. We have developed a detailed understanding of the physics of this process and through numerical modeling have been able to accurately fit transient response of the microwave phase shift when the qubit is suddenly flipped by a strong pi pulse. This fit requires no adjustable parameters other than the qubit lifetime T_1. From this quantitatively accurate fit we were able to demonstrate (see Paper #4) that the visibility (fidelity) of our Rabi flopping pi pulses were consistent with 100% (95 +- 5%). This is the first time that this has been done for superconducting qubits and is possible because of the simple and well-controlled nature of the cavity QED readout and the fact that it leaves no energy behind to form quasiparticles.

Paper 3 is a joint experimental/theoretical study of the spectroscopy of a CPB qubit in a cavity being driven by the readout microwave beam. The RF field from the beam induces a strong (0.5 MHz/photon) 'light shift' (ac Stark shift) of the qubit transition frequency. In addition, because this beam measures the state of the qubit, there is a measurement induced dephasing of the qubit transition. This is also the first time that this has been observed and accurate agreement with theory not only confirms our understanding of the physics but is a useful tool for calibrating the number of photons in the cavity. In separate unpublished work, we have shown that driving the cavity off resonance produces a light shift of the qubit, but no broadening of the transition (because no measurement is being made). This effect makes for a high fidelity RF controlled phase gate for the qubits.

A long follow up to our initial *Phys. Rev. Lett.* on the ac Stark shift is in preparation
(Paper 6). Among other things we are developing an understanding of the inelastic Raman processes that occur in the cavity when the qubit is suddenly flipped.

During the past year, senior undergraduate Will Braff worked together with Schoelkopf and Girvin to develop optimal protocols for the cQED readout system using a linear filter on the phase shift measurement record. Postdoc Jay Gambetta is bringing his expertise in quantum trajectory theory to this problem to understand the full non-linear dynamics of the time evolution of the system conditioned on the measurement record. This will allows us to model how coherent Rabi flopping crosses over to incoherent quantum jumps as the measurement strength is increased and allow us to understand how to optimize the single-shot fidelity of the cQED measurement system. A paper (Paper 5) is in preparation.

Squeezing and Parametric Down Conversion
Paper 7 represents a continuation of our quest to fully extend quantum optics to the microwave regime. Together with visiting Professor Kyungsun Moon, we predicted that the cavity QED architecture is well-suited for studying parametric down conversion. A single photon at the first harmonic of the resonator can be converted to two photons at the fundamental frequency via three-wave mixing induced by a single 'atom' (CPB) in the cavity. Non-linear optics faces two difficulties in the visible regime. First most optical media have only extremely weak non-linearities. This weak non-linearity means that large crystals are required which produces the second problem: wave vector matching (momentum conservation) which is very difficult because of the nature of the material dispersion. Here we use a cavity only one wavelength long and the non-linear medium is a single point-like 'atom' so momentum conservation is not an issue. Furthermore the coupling strengths available in our system are so large that non-linearities can be enormous. Parametric down conversion will be strongly driven with relatively small numbers of photons in the cavity. For even modest driving the parametric down conversion should be so efficient that it becomes coherent leading to production of a squeezed vacuum state exiting the cavity at its fundamental frequency.

Additional work presently underway by postdoc Jay Gambetta in collaboration with the Devoret group is examining related non-linear physics in the form of four wave mixing in the JBA and CBA amplifiers. We now realize that this can be

exploited to produce both squeezing and parametric amplificiation. Such effects might lead to higher readout fidelity for the JBA detector and also lead to new types of ultra-low noise microwave amplifiers that could be used to improve the cQED readout as well.

Two-Qubit Gates

During the past year Devoret's group developed a new universal gate protocol, FLICFORQ. Postdoc Alexandre Blais developed a very simple and efficient analytical scheme which greatly simplified the analysis of this RF controlled gate. [see Paper 8]. Postdocs Blais and Gambetta have also made considerable progress on a general analysis of many different types of two qubit gates in the cQED architecture. One of these, inspired by a visit from Peter Zoller in the spring of 2005, is a phase gate analogous to those used in ion traps. A long paper analyzing the speed and fidelity of different possible gates is in preparation.

Publications during this period:

1) "Backaction Effects of an SSET Measuring a Qubit: Spectroscopy and Ground State Measurements," B. Turek, H. Majer, A. Clerk, S.M. Girvin, A. Wallraff, K. Bladh, D. Gunnarson, T. Duty, P. Delsing, and R.J. Schoelkopf, IEEE Trans. on Appl. Superconductivity **15**, 880 (2005).
2) "Single-Electron Transistor Backaction on the Single-Electron Box," B.A. Turek, K. W. Lehnert, D. Gunnarsson, K. Bladh, P. Delsing, and R.J. Schoelkopf, Phys. Rev. B. **71**, 193304 (2005).
3) "AC Stark Shift and Dephasing in a Superconducting Qubit Strongly Coupled to a Cavity Field," D.I. Schuster, A. Wallraff, Alexandre Blais, L. Frunzio, Ren-Shou Huang, J. Majer, S.M. Girvin, and R.J. Schoelkopf, Phys. Rev. Lett. **94**, 123602 (2005).
4) "Approaching Unit Visibility for Control of a Superconducting Qubit with Dispersive Readout," A. Wallraff, D.I. Schuster, A. Blais, L. Frunzio, J. Majer, M.H. Devoret, S.M. Girvin, and R.J. Schoelkopf, Phys. Rev. Lett. **95**, 060501 (2005).
5) "Theoretical Limits on Fidelity of Continuous Qubit Measurements," W. Braff, S.M. Girvin, and R.J. Schoelkopf, in preparation.
6) "Qubit-Photon Interactions in a Cavity: Measurement Dephasing and Number Splitting," Jay Gambetta, Alexandre Blais, D. I. Schuster, A. Wallraff, L. Frunzio, J. Majer, S. M. Girvin, and R. J. Schoelkopf, to appear in *Phys. Rev. A* (2006); and cond-mat/0602322.
7) "Theory of Microwave Parametric Down Conversion and Squeezing Using Circuit QED," K. Moon and S.M. Girvin, *Phys. Rev. Lett.* **95,** 140504 (2005).
8) "Two-qubit gates for the circuit QED architectures," Alexandre Blais, Jay Gambetta, R. J. Schoelkopf and S. M. Girvin, *Phys. Rev. A* (in preparation).

Summary of publications supported by this grant:
(copies are attached at end)

Publications in peer-reviewed journals:

1) "Measurement of the Excited-state Lifetime of a Microelectronic Circuit"K. W. Lehnert, K. Bladh, L.F. Spietz, D. Gunnarsson, D.I. Schuster, P. Delsing, and R.J. Schoelkopf, Phys. Rev. Lett. **90**, 027002 (2003).
2) "Quantum Fluctuations of Charge and the Polarizability of the Single-Electron Box," K. W. Lehnert, B.A. Turek, K. Bladh, D. Gunnarsson, P. Delsing, and R.J. Schoelkopf, Phys. Rev. Lett **91**, 106801 (2003).
3) "Single-Electron Transistor Backaction on the Single-Electron Box," B.A. Turek, K. W. Lehnert, D. Gunnarsson, K. Bladh, P. Delsing, and R.J. Schoelkopf,
Phys. Rev. B. **71**, 193304 (2005).
4) "Cavity Quantum Electrodynamics for Superconducting Electrical Circuits: an Architecture for Quantum Computation," Alexandre Blais, Ren-Shou Huang, Andreas Wallraff, S.M. Girvin, and R.J. Schoelkopf, Phys. Rev. A **69**, 062320 (2004).
5) "Coherent Coupling of a Single Photon to a Superconducting Qubit Using Circuit Quantum Electrodynamics," A. Wallraff, D. Schuster, Alexandre Blais, L. Frunzio, Ren-Shou Huang, J. Majer, S. Kumar, S.M. Girvin, and R.J. Schoelkopf, Nature **431**, 162 (2004).
6) "AC Stark Shift and Dephasing in a Superconducting Qubit Strongly Coupled to a Cavity Field," D.I. Schuster, A. Wallraff, Alexandre Blais, L. Frunzio, Ren-Shou Huang, J. Majer, S.M. Girvin, and R.J. Schoelkopf, Phys. Rev. Lett. **94**, 123602 (2005).
7) "Approaching Unit Visibility for Control of a Superconducting Qubit with Dispersive Readout," A. Wallraff, D.I. Schuster, A. Blais, L. Frunzio, J. Majer, M.H. Devoret, S.M. Girvin, and R.J. Schoelkopf, Phys. Rev. Lett. **95**, 060501 (2005).
8) "Backaction Effects of an SSET Measuring a Qubit: Spectroscopy and Ground State Measurements," B. Turek, H. Majer, A. Clerk, S.M. Girvin, A. Wallraff, K. Bladh, D. Gunnarson, T. Duty, P. Delsing, and R.J. Schoelkopf, IEEE Trans. on Appl. Superconductivity **15**, 880 (2005).
9) "Fabrication and Characterization of Superconducting Circuit QED Devices for Quantum Computation," L. Frunzio, A. Wallraff, D. Schuster, J. Majer, and R.J. Schoelkopf, IEEE Trans. on Applied Superconductivity **15**, 860 (2005).
10) "Theory of Microwave Parametric Down Conversion and Squeezing Using Circuit QED," K. Moon and S.M. Girvin, *Phys. Rev. Lett.* **95,** 140504 (2005).
11) "Resonant Cooper-Pair Tunneling: Quantum Noise and Measurement Characteristics," A.A. Clerk, S.M. Girvin, A.K. Nguyen, and A.D. Stone, Phys. Rev. Letters **89**, 176804 (2002).
12) "Quantum-Limited Measurement and Information in Mesoscopic Detectors," A.A. Clerk, S.M. Girvin, and A.D. Stone, Phys. Rev **B 67**, 165324 (2003).

Non-peer reviewed:

1) "Qubits as Spectrometers of Quantum Noise," R.J. Schoelkopf, A.A. Clerk, S.M. Girvin, K.W. Lehnert, and M.H. Devoret in "Quantum Noise in Mesoscopic Systems," Y.V. Nazarov (ed.), Kluwer Academic Publishers, Dordrecht, ISBN#1-4020-1239-X, April 2003.
2) "Prospects for Cavity QED with Superconducting Circuits: an Architecture for Solid-State Quantum Computing," S.M. Girvin, A. Blais, R. Huang, A. Wallraff, and R.J. Schoelkopf, Proceedings of the LXXIX Les Houches Summer School on Quantum Entanglement and Information Processing.
3) "Noise and Measurement Backaction in Superconducting Circuits: Qubits as Spectrometers of Quantum Noise," R.J. Schoelkopf, A.A. Clerk, K.W. Lehnert, and M.H. Devoret, Proceedings of the SPIE:Noise and Information in Nanoelectronics, Sensors, and Standards 5115, pp. 356-376 (2003).

Submitted:

1) "Qubit-Photon Interactions in a Cavity: Measurement Dephasing and Number Splitting,"
Jay Gambetta, Alexandre Blais, D. I. Schuster, A. Wallraff, L. Frunzio, J. Majer, S. M. Girvin, and R. J. Schoelkopf, submitted to *Phys. Rev. A* (2006).

In preparation:

1) "Theoretical Limits on Fidelity of Continuous Qubit Measurements," W. Braff, S.M. Girvin, and R.J. Schoelkopf, in preparation.

MASTER COPY: PLEASE KEEP THIS "MEMORANDUM OF TRANSMITTAL" BLANK FOR REPRODUCTION PURPOSES. WHEN REPORTS ARE GENERATED UNDER THE ARO SPONSORSHIP, FORWARD A COMPLETED COPY OF THIS FORM WITH EACH REPORT SHIPMENT TO THE ARO. THIS WILL ASSURE PROPER IDENTIFICATION. NOT TO BE USED FOR INTERIM PROGRESS REPORTS; SEE PAGE 2 FOR INTERIM PROGRESS REPORT INSTRUCTIONS.

MEMORANDUM OF TRANSMITTAL

U.S. Army Research Office
ATTN: AMSRL-RO-BI (TR)
P.O. Box 12211
Research Triangle Park, NC 27709-2211

☐ Reprint (Orig + 2 copies)
☐ Technical Report (Orig + 2 copies)
☐ Manuscript (1 copy)
☒ Final Progress Report (Orig + 2 copies)
☐ Related Materials, Abstracts, Theses (1 copy)

CONTRACT/GRANT NUMBER: DAAD19-02-1-0045

REPORT TITLE: Quantum Computing with Single Cooper-Pair Electronics

is forwarded for your information.

SUBMITTED FOR PUBLICATION TO (applicable only if report is manuscript):

Sincerely,

Robert J. Schoelkopf
Steven M. Girvin

Measurement of the Excited-State Lifetime of a Microelectronic Circuit

K. W. Lehnert,[1,*] K. Bladh,[2] L. F. Spietz,[1] D. Gunnarsson,[2] D. I. Schuster,[1] P. Delsing,[2] and R. J. Schoelkopf[1]

[1]*Department of Applied Physics and Physics, Yale University, New Haven, Connecticut 06511*

[2]*Microtechnology Center at Chalmers MC2, Department of Microelectronics and Nanoscience, Chalmers University of Technology and Göteborg University, SE-412 96, Göteborg, Sweden*

(Received 20 June 2002; published 17 January 2003)

We demonstrate that a continuously measured microelectronic circuit, the Cooper-pair box measured by a radio-frequency single-electron transistor, approximates a quantum two-level system. We extract the Hamiltonian of the circuit through resonant spectroscopy and measure the excited-state lifetime. The lifetime is more than 10^5 times longer than the inverse transition frequency of the two-level system, even though the measurement is active. This lifetime is also comparable to an estimate of the known upper limit, set by spontaneous emission, for this circuit.

DOI: 10.1103/PhysRevLett.90.027002 PACS numbers: 74.40.+k, 85.25.Hv, 85.35.Gv

Recently, microelectronic circuits have been coaxed into behaving as quantum two-level systems (TLS) [1–5]. The TLS behavior of circuits is revolutionary because it demonstrates the quantum behavior of a macroscopic degree of freedom composed of many microscopic degrees of freedom. Quantum coherence was believed to be fragile in electrical circuits both because it required the suppression of the dynamics of the microscopic elements in a condensed matter system and because the quantum oscillations of an electric or magnetic degree of freedom would efficiently radiate energy into the electromagnetic environment. Discussed in terms of the Bloch equations [6], familiar from nuclear magnetic resonance, a TLS in a coherent superposition of states has characteristic times T_2 to become an incoherent mixture and T_1 to relax back to its ground state.

In this Letter, we observe that a microelectronic circuit, the Cooper-pair box, may be measured continuously while still behaving approximately as a two-level system. The box is integrated with a radio-frequency single-electron transistor (RF-SET) measurement apparatus, which we operate as weak, continuous measurement of the box's state. Under these conditions we are able to determine the parameters that appear in the box's Hamiltonian, make a worst-case estimate T_2^* of the decoherence time T_2, and measure the excited-state lifetime T_1 of the two-level system. We determine the parameters in the Hamiltonian through a kind of spectroscopy where we observe a resonant change in the box's state when its transition frequency matches a multiple of the frequency of an oscillatory excitation. From the width in frequency of these resonances we can find T_2^* [7]. We stimulate the box into its excited state and measure T_1 directly by exploiting the large measurement bandwidth of the RF-SET to resolve in time the circuit's decay to its ground state. Most remarkably, the value of T_1 that we find while *continuously measuring* the state of the box is comparable to estimates of the excited-state lifetime limited by the quantum fluctuations of the electromagnetic environment. This demonstrates that the Cooper-pair box, when embedded in a circuit for control and measurement, remains well decoupled from other sources of dissipation. Based on the observed noise in the readout and the lifetime, we conclude that RF-SET is a promising qubit readout because a "single-shot" measurement, where the box is observed in its excited state before it has relaxed into its ground state, is possible.

The Cooper-pair box is a microelectronic circuit composed of an isolated superconducting island, attached to a superconducting lead through a tunnel junction. An additional lead, called the gate lead, lies near the island and changes the electrostatic potential of the island with the application of a voltage V_g to the gate lead through the gate capacitance C_g [Fig. 1(a)]. The island's total capacitance C_Σ is small enough to suppress fluctuations of charge on the island. Because the island and the lead are superconducting, all of the electrons form Cooper pairs and participate in the macroscopic quantum ground state of the island. The only degree of freedom is the number of pairs n on the island. Because of the large charging energy $E_C = e^2/2C_\Sigma$, we need consider only two states, a state $|0\rangle$ with no excess Cooper pairs ($n = 0$) and a state $|1\rangle$ with one excess Cooper pair ($n = 1$), as reckoned from electrical neutrality. The Hamiltonian of the Cooper-pair box circuit is

$$\mathbf{H} = -2E_c(1 - 2n_g)\boldsymbol{\sigma}_z - \frac{E_J}{2}\boldsymbol{\sigma}_x, \tag{1}$$

where $\boldsymbol{\sigma}_z$ and $\boldsymbol{\sigma}_x$ are the Pauli spin matrices and n_g is the total polarization charge applied to the gate electrode, $n_g = C_g V_g/2e - n_{\text{off}}$, in units of a Cooper-pair's charge [10,11]. The offset charge n_{off} accounts for the uncontrolled potential arising from charges nearby the box island. The Josephson energy, $E_J^{\max} = h\Delta/8e^2R_\Sigma$, is the effective tunneling matrix element for Cooper pairs across a junction with resistance R_Σ in a superconductor with BCS gap Δ. The junction is, in fact, a composite of two parallel junctions connected to form a loop with

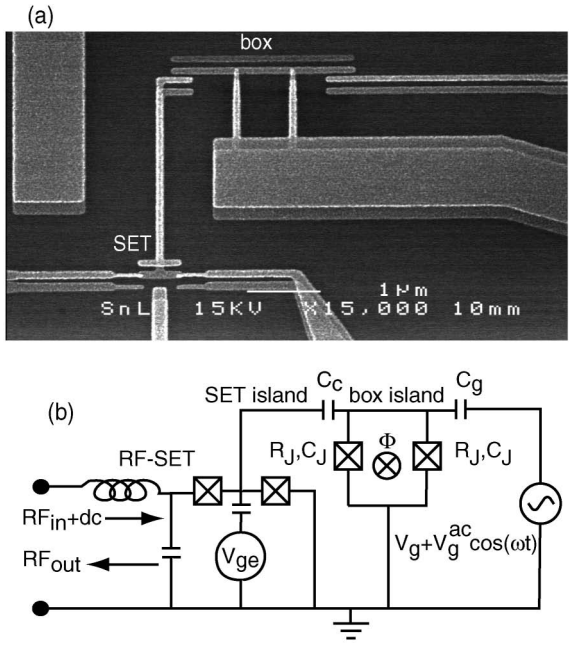

FIG. 1. (a) An SEM micrograph of the Cooper-pair box and SET electrometer. The device is made from an evaporated aluminum film (light gray regions) on an insulating SiO_2 substrate (dark gray regions) by the technique of double angle evaporation [8], which gives the double image. The aluminum has BCS gap $\Delta/k_B = 2.4\,\mathrm{K}$. (b) A circuit diagram of the box and RF-SET electrometer. The SET gate voltage V_{ge}, the 500 MHz oscillatory bias, and the dc bias ($\mathrm{RF_{in}}+\mathrm{dc}$) determine the electrometer's operating point. The charge on the box is inferred from variation in the amount of applied RF power that is reflected ($\mathrm{RF_{out}}$) from the SET electrometer, which is a sensitive function of SET's conductance [9]. The tunnel junctions (crosses in boxes) are characterized by a junction resistance R_J and capacitance C_J, which enter the box's Hamiltonian through $C_\Sigma = C_C + 2C_J + C_g$ and $R_\Sigma = R_J/2$ (see text).

1 $(\mu\mathrm{m})^2$ area (Fig. 1). The effective Josephson energy E_J of the pair of junctions is then tunable with magnetic flux Φ through this loop, as $E_J = E_J^{\max}\cos(\pi\Phi/\Phi_0)$, where Φ_0 is the quantum of flux ($h/2e$). Equation (1) is the Hamiltonian of a quasispin 1/2 particle in a fictitious magnetic field that can be decomposed into two orthogonal fields. The z component of this fictitious field which accounts for the box's electrostatic energy, $E_{el}(V_g) = 2E_c(1 - 2n_g)$, is tuned with V_g and the x component, which accounts for the Josephson energy $E_J(\Phi) = E_J^{\max}\cos(\pi\Phi/\Phi_0)$, is tuned with Φ [11]. The box is an artificial two-level system and both of the terms in its Hamiltonian are tunable *in situ*.

In the box, states of definite numbers of Cooper pairs on the island are states of definite charge. In order to measure the charge of the Cooper-pair box, we fabricate the box next to a RF-SET [8,9], an exquisitely sensitive electrometer, so that the addition of a Cooper pair to the box's island causes a small fraction ($C_C/C_\Sigma = 3.7\%$) of the Cooper pair's charge to appear as polarization charge on the capacitor C_C that couples the box and the RF-SET (Fig. 1). The electrometer used here had a sensitivity of $4 \times 10^{-5}\ e/\sqrt{\mathrm{Hz}}$ and 10 MHz of measurement bandwidth. Because the RF-SET measures charge, its action can be described as projecting the state of the box into a state of definite Cooper-pair number. In the formal terms of Eq. (1), it measures $Q_{\mathrm{box}} = (1 + \langle\boldsymbol{\sigma}_z\rangle)e$ where Q_{box} is further averaged over the measurement time.

We perform spectroscopy by applying a continuous microwave stimulus to the gate of the Cooper-pair box and sweeping n_g to tune the parameters of the TLS and find the resonance condition (Fig. 2). A measurement of Q_{box} vs n_g shows that the box does not remain in its ground state over a range $0.3 < n_g < 0.7$. This behavior is caused by backaction [12,13] generated by currents flowing through RF-SET [14]. We proceed by studying the box in the range of n_g where it does remain in its ground state.

When a 35 GHz microwave signal is applied to the gate, we observe clear evidence that the box is a coherent two-level system. Resonant peaks appear [Fig. 2(b)] in Q_{box} that are sharp and symmetrically spaced about $n_g = 0.5$. The two features, a peak for $n_g < 0.5$ and a dip for

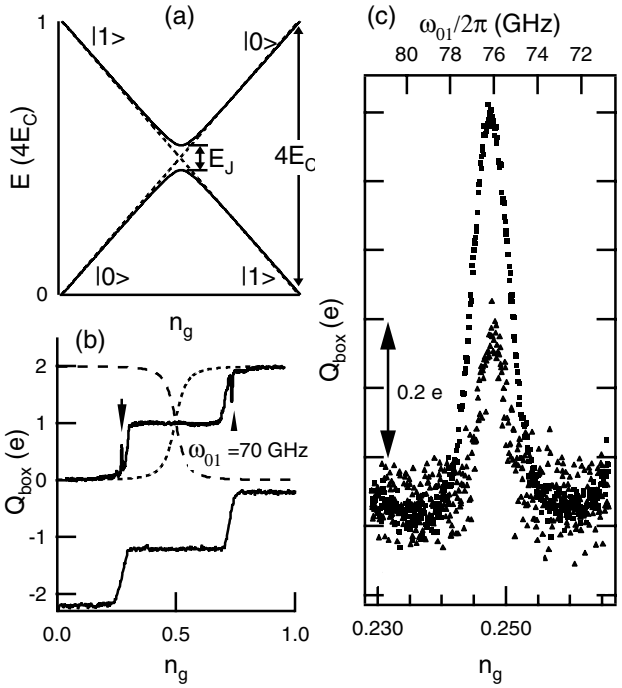

FIG. 2. (a) The ground and excited state energies versus n_g for Eq. (1), with $4E_C = 12E_J$ (solid line) and $E_J = 0$ (dotted lines). Energy eigenstates asymptotically approach charge states ($|1\rangle$ and $|0\rangle$) far from $n_g = 0.5$. (b) Q_{box} vs n_g, calculated for the ground state (dotted line), excited state (dashed line), and measured (solid line) with 35 GHz microwaves applied to the box gate. The arrows indicate resonant peaks. Also shown is Q_{box} measured with no microwaves applied (solid line), with the y axis shifted down by 2.2 e. (c) Two resonant peaks in Q_{box} vs n_g on the bottom axis and vs ω_{01} on the top axis, with $\omega = 38$ GHz and where the larger value of V_g^{ac} (squares) is twice the smaller value (triangles).

$n_g > 0.5$, both correspond to the change in $Q_{\rm box}$ when the box spends some time in the excited state. Because $Q_{\rm box}$ is an average of thousands of repeated measurements, the peak height indicates the probability of finding the box in its excited state [Fig. 2(c)].

The resonant peaks permit a spectroscopic determination of E_C and $E_J^{\rm max}$. By tuning n_g and Φ while exciting the box with a fixed microwave frequency, we find good agreement between the locations of resonant peaks and the difference between ground-state and excited-state energies $E_{01}(n_g, \Phi) = \hbar\omega_{01}$ expected from Eq. (1). An independent measurement of E_C [15] demonstrates that these peaks occur when the irradiating frequency ω is half ω_{01}, indicating that these peaks correspond to a two-photon transition [16]. At lower frequencies and for single-photon transitions, the peaks would appear at an n_g for which the box does not stay in the ground state while being measured and are therefore not visible. We find a single value for E_C and for $E_J^{\rm max}$ that account for the location of the resonant peaks at applied frequencies between 32 and 38 GHz giving resonant peaks for ω_{01} between 64 and 76 GHz [Fig. 3(a)]. We are able to extract the parameters of the Hamiltonian, $4E_C/h = 149.1 \pm 0.4$ GHz and $E_J^{\rm max}/h = 13.0 \pm 0.2$ GHz, which imply $C_\Sigma = 518$ aF and $R_\Sigma = 12.4\,\mathrm{k}\Omega$. Through spectroscopy we have measured the parameters of an electrical circuit that could not have been measured with transport [Fig. 1(b)]. Because these measurements were made at a temperature $T < 40$ mK, they are in the limit $k_B T \ll E_J < E_C$.

Consistent with the behavior of a TLS, the peaks disappear for $\Phi = \Phi_0/2$ when E_J approaches zero. This

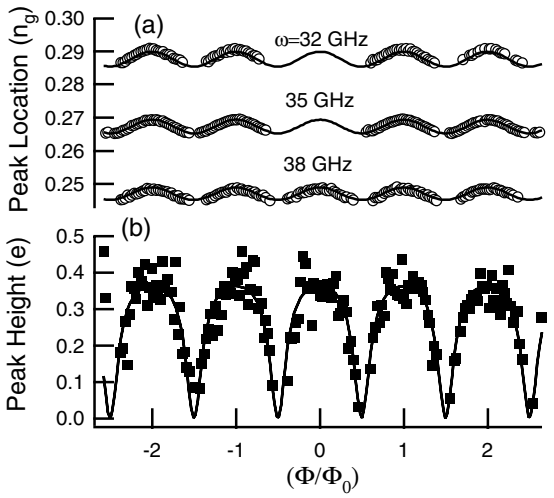

FIG. 3. Resonant spectroscopy of the box versus the two control parameters of the Hamiltonian, V_g and Φ. (a) The locations of resonant peaks (circles) in n_g and Φ, for $\omega = 32$, 35, and 38 GHz and fits (lines), using Eq. (1) for $\omega_{01} = 2\omega = 64$, 70, and 76 GHz to find a single value of E_C and of $E_J^{\rm max}$. The systematic uncertainty in n_g is represented by the size of the open circle symbols. (b) The height, in electrons, of a 76 GHz resonant peak as a function of Φ (squares) and a guide to the eye (line).

demonstrates that E_J provides the coupling between the charge states [Fig. 3(b)]. An oscillating gate voltage with amplitude V_g^{ac} adds a term to the Hamiltonian in Eq. (1), which is $(C_g V_g^{ac}/2e)\cos(\omega t)\boldsymbol{\sigma}_z$ and is collinear with the ground state of the quasispin described by Eq. (1) when $E_J = 0$. The microwave excitation therefore applies no torque which could excite the quasispin from its ground state [6].

The width of the resonant peaks we observe provides a worst-case estimate of the decoherence time of the two-level system. We express the width of a resonance δn_g as a width in frequency $\delta\omega_{01} = (1/\hbar)(dE_{01}/dn_g)\delta n_g$. In the absence of inhomogenous broadening, the half width at half maximum inferred for zero power is the decoherence rate $1/T_2$ of a TLS [6]. From $\delta\omega_{01}$ measured at the lowest value of V_g^{ac} applied, we estimate a time T_2^* of about 325 ps [7]. The resonant peaks have a Gaussian shape, and $n_{\rm off}$ drifts an amount comparable to δn_g during the 2 min required to complete a measurement. Both observations imply that the width of the peaks expresses not the intrinsic loss of phase coherence due to coupling the TLS to the environment, but rather the degree to which an ensemble of measurements are not identical, due to the well-known $1/f$ noise of single-electron devices [17]. This T_2^* is a worst-case estimate because it is extracted while the system is measured continuously by the RF-SET and because it represents an ensemble average of many single measurements that require about 2 min to complete. Nevertheless, T_2^* is about 150 times longer than $1/\omega_{01}$ [Fig. 2(c)] and is similar to the times found in [18], another Cooper-pair box implementation, as well as [5] a SQUID circuit. Reference [4] demonstrates that this inhomogenous broadening may be overcome by operating the Cooper box at $n_g = 0.5$ where E_{01} is to first order insensitive to fluctuations in $n_{\rm off}$.

In order to measure the excited-state lifetime T_1, we excite the box and then measure the time required to relax back to the ground state. A 38 GHz signal is continuously applied to the gate and the box gate is tuned to $n_g = 0.248$ and $E_J = E_J^{\rm max}$ so that the microwaves resonantly couple the ground and excited states through a two-photon transition. Abruptly, n_g is then shifted to $n_g = 0.171$ in 30 ns, slowly enough to be adiabatic but much faster than T_1. The microwave excitation then no longer resonantly couples the ground and excited states, and the probability of being in the excited state decays in a time T_1. By averaging many of the transient responses to this stimulus, we find $T_1 = 1.3\ \mu$s (Fig. 4). A similar T_1 was found in [4] for a Cooper-pair box with much smaller E_C and operated at $n_g = 0.5$. The lifetime is a quantity which is insensitive to slow drifts in $n_{\rm off}$ and demonstrates that the TLS, which oscillates $T_1 \times \omega_{01} = 6 \times 10^5$ times before relaxing into its ground state, is well decoupled from all other sources of dissipation.

We can compare this long lifetime with the spontaneous emission rate expected from the quantum fluctuations of a generic electromagnetic environment. Calculating the

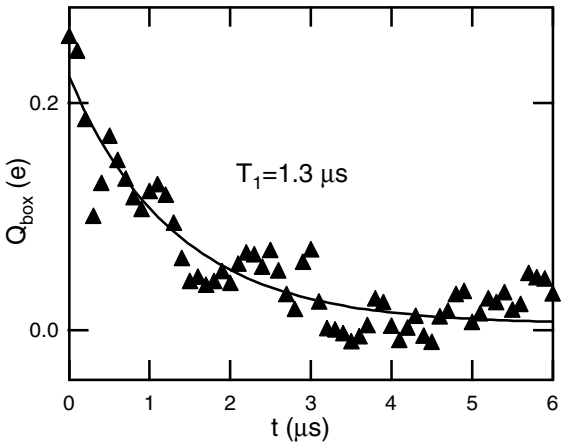

FIG. 4. A determination of the excited-state lifetime of the box. Q_{box} vs time t (triangles), relative to $t = 0$, when n_g is shifted from = 0.248 to 0.171 in 30 ns, with 38 GHz microwaves applied. The shift in n_g brings the box out of resonance with the microwave excitation. An exponential fit to the data implies $T_1 = 1.3$ μs (line).

rate using Fermi's golden rule gives

$$\frac{1}{T_1} = \left(\frac{C_g^T}{C_\Sigma}\right)^2 \left(\frac{e}{\hbar}\right)^2 \sin^2(\theta) S_V(\nu_{01} = \omega_{01}/2\pi), \qquad (2)$$

where $S_V(\nu) = 2h\nu(\text{Re}(Z_0))$ is the voltage spectral density of the quantum fluctuations of an environment with an impedance Z_0 at frequency ν and $\sin\theta = E_J/\hbar\omega_{01}$ [11]. The quantity C_g^T is the total capacitance of the box to nearby metal traces, including intentional coupling to the gate lead and other unintended capacitive coupling (Fig. 1). We calculate T_1 for a 50 Ω environment to be between 0.25 and 1 μs, extracting $C_g^T = 45 \pm 15$ aF from an electrostatic simulation of the chip layout [11,12]. We do not claim to have demonstrated that the lifetime is limited by spontaneous emission; however, if there are additional relaxation processes, either due to the electrometer or fluctuations of some microscopic degree of freedom in the box, their influence is at most comparable to that of spontaneous emission into a typical ($Z_0 \approx$ 50 Ω) electromagnetic environment.

In these experiments, we demonstrate that a Cooper-pair box is a coherent two-level system with a long excited-state lifetime. With spectroscopy, we determine the box's Hamiltonian and its spontaneous emission rate into a typical environment. We measure an excited-state lifetime of a box that is remarkable for two reasons. First, it shows that a quantum-coherent microelectronic circuit can have a T_1 that approaches the limit set by spontaneous emission of a photon into the electromagnetic environment. Second, it is observed by resolving, on submicrosecond time scales, the decay of the excited-state charge signal while the two-level system is continuously measured. Given the observed electrometer sensitivity of $4 \times 10^{-5}\ e/\sqrt{\text{Hz}}$, the excited-state lifetime is long enough that a single measurement can discriminate between the box in its excited state and the box in its ground state. In a coherent superposition of states the box oscillates 6×10^5 times before decaying to the ground state, demonstrating that the circuit is a promising qubit implementation if, as in [4], the sources of inhomogeneous broadening can be overcome.

This work was supported by the National Security Agency (NSA), Advanced Research and Development Activity (ARDA) under Army Research Office (ARO) Contract No. DAAD19-99-1-0346, the David and Lucile Packard Foundation, and the Wallenberg Foundation. The authors thank M. Devoret, S. Girvin, and A. Clerk for useful discussions.

*Email address: konrad.lehnert@yale.edu
Group Web site: www.eng.yale.edu/rslab

[1] Y. Nakamura, Y. A. Pashkin, and J. S. Tsai, Nature (London) **398**, 786 (1999).
[2] Y. Nakamura, C. D. Chen, and J. S. Tsai, Phys. Rev. Lett. **79**, 2328 (1997).
[3] J. R. Friedman *et al.*, Nature (London) **406**, 43 (2000).
[4] D. Vion *et al.*, Science **296**, 886 (2002).
[5] C. H. van der Wal *et al.*, Science **290**, 773 (2000).
[6] A. Abragam, *The Principles of Nuclear Magnetism: The International Series of Monographs on Physics 32* (Oxford University Press, Oxford, 1983).
[7] We refer to the inverse linewidth as T_2^* because our measurements share some features of liquid-state NMR in a spatially inhomogenous magnetic field [6].
[8] T. A. Fulton and G. J. Dolan, Phys. Rev. Lett. **59**, 109 (1987).
[9] R. J. Schoelkopf *et al.*, Science **280**, 1238 (1998).
[10] V. Bouchiat *et al.*, Phys. Scr. **T76**, 165 (1998).
[11] Y. Makhlin, G. Schön, and A. Shnirman, Rev. Mod. Phys. **73**, 357 (2001).
[12] M. H. Devoret and R. J. Schoelkopf, Nature (London) **406**, 1039 (2000).
[13] A. A. Clerk, S. M. Girvin, A. K. Nguyen, and A. D. Stone, Phys. Rev. Lett. **89**, 176804 (2002).
[14] The 1 electron step around $n_g = 0.5$ arises from nonequilibrium quasiparticle excitations on the box island, generated by currents flowing in the RF-SET electrometer. The RF-SET's bias is selected as a compromise between minimizing the width of this feature and maximizing the RF-SET's sensitivity. See Ref. [10] and references therein.
[15] We determine E_c by measuring the thermal broadening of the transitions between charge states when the box is driven into its normal state. This method is used in Ref. [10].
[16] C. Cohen-Tannoudji, B. Diu, and F. Laloë, *Quantum Mechanics* (John Wiley and Sons, New York, 1977), Vol. 2, Chap. B13, pp. 1336–1338.
[17] N. M. Zimmerman, J. L. Cobb, and A. F. Clark, Phys. Rev. B **56**, 7675 (1997).
[18] Y. Nakamura, Y. A. Pashkin, T. Yamamoto, and J. S. Tsai, Phys. Rev. Lett. **88**, 047901 (2002).

Quantum Charge Fluctuations and the Polarizability of the Single-Electron Box

K.W. Lehnert,[1,*] B. A. Turek,[1] K. Bladh,[2] L. F. Spietz,[1] D. Gunnarsson,[2] P. Delsing,[2] and R. J. Schoelkopf[1,†]

[1]*Department of Applied Physics and Physics, Yale University, New Haven, Connecticut 06511 USA*

[2]*Microtechnology Center at Chalmers MC2, Department of Microelectronics and Nanoscience, Chalmers University of Technology and Göteborg University, SE-412 96, Göteborg, Sweden*

(Received 20 February 2003; published 5 September 2003)

We measure the average charge on the island of a single-electron box, with an accuracy of two thousandths of an electron. Thermal fluctuations alone cannot account for the dependence of the average charge on temperature, on external potential, or on the quasiparticle density of states in the metal from which the box is formed. In contrast, we find excellent agreement between these measurements and a theory that treats the quantum fluctuations of charge perturbatively.

DOI: 10.1103/PhysRevLett.91.106801 PACS numbers: 73.23.Hk, 73.63.Kv, 85.35.Gv

A general feature of quantum many-body phenomena is the screening of a single degree of freedom by a bath of virtual excitations. The Lamb shift and the Kondo effect are well-known examples, where the discrete states of a hydrogen atom or a magnetic impurity are renormalized by the quantum fluctuations of an environment of virtual photons or virtual spin flips. In single-electron circuits [1], such as the single-electron transistor (SET) [2], the charge pump [3], or the single-electron box [4], the same sort of quantum fluctuations exist in a system which can be controlled and measured electrically. These fluctuations arise from the virtual tunneling of electrons between the metal islands and the metal leads that comprise single-electron devices. Electron-hole pairs, generated by the virtual tunneling, partially screen the charge on the islands and modify the discrete spectrum of charge states. The single-electron box, the simplest single-electron circuit, is the ideal system in which to test the theory of quantum charge fluctuations.

The box has been studied theoretically [5–9] because it is a model system for understanding electron-electron interactions and because the quantum fluctuations in the box are analogous to both the Kondo effect [5] and the Lamb shift. In spite of the extensive theoretical work, few experiments have probed the fluctuations described by Refs. [5–9]. Those experiments that have done so are mostly in semiconductor dots [10–12]; whereas the theory of Refs. [6–9] describes metallic systems, such as our box or Refs. [13,14], in which the tunnel junctions comprise many nearly opaque channels. Because the quantum fluctuations screen an electron with a polarization charge much less than one electron, very sensitive charge measurements are required to resolve the fine structure associated with these fluctuations.

In this Letter, we measure the time-averaged charge on the island of a single-electron box with an accuracy much better than one electron using a radio-frequency SET (rf-SET) [15]. We observe quantum fluctuations of charge, and we modify the strength of these quantum fluctuations by changing the temperature, the external potential, and the quasiparticle density of states of the metal in which the tunnel junction is embedded. In each case, we find quantitative agreement between our results and the theory of quantum fluctuations.

Our single-electron box is composed of an isolated aluminum island attached to an aluminum lead through a thin insulating layer across which electrons can tunnel. A 1 T magnetic field is applied to keep the aluminum in its normal (nonsuperconducting) state. An additional lead, called the gate lead, lies near the island and changes the electrostatic potential of the island with the application of a voltage V_g to the gate lead through the gate capacitance C_g. The total island capacitance C_Σ^0 is small enough that the addition of a single electron to the island requires a large electrostatic energy

$$U_n = E_C^0(n - n_g)^2, \tag{1}$$

where $E_C^0 = e^2/2C_\Sigma^0$ is the charging energy, n is the number of excess electrons on the box, and $n_g = C_g V_g/e$. The minimum energy is clearly achieved when n is the integer nearest n_g; when $n_g = 0.5$ the two lowest-energy charge states are degenerate.

Equation (1) ignores the quantum fluctuations, or the effects of the coupling of island and lead through the tunnel junction. The junction couples the charge states to each other and to quasiparticle excitations in the metal on either side of the junction. This alters the spectrum of states in Eq. (1) in three ways. First, the charging energy is reduced (C_Σ^0 is enhanced) from its bare value E_C^0 to a renormalized value $E_C^N = e^2/2C_\Sigma^N$ in the normal state or $E_C^S = e^2/2C_\Sigma^S$ in the superconducting state. Second, when a pair of states are nearly degenerate their energy difference becomes temperature dependent. Finally, the electrostatic energy U_n of the charge states is no longer quadratic in n_g. The magnitude of these three effects is calculated with a theory perturbative in the dimensionless conductance $g = R_K/(4\pi^2 R_j) = (h/e^2)/(4\pi^2 R_j)$ [6,7,9], where R_j is the box junction resistance. By measuring the average charge on the box island Q_{box}/e versus n_g (Coulomb staircase) with an uncertainty less than g, we can compare all three effects with theory.

We measure $Q_{\rm box}$ as a function of n_g by coupling the box island to an rf-SET electrometer through a capacitor C_C [15] [Fig. 1(a)]. The quantity that we measure directly is the charge coupled to the electrometer $Q_{\rm elec}$ versus n_g, which approximates a sawtooth function (Coulomb sawtooth). We infer the Coulomb staircase as $Q_{\rm box} = (n_g e\kappa - Q_{\rm elec})/\kappa$ [Fig. 1(c)], where $\kappa = C_C/C_\Sigma^N$ is the fraction of the charge on the box that couples to the electrometer. The value of $e\kappa$ is not an independently known parameter; rather, it is determined as the slope of the Coulomb sawtooth at $n_g = 0$, *assuming* that $Q_{\rm box}$ is independent of n_g at $n_g = 0$. Following this procedure, we extract a value of $\kappa = (3.35 \pm 0.05) \times 10^{-2}$. Our assumption is valid if we interpret C_Σ^N (and E_C^N) determined in our experiments as a value renormalized by tunneling, not the bare, geometrical value C_Σ^0, which is a parameter in the theory of Refs. [6,7]. While we cannot prevent tunneling and measure C_Σ^0, we can suppress tunneling and observe a variation in the total box capacitance.

We find the first evidence of quantum fluctuations by examining the temperature dependence of the Coulomb staircase. We measure the staircase at a high temperature ($T = 500$ mK) and extract a value of $E_C^N/k_B = 1.57 \pm 0.05$ K ($C_\Sigma^N = 590 \pm 20$ aF) by assuming thermal broadening, that is, a Boltzmann occupation of the states in [Eq. (1)]. In the range 200–500 mK, we find excellent agreement [Fig. 2(a)] between the measured staircase and thermal broadening in a comparison with no adjustable parameters. Below 200 mK, thermal fluctuations characterized by any single temperature cannot account for the measured staircase [Fig. 2(b)]. As the temperature of the cryogenic apparatus is reduced, away from $n_g = 0.5$ the staircase remains rounded as if the box's temperature were saturating around 130 mK. Nevertheless, the staircase grows continually sharper at

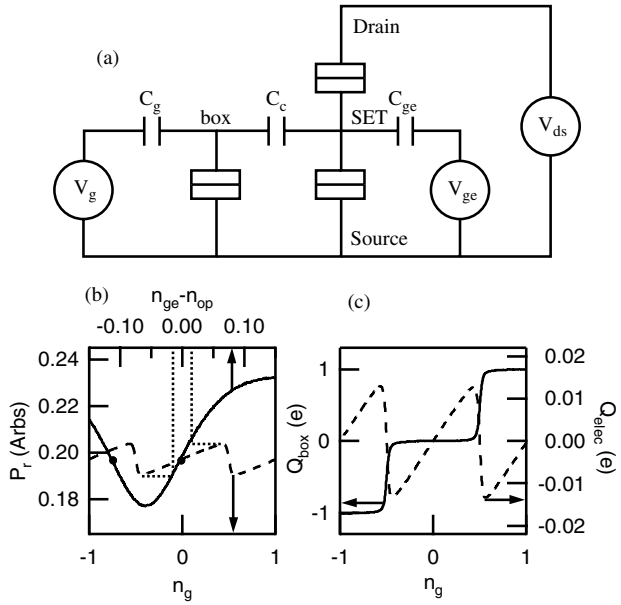

FIG. 1. (a) Circuit diagram of the single-electron box capacitively coupled to an rf-SET electrometer. The tunnel junctions are represented by boxes divided by a horizontal line. The junction capacitance C_J is the dominant component of the total box capacitance, $C_\Sigma^0 = C_J + C_g + C_C$. Additional circuit elements (not shown) apply an rf signal between the SET's drain and source and detect the amount of rf power reflected P_r from the rf-SET [15]. (b) Calibration of the Coulomb sawtooth is accomplished by varying the SET's control gate voltage $V_{\rm ge} = n_{\rm ge}(e/C_{\rm ge})$ about a fixed operating voltage $V_{\rm op} = n_{\rm op}(e/C_{\rm ge})$ while the box gate is held at $n_g = 0$. This applies a known charge signal $Q_{\rm elec} = e(n_{\rm ge} - n_{\rm op})$ to the SET. The plot P_r versus $n_{\rm ge} - n_{\rm op} = Q_{\rm elec}/e$ (solid line, top axis) is a nonlinear map (implied by dotted lines) that converts P_r versus n_g (dashed lines, bottom axis) into $Q_{\rm elec}$ versus n_g. The electrometer's operating point $n_{\rm op} = 0.44$ and an alternative $n_{\rm op} = 0.56$ and are indicated (two dots). (c) The Coulomb sawtooth, $Q_{\rm elec}$ versus n_g, (dashed line) on the right axis, and the Coulomb staircase, $Q_{\rm box}$ vs n_g, (solid line) on the left axis at $T = 30$ mK.

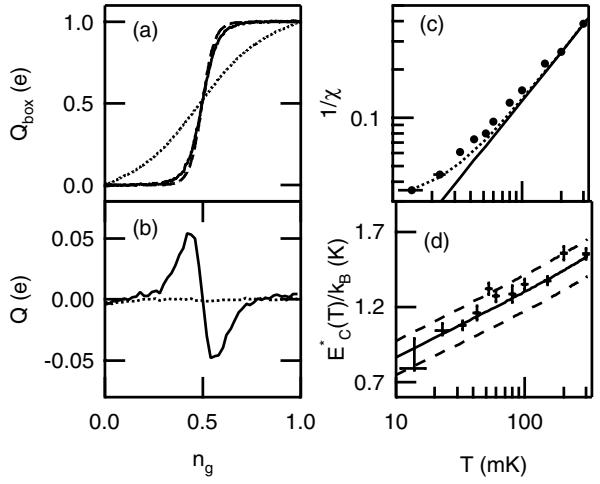

FIG. 2. (a) Coulomb staircases at $T = 500$ mK (dotted line) and $T = 100$ mK (solid line). The charging energy E_C^N is extracted by fitting to the 500 mK data a theoretical staircase (not shown) broadened only by thermal fluctuations. The 100 mK staircase is compared to the thermal fluctuation theory with no adjustable parameters (dashed line). (b) The residuals of the 500 mK fit (dotted line) and of the 100 mK comparison (solid line). (c) Plotted versus T on logarithmic scales are the measured value of $(1/\chi)$ (points), the expression $1/\chi = 2k_BT/E_C^N$ (line) showing the expected behavior in the absence of quantum fluctuations, and the expression $1/\chi = 2k_B\sqrt{(T^2 + T_{\rm sp}^2)}/E_C^N$ showing the expected behavior in the absence of quantum fluctuations but in the presence of a spurious broadening characterized by a phenomenological effective temperature $T_{\rm sp} = 25$ mK (dotted line). A model of temperature-independent spurious broadening does not contain the observed behavior of χ versus T. (d) The quantity $E_C^*(T) = 2k_BT\chi$ (points) and the prediction of [9] (line) versus T with no adjustable parameters. Dashed lines indicate the range of theory consistent with the uncertainties in g and E_C^N. The error bars of two lowest T points account for a systematic rounding introduced by the SET's backaction [16].

electrostatic degeneracy, $n_g = 0.5$, consistent with temperatures below 30 mK. Because the box is most sensitive to external noise at degeneracy, this surprising behavior is both inconsistent with an external source of noise and a qualitative hallmark of quantum fluctuations [10].

The theories of Refs. [5,8,9] predict the slope $\chi = (1/e)dQ_{\rm box}/dn_g$ of the Coulomb staircase, essentially the polarizability, at $n_g = 0.5$ as a function of temperature [8,9]. Because $\chi = E_C^N/2k_BT$ in the absence of quantum fluctuations, a plot of $1/\chi$ versus T reveals the quantum fluctuations in its deviation from a line with slope $2k_B/E_C^N$ [Fig. 2(c)]. Near $n_g = 0.5$, where the two lowest charges states are nearly degenerate, quantum fluctuations cause a temperature-dependent reduction in the energy separation, $U_1 - U_0 = E_C^*(0.5 - n_g)$, of the levels, described by a reduced $E_C^* = 2k_B\chi T < E_C^N$. Reference [9] implies $E_C^* = E_C^N[1 - 2g(3.154 + \ln(E_C^0/\pi k_BT))] + \mathcal{O}[g^2, (k_BT/E_C^N)^2]$, where $E_C^0 = E_C^N(1 + 4g + \mathcal{O}(g^2))$. Note the similarity to the Kondo effect where the screening of a localized magnetic impurity by itinerant spins leads to a logarithmic in T correction of the impurity's magnetic moment [5]. In Fig. 2(d), we plot $E_C^*(T)$ versus T and find good agreement with Ref. [9], in a comparison with no adjustable parameters. This same effect was observed in SET's by Joyez *et al.* [13].

To make the comparison with theory, we must have an independent determination of the dimensionless conductance of the box, $g = (4.2 \pm 0.2) \times 10^{-2}$, which can be obtained by studying the box in its superconducting state. With no applied magnetic field, the aluminum superconducts, and the parameters of the box, $C_\Sigma^S = 518 \pm 6$ aF and $R_j = 15.4 \pm 0.9\ \mathrm{k}\Omega$, can be extracted by microwave spectroscopy of the coherent two-level system formed by the coupling of Cooper pairs between the lead and the island [18]. What is directly measured is the charging energy in the superconducting state $E_C^S/k_B = 1.79 \pm 0.02$ K and the Josephson energy $E_J/k_B = (h\Delta/8e^2R_jk_B)F(E_C^0/\Delta) = 0.62 \pm 0.01$K, where $\Delta/k_B = 2.4 \pm 0.1$ K is the BCS gap in aluminum and $F(E_C^0/\Delta)$ is a function that accounts for Coulomb blockade effects by modifying the usual Ambegakor-Baratoff relation [19]. For our sample $F(E_C^0/\Delta) = 1.25$. Note that in the superconducting state $E_C^S = e^2/2C_\Sigma^S$ is not the same as $E_C^N = e^2/2C_\Sigma^N$ in the normal state. This difference reflects the different quantum fluctuations of a metal with a superconducting or with a normal quasiparticle density of states (DOS).

We are able to tune this influence of the DOS by continuously reducing Δ in the aluminum with an applied magnetic field $B_{\rm app}$. We observe that C_Σ^S is a function of $\Delta(B_{\rm app})$ by measuring $\kappa^S = C_C/C_\Sigma^S$, the slope of the Coulomb sawtooth at $n_g = 0$, as the aluminum is driven from the fully superconducting state to the normal state. With increasing $B_{\rm app}$, κ^S is reduced continuously from a value $\kappa^S = (3.70 \pm 0.05) \times 10^{-2}$ with $B_{\rm app} = 0$ to $\kappa = (3.35 \pm 0.05) \times 10^{-2}$ in the normal state (Fig. 3). Because both κ^S and E_C^S are proportional to $1/C_\Sigma^S(B_{\rm app})$ we infer $E_C^N/k_B = [E_C^S(B_{\rm app})/k_B][\kappa/\kappa^S(B_{\rm app})] = 1.62 \pm 0.04$ K, which is consistent with the value 1.57 ± 0.05 K extracted from the broadening of the Coulomb staircase at high temperatures.

The theory of the normal box [7] predicts that the effects of tunneling can be treated around $n_g = 0$ as a renormalization of C_Σ^0 to a value larger by the factor $[1 + 4g + 10.93g^2 + \mathcal{O}(g^3) = 1.18]$. The renormalization of the bare capacitance in the superconducting state C_Σ^S/C_Σ^0 is predicted to be smaller than in the normal state because the quasiparticle excitations have a minimum energy Δ, which suppresses the virtual tunneling. The bare capacitance is not an experimentally accessible parameter; however, the perturbative techniques of Ref. [7] can be used [20] to calculate the renormalization of C_Σ^0 for a metal with a BCS, rather than constant, DOS. Inverting this, we infer from the normal state ($C_\Sigma^0 = 498 \pm 16$ aF) and from the superconducting state ($C_\Sigma^0 = 478 \pm 7$ aF) values for the bare capacitance that are consistent with each other. By altering the DOS, we have observed that the capacitance of a tunnel junction is not a property of tunnel junction alone, but also of the spectrum of low-energy excitation in the metal from which it is made.

We have already seen that the electrostatic energy of the box is both a function of the temperature and of the

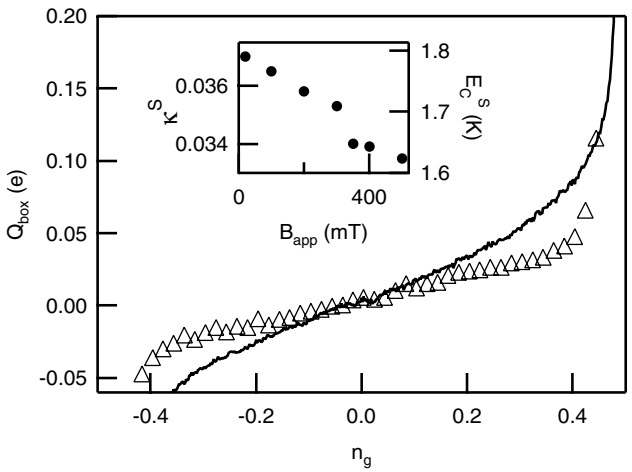

FIG. 3. Coulomb staircases with the box in its normal state (line) and in its superconducting state, $B_{\rm app} = 100$ mT (triangles). For both, the Coulomb sawtooths have been converted to staircases using $\kappa^0 = C_C/C_\Sigma^0 = 3.9 \times 10^{-2}$, which would be the slope of the Coulomb sawtooth around $n_g = 0$ in the absence of tunneling. The renormalization of C_Σ^0 is visible as the nonzero slope $(1/e)dQ_{\rm box}/dn_g$ of these plots at $n_g = 0$. The inset shows $\kappa^S(B_{\rm app})$ versus $B_{\rm app}$ and the value of $E_C^S(B_{\rm app})$ inferred from κ^S, as the aluminum is driven from its superconducting to its normal state. In the superconducting state, a single out-of-equilibrium quasiparticle on the box's island keeps the Coulomb staircase e periodic.

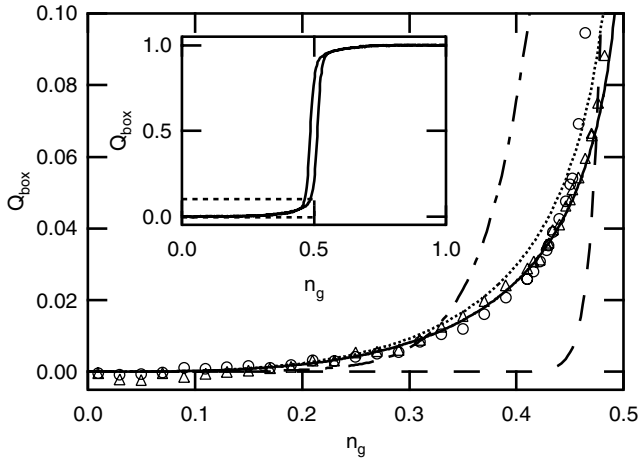

FIG. 4. Coulomb staircases with the box at two different electrometer operating points, $n_{op} = 0.44$ (triangles) and $n_{op} = 0.56$ (circles); $V_{ds} = 0$ for both. The SET's backaction causes these two curves to deviate from each other around $n_g = 0.5$. The theory plots are the charge on the box predicted for thermal fluctuations but no quantum fluctuations at $T = 125$ mK (dashed dotted line) and $T = 29$ mK (dashed line), and for the quantum fluctuations calculated to first order in g (dotted line) and second order in g (solid line) [6,7]. The second order calculation is fit to the data with the adjustable parameter $\kappa = (3.375 \pm 0.001) \times 10^{-2}$, which is better constrained by this fit than by extracting the slope of the Coulomb sawtooth. Note we have plotted both data and theory in the form with $dQ_{box}/dn_g = 0$ at $n_g = 0$ unlike Refs. [6,7]. Inset: the same data over a range $0 < n_g < 1$. The dashed box indicates the region plotted in the main figure.

quasiparticle DOS in metal lead and island. We now show that the ground-state energy deviates from the parabolas of Eq. (1). Because $Q_{box}/e = n_g - (1/2E_C^0)(dU_n/dn_g)$ at $T = 0$ [6], Eq. (1) implies perfectly flat steps in the Coulomb staircase, whereas we observe some curvature around $n_g = 0$ even at $T \ll E_C^N$. The ground-state energy cannot be quadratic in n_g. This modification of the ground-state energy is the Lamb shift in the single-electron box.

It is precisely the detailed shape of the Coulomb staircase at $T = 0$ that is predicted by [6,7] and which provides the most stringent test of the theory (Fig. 4). We find that Q_{box} deviates from a perfect step function by several percent in the range $0 < n_g < 0.45$ [16]. In this region at the base temperature of our cryogenic apparatus, we may consider the box to be in a zero temperature limit and ignore the influence of the electrometer (Fig. 4). To an accuracy of 2×10^{-3} e, limited by the linearity of the applied gate voltage, we find agreement with this theory. Our measurement is sufficiently accurate and sensitive that the perturbative calculation of Ref. [7] must be carried out to second order to show agreement with our experiment, even for the relatively small value of $g = 4.2 \times 10^{-2}$.

In these experiments, we have used an rf-SET electrometer to measure the polarizibility of a mesoscopic electrical circuit. We have chosen to apply this technique to the single-electron box, a model system for understanding electron-electron interactions whose Hamiltonian is analogous to the Kondo Hamiltonian. We find excellent agreement between our measurements and a perturbative treatment of the quantum fluctuations. The excellent agreement between our measurements and theory both supports this theory and demonstrates the precision electrometry possible with the rf-SET. The technique we demonstrate would be an ideal method for exploring the equilibrium behavior of more complicated mesoscopic circuits, such as semiconductor quantum dots or carbon nanotubes.

This work was supported by the National Security Agency (NSA), Advanced Research and Development Activity (ARDA) under Army Research Office (ARO) Contract No. DAAD-19-02-1-0045, the David and Lucile Packard Foundation, the Wallenberg Foundation, and the W. M. Keck Foundation. The authors thank M. Devoret, S. Girvin, A. Clerk, H. Grabert, and L. Glazman for useful discussions.

*Electronic address: konrad.lehnert@jila.colorado.edu
Permanent address: JILA, National Institute of Standards and Technology and University of Colorado, Boulder, CO, 80309-0440.
†Group website: www.eng.yale.edu\rslab

[1] *Single Charge Tunneling*, edited by H. Grabert and M. H. Devoret, Nato Advanced Study Institutes, Ser. B, Vol. 294 (Plenum, New York, 1992).
[2] T. A. Fulton and G. J. Dolan, Phys. Rev. Lett. **59**, 109 (1987).
[3] H. Pothier *et al.*, Europhys. Lett. **17**, 249 (1992).
[4] P. Lafarge *et al.*, Z. Phys. B **85**, 327 (1991).
[5] K. A. Matveev, Sov. Phys. JETP **72**, 892 (1991).
[6] G. Göppert *et al.*, Phys. Rev. Lett. **81**, 2324 (1998).
[7] G. Göppert and H. Grabert, Phys. Rev. B **63**, 125307 (2001), and references therein.
[8] H. Schoeller and G. Schön, Phys. Rev. B **50**, 18 436 (1994).
[9] H. Grabert, Phys. Rev. B **50**, 17 364 (1994).
[10] D. Berman *et al.*, Phys. Rev. Lett. **82**, 161 (1999).
[11] D. S. Duncan *et al.*, Appl. Phys. Lett. **74**, 1045 (1999).
[12] L. W. Molenkamp, K. Flensberg, and M. Kemerink, Phys. Rev. Lett. **75**, 4282 (1995).
[13] P. Joyez *et al.*, Phys. Rev. Lett. **79**, 1349 (1997).
[14] D. Chouvaev *et al.*, Phys. Rev. B **59**, 10 599 (1999).
[15] R. J. Schoelkopf *et al.*, Science **280**, 1238 (1998).
[16] In a region $0.45 < n_g < 0.55$ and $T < 50$ mK, Q_{box} depends on the operating point of the electrometer. While we can accurately model the electrometer's influence on the box [17], no theory yet accounts for quantum fluctuations and backaction simultaneously.
[17] B. A. Turek *et al.* (to be published).
[18] K. W. Lehnert *et al.*, Phys. Rev. Lett. **90**, 027002 (2003).
[19] P. Joyez, Ph.D. thesis, University of Paris, 1995.
[20] V. Bouchiat, Ph.D. thesis, University of Paris, 1997.

Single-electron transistor backaction on the single-electron box

B. A. Turek,[1] K. W. Lehnert,[1] A. Clerk,[1] D. Gunnarsson,[2] K. Bladh,[2] P. Delsing,[2] and R. J. Schoelkopf[1]
[1]*Department of Applied Physics and Department of Physics, Yale University, New Haven, Connecticut 06511, USA*
[2]*Microtechnology Center at Chalmers MC2, Department of Microelectronics and Nanoscience, Chalmers University of Technology and Goteborg University, SE-412 96 Goteborg, Sweden*
(Received 21 February 2005; published 26 May 2005)

We report an experimental observation of the backaction of a single-electron transistor (SET) measuring the Coulomb staircase of a single-electron box. As current flows through the SET, the charge state of the SET island fluctuates. These fluctuations capacitively couple to the box and cause changes in the position, width, and asymmetry of the Coulomb staircase. A sequential tunneling model accurately recreates these effects, confirming this mechanism of the backaction of a SET. This is a first step toward understanding the effects of quantum measurement on solid-state qubits.

DOI: 10.1103/PhysRevB.71.193304 PACS number(s): 73.23.Hk, 72.70.+m, 85.35.Gv

In the recent work toward the goal of quantum computing, and in the study of single quantum systems in general, the single-electron transistor (SET) is often used as a measurement device. It has been proposed as a readout device for mechanical,[1] spin,[2] and charge[3] quantum systems, and has been successfully used to measure superconducting charge qubits.[4] As with any amplifier, the SET must produce electrical noise on its input, perturbing the measured system and causing the unavoidable backaction of a quantum measurement.

SET backaction on a two-level system has been studied extensively in the theoretical literature. It has been determined that the SET should be able to approach the quantum limit of backaction, where it dephases a qubit as rapidly as it is reads the qubit state.[5] Spectral components of the SET backaction at the two-level system transition frequency can also contribute to transitions between two qubit states.[6,7] A qubit could thus form a spectrum analyzer capable of probing previously inaccessible frequencies.[8] These theoretical analyses presume SET backaction results from fluctuations in the charge state of the SET island caused by the drain-source current, but no experimental measurements exist confirming that this is the dominant or the sole mechanism of the SET's backaction. Indeed, it often appears that the SET can poison the Cooper-pair box, inducing nonequilibrium quasiparticles through other mechanisms.[9,10]

As a first quantitative test of SET backaction, we consider the SET and box operated in the normal (nonsuperconducting) state, created with the application of a 1-T magnetic field. Analysis of the normal box is simpler than in the superconducting state because the box is no longer sensitive to parity and quasiparticle generation. The normal SET can also be simply described by a sequential tunneling model, which avoids the complication of the many possible quasiparticle-pair tunneling cycles[11] in the superconducting SET. Nevertheless, the primary mechanism of SET backaction is still the capacitive electromagnetic coupling between the box and SET, and the box remains a mesoscopic device that is sensitive to this backaction. Just as with the SSET-Cooper-pair box system, sensitive measurements of the Coulomb staircase of the normal box can reveal the dynamics of the coupled system, and probe the nature of SET backaction.

The possibility of SET backaction on a single-electron box was proposed with experiments in the field,[12] but has proven difficult to quantify. The signature of SET electrical backaction is difficult to separate from simple heating of the sample.[13,14] The backaction has been measured with very strong coupling between the SET and the box,[15] but few measurements exist in systems that are as weakly coupled as the proposed Cooper pair box-SET experiments. In this Brief Report, we present an experimental analysis of a SET weakly coupled to a single-electron box. We vary the operating point of the SET, measure the Coulomb staircase of the box, and find the variations in the shift, width, and asymmetry of the staircases to be in agreement with a model that includes backaction caused by the charge-state fluctuations of the SET island. These variations in the measured staircases allow us to measure average properties of the noise of the SET.

The SET [Fig. 1(a)] consists of a aluminum island connected through tunnel junctions to two leads (the drain and the source) and capacitively coupled to a third (the gate). A SET is described by its charging energy ($E_c = e^2/2C_\Sigma$, the energy to add an additional electron to the island), by the tunneling resistance of the junctions on the drain and the source leads (R_j), and by the size of the capacitors coupling it to the external control voltage (C_{ge}) and to the measured

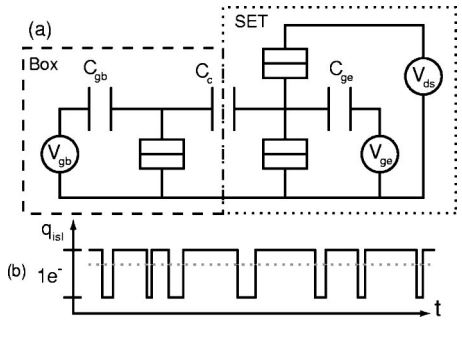

FIG. 1. (a) Circuit diagram of the single-electron box (dashed box) capacitively coupled to the SET (dotted box). The normal-state tunnel junctions are represented by boxes with a single line through them. (b) Plot of the charge state on the SET island vs time. The dotted line shows the mean value of the charge on the SET island.

system (C_c). A high tunneling resistance ($R_j > h/e^2$) and large charging energy ($E_c > k_B T$) suppress the addition of charge to the island by quantum or thermal fluctuations, so the island may be considered confined to a discrete set of charge states. A bias voltage (V_{ds}) provides the energy necessary for the system to switch between charge states, allowing current to flow from the drain to the source. The amount of current is controlled by the rate of transition between accessible charge states, which is a function of the potential of the island. Thus the SET forms a very sensitive electrometer, where changes in the total charge capacitively coupled to the island modulate the current flowing through the transistor. The SET is operated by fixing the values of the externally applied V_{ds} and V_{ge}, and observing variations in the conductance as the charge coupled to the SET from the measured system changes. The point at which V_{ds} and V_{ge} are fixed is termed the operating point; the same measurement can be performed by observing conductance variations about many different operating points.

The box [Fig. 1(a)] consists of another island capacitively gated by an external lead (V_{gb}) and connected through a tunnel junction to ground. As with the SET, the gate lead controls the potential of the box and changes the relative electrostatic energies of the available charge states. We express the gate voltages for both the box and the electrometer in terms of the number of electrons on the corresponding gate capacitors: $n_{gb} = C_{gb} V_{gb}/e$ and $n_{ge} = C_{ge} V_{ge}/e$. When n_{gb} is raised by one electron, the island charge state of minimum energy changes, and a single electron tunnels on to the island to keep it in its ground state. Plotting the time-averaged number of additional electrons on the island as a function of n_{gb} gives the familiar "Coulomb staircase" [Fig. 2(b)].[12] The width of this staircase is normally a function only of the temperature of the sample. In this Brief Report we quantify SET backaction by observing additional variations in the Coulomb staircase that are systematic with the SET operating point.

The coupling capacitor [C_c in Fig. 1(a)] couples together the potential on the two islands, allowing the SET to measure the box and also allowing the potential on the SET island to affect the box. The strength of this coupling is expressed either as the fraction of the electrometer charge coupled to the box ($\kappa = C_c/C_{\Sigma_{SET}}$) or as the temperature necessary to cause changes in a Coulomb staircase comparable to those caused by backaction ($T_\kappa = \kappa E_{c_{box}}/k_B$). As the polarization charge on C_c changes, the total charge coupled to the SET changes, changing the tunneling rates in the SET and modulating the current that flows from the drain to the source. The charge on the box is then inferred from the change in current through the SET. C_c also couples the charge on the SET island to the box, and in doing so creates the effects that we see as the SET's backaction.

The discrete nature of charge causes two kinds of noise in the SET. The drain-source current flows not as a continuous fluid, but as individual charges, causing an uncertainty in the SET's measurement due to shot noise. In addition to shot noise on the output (the drain-source current), there is also charge noise on the SET input (the gate capacitor) that affects the measured system. Electrons tunneling on and off the island cause both the charge state and the potential of the SET island to fluctuate between two values [Fig. 1(b)]. The fluctuating potential on the SET island coupled through C_c is found to be the source of the SET's backaction. Three averaged properties of the fluctuating potential have effects visible on the Coulomb staircase and can be varied with the operating point of the SET. The mean charge on the SET island varies by as much as one electron, and leads to shifts in the position of the Coulomb staircase by as much as κe. The rms magnitude of the charge fluctuations on the SET island broaden the measured Coulomb staircase by an amount that varies with n_{ge}. Finally, the telegraph-noise nature of the charge-state fluctuations on the SET island causes the staircases to be asymmetric; the magnitude and direction of that asymmetry varies with the SET's operating point.

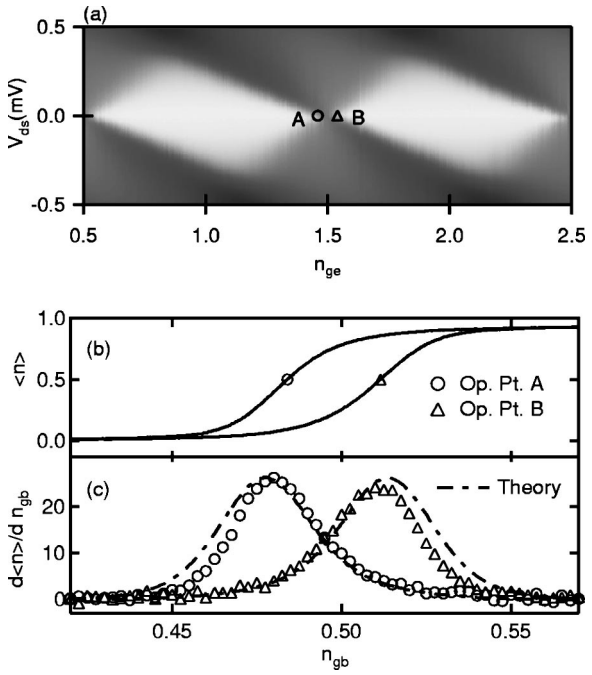

FIG. 2. (a) Plot of the reflected power from the SET as a function of gate (n_{ge}) and drain-source (V_{ds}) voltage. (b) Coulomb staircases measured at the operating points marked in (a) as a function of the box gate voltage n_{gb}. The time-averaged number of electrons on the box is measured with a precision of $\pm 1 \times 10^{-3}$ and an accuracy of $\pm 2 \times 10^{-3}$. (c) Derivatives of these Coulomb staircases and of the corresponding Coulomb staircases generated with a sequential tunneling model with $E_{C_{SET}}/k_B = 2.3$ K, $E_{C_{box}}/k_B = 1.6$ K, $R_{j_{SET}} = 47$ kΩ, $R_{j_{box}} = 15.4$ kΩ, and $C_c/C_{\Sigma_{SET}} = 0.048$. The derivative of the Coulomb staircase is reported with an accuracy of ±0.4.

A sequential tunneling model for the full SET-box system accurately recreates both the measurement and the backaction. The tunneling rates between any two box and SET charge states are calculated as a function of n_{ge}, n_{gb}, and V_{ds} (for details, see Ref. 16). The time-averaged charge state of the SET-box system corresponds to the steady state of these coupled rates. The current through the transistor is calculated as the product of the time-averaged charge on the SET island and the rate at which charge tunnels off the island. This model allows us to replicate the Coulomb staircases taken at various operating points with only the electron temperature

as a free parameter. The elevated temperature of the best-fit model steps ($T=27\pm1$ mK in a fridge at $T=13$ mK) reflected the broadening of the measured steps due to quantum fluctuations of charge,[17] and is well understood. Theoretical curves also correctly account for higher-order effects in the box-SET system. At certain operating points (e.g., $n_{ge}=\frac{1}{2}$, $V_{ds}=0$, $n_{gb}=\frac{1}{2}$), the SET's backaction is a sensitive function of the state of the box. Changes in the Coulomb staircase measured at such operating points can only be understood by a sequential tunneling model for the full coupled box-SET system.

Coulomb staircases were measured in a dilution refrigerator at 13 mK, where the available thermal energy was far less than the charging energy of either the SET or the box island. The SET was operated as a rf-SET,[18] with a LC resonant circuit reflecting an amount of microwave power that varied as the oscillator was damped by the varying conductance of the SET. Staircases were measured by sweeping n_{gb} over a range corresponding to $1/4e$. While the box gate was swept, the SET gate was swept in the opposite direction to cancel the parasitic capacitance of the box lead to the electrometer's island. Before each Coulomb staircase was measured, n_{ge} was swept to find the reflected microwave power as a function of charge coupled to the SET island. Variations in reflected power with n_{gb} were then converted (via this lookup table) to charge on C_c (for a more detailed description, see Ref. 17). The measured charge on the box is thus reported from the amount of charge on C_{ge} necessary to cause an equivalent electrometer response.

Backaction effects were found to be very sensitive to variations in n_{gb} and n_{ge} and our experiment therefore required that these voltages be set with high precision. Drifts were removed by referencing the steps to a fiducial step every 20 min. First, n_{ge} was swept at $V_{ds}=0$ and the value of n_{ge} that maximized SET conductance was determined as $n_{ge}=\frac{1}{2}$ [see Fig. 2(a)]. Next, a Coulomb staircase was measured with the SET operated at $n_{ge}=0.44$, $V_{ds}=0$. The value of n_{gb} at the center of this step was determined. Charge offset noise and $1/f$ noise drifts add constant offsets to either n_{ge} or n_{gb}; measuring the fiducial step as described here allows us to quantify the change in these offsets on both the box and the SET. Measurements found to contain large charge jumps in n_{ge} or n_{gb} were discarded. This procedure allowed measurement of Coulomb staircases with an uncertainty of $1\times10^{-3}e$ in the charge and an uncertainty of $5.5\times10^{-4}e$ in the horizontal position of the steps. The uncertainty in the applied n_{ge} was found to be $5\times10^{-3}e$.

The differences in Coulomb staircases measured at different operating points allow us to measure average properties of the fluctuating potential of the SET island. Staircases measured at different operating points are shifted in n_{gb} [Fig. 2(b)]. The shift of each staircase is proportional to the mean charge on the SET island. The mean charge on the SET island varies by as much as one electron with SET operating point, and the corresponding charge that couples to the box and adds to n_{gb} varies by as much as κe. We measure staircase shift by reporting the value of n_{gb} at each step's midpoint, measured relative to the center of a fiducial step [Fig. 3(a)]. The sequential tunneling model accurately recreates these variations in the step position.

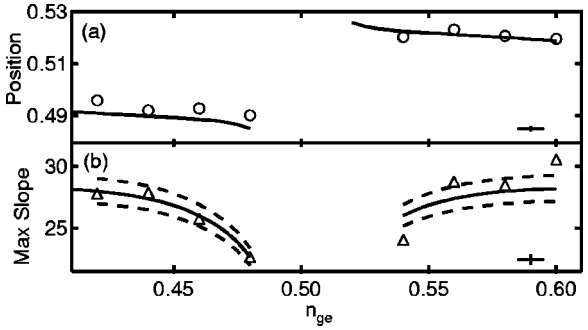

FIG. 3. (a) The horizontal position of the center of the Coulomb staircase for various operating points of the SET. The model is a solid line, and circles are experimental measurements. No measurements exist near $n_{ge}=\frac{1}{2}$ where the electrometer had no gain. Representative error bars are shown in the bottom right-hand side of the plot. Horizontal uncertainty reflects the measured instability of the SET operating point due to charge noise. (b) The maximum slope of the staircases measured with the SET at the same series of operating points. Confidence bands show the model curve for 27 ± 1 mK.

The measured Coulomb staircases also exhibit variations in width that change with operating point [Fig. 3(b)]. Three different mechanisms broaden the Coulomb staircase: quantum fluctuations, thermal excitation, and SET backaction. Quantum fluctuations of charge on the box cause broadening, but only away from the center of the step.[17] Our measurement, which quantifies broadening as the maximum slope at the center of each Coulomb step, is therefore insensitive to quantum broadening. Thermal excitations of the box also broaden the Coulomb staircase. SET heating varies with operating point, and, for large values of V_{ds}, can produce a trend in staircase width similar to the effects of backaction. All of our data were taken, however, at $V_{ds}=0$, where heating from the SET was negligible. Finally, SET backaction broadens the Coulomb staircase when the charge-state fluctuations of the SET island cause the box to switch between charge states. SET backaction broadens staircases by as much as κe, and broadens staircases most at operating points where the

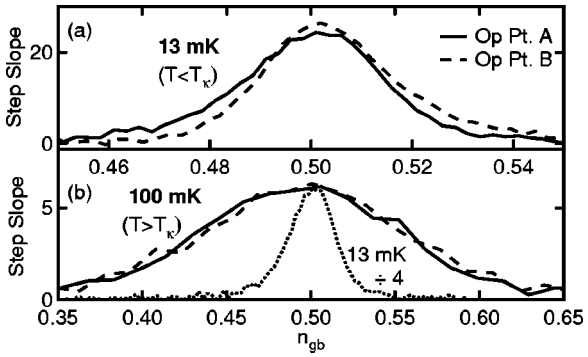

FIG. 4. (a) Derivatives of steps measured at the operating points in Fig. 2(a), offset in n_{gb} to eliminate the shift in position of the steps. Note that the tails of the two steps are asymmetric. (b) Steps measured at the same operating points with the sample at 100 mK. The asymmetry is no longer visible. The inset demonstrates the thermal broadening by showing a $1/4$ scale curve from the top graph plotted on the x axis for the bottom graph.

rms magnitude of the SET charge-state fluctuations is largest. The observed variations in staircase broadening with operating point [Fig. 3(b)] are fully accounted for with our sequential tunneling model.

The staircases are also asymmetric in a manner that varies predictably with operating point. Each staircase was found to have a longer tail in the direction away from which the staircase was shifted. The asymmetry of the Coulomb staircase is best viewed in the derivative of the steps [Fig. 2(b), or with the curves shifted to overlay in Fig. 4(a)], where it clearly follows the same trend as the model produces. Unfortunately, differentiating our data increased the noise and made it difficult to quantify the asymmetry; qualitatively, however, the model reproduces the experimentally observed trends. The staircase asymmetry is caused by the nature of the charge-state fluctuations on the SET island. The potential of the SET island lies preferentially to one side of the mean potential, with infrequent fluctuations far to the other side [Fig. 1(b)]. The staircases are thus broadened asymmetrically in the $+n_{gb}$ and $-n_{gb}$ directions. The preferred charge state, and thus the asymmetry of the measured staircase, is found to switch at $n_{ge}=\frac{1}{2}$.

The model also shows good agreement with our data at higher temperatures, where the various effects of the backaction change predictably. At higher temperatures, the mean potential of the SET island still changes with n_{ge}, and thus step shifts are still visible. For $T>T_{\kappa}$, however, the range (in n_{gb}) of thermal broadening is greater than the range of the backaction broadening or the asymmetry, and neither of these effects are therefore visible [Fig. 4(b)].

In these experiments we confirm that charge-state fluctuations of the SET island are the primary source of SET backaction. We observe the differences in Coulomb staircases measured with the SET biased at a variety of different operating points, and note changes in the shift, width, and asymmetry of the steps that are accurately recreated by a sequential tunneling model. This confirms that electromagnetic coupling to the fluctuating SET island potential can provide the ultimate lower bound on SET backaction.

This work was supported by the National Security Agency (NSA) and Advanced Research and Development Activity (ARDA) under Army Research Office (ARO) Contracts No. DAAD-19-02-1-0045 and DAAD-19–01–1–0611, the NSF ITR program under Grant No. DMR-0325580, the NSF under Grant No. DMR-0342157, the W. M. Keck Foundation, and the David and Lucile Packard Foundation.

[1] M. Blencowe and M. Wybourne, Appl. Phys. Lett. **77**, 3845 (2000).
[2] B. E. Kane, N. S. McAlpine, A. S. Dzurak, R. G. Clark, G. J. Milburn, H. B. Sun, and H. Wiseman, Phys. Rev. B **61**, 2961 (2000).
[3] V. Bouchiat, D. Vion, P. Joyez, D. Esteve, and M. Devoret, Phys. Scr., T **T76**, 165 (1998).
[4] K. W. Lehnert, K. Bladh, L. F. Spietz, D. Gunnarsson, D. I. Schuster, P. Delsing, and R. J. Schoelkopf, Phys. Rev. Lett. **90**, 027002 (2003).
[5] M. Devoret and R. Schoelkopf, Nature (London) **406**, 1039 (2000).
[6] A. Aassime, G. Johansson, G. Wendin, R. J. Schoelkopf, and P. Delsing, Phys. Rev. Lett. **86**, 3376 (2001).
[7] G. Johansson, A. Kack, and G. Wendin, Phys. Rev. Lett. **88**, 046802 (2002).
[8] R. J. Schoelkopf, A. A. Clerk, S. M. Girvin, K. W. Lehnert, and M. H. Devoret, cond-mat/0210247.
[9] B. Turek, J. B. Majer, A. Clerk, S. M. Girvin, A. Wallraff, K. Bladh, D. Gunnarsson, T. Duty, P. Delsing, and R. J. Schoelkopf. Accepted for Publication, IEEE Transactions on Applied Superconductivity.
[10] J. Mannik and J. E. Lukens, Phys. Rev. Lett. **92**, 057004 (2004).
[11] S. Pohlen, Ph.D. thesis, Harvard University, 1999.
[12] P. Lafarge, H. Pothier, E. R. Williams, D. Esteve, C. Urbina, and M. H. Devoret, Z. Phys. B: Condens. Matter **85**, 327 (1991).
[13] R. Schafer, B. Limbach, P. vom Stein, and C. Wallisser, cond-mat/0205223.
[14] V. A. Krupenin, S. V. Lotkhov, H. Scherer, Th. Weimann, A. B. Zorin, F.-J. Ahlers, J. Niemeyer, and H. Wolf, Phys. Rev. B **59**, 10 778 (1999).
[15] C. P. Heij, P. Hadley, and J. E. Mooij, Phys. Rev. B **64**, 245116 (2001).
[16] *Single Charge Tunneling*, edited by M. Devoret and H. Grabert, Nato Advanced Study Institutes Ser. B Vol. 294 (Plenum, New York, 1992).
[17] K. W. Lehnert, B. A. Turek, K. Bladh, L. F. Spietz, D. Gunnarsson, P. Delsing, and R. J. Schoelkopf, Phys. Rev. Lett. **91**, 106801 (2003).
[18] R. J. Schoelkopf, P. Wahlgren, A. Kozhevnikov, P. Delsing, and D. Prober, Science **280**, 1238 (1998).

Cavity quantum electrodynamics for superconducting electrical circuits: An architecture for quantum computation

Alexandre Blais,[1] Ren-Shou Huang,[1,2] Andreas Wallraff,[1] S. M. Girvin,[1] and R. J. Schoelkopf[1]
[1]*Departments of Physics and Applied Physics, Yale University, New Haven, Connecticut 06520, USA*
[2]*Department of Physics, Indiana University, Bloomington, Indiana 47405, USA*
(Received 7 February 2004; published 29 June 2004)

We propose a realizable architecture using one-dimensional transmission line resonators to reach the strong-coupling limit of cavity quantum electrodynamics in superconducting electrical circuits. The vacuum Rabi frequency for the coupling of cavity photons to quantized excitations of an adjacent electrical circuit (qubit) can easily exceed the damping rates of both the cavity and qubit. This architecture is attractive both as a macroscopic analog of atomic physics experiments and for quantum computing and control, since it provides strong inhibition of spontaneous emission, potentially leading to greatly enhanced qubit lifetimes, allows high-fidelity quantum nondemolition measurements of the state of multiple qubits, and has a natural mechanism for entanglement of qubits separated by centimeter distances. In addition it would allow production of microwave photon states of fundamental importance for quantum communication.

DOI: 10.1103/PhysRevA.69.062320 PACS number(s): 03.67.Lx, 73.23.Hk, 74.50.+r, 32.80.−t

I. INTRODUCTION

Cavity quantum electrodynamics (CQED) studies the properties of atoms coupled to discrete photon modes in high Q cavities. Such systems are of great interest in the study of the fundamental quantum mechanics of open systems, the engineering of quantum states, and measurement-induced decoherence [1–3] and have also been proposed as possible candidates for use in quantum information processing and transmission [1–3]. Ideas for novel CQED analogs using nanomechanical resonators have recently been suggested by Schwab and collaborators [4,5]. We present here a realistic proposal for CQED via Cooper pair boxes coupled to a one-dimensional (1D) transmission line resonator, within a simple circuit that can be fabricated on a single microelectronic chip. As we discuss, 1D cavities offer a number of practical advantages in reaching the strong-coupling limit of CQED over previous proposals using discrete LC circuits [6,7], large Josephson junctions [8–10], or 3D cavities [11–13]. Besides the potential for entangling qubits to realize two-qubit gates addressed in those works, in the present work we show that the CQED approach also gives strong and controllable isolation of the qubits from the electromagnetic environment, permits high-fidelity quantum nondemolition (QND) readout of multiple qubits, and can produce states of microwave photon fields suitable for quantum communication. The proposed circuits therefore provide a simple and efficient architecture for solid-state quantum computation, in addition to opening up a new avenue for the study of entanglement and quantum measurement physics with macroscopic objects. We will frame our discussion in a way that makes contact between the language of atomic physics and that of electrical engineering.

We begin in Sec. II with a brief general overview of CQED before turning to a discussion of our proposed solid-state realization of cavity QED in Sec. III. We then discuss in Sec. IV the case where the cavity and qubit are tuned in resonance and in Sec. V the case of large detuning which leads to lifetime enhancement of the qubit. In Sec. VI, a quantum nondemolition readout protocol is presented. Realization of one-qubit logical operations is discussed in Sec. VII and two-qubit entanglement in Sec. VIII. We show in Sec. IX how to take advantage of encoded universality and decoherence-free subspace in this system.

II. BRIEF REVIEW OF CAVITY QED

Cavity QED studies the interaction between atoms and the quantized electromagnetic modes inside a cavity. In the optical version of CQED [2], schematically shown in Fig. 1(a), one drives the cavity with a laser and monitors changes in the cavity transmission resulting from coupling to atoms falling through the cavity. One can also monitor the spontaneous emission of the atoms into transverse modes not confined by the cavity. It is not generally possible to directly determine the state of the atoms after they have passed through the cavity because the spontaneous emission lifetime is on the scale of nanoseconds. One can, however, infer information about the state of the atoms inside the cavity from real-time monitoring of the cavity optical transmission.

In the microwave version of CQED [3], one uses a very-high-Q superconducting 3D resonator to couple photons to transitions in Rydberg atoms. Here one does not directly monitor the state of the photons, but is able to determine with high efficiency the state of the atoms after they have passed through the cavity (since the excited state lifetime is of the order of 30 ms). From this state-selective detection one can infer information about the state of the photons in the cavity.

The key parameters describing a CQED system (see Table I) are the cavity resonance frequency ω_r, the atomic transition frequency Ω, and the strength of the atom-photon coupling g appearing in the Jaynes-Cummings Hamiltonian [14]

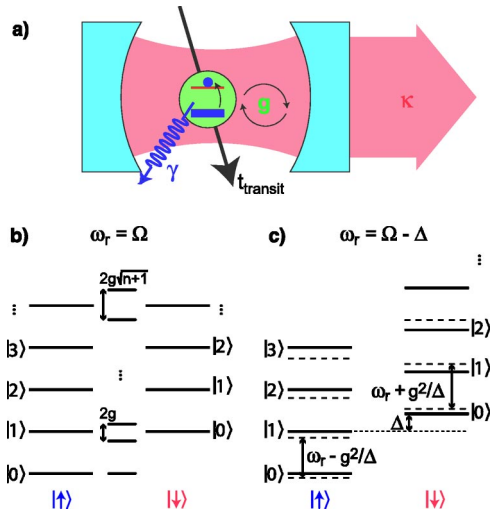

FIG. 1. (Color online) (a) Standard representation of a cavity quantum electrodynamic system, comprising a single mode of the electromagnetic field in a cavity with decay rate κ coupled with a coupling strength $g=\mathcal{E}_{\rm rms}d/\hbar$ to a two-level system with spontaneous decay rate γ and cavity transit time $t_{\rm transit}$. (b) Energy spectrum of the uncoupled (left and right) and dressed (center) atom-photon states in the case of zero detuning. The degeneracy of the two-dimensional manifolds of states with $n-1$ quanta is lifted by $2g\sqrt{n+1}$. (c) Energy spectrum in the dispersive regime (long-dashed lines). To second order in g, the level separation is independent of n, but depends on the state of the atom.

$$H=\hbar\omega_{\rm r}\left(a^{\dagger}a+\frac{1}{2}\right)+\frac{\hbar\Omega}{2}\sigma^{z}+\hbar g(a^{\dagger}\sigma^{-}+\sigma^{+}a)+H_{\kappa}+H_{\gamma}. \tag{1}$$

Here H_{κ} describes the coupling of the cavity to the continuum which produces the cavity decay rate $\kappa=\omega_{\rm r}/Q$, while H_{γ} describes the coupling of the atom to modes other than the cavity mode which cause the excited state to decay at rate γ (and possibly also produce additional dephasing effects). An additional important parameter in the atomic case is the transit time $t_{\rm transit}$ of the atom through the cavity.

In the absence of damping, exact diagonalization of the Jaynes-Cumming Hamiltonian yields the excited eigenstates (dressed states) [15]

$$|\overline{+,n}\rangle=\cos\ \theta_n|\downarrow,n\rangle+\sin\ \theta_n|\uparrow,n+1\rangle, \tag{2}$$

$$|\overline{-,n}\rangle=-\sin\ \theta_n|\downarrow,n\rangle+\cos\ \theta_n|\uparrow,n+1\rangle, \tag{3}$$

and ground state $|\uparrow,0\rangle$ with corresponding eigenenergies

$$E_{\overline{\pm},n}=(n+1)\hbar\omega_{\rm r}\pm\frac{\hbar}{2}\sqrt{4g^{2}(n+1)+\Delta^{2}}, \tag{4}$$

$$E_{\uparrow,0}=-\frac{\hbar\Delta}{2}. \tag{5}$$

In these expressions,

$$\theta_n=\frac{1}{2}\tan^{-1}\left(\frac{2g\sqrt{n+1}}{\Delta}\right), \tag{6}$$

and $\Delta\equiv\Omega-\omega_{\rm r}$ the atom-cavity detuning.

Figure 1(b) shows the spectrum of these dressed states for the case of zero detuning, $\Delta=0$, between the atom and cavity. In this situation, degeneracy of the pair of states with $n+1$ quanta is lifted by $2g\sqrt{n+1}$ due to the atom-photon interaction. In the manifold with a single excitation, Eqs. (2) and (3) reduce to the maximally entangled atom-field states $|\overline{\pm,0}\rangle=(|\uparrow,1\rangle\pm|\downarrow,0\rangle)/\sqrt{2}$. An initial state with an excited atom and zero photons $|\uparrow,0\rangle$ will therefore flop into a photon $|\downarrow,1\rangle$ and back again at the vacuum Rabi frequency g/π. Since the excitation is half atom and half photon, the decay rate of $|\overline{\pm,0}\rangle$ is $(\kappa+\gamma)/2$. The pair of states $|\overline{\pm,0}\rangle$ will be resolved in a transmission experiment if the splitting $2g$ is larger than this linewidth. The value of $g=\mathcal{E}_{\rm rms}d/\hbar$ is determined by the transition dipole moment d and the rms zero-point electric field of the cavity mode. Strong coupling is achieved when $g\gg\kappa,\gamma$ [15].

TABLE I. Key rates and CQED parameters for optical [2] and microwave [3] atomic systems using 3D cavities, compared against the proposed approach using superconducting circuits, showing the possibility for attaining the strong cavity QED limit ($n_{\rm Rabi}\gg1$). For the 1D superconducting system, a full-wave ($L=\lambda$) resonator, $\omega_{\rm r}/2\pi=10$ GHz, a relatively low Q of 10^4, and coupling $\beta=C_g/C_{\Sigma}=0.1$ are assumed. For the 3D microwave case, the number of Rabi flops is limited by the transit time. For the 1D circuit case, the intrinsic Cooper-pair box decay rate is unknown; a conservative value equal to the current experimental upper bound $\gamma\leqslant1/(2\ \mu{\rm s})$ is assumed.

Parameter	Symbol	3D optical	3D microwave	1D circuit
Resonance or transition frequency	$\omega_{\rm r}/2\pi$, $\Omega/2\pi$	350 THz	51 GHz	10 GHz
Vacuum Rabi frequency	g/π, $g/\omega_{\rm r}$	220 MHz, 3×10^{-7}	47 kHz, 1×10^{-7}	100 MHz, 5×10^{-3}
Transition dipole	d/ea_0	~1	1×10^{3}	2×10^{4}
Cavity lifetime	$1/\kappa, Q$	10 ns, 3×10^{7}	1 ms, 3×10^{8}	160 ns, 10^{4}
Atom lifetime	$1/\gamma$	61 ns	30 ms	2 μs
Atom transit time	$t_{\rm transit}$	$\geqslant50$ μs	100 μs	∞
Critical atom number	$N_0=2\gamma\kappa/g^2$	6×10^{-3}	3×10^{-6}	$\leqslant6\times10^{-5}$
Critical photon number	$m_0=\gamma^2/2g^2$	3×10^{-4}	3×10^{-8}	$\leqslant1\times10^{-6}$
Number of vacuum Rabi flops	$n_{\rm Rabi}=2g/(\kappa+\gamma)$	~10	~5	$\sim10^{2}$

For large detuning, $g/\Delta \ll 1$, expansion of Eq. (4) yields the dispersive spectrum shown in Fig. 1(c). In this situation, the eigenstates of the one excitation manifold take the form [15]

$$|\overline{-,0}\rangle \sim -(g/\Delta)|\downarrow,0\rangle + |\uparrow,1\rangle, \tag{7}$$

$$|\overline{+,0}\rangle \sim |\downarrow,0\rangle + (g/\Delta)|\uparrow,1\rangle. \tag{8}$$

The corresponding decay rates are then simply given by

$$\Gamma_{\overline{-,0}} \simeq (g/\Delta)^2\gamma + \kappa, \tag{9}$$

$$\Gamma_{\overline{+,0}} \simeq \gamma + (g/\Delta)^2\kappa. \tag{10}$$

More insight into the dispersive regime is gained by making the unitary transformation

$$U = \exp\left[\frac{g}{\Delta}(a\sigma^+ - a^\dagger\sigma^-)\right] \tag{11}$$

and expanding to second order in g (neglecting damping for the moment) to obtain

$$UHU^\dagger \approx \hbar\left[\omega_r + \frac{g^2}{\Delta}\sigma^z\right]a^\dagger a + \frac{\hbar}{2}\left[\Omega + \frac{g^2}{\Delta}\right]\sigma^z. \tag{12}$$

As is clear from this expression, the atom transition is ac Stark/Lamb shifted by $(g^2/\Delta)(n+1/2)$. Alternatively, one can interpret the ac Stark shift as a dispersive shift of the cavity transition by $\sigma^z g^2/\Delta$. In other words, the atom pulls the cavity frequency by $\pm g^2/\kappa\Delta$.

III. CIRCUIT IMPLEMENTATION OF CAVITY QED

We now consider the proposed realization of cavity QED using the superconducing circuits shown in Fig. 2. A 1D transmission line resonator consisting of a full-wave section of superconducting coplanar waveguide plays the role of the cavity and a superconducting qubit plays the role of the atom. A number of superconducting quantum circuits could function as artificial atom, but for definiteness we focus here on the Cooper-pair box [6,16–18].

A. Cavity: Coplanar stripline resonator

An important advantage of this approach is that the zero-point energy is distributed over a very small effective volume ($\approx 10^{-5}$ cubic wavelengths) for our choice of a quasi-one-dimensional transmission line "cavity." As shown in Appendix A, this leads to significant rms voltages $V^0_{\rm rms} \sim \sqrt{\hbar\omega_r/cL}$ between the center conductor and the adjacent ground plane at the antinodal positions, where L is the resonator length and c is the capacitance per unit length of the transmission line. At a resonant frequency of 10 GHz ($h\nu/k_B \sim 0.5$ K) and for a 10 μm gap between the center conductor and the adjacent ground plane, $V_{\rm rms} \sim 2$ μV corresponding to electric fields $\mathcal{E}_{\rm rms} \sim 0.2$ V/m, some 100 times larger than achieved in the 3D cavity described in Ref. [3]. Thus, this geometry might also be useful for coupling to Rydberg atoms [19].

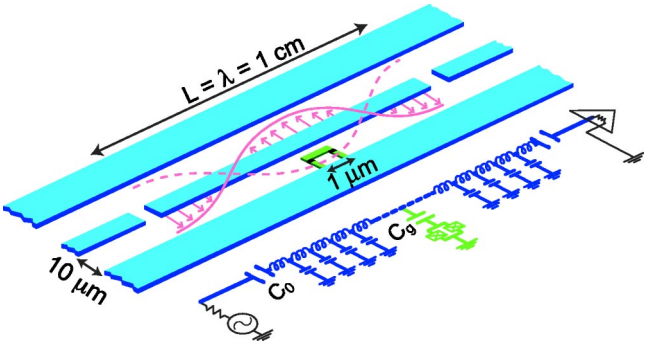

FIG. 2. (Color online). Schematic layout and equivalent lumped circuit representation of proposed implementation of cavity QED using superconducting circuits. The 1D transmission line resonator consists of a full-wave section of superconducting coplanar waveguide, which may be lithographically fabricated using conventional optical lithography. A Cooper-pair box qubit is placed between the superconducting lines and is capacitively coupled to the center trace at a maximum of the voltage standing wave, yielding a strong electric dipole interaction between the qubit and a single photon in the cavity. The box consists of two small ($\sim$100 nm$\times$100 nm) Josephson junctions, configured in a ~ 1 μm loop to permit tuning of the effective Josephson energy by an external flux $\Phi_{\rm ext}$. Input and output signals are coupled to the resonator, via the capacitive gaps in the center line, from 50Ω transmission lines which allow measurements of the amplitude and phase of the cavity transmission, and the introduction of dc and rf pulses to manipulate the qubit states. Multiple qubits (not shown) can be similarly placed at different antinodes of the standing wave to generate entanglement and two-bit quantum gates across distances of several millimeters.

In addition to the small effective volume and the fact that the on-chip realization of CQED shown in Fig. 2 can be fabricated with existing lithographic techniques, a transmission-line resonator geometry offers other practical advantages over lumped LC circuits or current-biased large Josephson junctions. The qubit can be placed within the cavity formed by the transmission line to strongly suppress the spontaneous emission, in contrast to a lumped LC circuit, where without additional special filtering, radiation and parasitic resonances may be induced in the wiring [20]. Since the resonant frequency of the transmission line is determined primarily by a fixed geometry, its reproducibility and immunity to $1/f$ noise should be superior to Josephson junction plasma oscillators. Finally, transmission-line resonances in coplanar waveguides with $Q \sim 10^6$ have already been demonstrated [21,22], suggesting that the internal losses can be very low. The optimal choice of the resonator Q in this approach is strongly dependent on the intrinsic decay rates of superconducting qubits which, as described below, are presently unknown, but can be determined with the setup proposed here. Here we assume the conservative case of an overcoupled resonator with a $Q \sim 10^4$, which is preferable for the first experiments.

B. Artificial atom: The Cooper-pair box

Our choice of "atom," the Cooper-pair box [6,16], is a mesoscopic superconducting island. As shown in Fig. 3, the

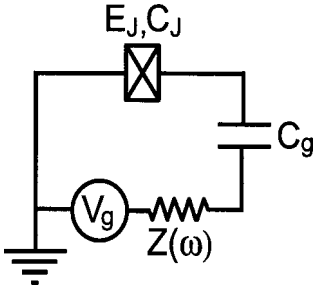

FIG. 3. Circuit diagram of the Cooper-pair box. The gate voltage is connected to the island through an environmental impedance $Z(\omega)$.

island is connected to a large reservoir through a Josephson junction with Josephson energy E_J and capacitance C_J. It is voltage biased from a lead having capacitance C_g to the island. If the superconducting gap is larger than both the charging energy $E_c=e^2/2C_\Sigma$ (where $C_\Sigma=C_J+C_g$ is the total box capacitance) and temperature, the only relevant degree of freedom is the number of Cooper pairs N on the island. In this basis, the Hamiltonian describing the superconducting island takes the form

$$H_Q = 4E_c\sum_N (N-N_g)^2|N\rangle\langle N| - \frac{E_J}{2}\sum_N (|N+1\rangle\langle N| + \text{H.c.}), \tag{13}$$

where $N_g=C_gV_g/2e$ is the dimensionless gate charge representing the total polarization charge injected into the island by the voltage source.

In the charge regime $4E_c \gg E_J$ and restricting the gate charge to the range $N_g \in [0,1]$, only a pair of adjacent charge states on the island are relevant and the Hamiltonian then reduces to a 2×2 matrix

$$H_Q = -\frac{E_{\rm el}}{2}\overline{\sigma^z} - \frac{E_J}{2}\overline{\sigma^x}, \tag{14}$$

with $E_{\rm el}=4E_C(1-2N_g)$. The Cooper-pair box can in this case be mapped to a pseudospin-1/2 particle, with effective fields in the x and z directions.

Replacing the Josephson junction by a pair of junctions in parallel, each with energy $E_J/2$, the effective field in the x direction becomes $E_J\cos(\pi\Phi_{\rm ext}/\Phi_0)/2$. By threading a flux $\Phi_{\rm ext}$ in the loop formed by the pair of junctions and changing the gate voltage V_g, it is possible to control the effective fields acting on the qubit. In the setup of Fig. 2, application of dc gate voltage on the island can be conveniently achieved by applying a bias voltage to the center conductor of the transmission line. The resonator coupling capacitance C_0, the gate capacitance C_g (the capacitance between the center conductor of the resonator and the island), and the capacitance to ground of the resonator then act as a voltage divider.

C. Combined system: Superconducting cavity QED

For a superconducting island fabricated inside a resonator, in addition to a dc part $V_g^{\rm dc}$, the gate voltage has a quantum part v. As shown in Appendix A, if the qubit is placed in the center of the resonator, this latter contribution is given by $v=V_{\rm rms}^0(a^\dagger+a)$. Taking into account both $V_{\rm g}^{\rm dc}$ and v in Eq. (14), we obtain

$$H_Q = -2E_C(1-2N_g^{\rm dc})\overline{\sigma^z} - \frac{E_J}{2}\overline{\sigma^x} - e\frac{C_g}{C_\Sigma}\sqrt{\frac{\hbar\omega_{\rm r}}{Lc}}(a^\dagger+a) \times(1-2N_g-\overline{\sigma^z}). \tag{15}$$

Working in the eigenbasis $\{|\uparrow\rangle,|\downarrow\rangle\}$ of the first two terms of the above expression [23] and adding the Hamiltonian of the oscillator mode coupled to the qubit, the Hamiltonian of the interacting qubit and resonator system takes the form

$$H = \hbar\omega_{\rm r}\left(a^\dagger a+\frac{1}{2}\right) + \frac{\hbar\Omega}{2}\sigma^z - e\frac{C_g}{C_\Sigma}\sqrt{\frac{\hbar\omega_{\rm r}}{Lc}}(a^\dagger+a) \times[1-2N_g-\cos(\theta)\sigma^z+\sin(\theta)\sigma^x]. \tag{16}$$

Here, σ^x and σ^z are Pauli matrices in the eigenbasis $\{|\uparrow\rangle,|\downarrow\rangle\}$, $\theta=\arctan[E_J/4E_C(1-2N_g^{\rm dc})]$ is the mixing angle, and the energy splitting of the qubit is $\Omega=\sqrt{E_J^2+[4E_C(1-2N_g^{\rm dc})]^2}/\hbar$ [23]. Note that contrary to the case of a qubit fabricated outside the cavity where the N_g^2 term in Eq. (13) has no effect, here this term slightly renormalizes the cavity frequency $\omega_{\rm r}$ and displaces the oscillator coordinate. These effects are implicit in Eq. (16).

At the charge degeneracy point (where $N_g^{\rm dc}=C_gV_g^{\rm dc}/2e=1/2$ and $\theta=\pi/2$), neglecting rapidly oscillating terms and omitting damping for the moment, Eq. (16) reduces to the Jaynes-Cummings Hamiltonian (1) with $\Omega=E_J/\hbar$ and coupling

$$g = \frac{\beta e}{\hbar}\sqrt{\frac{\hbar\omega_r}{cL}}, \tag{17}$$

where $\beta\equiv C_g/C_\Sigma$. The quantum electrical circuit of Fig. 2 is therefore mapped to the problem of a two-level atom inside a cavity. Away from the degeneracy point, this mapping can still be performed, but with a coupling strength reduced by $\sin(\theta)$ and an additional term proportional to $(a^\dagger+a)$.

In this circuit, the "atom" is highly polarizable at the charge degeneracy point, having transition dipole moment $d\equiv\hbar g/\mathcal{E}_{\rm rms}\sim 2\times 10^4$ atomic units (ea_0), or more than an order of magnitude larger than even a typical Rydberg atom [15]. An experimentally realistic [18] coupling $\beta\sim 0.1$ leads to a vacuum Rabi rate $g/\pi\sim 100$ MHz, which is three orders of magnitude larger than in corresponding atomic microwave CQED experiments [3] or approximately 1% of the transition frequency. Unlike the usual CQED case, these artificial "atoms" remain at fixed positions indefinitely and so do not suffer from the problem that the coupling g varies with position in the cavity.

A comparison of the experimental parameters for implementations of cavity QED with optical and microwave atomic systems and for the proposed implementation with superconducting circuits is presented in Table I. We assume here a relatively low $Q=10^4$ and a worst case estimate, con-

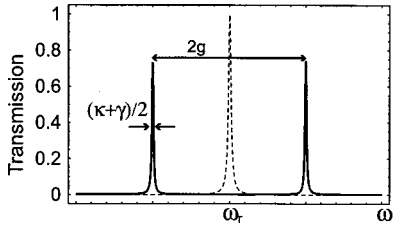

FIG. 4. Expected transmission spectrum of the resonator in the absence (dashed line) and presence (solid line) of a superconducting qubit biased at its degeneracy point. Parameters are those presented in Table I. The splitting exceeds the line width by two orders of magnitude.

sistent with the bound set by previous experiments with superconducting qubits (discussed further below), for the intrinsic qubit lifetime of $1/\gamma \geqslant 2\ \mu$s.

The standard figures of merit [24] for strong coupling are the critical photon number needed to saturate the atom on resonance, $m_0 = \gamma^2/2g^2 \leqslant 1\times 10^{-6}$, and the minimum atom number detectable by measurement of the cavity output, $N_0 = 2\gamma\kappa/g^2 \leqslant 6\times 10^{-5}$. These remarkably low values are clearly very favorable and show that superconducting circuits could access the interesting regime of very strong coupling.

IV. ZERO DETUNING

In the case of a low-Q cavity ($g < \kappa$) and zero detuning, the radiative decay rate of the qubit into the transmission line becomes strongly *enhanced* by a factor of Q relative to the rate in the absence of the cavity [15]. This is due to the resonant enhancement of the density of states at the atomic transition frequency. In electrical engineering language, the $\sim 50\Omega$ external transmission-line impedance is transformed on resonance to a high value which is better matched to extract energy from the qubit.

For strong coupling $g > \kappa, \gamma$, the first excited state becomes a doublet with linewidth $(\kappa+\gamma)/2$, as explained in Sec. II. As can be seen from Table I, the coupling in the proposed superconducting implementation is so strong that, even for the low $Q = 10^4$ we have assumed, $2g/(\kappa+\gamma) \sim 100$ vacuum Rabi oscillations are possible. Moreover, as shown in Fig. 4, the frequency splitting ($g/\pi \sim 100$ MHz) will be readily resolvable in the transmission spectrum of the resonator. This spectrum, calculated here following Ref. [25], can be observed in the same manner as employed in optical atomic experiments, with a continuous-wave measurement at low drive, and will be of practical use to find the dc gate voltage needed to tune the box into resonance with the cavity.

Of more fundamental importance than this simple avoided level crossing, however, is the fact that the Rabi splitting scales with the square root of the photon number, making the level spacing anharmonic. This should cause a number of novel nonlinear effects [14] to appear in the spectrum at higher drive powers when the average photon number in the cavity is large ($\langle n\rangle > 1$).

A conservative estimate of the noise energy for a 10 GHz cryogenic high-electron-mobility (HEMT) amplifier is $n_{\rm amp} = k_B T_N/\hbar\omega_r \sim 100$ photons, where T_N is the noise temperature of the amplification circuit. As a result, these spectral features should be readily observable in a measurement time $t_{\rm meas} = 2n_{\rm amp}/\langle n\rangle\kappa$ or only $\sim 32\ \mu$s for $\langle n\rangle \sim 1$.

V. LARGE DETUNING: LIFETIME ENHANCEMENT

For qubits *not* inside a cavity, fluctuation of the gate voltage acting on the qubit is an important source of relaxation and dephasing. As shown in Fig. 3, in practice the qubit's gate is connected to the voltage source through external wiring having, at the typical microwave transition frequency of the qubit, a real impedance of value close to the impedance of free space ($\sim 50\ \Omega$). The relaxation rate expected from purely quantum fluctuations across this impedance (spontaneous emission) is [18,23]

$$\frac{1}{T_1} = \frac{E_{\rm J}^2}{E_{\rm J}^2 + E_{\rm el}^2}\left(\frac{e}{\hbar}\right)^2 \beta^2 S_V(+\Omega), \tag{18}$$

where $S_V(+\Omega) = 2\hbar\Omega\ {\rm Re}[Z(\Omega)]$ is the spectral density of voltage fluctuations across the environmental impedance (in the quantum limit). It is difficult in most experiments to precisely determine the real part of the high-frequency environmental impedance presented by the leads connected to the qubit, but reasonable estimates [18] yield values of T_1 in the range of 1 μs.

For qubits fabricated inside a cavity, the noise across the environmental impedance does not couple directly to the qubit, but only indirectly through the cavity. For the case of strong detuning, coupling of the qubit to the continuum is therefore substantially reduced. One can view the effect of the detuned resonator as filtering out the vacuum noise at the qubit transition frequency or, in electrical engineering terms, as providing an impedance transformation which strongly *reduces* the real part of the environmental impedance seen by the qubit.

Solving for the normal modes of the resonator and transmission lines, including an input impedance R at each end of the resonator, the spectrum of voltage fluctuations as seen by the qubit fabricated in the center of the resonator can be shown to be well approximated by

$$S_V(\Omega) = \frac{2\hbar\omega_{\rm r}}{Lc}\frac{\kappa/2}{\Delta^2 + (\kappa/2)^2}. \tag{19}$$

Using this transformed spectral density in Eq. (18) and assuming a large detuning between the cavity and qubit, the relaxation rate due to vacuum fluctuations takes a form that reduces to $1/T_1 \equiv \gamma_\kappa = (g/\Delta)^2\kappa \sim 1/(64\ \mu{\rm s})$, at the qubit's degeneracy point. This is the result already obtained in Eq. (10) using the dressed-state picture for the coupled atom and cavity, except for the additional factor γ reflecting a loss of energy to modes outside of the cavity. For large detuning, damping due to spontaneous emission can be much less than κ.

One of the important motivations for this CQED experiment is to determine the various contributions to the qubit

decay rate so that we can understand their fundamental physical origins as well as engineer improvements. Besides γ_κ evaluated above, there are two additional contributions to the total damping rate $\gamma=\gamma_\kappa+\gamma_\perp+\gamma_{\rm NR}$. Here $\gamma_\perp$ is the decay rate into photon modes other than the cavity mode and $\gamma_{\rm NR}$ is the rate of other (possibly nonradiative) decays. Optical cavities are relatively open and $\gamma_\perp$ is significant, but for 1D microwave cavities, $\gamma_\perp$ is expected to be negligible (despite the very large transition dipole). For Rydberg atoms the two qubit states are both highly excited levels and $\gamma_{\rm NR}$ represents (radiative) decay out of the two-level subspace. For Cooper-pair boxes, $\gamma_{\rm NR}$ is completely unknown at the present time, but could have contributions from phonons, two-level systems in insulating [20] barriers and substrates, or thermally excited quasiparticles.

For Cooper box qubits *not* inside a cavity, recent experiments [18] have determined a relaxation time $1/\gamma=T_1 \sim 1.3\ \mu$s despite the backaction of continuous measurement by a SET electrometer. Vion *et al.* [17] found $T_1 \sim 1.84\ \mu$s (without measurement backaction) for their charge-phase qubit. Thus, in these experiments, if there are nonradiative decay channels, they are at most comparable to the vacuum radiative decay rate (and may well be much less) estimated using Eq. (18). Experiments with a cavity will present the qubit with a simple and well-controlled electromagnetic environment, in which the radiative lifetime can be enhanced with detuning to $1/\gamma_\kappa > 64\ \mu$s, allowing $\gamma_{\rm NR}$ to dominate and yielding valuable information about any nonradiative processes.

VI. DISPERSIVE QND READOUT OF QUBITS

In addition to lifetime enhancement, the dispersive regime is advantageous for readout of the qubit. This can be realized by microwave irradiation of the cavity and then probing the transmitted or reflected photons [26].

A. Measurement protocol

A drive of frequency $\omega_{\mu w}$ on the resonator can be modeled by [15]

$$H_{\mu w}(t)=\hbar\varepsilon(t)(a^\dagger e^{-i\omega_{\mu w}t}+ae^{+i\omega_{\mu w}t}), \tag{20}$$

where $\varepsilon(t)$ is a measure of the drive amplitude. In the dispersive limit, one expects from Fig. 1(c) peaks in the transmission spectrum at ω_r-g^2/Δ and $\Omega+2g^2/\Delta$ if the qubit is initially in its ground state. In a frame rotating at the drive frequency, the matrix elements for these transitions are, respectively,

$$\langle\uparrow,0|H_{\mu w}|\overline{-,n}\rangle \sim \varepsilon,$$

$$\langle\uparrow,0|H_{\mu w}|\overline{+,n}\rangle \sim \frac{\varepsilon g}{\Delta}. \tag{21}$$

In the large detuning case, the peak at $\Omega+2g^2/\Delta$, corresponding approximatively to a qubit flip, is highly suppressed.

The matrix element corresponding to a qubit flip from the excited state is also suppressed and, as shown in Fig. 5, depending on the qubit being in its ground or excited states, the transmission spectrum will present a peak of width κ at ω_r-g^2/Δ or ω_r+g^2/Δ. With the parameters of Table I, this dispersive pull of the cavity frequency is $\pm g^2/\kappa\Delta=\pm 2.5$ linewidths for a 10% detuning. Exact diagonalization (4) shows that the pull is power dependent and decreases in magnitude for cavity photon numbers on the scale $n=n_{\rm crit}\equiv\Delta^2/4g^2$. In the regime of nonlinear response, single-atom optical bistability [14] can be expected when the drive frequency is off resonance at low power but on resonance at high power [29].

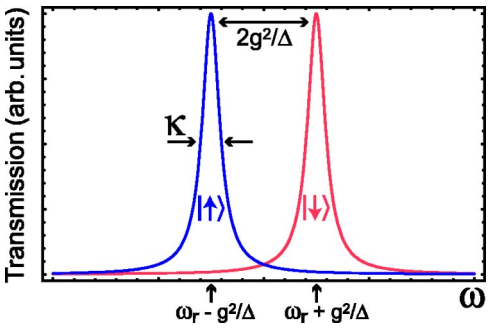

FIG. 5. (Color online) Transmission spectrum of the cavity, which is "pulled" by an amount $\pm g^2/\Delta=\pm 2.5\omega_r\times 10^{-4}$, depending on the state of the qubit (red for the excited state, blue for the ground state). To perform a measurement of the qubit, a pulse of microwave photons, at a probe frequency $\omega_{\mu w}=\omega_r$ or $\omega_r\pm g^2/\Delta$, is sent through the cavity. Additional peaks near Ω corresponding to qubit flips are suppressed by g/Δ.

The state-dependent pull of the cavity frequency by the qubit can be used to entangle the state of the qubit with that of the photons transmitted or reflected by the resonator. For $g^2/\kappa\Delta>1$, as in Fig. 5, the pull is greater than the linewidth, and irradiating the cavity at one of the pulled frequencies $\omega_r\pm g^2/\Delta$, the transmission of the cavity will be close to unity for one state of the qubit and close to zero for the other [30].

Choosing the drive to be instead at the bare cavity frequency ω_r, the state of the qubit is encoded in the phase of the reflected and transmitted microwaves. An initial qubit state $|\chi\rangle=\alpha|\uparrow\rangle+\beta|\downarrow\rangle$ evolves under microwave irradiation into the entangled state $|\psi\rangle=\alpha|\uparrow,\theta\rangle+\beta|\downarrow,-\theta\rangle$, where $\tan\theta=2g^2/\kappa\Delta$ and $|\pm\theta\rangle$ are (interaction representation) coherent states with the appropriate mean photon number and opposite phases. In the situation where $g^2/\kappa\Delta\ll 1$, this is the most appropriate strategy.

It is interesting to note that such an entangled state can be used to couple qubits in distant resonators and allow quantum communication [31]. Moreover, if an independent measurement of the qubit state can be made, such states can be turned into photon Schrödinger cats [15].

To characterize these two measurement schemes corresponding to two different choices of the drive frequency, we compute the average photon number inside the resonator $\overline{n}$ and the homodyne voltage on the 50Ω impedance at the output of the resonator. Since the power coupled to the outside of the resonator is $P=\langle n\rangle\hbar\omega_r\kappa/2=\langle V_{\rm out}\rangle^2/R$, the homodyne voltage can be expressed as $\langle V_{\rm out}\rangle=\sqrt{R\hbar\omega_r\kappa}\langle a+a^\dagger\rangle/2$ and is proportional to the real part of the field inside the cavity.

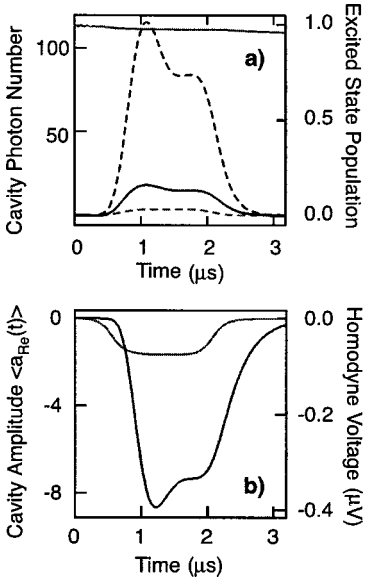

FIG. 6. (Color online) Results of numerical simulations using the quantum-state diffusion method. A microwave pulse of duration $\sim 15/\kappa$ and centered at the pulled frequency $\omega_r + g^2/\Delta$ drives the cavity. (a) The occupation probability of the excited state (right axis, solid lines), for the case in which the qubit is initially in the ground (blue) or excited (red) state and intracavity photon number (left axis, dash lines), are shown as a function of time. Though the qubit states are temporarily coherently mixed during the pulse, the probability of real transitions is seen to be small. Depending on the qubit's state, the pulse is either on or away from the combined cavity-qubit resonance and therefore is mostly transmitted or mostly reflected. (b) The real component of the cavity electric field amplitude (left axis) and the transmitted voltage phasor (right axis) in the output transmission line for the two possible initial qubit states. The parameters used for the simulation are presented in Table I.

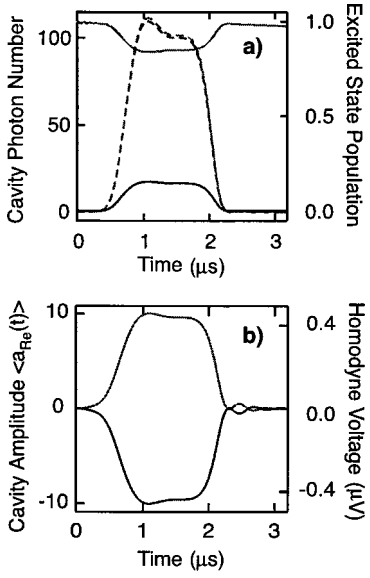

FIG. 7. (Color online) Same as Fig. 6 for the drive at the bare cavity frequency ω_r. Depending on the qubit's state, the pulse is either above or below the combined cavity-qubit resonance and so is partly transmitted and reflected but with a large relative phase shift that can be detected with homodyne detection. In (b), the opposing phase shifts cause a change in sign of the output, which can be measured with high signal to noise to realize a single-shot, QND measurement of the qubit.

In the absence of dissipation, the time dependence of the field inside the cavity can be obtained in the Heisenberg picture from Eqs. (12) and (20). This leads to a closed set of differential equations for a, σ^z, and $a\sigma^z$ which is easily solved. In the presence of dissipation, however [i.e., performing the transformation (11) on H_κ and H_γ, and adding the resulting terms to Eqs. (12) and (20)], the set is no longer closed and we resort to numerical stochastic wave function calculations [32]. See Appendix B for a brief presentation of this numerical method.

Figures 6 and 7 show the numerical results for the two choices of drive frequency and using the parameters of Table I. For these calculations, a pulse of duration $\sim 15/\kappa$ with a hyperbolic tangent rise and fall is used to excite the cavity. Figure 6 corresponds to a drive at the pulled frequency $\omega_r + g^2/\Delta$. In Fig. 6(a) the probability $P_\downarrow$ to find the qubit in its excited state (right axis) is plotted as a function of time for the qubit initially in the ground (blue) or excited state (red). The dashed lines represent the corresponding number of photons in the cavity (left axis). Figure 6(b) shows, in a frame rotating at the drive frequency, the real part of the cavity electric field amplitude (left axis) and transmitted voltage phase (right axis) in the output transmission line, again for the two possible initial qubit states. These quantities are shown in Fig. 7 for a drive at the bare frequency ω_r.

As expected, for the first choice of drive frequency, the information about the state of the qubit is mostly stored in the number of transmitted photons. When the drive is at the bare frequency, however, there is very little information in the photon number, with most of the information being stored in the phase of the transmitted and reflected signal. This phase shift can be measured using standard heterodyne techniques. As also discussed in Appendix C, both approaches can serve as a high-efficiency quantum nondemolition dispersive readout of the state of the qubit.

B. Measurement time and backaction

As seen from Eq. (12), the backaction of the dispersive CQED measurement is due to quantum fluctuations of the number of photons n within the cavity. These fluctuations cause variations in the ac Stark shift $(g^2/\Delta)n\sigma^z$, which in turn dephase the qubit. It is useful to compute the corresponding dephasing rate and compare it with the measurement rate—i.e., the rate at which information about the state of the qubit can be acquired.

To determine the dephasing rate, we assume that the cavity is driven at the bare cavity resonance frequency and that the pull of the resonance is small compared to the linewidth κ. The relative phase accumulated between the ground and excited states of the qubit is

$$\varphi(t) = 2\frac{g^2}{\Delta}\int_0^t dt' n(t'), \tag{22}$$

which yields a mean phase advance $\langle\varphi\rangle = 2\theta_0 N$ with $\theta_0 = 2g^2/\kappa\Delta$ and $N = \kappa\bar{n}t/2$ the total number of transmitted pho-

tons [14]. For weak coupling, the dephasing time will greatly exceed $1/\kappa$ and, in the long-time limit, the noise in φ induced by the ac Stark shift will be Gaussian. Dephasing can then be evaluated by computing the long-time decay of the correlator

$$\langle \sigma^+(t)\sigma^-(0)\rangle = \left\langle \exp\left(i\int_0^t dt'\varphi(t')\right)\right\rangle \simeq \exp\left[-\frac{1}{2}\left(2\frac{g^2}{\Delta}\right)^2 \int_0^t\int_0^t dt_1 dt_2 \langle n(t_1)n(t_2)\rangle\right]. \tag{23}$$

To evaluate this correlator in the presence of a continuous-wave (cw) drive on the cavity, we first perform a canonical transformation on the cavity operators $a^{(\dagger)}$ by writing them in terms of a classical $\alpha^{(*)}$ and a quantum part $d^{(\dagger)}$:

$$a(t) = \alpha(t) + d(t). \tag{24}$$

Under this transformation, the coherent state obeying $a|\alpha\rangle = \alpha|\alpha\rangle$ is simply the vacuum for the operator d. It is then easy to verify that

$$\langle [n(t) - \bar{n}][n(0) - \bar{n}]\rangle = \alpha^2\langle d(t)d^\dagger(0)\rangle = \bar{n}e^{-\kappa|t|/2}. \tag{25}$$

It is interesting to note that the factor of $1/2$ in the exponent is due to the presence of the coherent drive. If the resonator is not driven, the photon number correlator rather decays at a rate κ. Using this result in Eq. (23) yields the dephasing rate

$$\Gamma_\varphi = 4\theta_0^2\frac{\kappa}{2}\bar{n}. \tag{26}$$

Since the rate of transmission on resonance is $\kappa\bar{n}/2$, this means that the dephasing per transmitted photon is $4\theta_0^2$.

To compare this result to the measurement time $T_{\rm meas}$, we imagine a homodyne measurement to determine the transmitted phase. Standard analysis of such an interferometric setup [14] shows that the minimum phase change which can be resolved using N photons is $\delta\theta = 1/\sqrt{N}$. Hence the measurement time to resolve the phase change $\delta\theta = 2\theta_0$ is

$$T_{\rm m} = \frac{1}{2\kappa\bar{n}\theta_0^2}, \tag{27}$$

which yields

$$T_{\rm m}\Gamma_\varphi = 1. \tag{28}$$

This exceeds the quantum limit [33] $T_{\rm m}\Gamma_\varphi = 1/2$ by a factor of 2. Equivalently, in the language of Ref. [34] (which uses a definition of the measurement time twice as large as that above) the efficiency ratio is $\chi \equiv 1/(T_{\rm m}\Gamma_\varphi) = 0.5$.

The failure to reach the quantum limit can be traced [35] to the fact that that the coupling of the photons to the qubit is not adiabatic. A small fraction $R \approx \theta_0^2$ of the photons incident on the resonator are reflected rather than transmitted. Because the phase shift of the reflected wave [14] differs by π between the two states of the qubit, it turns out that, despite its weak intensity, the reflected wave contains precisely the same amount of information about the state of the qubit as the transmitted wave which is more intense but has a smaller phase shift. In the language of Ref. [34], this "wasted" information accounts for the excess dephasing relative to the measurement rate. By measuring also the phase shift of the reflected photons, it could be possible to reach the quantum limit.

Another form of possible backaction is mixing transitions between the two qubit states induced by the microwaves. First, as seen from Fig. 6(a) and 7(a), increasing the average number of photons in the cavity induces mixing. This is simply caused by dressing of the qubit by the cavity photons. Using the dressed states (2) and (3), the level of this coherent mixing can be estimated as

$$P_{\downarrow,\uparrow} = \frac{1}{2}\langle \pm,\bar{n}|\mathbb{1} \pm \sigma^z|\pm,\bar{n}\rangle \tag{29}$$

$$= \frac{1}{2}\left(1 \pm \frac{\Delta}{\sqrt{4g^2(n+1)+\Delta^2}}\right). \tag{30}$$

Exciting the cavity to $n = n_{\rm crit}$ yields $P_\downarrow \sim 0.85$. As is clear from the numerical results, this process is completely reversible and does not lead to errors in the readout.

The drive can also lead to real transitions between the qubit states. However, since the coupling is so strong, large detuning $\Delta = 0.1\ \omega_{\rm r}$ can be chosen, making the mixing rate limited not by the frequency spread of the drive pulse, but rather by the width of the qubit excited state itself. The rate of driving the qubit from ground to excited state when n photons are in the cavity is $R \approx n(g/\Delta)^2\gamma$. If the measurement pulse excites the cavity to $n = n_{\rm crit}$, we see that the excitation rate is still only 1/4 of the relaxation rate. As a result, the main limitation on the fidelity of this QND readout is the decay of the excited state of the qubit during the course of the readout. This occurs (for small γ) with probability $P_{\rm relax} \sim \gamma t_{\rm meas} \sim 15\gamma/\kappa \sim 3.75\%$ and leads to a small error $P_{\rm err} \sim 5\gamma/\kappa \sim 1.5\%$ in the measurement, where we have taken $\gamma = \gamma_\kappa$. As confirmed by the numerical calculations of Fig. 6 and 7, this dispersive measurement is therefore highly nondemolition.

C. Signal to noise

For homodyne detection in the case where the cavity pull $g^2/\Delta\kappa$ is larger than 1, the signal-to-noise ratio (SNR) is given by the ratio of the number of photons, $n_{\rm sig} = n\kappa\Delta t/2$, accumulated over an integration period Δt, divided by the detector noise $n_{\rm amp} = k_B T_N/\hbar\omega_{\rm r}$. Assuming the integration time to be limited by the qubit's decay time $1/\gamma$ and exciting the cavity to a maximal amplitude $n_{\rm crit} = 100 \sim n_{\rm amp}$, we obtain SNR $= (n_{\rm crit}/n_{\rm amp})(\kappa/2\gamma)$. If the qubit lifetime is longer than a few cavity decay times ($1/\kappa = 160$ ns), this SNR can be very large. In the most optimistic situation where $\gamma = \gamma_\kappa$, the signal-to-noise ratio is SNR = 200.

When taking into account the fact that the qubit has a finite probability to decay during the measurement, a better strategy than integrating the signal for a long time is to take advantage of the large SNR to measure quickly. Simulations have shown that in the situation where $\gamma = \gamma_\kappa$, the optimum

TABLE II. Figures of merit for readout and multiqubit entanglement of superconducting qubits using dispersive (off-resonant) coupling to a 1D transmission-line resonator. The same parameters as Table I and a detuning of the Cooper-pair box from the resonator of 10% ($\Delta=0.1\omega_r$) are assumed. Quantities involving the qubit decay γ are computed both for the theoretical lower bound $\gamma=\gamma_\kappa$ for spontaneous emission via the cavity and (in parentheses) for the current experimental upper bound $1/\gamma \geqslant 2$ μs. Though the signal to noise of the readout is very high in either case, the estimate of the readout error rate is dominated by the probability of qubit relaxation during the measurement, which has a duration of a few cavity lifetimes [$\sim(1-10)\kappa^{-1}$]. If the qubit nonradiative decay is low, both high-efficiency readout and more than 10^3 two-bit operations could be attained.

Parameter	Symbol	1D circuit
Dimensionless cavity pull	$g^2/\kappa\Delta$	2.5
Cavity-enhanced lifetime	$\gamma_\kappa^{-1}=(\Delta/g)^2\kappa^{-1}$	64 μs
Readout SNR	SNR $=(n_{\rm crit}/n_{\rm amp})\kappa/2\gamma$	200 (6)
Readout error	$P_{\rm err}\sim 5\times\gamma/\kappa$	1.5%(14%)
One-bit operation time	$T_\pi > 1/\Delta$	>0.16 ns
Entanglement time	$t_{\sqrt{i\rm SWAP}}=\pi\Delta/4g^2$	$\sim$0.05 μs
Two-bit operations	$N_{\rm op}=1/[\gamma\, t_{\sqrt{i\rm SWAP}}]$	>1200(40)

integration time is roughly 15 cavity lifetimes. This is the pulse length used for the stochastic numerical simulations shown above. The readout fidelity, including the effects of this stochastic decay, and related figures of merit of the single-shot high efficiency QND readout are summarized in Table II.

This scheme has other interesting features that are worth mentioning here. First, since nearly all the energy used in this dispersive measurement scheme is dissipated in the remote terminations of the input and output transmission lines, it has the practical advantage of avoiding quasiparticle generation in the qubit.

Another key feature of the cavity QED readout is that it lends itself naturally to operation of the box at the charge degeneracy point ($N_g=1/2$), where it has been shown that T_2 can be enormously enhanced [17] because the energy splitting has an extremum with respect to gate voltage and isolation of the qubit from $1/f$ dephasing is optimal. The derivative of the energy splitting with respect to gate voltage is the charge difference in the two qubit states. At the degeneracy point this derivative vanishes and the environment cannot distinguish the two states and thus cannot dephase the qubit. This also implies that a charge measurement cannot be used to determine the state of the system [4,5]. While the first derivative of the energy splitting with respect to gate voltage vanishes at the degeneracy point, the second derivative, corresponding to the difference in charge *polarizability* of the two quantum states, is *maximal*. One can think of the qubit as a nonlinear quantum system having a state-dependent capacitance (or in general, an admittance) which changes sign between the ground and excited states [36]. It is this change in polarizability which is measured in the dispersive QND measurement.

In contrast, standard charge measurement schemes [37,18] require moving away from the optimal point. Simmonds *et al.* [20] have recently raised the possibility that there are numerous parasitic environmental resonances which can relax the qubit when its frequency Ω is changed during the course of moving the operating point. The dispersive CQED measurement is therefore highly advantageous since it operates best at the charge degeneracy point. In general, such a measurement of an ac property of the qubit is strongly desirable in the usual case where dephasing is dominated by low-frequency ($1/f$) noise. Notice also that the proposed quantum nondemolition measurement would be the inverse of the atomic microwave CQED measurement in which the state of the photon field is inferred nondestructively from the phase shift in the state of atoms sent through the cavity [3].

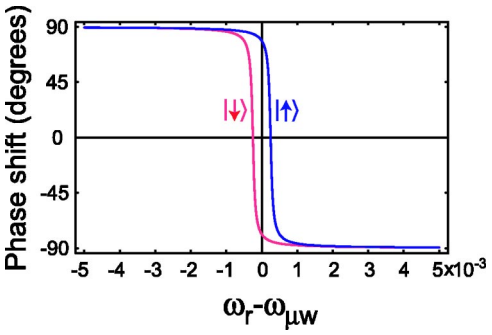

FIG. 8. (Color online) Phase shift of the cavity field for the two states of the qubit as a function of detuning between the driving and resonator frequencies. Obtained from the steady-state solution of the equation of motion for $a(t)$ while only taking into account damping on the cavity and using the parameters of Table I. Readout of the qubit is realized at, or close to, zero detuning between the drive and resonator frequencies where the dependence of the phase shift on the qubit state is largest. Coherent manipulations of the qubit are realized close to the qubit frequency which is 10% detuned from the cavity (not shown on this scale). At such large detunings, there is little dependence of the phase shift on the qubit's state.

VII. COHERENT CONTROL

While microwave irradiation of the cavity at its resonance frequency constitutes a measurement, irradiation close to the qubit's frequency can be used to coherently control the state of the qubit. In the former case, the phase shift of the transmitted wave is strongly dependent on the state of the qubit and hence the photons become entangled with the qubit, as shown in Fig. 8. In the latter case, however, driving is *not* a measurement because, for large detuning, the photons are largely reflected with a phase shift which is independent of the state of the qubit. There is therefore little entanglement between the field and qubit in this situation and the rotation fidelity is high.

To model the effect of the drive on the qubit, we add the microwave drive of Eq. (20) to the Jaynes-Cumming Hamiltonian (1) and apply the transformation (11) (again neglecting damping) to obtain the effective one-qubit Hamiltonian

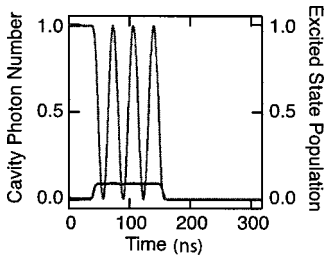

FIG. 9. (Color online) Numerical stochastic wave function simulation showing coherent control of a qubit by microwave irradiation of the cavity at the ac Stark- and Lamb-shifted qubit frequency. The qubit (red line) is first left to evolve freely for about 40 ns. The drive is turned on for $t=7\pi\Delta/2g\varepsilon\sim 115$ ns, corresponding to 7π pulses, and then turned off. Since the drive is tuned far away from the cavity, the cavity photon number (black line) is small even for the moderately large drive amplitude $\varepsilon=0.03\ \omega_r$ used here.

$$H_{1q}=\frac{\hbar}{2}\left[\Omega+2\frac{g^2}{\Delta}\left(a^\dagger a+\frac{1}{2}\right)-\omega_{\mu w}\right]\sigma^z+\hbar\frac{g\varepsilon(t)}{\Delta}\sigma^x+\hbar(\omega_r-\omega_{\mu w})a^\dagger a+\hbar\varepsilon(t)(a^\dagger+a) \tag{31}$$

in a frame rotating at the drive frequency $\omega_{\mu w}$. Choosing $\omega_{\mu w}=\Omega+(2n+1)g^2/\Delta$, H_{1q} generates rotations of the qubit about the x axis with Rabi frequency $g\varepsilon/\Delta$. Different drive frequencies can be chosen to realize rotations around arbitrary axes in the $x-z$ plane. In particular, choosing $\omega_{\mu w}=\Omega+(2n+1)g^2/\Delta-2g\varepsilon/\Delta$ and $t=\pi\Delta/2\sqrt{2}g\varepsilon$ generates the Hadamard transformation H. Since $H\sigma^xH=\sigma^z$, these two choices of frequency are sufficient to realize any one-qubit logical operation.

Assuming that we can take full advantage of lifetime enhancement inside the cavity (i.e., that $\gamma=\gamma_\kappa$), the number of π rotations about the x axis which can be carried out is $N_\pi=2\varepsilon\Delta/\pi g\kappa\sim 10^5\varepsilon$ for the experimental parameters assumed in Table I. For large ε, the choice of drive frequency must take into account the power dependence of the cavity frequency pulling.

Numerical simulation shown in Fig. 9 confirms this simple picture and that single-bit rotations can be performed with very high fidelity. It is interesting to note that since detuning between the resonator and the drive is large, the cavity is only virtually populated, with an average photon number $\bar{n}\approx\varepsilon^2/\Delta^2\sim 0.1$. Virtual population and depopulation of the cavity can be realized much faster than the cavity lifetime $1/\kappa$ and, as a result, the qubit feels the effect of the drive rapidly after the drive has been turned on. The limit on the speed of turn on and off of the drive is set by the detuning Δ. If the drive is turned on faster than $1/\Delta$, the frequency spread of the drive is such that part of the drive's photons will pick up phase information (see Fig. 8) and dephase the qubit. As a result, for large detuning, this approach leads to a fast and accurate way to coherently control the state of the qubit.

To model the effect of the drive on the resonator an alternative model is to use the cavity-modified Maxwell-Bloch equations [25]. As expected, numerical integration of the Maxwell-Bloch equations reproduce very well the stochastic numerical results when the drive is at the qubit's frequency but do *not* reproduce these numerical results when the drive is close to the bare resonator frequency (Figs. 6 and 7)—i.e., when entanglement between the qubit and photons cannot be neglected.

VIII. RESONATOR AS QUANTUM BUS: ENTANGLEMENT OF MULTIPLE QUBITS

The transmission-line resonator has the advantage that it should be possible to place multiple qubits along its length ($\sim$1 cm) and entangle them together, which is an essential requirement for quantum computation. For the case of two qubits, they can be placed closer to the ends of the resonator but still well isolated from the environment and can be separately dc biased by capacitive coupling to the left and right center conductors of the transmission line. Additional qubits would have to have separate gate bias lines installed.

For the pair of qubits labeled i and j, both coupled with strength g to the cavity and detuned from the resonator but in resonance with each other, the transformation (11) yields the effective two-qubit Hamiltonian [3,38,39]

$$H_{2q}\approx\hbar\left[\omega_r+\frac{g^2}{\Delta}(\sigma_i^z+\sigma_j^z)\right]a^\dagger a+\frac{1}{2}\hbar\left[\Omega+\frac{g^2}{\Delta}\right](\sigma_i^z+\sigma_j^z)+\hbar\frac{g^2}{\Delta}(\sigma_i^+\sigma_j^-+\sigma_i^-\sigma_j^+). \tag{32}$$

In addition to ac Stark and Lamb shifts, the last term couples the qubits through virtual excitations of the resonator.

In a frame rotating at the qubit's frequency Ω, H_{2q} generates the evolution

$$U_{2q}(t)=\exp\left[-i\frac{g^2}{\Delta}t\left(a^\dagger a+\frac{1}{2}\right)(\sigma_i^z+\sigma_j^z)\right]\times\begin{pmatrix}1&&&\\&\cos\frac{g^2}{\Delta}t&i\sin\frac{g^2}{\Delta}t&\\&i\sin\frac{g^2}{\Delta}t&\cos\frac{g^2}{\Delta}t&\\&&&1\end{pmatrix}\otimes\mathbb{1}_r, \tag{33}$$

where $\mathbb{1}_r$ is the identity operator in resonator space. Up to phase factors, this corresponds at $t=\pi\Delta/4g^2\sim 50$ ns to a $\sqrt{i\text{SWAP}}$ logical operation. Up to one-qubit gates, this operation is equivalent to the controlled-NOT gate. Together with one-qubit gates, the interaction H_{2q} is therefore sufficient for universal quantum computation [40]. Assuming again that we can take full advantage of the lifetime enhancement inside the cavity, the number of $\sqrt{i\text{SWAP}}$ operations which can be carried out is $N_{2q}=4\Delta/\pi\kappa\sim 1200$ for the parameters assumed above. This can be further improved if the qubit's nonradiative decay is sufficiently small and higher Q cavities are employed.

When the qubits are detuned from each other, the off-diagonal coupling provided by H_{2q} is only weakly effective and the coupling is for all practical purposes turned off. Two-

qubit logical gates in this setup can therefore be controlled by individually tuning the qubits. Moreover, single-qubit and two-qubit logical operations on different qubits and pairs of qubits can both be realized simultaneously, a requirement to reach presently known thresholds for fault-tolerant quantum computation [41].

It is interesting to point out that the dispersive QND readout presented in Sec. VI may be able to determine the state of multiple qubits in a single shot without the need for additional signal ports. For example, for the case of two qubits with different detunings, the cavity pull will take four different values $\pm g_1^2/\Delta_1 \pm g_2^2/\Delta_2$, allowing single-shot readout of the coupled system. This can in principle be extended to N qubits provided that the range of individual cavity pulls can be made large enough to distinguish all the combinations. Alternatively, one could read them out in small groups at the expense of having to electrically vary the detuning of each group to bring them into strong coupling with the resonator.

IX. ENCODED UNIVERSALITY AND DECOHERENCE-FREE SUBSPACE

Universal quantum computation can also be realized in this architecture under the encoding $\mathcal{L}=\{|\uparrow\downarrow\rangle,|\downarrow\uparrow\rangle\}$ by controlling only the qubit's detuning and, therefore, by turning on and off the interaction term in H_{2q} [42].

An alternative encoded two-qubit logical operation to the one suggested in Ref. [42] can be realized here by tuning the four qubits forming the pair of encoded qubits in resonance for a time $t=\pi\Delta/3g^2$. The resulting effective evolution operator can be written as $\hat{U}_{2q}=\exp[-i(\pi\Delta/3g^2)\hat{\sigma}_{x1}\hat{\sigma}_{x2}]$, where $\hat{\sigma}_{xi}$ is a Pauli operator acting on the ith encoded qubit. Together with encoded one-qubit operations, $\hat{U}_{2q}$ is sufficient for universal quantum computation using the encoding $\mathcal{L}$.

We point out that the subspace $\mathcal{L}$ is a decoherence-free subspace with respect to global dephasing [43] and use of this encoding will provide some protection against noise. The application of $\hat{U}_{2q}$ on the encoded subspace $\mathcal{L}$, however, causes temporary leakage out of this protected subspace. This is also the case with the approach of Ref. [42]. In the present situation, however, since the Hamiltonian generating $\hat{U}_{2q}$ commutes with the generator of global dephasing, this temporary excursion out of the protected subspace does not induce noise on the encoded qubit.

X. SUMMARY AND CONCLUSIONS

In summary, we propose that the combination of one-dimensional superconducting transmission-line resonators, which confine their zero-point energy to extremely small volumes, and superconducting charge qubits, which are electrically controllable qubits with large electric dipole moments, constitutes an interesting system to access the strong-coupling regime of cavity quantum electrodynamics. This combined system is an advantageous architecture for the coherent control, entanglement, and readout of quantum bits for quantum computation and communication. Among the practical benefits of this approach are the ability to suppress radiative decay of the qubit while still allowing one-bit operations, a simple and minimally disruptive method for readout of single and multiple qubits, and the ability to generate tunable two-qubit entanglement over centimeter-scale distances. We also note that in the structures described here, the emission or absorption of a single photon by the qubit is tagged by a sudden large change in the resonator transmission properties [29], making them potentially useful as single-photon sources and detectors.

ACKNOWLEDGEMENTS

We are grateful to David DeMille, Michel Devoret, Clifford Cheung, and Florian Marquardt for useful conversations. We also thank André-Marie Tremblay and the Canadian Foundation for Innovation for access to computing facilities. This work was supported in part by the National Security Agency (NSA) and Advanced Research and Development Activity (ARDA) under Army Research Office (ARO) Contract No. DAAD19-02-1-0045, NSF DMR-0196503, NSF DMR-0342157, the NSF ITR program under Grant No. DMR-0325580, the David and Lucile Packard Foundation, the W.M. Keck Foundation, and NSERC.

APPENDIX A: QUANTIZATION OF THE 1D TRANSMISSION-LINE RESONATOR

A transmission line of length L, whose cross-section dimension is much less then the wavelength of the transmitted signal, can be approximated by a 1D model. For relatively low frequencies it is well described by an infinite series of inductors with each node capacitively connected to ground, as shown in Fig. 2. Denoting the inductance per unit length l and the capacitance per unit length c, the Lagrangian of the circuit is

$$\mathcal{L}=\int_{-L/2}^{L/2} dx\left(\frac{l}{2}j^2-\frac{1}{2c}q^2\right), \tag{A1}$$

where $j(x,t)$ and $q(x,t)$ are the local current and charge density, respectively. We have ignored for the moment the two semi-infinite transmission lines capacitively coupled to the resonator. Defining the variable $\theta(x,t)$,

$$\theta(x,t)\equiv\int_{-L/2}^{x} dx' q(x',t), \tag{A2}$$

the Lagrangian can be rewritten as

$$L=\int_{-L/2}^{L/2} dx\left(\frac{l}{2}\dot{\theta}^2-\frac{1}{2c}(\nabla\theta)^2\right). \tag{A3}$$

The corresponding Euler-Lagrange equation is a wave equation with the speed $v=\sqrt{1/lc}$. Using the boundary conditions due to charge neutrality,

$$\theta(-L/2,t)=\theta(L/2,t)=0, \tag{A4}$$

we obtain

$$\theta(x,t) = \sqrt{\frac{2}{L}} \sum_{k_o=1}^{k_{o,\mathrm{cutoff}}} \phi_{k_o}(t)\cos\frac{k_o \pi x}{L} + \sqrt{\frac{2}{L}} \sum_{k_e=2}^{k_{e,\mathrm{cutoff}}} \phi_{k_e}(t)\sin\frac{k_e \pi x}{L}, \tag{A5}$$

for odd and even modes, respectively. For finite length L, the transmission line acts as a resonator with resonant frequencies $\omega_k = k\pi v/L$. The cutoff is determined by the fact that the resonator is not strictly one dimensional.

Using the normal-mode expansion (A5) in (A3), one obtains, after spatial integration, the Lagrangian in the form of a set of harmonic oscillators:

$$\mathcal{L} = \sum_k \frac{l}{2}\dot{\phi}_k^2 - \frac{1}{2c}\left(\frac{k\pi}{L}\right)^2 \phi_k^2. \tag{A6}$$

Promoting the variable ϕ_k and its canonically conjugated momentum $\pi_k = l\dot{\phi}_k$ to conjugate operators and introducing the boson creation and annihilation operators $a_k^\dagger$ and a_k satisfying $[a_k, a_{k'}^\dagger] = \delta_{kk'}$, we obtain the usual relations diagonalizing the Hamiltonian obtained from the Lagrangian (A6):

$$\hat{\phi}_k(t) = \sqrt{\frac{\hbar\omega_k c}{2}}\frac{L}{k\pi}[a_k(t) + a_k^\dagger(t)], \tag{A7}$$

$$\hat{\pi}_k(t) = -i\sqrt{\frac{\hbar\omega_k l}{2}}[a_k(t) - a_k^\dagger(t)]. \tag{A8}$$

From these relations, the voltage on the resonator can be expressed as

$$\begin{aligned} V(x,t) &= \frac{1}{c}\frac{\partial\,\theta(x,t)}{\partial x} \\ &= -\sum_{k_o=1}^{\infty} \sqrt{\frac{\hbar\omega_{k_o}}{Lc}}\sin\left(\frac{k_o\pi x}{L}\right)[a_{k_o}(t) + a_{k_o}^\dagger(t)] \\ &\quad + \sum_{k_e=1}^{\infty} \sqrt{\frac{\hbar\omega_{k_e}}{Lc}}\cos\left(\frac{k_e\pi x}{L}\right)[a_{k_e}(t) + a_{k_e}^\dagger(t)]. \end{aligned} \tag{A9}$$

In the presence of the two semi-infinite transmission lines coupled to the resonator, the Lagrangian (A3) and the boundary conditions (A4) are modified to take into account the voltage drop on the coupling capacitors C_0. Assuming no spatial extent for the capacitors C_0, the problem is still solvable analytically. Due to this coupling, the wave function can now extend outside of the central segment which causes a slight redshift, of order C_0/Lc, of the cavity resonant frequency.

As shown in Fig. 2, we assume the qubit to be fabricated at the center of the resonator. As a result, at low temperatures, the qubit is coupled to the mode $k=2$ of the resonator, which as an antinode of the voltage in its center. The rms voltage between the center conductor and the ground plane is then $V_{\mathrm{rms}}^0 = \sqrt{\hbar\omega_r/cL}$ with $\omega_r = \omega_2$ and the voltage felt by the qubit is $V(0,t) = V_{\mathrm{rms}}^0[a_2(t) + a_2^\dagger(t)]$. In the main body of this paper, we work only with this second harmonic and drop the mode index on the resonator operators.

APPENDIX B: TREATMENT OF DISSIPATION

The evolution of the total density matrix, including the qubit, cavity mode, and baths, is described by the von Neuman equation

$$\dot{\rho}_{tot} = -\frac{i}{\hbar}[H_{\mathrm{sys}} + H_\kappa + H_\gamma, \rho_{\mathrm{tot}}], \tag{B1}$$

where H_{sys} stands for the first three terms of Eq. (1) plus the drive Hamiltonian of Eq. (20). An explicit expression for H_κ can be found in Ref. [14]. When the coupling between the system (qubit plus cavity mode) and the baths is weak, the reduced density operator for the system can be shown to obey the master equation [14]

$$\dot{\rho} = -\frac{i}{\hbar}[H_{\mathrm{sys}}, \rho] - \frac{1}{2}\sum_{m=\{\kappa,\gamma\}} (L_m^\dagger L_m \rho + \rho L_m^\dagger L_m - 2L_m \rho L_m^\dagger) \tag{B2}$$

in the Markov approximation. Here, L_m are Lindblad operators describing the effect of the baths on the system and can be expressed as $L_\kappa = \sqrt{\kappa}a$ and $L_\gamma = \sqrt{\gamma}\sigma^-$. The effect of finite temperature and pure dephasing, for example, can also be taken into account easily by introducing additional Lindblad operators.

The master equation is solved numerically by truncating the cavity Hilbert space to N photons. This leads to $(2N)^2$ coupled differential equations which, for large N, can be difficult to solve in practice. An alternative approach is to write an equivalent stochastic differential equation for the wave function [32,44]. There exist different such "unravelings" of the master equation and here we use the quantum state diffusion equation [32,44]

$$\begin{aligned} |d\psi\rangle &= -\frac{i}{\hbar}H_{\mathrm{sys}}|\psi\rangle dt + \sum_m (L_m - \langle L_m\rangle_\psi)|\psi\rangle d\xi_m \\ &\quad - \frac{1}{2}\sum_m (L_m^\dagger L_m + \langle L_m^\dagger\rangle_\psi\langle L_m\rangle_\psi - 2\langle L_m^\dagger\rangle_\psi L_m)|\psi\rangle dt. \end{aligned} \tag{B3}$$

The $d\xi_m$ are complex independent Wiener processes satisfying for their ensemble averages

$$\overline{d\xi_m} = \overline{d\xi_m d\xi_n} = 0, \tag{B4}$$

$$\overline{d\xi_m^* d\xi_n} = \delta_{mn}dt. \tag{B5}$$

An advantage of this approach is that now only $2N$ coupled differential equations have to be solved. A drawback is that the results must be averaged over many realizations of the noise to obtain accurate results. Still, this leads to much less important memory usage and to speedup in the numerical calculations [32,45].

APPENDIX C: QUANTUM NONDEMOLITION MEASUREMENTS

Readout of a qubit can lead to both mixing and dephasing [23,33]. While dephasing is unavoidable, mixing of the measured observable can be eliminated in a QND measurement by choosing the qubit-measurement apparatus interaction such that the measured observable is a constant of motion. In that situation, the measurement-induced mixing is rather introduced in the operator conjugate to the operator being measured.

In the situation of interest in this paper, the operator being probed is σ^z and, from Eq. (12), the qubit-measurement apparatus interaction Hamiltonian is given for large detuning by $H_{\rm int}=(g^2/\Delta)\sigma^z a^\dagger a$, such that $[\sigma^z,H_{\rm int}]=0$. For σ^z to be a constant of motion also requires that it commute with the qubit Hamiltonian. This condition is also satisfied in Eq. (12).

That the measured observable is a constant of motion implies that repeated observations will yield the same result. This allows for the measurement result to reach arbitrary large accuracy by accumulating signal. In practice, however, there are always environmental dissipation mechanisms acting on the qubit independently of the readout. Even in a QND situation, these will lead to a finite mixing rate $1/T_1$ of the qubit in the course of the measurement. Hence, high fidelity can only be achieved by a strong measurement completed in a time $T_{\rm m}\ll T_1$. This simple point is not as widely appreciated as it should be.

[1] H. Mabuchi and A. Doherty, Science **298**, 1372 (2002).
[2] C. J. Hood, T. W. Lynn, A. C. Doherty, A. S. Parkins, and H. J. Kimble, Science **287**, 1447 (2000).
[3] J. Raimond, M. Brune, and S. Haroche, Rev. Mod. Phys. **73**, 565 (2001).
[4] A. Armour, M. Blencowe, and K. C. Schwab, Phys. Rev. Lett. **88**, 148301 (2002).
[5] E. K. Irish and K. Schwab, Phys. Rev. B **68**, 155311 (2003).
[6] Y. Makhlin, G. Schön, and A. Shnirman, Rev. Mod. Phys. **73**, 357 (2001).
[7] O. Buisson and F. Hekking, in *Macroscopic Quantum Coherence and Quantum Computing*, edited by D. V. Averin, B. Ruggiero, and P. Silvestrini (Kluwer, New York, 2001).
[8] F. Marquardt and C. Bruder, Phys. Rev. B **63**, 054514 (2001).
[9] F. Plastina and G. Falci, Phys. Rev. B **67**, 224514 (2003).
[10] A. Blais, A. Maassen van den Brink, and A. Zagoskin, Phys. Rev. Lett. **90**, 127901 (2003).
[11] W. Al-Saidi and D. Stroud, Phys. Rev. B **65**, 014512 (2001).
[12] C.-P. Yang, S.-I. Chu, and S. Han, Phys. Rev. A **67**, 042311 (2003).
[13] J. Q. You and F. Nori, Phys. Rev. B **68**, 064509 (2003).
[14] D. Walls and G. Milburn, *Quantum Optics* (Spinger-Verlag, Berlin, 1994).
[15] S. Haroche, in *Fundamental Systems in Quantum Optics* , edited by J. Dalibard, J. Raimond, and J. Zinn-Justin (Elsevier, New York, 1992), p. 767.
[16] V. Bouchiat, D. Vion, P. Joyez, D. Esteve, and M. Devoret, Phys. Scr. **T76**, 165 (1998).
[17] D. Vion, A. Aassime, A. Cottet, P. Joyez, H. Pothier, C. Urbina, D. Esteve, and M. Devoret, Science **296**, 886 (2002).
[18] K. Lehnert, K. Bladh, L. Spietz, D. Gunnarsson, D. Schuster, P. Delsing, and R. Schoelkopf, Phys. Rev. Lett. **90**, 027002 (2003).
[19] A. S. Sorensen, C. H. van der Wal, L. Childress, and M. D. Lukin, Phys. Rev. Lett. **92**, 063601 (2004).
[20] R. W. Simmonds, K. M. Lang, D. A. Hite, D. P. Pappas, and J. Martinis (unpublished).
[21] P. K. Day, H. G. LeDuc, B. A. Mazin, A. Vayonakis, and J. Zmuidzinas, Nature (London) **425**, 817 (2003).
[22] A. Wallraff and R. Schoelkopf (unpublished).
[23] R. Schoelkopf, A. Clerk, S. Girvin, K. Lehnert, and M. Devoret, *Quantum Noise in Mesoscopic Physics* (Kluwer Academic, Dordrecht, 2003), Chap. 9, pp. 175–203.
[24] H. Kimble, *Cavity Quantum Electrodynamics* (Academic Press, San Diego, 1994).
[25] C. Wang and R. Vyas, Phys. Rev. A **55**, 823 (1997).
[26] A lumped *LC* circuit was used in Refs. [27,28] to probe flux qubits in a different way.
[27] E. Il'ichev, N. Oukhanski, A. Izmalkov, T. Wagner, M. Grajcar, H.-G. Meyer, A. Y. Smirnov, A. Maassen van den Brink, M. Amin, and A. Zagoskin, Phys. Rev. Lett. **91**, 097906 (2003).
[28] A. Izmalkov, M. Grajcar, E. Il'ichev, T. Wagner, H.-G. Meyer, A. Smirnov, M. Amin, A. Maassen van den Brink, and A. Zagoskin, eprint cond-mat/0312332.
[29] S. Girvin, A. Blais, and R. Huang (unpublished).
[30] We note that for the case of $Q=10^6$, the cavity pull is a remarkable ±250 linewidths, but depending on the nonradiative decay rate of the qubit, this may be in the regime $\kappa<\gamma$, making the state measurement too slow.
[31] S. van Enk, J. Cirac, and P. Zoller, Science **279**, 2059 (1998).
[32] R. Schack and T. A. Brun, Comput. Phys. Commun. **102**, 210 (1997).
[33] M. Devoret and R. Schoelkopf, Nature (London) **406**, 1039 (2000).
[34] A. Clerk, S. Girvin, and A. Stone, Phys. Rev. B **67**, 165324 (2003).
[35] F. Marquardt (unpublished).
[36] D. Averin and C. Bruder, Phys. Rev. Lett. **91**, 057003 (2003).
[37] Y. Nakamura, Y. Pashkin, and J. Tsai, Nature (London) **398**, 786 (1999).
[38] A. Sørensen and K. Mølmer, Phys. Rev. Lett. **82**, 1971 (1999).
[39] S.-B. Zheng and G.-C. Guo, Phys. Rev. Lett. **85**, 2392 (2000).
[40] A. Barenco, C. Bennett, R. Cleve, D. DiVincenzo, N. Margolus, S. P, T. Sleator, J. Smolin, and H. Weinfurter, Phys. Rev. A **52**, 3457 (1995).
[41] D. Aharonov and M. Ben-Or, in *Proceedings of the 37th Annual Symposium on Foundations of Computer Science* (IEEE Computer Society Press, Los Alamitos, CA, 1996), p. 46.
[42] D. Lidar and L.-A. Wu, Phys. Rev. Lett. **88**, 017905 (2002).

[43] J. Kempe, D. Bacon, D. Lidar, and K. B. Whaley, Phys. Rev. A **63**, 042307 (2001).
[44] C. Gardiner and P. Zoller, *Quantum Noise* (Springer-Verlarg, Berlin, 2000).
[45] K. Molmer, Y. Castin, and J. Dalibard, J. Opt. Soc. Am. B **10**, 524 (1993).

coupled system by applying pulses of varying length. In Fig. 3b, Rabi oscillations are shown for the $|00\rangle$ to $|11\rangle$ transition. When the microwave frequency is detuned from resonance, the Rabi oscillations are accelerated (bottom four curves, to be compared with the fifth curve). After a π pulse which prepares the system in the $|10\rangle$ state, these oscillations are suppressed (second curve in Fig. 3b). After a 2π pulse they are revived (first curve in Fig. 3b). In the case of Fig. 3c, the qubit is first excited onto the $|10\rangle$ state by a π pulse, and a second pulse in resonance with the red sideband transition drives the system between the $|10\rangle$ and $|01\rangle$ states. The Rabi frequency depends linearly on the microwave amplitude, with a smaller slope compared to the bare qubit driving. During the time evolution of the coupled Rabi oscillations shown in Fig. 3b and c, the qubit and the oscillator experience a time-dependent entanglement, although the present data do not permit us to quantify it to a sufficient degree of confidence.

The sideband Rabi oscillations of Fig. 3 show a short coherence time ($\sim$3 ns), which we attribute mostly to the oscillator relaxation. To determine its relaxation time, we performed the following experiment. First, we excite the oscillator with a resonant low power microwave pulse. After a variable delay Δt, during which the oscillator relaxes towards $n = 0$, we start recording Rabi oscillations on the red sideband transition (see Fig. 4a for $\Delta t = 1$ ns). The decay of the oscillation amplitude as a function of Δt corresponds to an oscillator relaxation time of $\sim$6 ns (Fig. 4b), consistent with a quality factor of 100–150 estimated from the width of the υ_p resonance. The exponential fit (continuous line in Fig. 4b) shows an offset of $\sim$4% due to thermal effects. To estimate the higher bound of the sample temperature, we consider that the visibility of the oscillations presented here (Figs 2–4) is set by the detection efficiency and not by the state preparation. When related to the maximum signal of the qubit Rabi oscillations of $\sim$40%, the 4%-offset corresponds to $\sim$10% thermal occupation of oscillator excited states (an effective temperature of $\sim$60 mK). Consistently, we also observe low-amplitude red sideband oscillations without preliminary microwave excitation of the oscillator.

We have demonstrated coherent dynamics of a coupled superconducting two-level plus harmonic oscillator system, implying that the two subsystems are entangled. Increasing the coupling strength and the oscillator relaxation time should allow us to quantify the entanglement, as well as to study non-classical states of the oscillator. Our results provide strong indications that solid-state quantum devices could in future be used as elements for the manipulation of quantum information. □

Received 25 May; accepted 5 July 2004; doi:10.1038/nature02831.

1. Nielsen, M. A. & Chuang, I. L. *Quantum Computation and Quantum Information* (Cambridge Univ. Press, Cambridge, 2000).
2. Nakamura, Y. *et al.* Coherent control of macroscopic quantum states in a single-Cooper-pair box. *Nature* **398,** 786–788 (1999).
3. Vion, D. *et al.* Manipulating the quantum state of an electrical circuit. *Science* **296,** 886–889 (2002).
4. Yu, Y., Han, S., Chu, X., Chu, S. & Wang, Z. Coherent temporal oscillations of macroscopic quantum states in a Josephson junction. *Science* **296,** 889–892 (2002).
5. Martinis, J. M., Nam, S., Aumentado, J. & Urbina, C. Rabi oscillations in a large Josephson-junction qubit. *Phys. Rev. Lett.* **89,** 117901 (2002).
6. Chiorescu, I., Nakamura, Y., Harmans, C. J. P. M. & Mooij, J. E. Coherent quantum dynamics of a superconducting flux qubit. *Science* **299,** 1869–1871 (2003).
7. Pashkin, Yu. A. *et al.* Quantum oscillations in two coupled charge qubits. *Nature* **421,** 823–826 (2003).
8. Berkley, A. J. *et al.* Entangled macroscopic quantum states in two superconducting qubits. *Science* **300,** 1548–1550 (2003).
9. Majer, J. B., Paauw, F. G., ter Haar, A. C. J., Harmans, C. J. P. M. & Mooij, J. E. Spectroscopy on two coupled flux qubits. Preprint at ⟨http://arxiv.org/abs/cond-mat/0308192⟩ (2003).
10. Izmalkov, A. *et al.* Experimental evidence for entangled states formation in a system of two coupled flux qubits. Preprint at ⟨http://arxiv.org/abs/cond-mat/0312332⟩ (2003).
11. Yamamoto, T., Pashkin, Yu. A., Astafiev, O., Nakamura, Y. & Tsai, J. S. Demonstration of conditional gate operation using superconducting charge qubits. *Nature* **425,** 941–944 (2003).
12. Leibfried, D., Blatt, R., Monroe, C. & Wineland, D. Quantum dynamics of single trapped ions. *Rev. Mod. Phys.* **75,** 281–324 (2003).
13. Mandel, O. *et al.* Controlled collisions for multi-particle entanglement of optically trapped atoms. *Nature* **425,** 937–940 (2003).
14. Raimond, J. M., Brune, M. & Haroche, S. Manipulating quantum entanglement with atoms and photons in a cavity. *Rev. Mod. Phys.* **73,** 565–582 (2001).
15. Mooij, J. E. *et al.* Josephson persistent-current qubit. *Science* **285,** 1036–1039 (1999).
16. van der Wal, C. H. *et al.* Quantum superposition of macroscopic persistent-current states. *Science* **290,** 773–777 (2000).
17. Burkard, G. *et al.* Asymmetry and decoherence in double-layer persistent-current qubit. Preprint at ⟨http://arxiv.org/abs/cond-mat/0405273⟩ (2004).
18. Goorden, M. C., Thorwart, M. & Grifoni, M. Entanglement spectroscopy of a driven solid-state qubit and its detector. Preprint at ⟨http://arxiv.org/abs/cond-mat/0405220⟩ (2004).
19. Tinkham, M. *Introduction to Superconductivity* 2nd edn (McGraw-Hill, New York, 1996).
20. Cohen-Tannoudji, C., Dupont-Roc, J. & Grynberg, G. *Atom-photon Interactions: Basic Processes and Applications* Ch. II E (Wiley & Sons, New York, 1992).

Acknowledgements We thank A. Blais, G. Burkard, D. DiVincenzo, G. Falci, M. Grifoni, S. Lloyd, S. Miyashita, T. Orlando, R. N. Schouten, L. Vandersyepen and F. K. Wilhelm for discussions. This work was supported by the Dutch Foundation for Fundamental Research on Matter (FOM), the EU Marie Curie and SQUBIT grants, and the US Army Research Office.

Competing interests statement The authors declare that they have no competing financial interests.

Correspondence and requests for materials should be addressed to I.C. (chiorescu@pa.msu.edu) and J.E.M. (mooij@qt.tn.tudelft.nl).

Strong coupling of a single photon to a superconducting qubit using circuit quantum electrodynamics

A. Wallraff[1], D. I. Schuster[1], A. Blais[1], L. Frunzio[1], R.- S. Huang[1,2], J. Majer[1], S. Kumar[1], S. M. Girvin[1] & R. J. Schoelkopf[1]

[1]*Departments of Applied Physics and Physics, Yale University, New Haven, Connecticut 06520, USA*
[2]*Department of Physics, Indiana University, Bloomington, Indiana 47405, USA*

The interaction of matter and light is one of the fundamental processes occurring in nature, and its most elementary form is realized when a single atom interacts with a single photon. Reaching this regime has been a major focus of research in atomic physics and quantum optics[1] for several decades and has generated the field of cavity quantum electrodynamics[2,3]. Here we perform an experiment in which a superconducting two-level system, playing the role of an artificial atom, is coupled to an on-chip cavity consisting of a superconducting transmission line resonator. We show that the strong coupling regime can be attained in a solid-state system, and we experimentally observe the coherent interaction of a superconducting two-level system with a single microwave photon. The concept of circuit quantum electrodynamics opens many new possibilities for studying the strong interaction of light and matter. This system can also be exploited for quantum information processing and quantum communication and may lead to new approaches for single photon generation and detection.

In atomic cavity quantum electrodynamics (QED), an isolated atom with electric dipole moment d interacts with the vacuum state electric field E_0 of a cavity. The quantum nature of the field gives rise to coherent oscillations of a single excitation between the atom and the cavity at the vacuum Rabi frequency $\nu_{\mathrm{Rabi}} = 2dE_0/h$, which can be observed when ν_{Rabi} exceeds the rates of relaxation and decoherence of both the atom and the field. This effect has been observed in the time domain using Rydberg atoms in three-dimensional microwave cavities[3] and spectroscopically using alkali atoms in very small optical cavities with large vacuum fields[4].

Coherent quantum effects have been recently observed in several superconducting circuits[5–10], making these systems well suited for use as quantum bits (qubits) for quantum information processing.

Of the various superconducting qubits, the Cooper pair box[11] is especially well suited for cavity QED because of its large effective electric dipole moment d, which can be 10^4 times larger than in an alkali atom and ten times larger than a typical Rydberg atom[12]. As suggested in our earlier theoretical study[12], the simultaneous combination of this large dipole moment and the large vacuum field strength—due to the small size of the quasi one-dimensional transmission line cavity—in our implementation is ideal for reaching the strong coupling limit of cavity QED in a circuit. Other solid-state analogues of strong coupling cavity QED have been envisaged in superconducting[13–20], semiconducting[21,22], and even micromechanical systems[23]. First steps towards realizing such a regime have been made for semiconductors[21,24,25]. To our knowledge, our experiments constitute the first experimental observation of strong coupling cavity QED with a single artificial atom and a single photon in a solid-state system.

The on-chip cavity is made by patterning a thin superconducting film deposited on a silicon chip. The quasi-one-dimensional coplanar waveguide resonator[26] consists of a narrow centre conductor of length l and two nearby lateral ground planes, see Fig. 1a. Close to its full-wave ($l = \lambda$) resonance frequency, $\omega_r = 2\pi\nu_r = 1/\sqrt{LC} = 2\pi\,6.044\,\mathrm{GHz}$, where ν_r is the bare resonance frequency, the resonator can be modelled as a parallel combination of a capacitor C and an inductor L (the internal losses are negligible). This simple resonant circuit behaves as a harmonic oscillator described by the hamiltonian $H_r = \hbar\omega_r(a^\dagger a + 1/2)$, where $\langle a^\dagger a\rangle = \langle \hat{n}\rangle = n$ is the average photon number. At our operating temperature of $T < 100\,\mathrm{mK}$, much less than $\hbar\omega_r/k_B \approx 300\,\mathrm{mK}$, the resonator is nearly in its ground state, with a thermal occupancy $n < 0.06$. The vacuum fluctuations of the resonator give rise to a root mean square (r.m.s.) voltage $V_{rms} = \sqrt{\hbar\omega_r/2C} \approx 1\,\mu\mathrm{V}$ on its centre conductor, and an electric field between the centre conductor and the ground plane that is a remarkable $E_{rms} \approx 0.2\,\mathrm{V\,m^{-1}}$, some hundred times larger than in the three-dimensional cavities used in atomic microwave cavity QED[3]. The large vacuum field strength results from the extremely small effective mode volume ($\sim 10^{-6}$ cubic wavelengths) of the resonator[12].

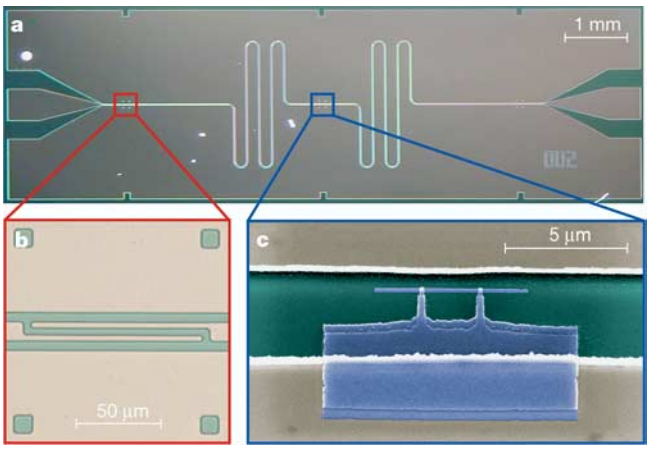

Figure 1 Integrated circuit for cavity QED. **a**, The superconducting niobium coplanar waveguide resonator is fabricated on an oxidized $10 \times 3\,\mathrm{mm}^2$ silicon chip using optical lithography. The width of the centre conductor is 10 μm separated from the lateral ground planes extending to the edges of the chip by a gap of width 5 μm resulting in a wave impedance of the structure of $Z = 50\,\Omega$ being optimally matched to conventional microwave components. The length of the meandering resonator is $l = 24\,\mathrm{mm}$. It is coupled by a capacitor at each end of the resonator (see **b**) to an input and output feed line, fanning out to the edge of the chip and keeping the impedance constant. **b**, The capacitive coupling to the input and output lines and hence the coupled quality factor Q is controlled by adjusting the length and separation of the finger capacitors formed in the centre conductor. **c**, False colour electron micrograph of a Cooper pair box (blue) fabricated onto the silicon substrate (green) into the gap between the centre conductor (top) and the ground plane (bottom) of a resonator (beige) using electron beam lithography and double angle evaporation of aluminium. The Josephson tunnel junctions are formed at the overlap between the long thin island parallel to the centre conductor and the fingers extending from the much larger reservoir coupled to the ground plane.

The resonator is coupled via two coupling capacitors $C_{in/out}$, one at each end (see Fig. 1b), to the input and output transmission lines that allow its microwave transmission to be probed (see Fig. 2a–c). The predominant source of dissipation is the loss of photons from the resonator through these ports at a rate $\kappa = \omega_r/Q$, where Q is the (loaded) quality factor of the resonator. The internal (uncoupled) loss of the resonator is negligible ($Q_{int} \approx 10^6$). Thus, the average photon lifetime in the resonator $T_r = 1/\kappa$ exceeds 100 ns, even for our initial choice of a moderate quality factor $Q \approx 10^4$.

The Cooper pair box (CPB) consists of a several micrometre long and submicrometre wide superconducting island which is coupled via two submicrometre size Josephson tunnel junctions to a much larger superconducting reservoir, and is fabricated in the gap between the centre conductor and the ground plane of the resonator, at an antinode of the field (see Fig. 1c). The CPB is a two-state system described by the hamiltonian[13] $H_a = -(E_{el}\sigma_x + E_J\sigma_z)/2$, where $E_{el} = 4E_C(1 - n_g)$ is the electrostatic energy and $E_J = E_{J,max}\cos(\pi\Phi_b)$ is the Josephson energy. The overall energy scales of these terms, the charging energy E_C and the Josephson energy $E_{J,max}$, can be readily engineered during the fabrication by the choice of the total box capacitance and resistance respectively, and then further tuned in situ by electrical means. A gate voltage V_g applied to the input port (see Fig. 2a), induces a gate charge $n_g = V_g C_g^\star/e$ that controls E_{el}, where $C_g^\star$ is the effective capacitance between the input port of the resonator and the island of the CPB. A flux bias $\Phi_b = \Phi/\Phi_0$, applied with an external coil to the loop of the box, controls E_J. Denoting the ground state of the box as $|\downarrow\rangle$ and the first excited state as $|\uparrow\rangle$ (see Fig. 2d), we have a two-level system whose energy separation $E_a = \hbar\omega_a$ can be widely varied as shown in Fig. 3c. Coherence of the CPB is limited by relaxation from the excited state at a rate γ_1, and by fluctuations of the level separation giving rise to dephasing at a rate γ_φ, for a total decoherence rate $\gamma = \gamma_1/2 + \gamma_\varphi$ (ref. 13).

The Cooper pair box couples to photons stored in the resonator by an electric dipole interaction, via the coupling capacitance C_g. The vacuum voltage fluctuations V_{rms} on the centre conductor of the resonator change the energy of a Cooper pair on the box island by an amount $\hbar g = dE_0 = eV_{rms}C_g/C_\Sigma$. We have shown[12] that this coupled system is described by the Jaynes–Cummings hamiltonian $H_{JC} = H_r + H_a + \hbar g(a^\dagger\sigma^- + a\sigma^+)$, where σ^+ (σ^-) creates (annihilates) an excitation in the CPB. It describes the coherent exchange of energy between a quantized electromagnetic field and a quantum two-level system at a rate $g/2\pi$, which is observable if g is much larger than the decoherence rates γ and κ. This strong coupling limit[3] $g > [\gamma, \kappa]$ is achieved in our experiments. When the detuning $\Delta = \omega_a - \omega_r$ is equal to zero, the eigenstates of the coupled system are symmetric and antisymmetric superpositions of a single photon and an excitation in the CPB $|\pm\rangle = (|0,\uparrow\rangle \pm |1,\downarrow\rangle)/\sqrt{2}$ with energies $E_\pm = \hbar(\omega_r \pm g)$. Although the cavity and the CPB are entangled in the eigenstates $|\pm\rangle$, their entangled character is not addressed in our current cavity QED experiment which spectroscopically probes the energies $E_\pm$ of the coherently coupled system.

The strong coupling between the field in the resonator and the CPB can be used to perform a quantum nondemolition (QND) measurement of the state of the CPB in the non-resonant (dispersive) limit $|\Delta| \gg g$. Diagonalization of the coupled quantum system leads to the effective hamiltonian[12]:

$$H \approx \hbar\left(\omega_r + \frac{g^2}{\Delta}\sigma_z\right)a^\dagger a + \frac{1}{2}\hbar\left(\omega_a + \frac{g^2}{\Delta}\right)\sigma_z$$

The transition frequency $\omega_r \pm g^2/\Delta$ is now conditioned by the qubit state $\sigma_z = \pm 1$. Thus, by measuring the transition frequency of the resonator, the qubit state can be determined. Similarly, the level separation in the qubit $\hbar(\omega_a + 2a^\dagger a\ g^2/\Delta + g^2/\Delta)$ depends on the number of photons in the resonator. The term $2a^\dagger a\ g^2/\Delta$, linear in $\hat{n}$, is the alternating current (a.c.) Stark shift and g^2/Δ is the Lamb shift. All terms in this hamiltonian, with the exception of the Lamb shift, are clearly identified in the results of our circuit QED experiments.

The properties of this coupled system are determined by probing the resonator spectroscopically[12]. The amplitude T and phase ϕ of a microwave probe beam of power P_{RF} transmitted through the resonator are measured versus probe frequency ω_{RF}. A simplified schematic of the microwave circuit is shown in Fig. 2a. In this set-up, the CPB acts as an effective capacitance that is dependent on its σ_z eigenstate, the coupling strength g, and detuning Δ. This variable capacitance changes the resonator frequency and its transmission spectrum. The transmission T^2 and phase ϕ of the resonator for a far-detuned qubit ($g^2/\kappa\Delta \ll 1$), that is, when the qubit is effectively decoupled from the resonator, are shown in Fig. 2b and c. In this case, the transmission is a lorentzian of width $\delta\nu_r = \nu_r/Q = \kappa/2\pi$ at ν_r, and the phase ϕ displays a corresponding step of π. The expected transmission at smaller detuning corresponding to a frequency shift $\pm g^2/\Delta = \kappa$ are shown by dashed lines in Fig. 2b and c. Such small shifts in the resonator frequency are sensitively measured as a phase shift $\phi = \pm\tan^{-1}(2g^2/\kappa\Delta)$ of the transmitted microwave at a fixed probe frequency ω_{RF} using beam powers P_{RF} which controllably populate the resonator with average photon numbers from $n \approx 10^3$ down to the sub-photon level $n \ll 1$. We note that both the resonator and qubit can be controlled and measured using capacitive and inductive coupling only, that is, without attaching any d.c. connections to either system.

Measurements of the phase ϕ versus n_g are shown in Fig. 3b, and two different cases can be identified for a Cooper pair box with Josephson energy $E_{J,max}/h > \nu_r$. In the first case, for bias fluxes such that $E_J(\Phi_b)/h > \nu_r$, the qubit does not come into resonance with the resonator for any value of gate charge n_g (see Fig. 3a). As a result, the measured phase shift ϕ is maximum for the smallest detuning Δ at $n_g = 1$ and gets smaller as Δ increases (see Fig. 3b). Moreover, ϕ is periodic in n_g with a period of $2e$, as expected. In the second case, for values of Φ_b resulting in $E_J(\Phi_b)/h < \nu_r$, the qubit goes through resonance with the resonator at two values of n_g. Thus, the phase shift ϕ is largest as the qubit approaches resonance ($\Delta \rightarrow 0$) at the points indicated by red arrows (see Fig. 3a, b). As the qubit goes through resonance, the phase shift ϕ changes sign when Δ changes sign. This behaviour is in perfect agreement with predictions based on the analysis of the circuit QED hamiltonian in the dispersive regime.

In Fig. 3c the qubit level separation $\nu_a = E_a/h$ is plotted versus the bias parameters n_g and Φ_b. The qubit is in resonance with the resonator at the points $[n_g, \Phi_b]$, indicated by the red curve in one quadrant of the plot. The measured phase shift ϕ is plotted versus

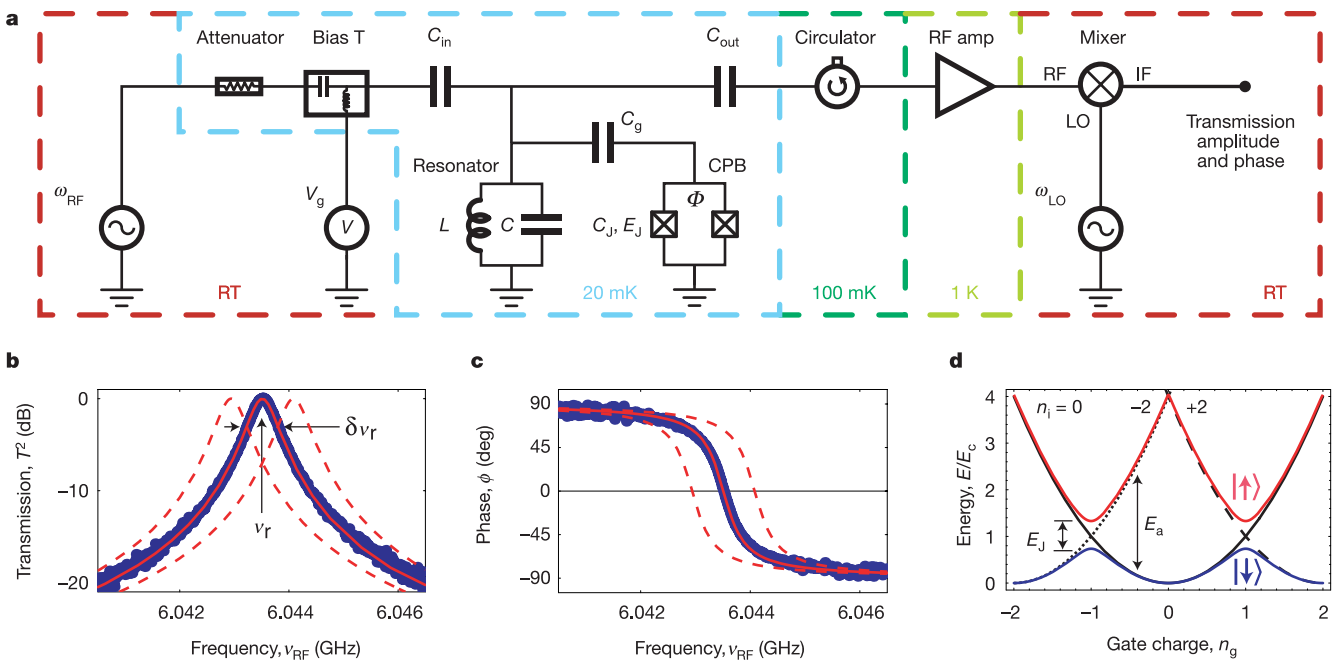

Figure 2 Measurement scheme, resonator and Cooper pair box. **a**, The resonator with effective inductance L and capacitance C coupled through the capacitor C_g to the Cooper pair box with junction capacitance C_J and Josephson energy E_J forms the circuit QED system which is coupled through $C_{in/out}$ to the input/output ports. The value of E_J is controllable by the magnetic flux Φ. The input microwave at frequency ω_{RF} is added to the gate voltage V_g using a bias-tee. After the transmitted signal at ω_{RF} is amplified using a cryogenic high electron mobility (HEMT) amplifier and mixed with the local oscillator at ω_{LO}, its amplitude and phase are determined. The circulator and the attenuator prevent leakage of thermal radiation into the resonator. The temperature of individual components is indicated. **b**, Measured transmission power spectrum of the resonator (blue dots), the full linewidth $\delta\nu_r$ at half-maximum and the centre frequency ν_r are indicated. The solid red line is a fit to a lorentzian with $Q = \nu_r/\delta\nu_r \approx 10^4$. **c**, Measured transmission phase ϕ (blue dots) with fit (red line). In panels **b** and **c** the dashed lines are theory curves shifted by $\pm\delta\nu_r$ with respect to the data. **d**, Energy level diagram of a Cooper pair box. The electrostatic energy $E_C(n_i - n_g)^2$, with charging energy $E_C = e^2/2C_\Sigma$, is indicated for $n_i = 0$ (solid black line), -2 (dotted line) and $+2$ (dashed line) excess electrons forming Cooper pairs on the island. C_Σ is the total capacitance of the island given by the sum of the capacitances C_J of the two tunnel junctions, the coupling capacitance C_g to the centre conductor of the resonator and any stray capacitances. In the absence of Josephson tunnelling the states with n_i and $n_i + 2$ electrons on the island are degenerate at $n_g = 1$. The Josephson coupling mediated by the weak link formed by the tunnel junctions between the superconducting island and the reservoir lifts this degeneracy and opens up a gap proportional to the Josephson energy $E_J = E_{J,max}\cos(\pi\Phi_b)$, where $E_{J,max} = h\Delta_{Al}/8e^2R_J$, with the superconducting gap of aluminium Δ_{Al} and the tunnel junction resistance R_J. A ground-state band $|\downarrow\rangle$ and an excited-state band $|\uparrow\rangle$ are formed with a gate charge and flux-bias-dependent energy level separation of E_a.

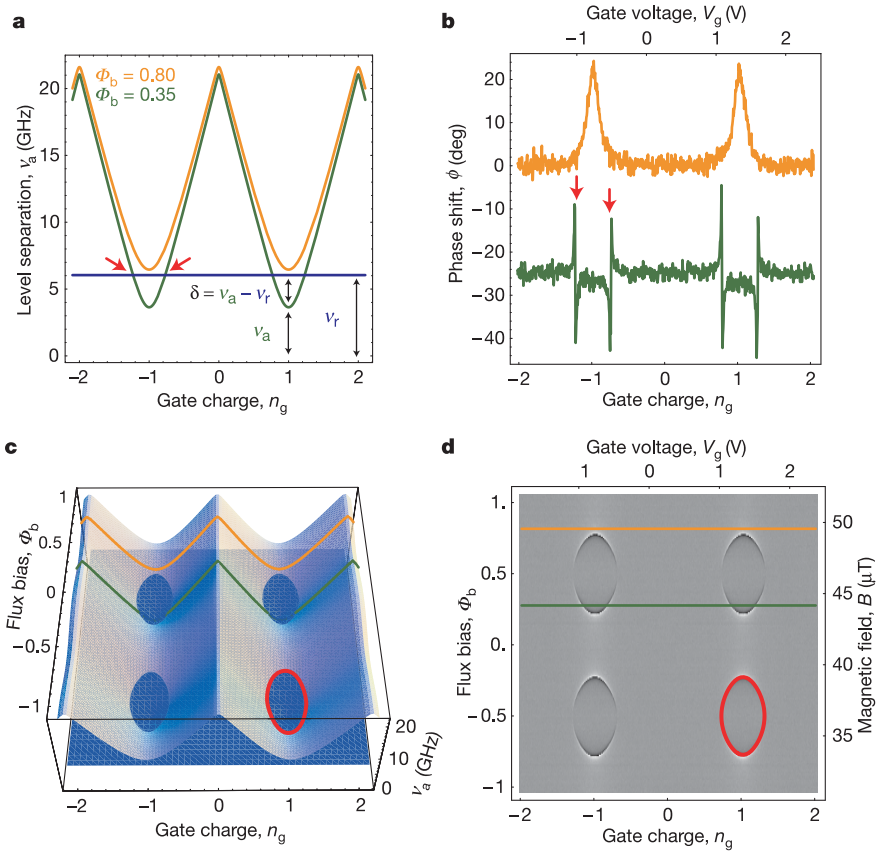

Figure 3 Strong coupling circuit QED in the dispersive regime. **a**, Calculated level separation $\nu_a = \omega_a/2\pi = E_a/h$ between ground $|\downarrow\rangle$ and excited state $|\uparrow\rangle$ of qubit for two values of flux bias $\Phi_b = 0.8$ (orange line) and $\Phi_b = 0.35$ (green line). The resonator frequency $\nu_r = \omega_r/2\pi$ is shown by a blue line. Resonance occurs at $\nu_a = \nu_r$ symmetrically around degeneracy $n_g = \pm 1$; also see red arrows. The detuning $\Delta/2\pi = \delta = \nu_a - \nu_r$ is indicated. **b**, Measured phase shift ϕ of the transmitted microwave for values of Φ_b in **a**. Green curve is offset by −25 deg for visibility. **c**, Calculated qubit level separation ν_a versus bias parameters n_g and Φ_b. The resonator frequency ν_r is indicated by the blue plane. At the intersection, also indicated by the red curve in the lower right-hand quadrant, resonance between the qubit and the resonator occurs ($\delta = 0$). For qubit states below the resonator plane the detuning is $\delta < 0$, above $\delta > 0$. **d**, Density plot of measured phase shift ϕ versus n_g and Φ_b. Light colours indicate positive ϕ ($\delta > 0$), dark colours negative ϕ ($\delta < 0$). The red line is a fit of the data to the resonance condition $\nu_a = \nu_r$. In **c** and **d**, the line cuts presented in **a** and **b** are indicated by the orange and the green line, respectively. The microwave probe power P_{RF} used to acquire the data is adjusted such that the maximum intra-resonator photon number n at ν_r is about ten for $g^2/\kappa\Delta \ll 1$. The calibration of the photon number has been performed in situ by measuring the a.c.-Stark shift of the qubit levels.

both n_g and Φ_b in Fig. 3d. We observe the expected periodicity in flux bias Φ_b with one flux quantum Φ_0. The set of parameters $[n_g, \Phi_b]$ for which the resonance condition is met is marked by a sudden sign change in ϕ, which allows a determination of the Josephson energy $E_{J,max} = 8.0\ (\pm 0.1)$ GHz and the charging energy $E_C = 5.2\ (\pm 0.1)$ GHz.

These data clearly demonstrate that the properties of the qubit can be determined in a transmission measurement of the resonator and that full in situ control over the qubit parameters is achieved. We note that in the dispersive regime this new read-out scheme for the Cooper pair box is most sensitive at charge degeneracy ($n_g = 1$), where the qubit is to first order decoupled from $1/f$ fluctuations in its charge environment, which minimizes dephasing[6]. This property is advantageous for quantum control of the qubit at $n_g = 1$, a point where traditional electrometry, using a single electron transistor (SET) for example[27], is unable to distinguish the qubit states. We note that this dispersive QND measurement of the qubit state[12] is the complement of the atomic microwave cavity QED measurement in which the state of the cavity is inferred non-destructively from the phase shift in the state of a beam of atoms sent through the cavity[3,28].

Making use of the full control over the qubit hamiltonian, we then tune the flux bias Φ_b so that the qubit is at $n_g = 1$ and in resonance with the resonator. Initially, the resonator and the qubit are cooled into their combined ground state $|0, \downarrow\rangle$; see inset in Fig. 4b. Owing to the coupling, the first excited states become a doublet $|\pm\rangle$. Similarly to ref. 4, we probe the energy splitting of this doublet spectroscopically using a weak probe beam so that $n \ll 1$. The intra-resonator photon number, n, is calibrated by measuring the a.c.-Stark shift of the qubit in the dispersive case. The resonator transmission T^2 is first measured for large detuning Δ with a probe beam populating the resonator with a maximum of $n \approx 1$ at resonance; see Fig. 4a. From the lorentzian line the photon decay rate of the resonator is determined as $\kappa/2\pi = 0.8$ MHz. The probe beam power is subsequently reduced by 5 dB and the transmission spectrum T^2 is measured in resonance ($\Delta = 0$); see Fig. 4b. We clearly observe two well-resolved spectral lines separated by the vacuum Rabi frequency $\nu_{Rabi} \approx 11.6$ MHz. The individual lines have a width determined by the average of the photon decay rate κ and the qubit decoherence rate γ. The data are in excellent agreement with the transmission spectrum numerically calculated using the given value $\kappa/2\pi = 0.8$ MHz and the single adjustable parameter $\gamma/2\pi = 0.7$ MHz.

The transmission spectrum shown in Fig. 4b is highly sensitive to the photon number in the cavity. The measured transmission spectrum is consistent with the expected thermal photon number of $n \lesssim 0.06$ ($T < 100$ mK); see red curve in Fig. 4b. Owing to the anharmonicity of the coupled atom-cavity system in the resonant case, an increased thermal photon number would reduce trans-

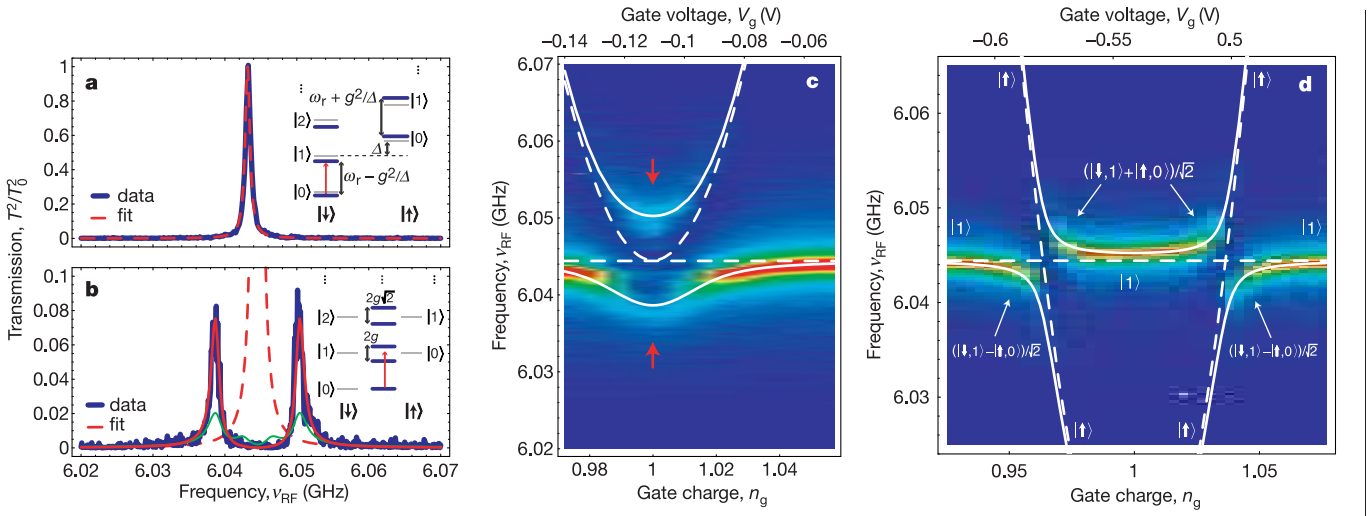

Figure 4 Vacuum Rabi mode splitting. **a**, Measured transmission T^2 (blue line) versus microwave probe frequency ν_{RF} for large detuning ($g^2/\Delta\kappa \ll 1$) and fit to lorentzian (dashed red line). The peak transmission amplitude is normalized to unity. The inset shows the dispersive dressed states level diagram. **b**, Measured transmission spectrum for the resonant case $\Delta = 0$ at $n_g = 1$ (blue line) showing the vacuum Rabi mode splitting compared to numerically calculated transmission spectra (red and green lines) for thermal photon numbers of $n = 0.06$ and 0.5, respectively. The dashed red line is the calculated transmission for $g = 0$ and $\kappa/2\pi = 0.8$ MHz. The inset shows the resonant dressed states level diagram. **c**, Resonator transmission amplitude T plotted versus probe frequency ν_{RF} and gate charge n_g for $\Delta = 0$ at $n_g = 1$. Blue colour corresponds to small T, red colour to large T. Dashed lines are uncoupled qubit level separation ν_a and resonator resonance frequency ν_r. Solid lines are level separations found from exact diagonalization of H_{JC}. Spectrum shown in **b** corresponds to line cut along red arrows. **d**, As in **c**, but for $E_J/h < \nu_r$. The dominant character of the corresponding eigenstates is indicated.

mission and give rise to additional peaks in the spectrum owing to transitions between higher excited doublets[30]. The transmission spectrum calculated for a thermal photon number of $n = 0.5$ (see green curve in Fig. 4b) is clearly incompatible with our experimental data, indicating that the coupled system has in fact cooled to near its ground state, and that we measure the coupling of a single qubit to a single photon. The nonlinearity of the cavity QED system is also observed at higher probe beam powers, as transitions are driven between states higher up the dressed state ladders (not shown).

We also observe the anti-crossing between the single photon resonator state and the first excited qubit state by tuning the qubit into and out of resonance with a gate charge near $n_g = 1$ and measuring the transmission spectrum (see Fig. 4c). The vacuum Rabi peaks evolve from a state with equal weight in the photon and qubit at $n_g = 1$ (as shown in Fig. 4b) to predominantly photon states for $n_g \gg 1$ or $n_g \ll 1$. The observed peak positions agree well with calculations considering the qubit with level separation ν_a, a single photon in the resonator with frequency ν_r and a coupling strength of $g/2\pi$; see solid lines in Fig. 4c. For a different value of flux bias Φ_b such that $E_a/h < \nu_r$ at $n_g = 1$, two anti-crossings are observed (see Fig. 4d) again in agreement with theory.

The observation of the vacuum Rabi mode splitting and the corresponding avoided crossings demonstrates that the strong coupling limit of cavity QED has been achieved, and that coherent superpositions of a single qubit and a single photon can be generated on a superconducting chip. This opens up many new possibilities for quantum optical experiments with circuits. Possible applications include using the cavity as a quantum bus to couple widely separated qubits in a quantum computer, or as a quantum memory to store quantum information, or even as a generator and detector of single microwave photons for quantum communication. □

Received 11 June; accepted 12 July 2004; doi:10.1038/nature02851.

1. Walls, D. & Milburn, G. *Quantum Optics* (Springer, Berlin, 1994).
2. Mabuchi, H. & Doherty, A. Cavity quantum electrodynamics: Coherence in context. *Science* **298,** 1372–1377 (2002).
3. Raimond, J., Brune, M. & Haroche, S. Manipulating quantum entanglement with atoms and photons in a cavity. *Rev. Mod. Phys.* **73,** 565–582 (2001).
4. Thompson, R. J., Rempe, G. & Kimble, H. J. Observation of normal-mode splitting for an atom in an optical cavity. *Phys. Rev. Lett.* **68,** 1132–1135 (1992).
5. Nakamura, Y., Pashkin, Y. A. & Tsai, J. S. Coherent control of macroscopic quantum states in a single-Cooper-pair box. *Nature* **398,** 786–788 (1999).
6. Vion, D. *et al.* Manipulating the quantum state of an electrical circuit. *Science* **296,** 886–889 (2002).
7. Martinis, J. M., Nam, S., Aumentado, J. & Urbina, C. Rabi oscillations in a large Josephson-junction qubit. *Phys. Rev. Lett.* **89,** 117901 (2002).
8. Chiorescu, I., Nakmura, Y., Harmans, C. J. P. M. & Mooij, J. E. Coherent quantum dynamics of a superconducting flux qubit. *Science* **299,** 1869–1871 (2003).
9. Yamamoto, T., Pashkin, Y. A., Astafiev, O., Nakamura, Y. & Tsai, J. S. Demonstration of conditional gate operation using superconducting charge qubits. *Nature* **425,** 941–944 (2003).
10. Berkley, A. J. *et al.* Entangled macroscopic quantum states in two superconducting qubits. *Science* **300,** 1548–1550 (2003).
11. Bouchiat, V., Vion, D., Joyez, P., Esteve, D. & Devoret, M. H. Quantum coherence with a single Cooper pair. *Phys. Scr.* **T76,** 165–170 (1998).
12. Blais, A., Huang, R.-S., Wallraff, A., Girvin, S. & Schoelkopf, R. Cavity quantum electrodynamics for superconducting electrical circuits: an architecture for quantum computation. *Phys. Rev. A* **69,** 062320 (2004).
13. Makhlin, Y., Schön, G. & Shnirman, A. Quantum-state engineering with Josephson-junction devices. *Rev. Mod. Phys.* **73,** 357–400 (2001).
14. Buisson, O. & Hekking, F. in *Macroscopic Quantum Coherence and Quantum Computing* (eds Averin, D. V., Ruggiero, B. & Silvestrini, P.) (Kluwer, New York, 2001).
15. Marquardt, F. & Bruder, C. Superposition of two mesoscopically distinct quantum states: Coupling a Cooper-pair box to a large superconducting island. *Phys. Rev. B* **63,** 054514 (2001).
16. Al-Saidi, W. A. & Stroud, D. Eigenstates of a small Josephson junction coupled to a resonant cavity. *Phys. Rev. B* **65,** 014512 (2001).
17. Plastina, F. & Falci, G. Communicating Josephson qubits. *Phys. Rev. B* **67,** 224514 (2003).
18. Blais, A., Maassen van den Brink, A. & Zagoskin, A. Tunable coupling of superconducting qubits. *Phys. Rev. Lett.* **90,** 127901 (2003).
19. Yang, C.-P., Chu, S.-I. & Han, S. Possible realization of entanglement, logical gates, and quantum-information transfer with superconducting-quantum-interference-device qubits in cavity QED. *Phys. Rev. A* **67,** 042311 (2003).
20. You, J. Q. & Nori, F. Quantum information processing with superconducting qubits in a microwave field. *Phys. Rev. B* **68,** 064509 (2003).
21. Kiraz, A. *et al.* Cavity-quantum electrodynamics using a single InAs quantum dot in a microdisk structure. *Appl. Phys. Lett.* **78,** 3932–3934 (2001).
22. Childress, L., Sørensen, A. S. & Lukin, M. D. Mesoscopic cavity quantum electrodynamics with quantum dots. *Phys. Rev. A* **69,** 042302 (2004).
23. Irish, E. K. & Schwab, K. Quantum measurement of a coupled nanomechanical resonator–Cooper-pair box system. *Phys. Rev. B* **68,** 155311 (2003).
24. Weisbuch, C., Nishioka, M., Ishikawa, A. & Arakawa, Y. Observation of the coupled exciton-photon mode splitting in a semiconductor quantum microcavity. *Phys. Rev. Lett.* **69,** 3314–3317 (1992).
25. Vuckovic, J., Fattal, D., Santori, C., Solomon, G. S. & Yamamoto, Y. Enhanced single-photon emission from a quantum dot in a micropost microcavity. *Appl. Phys. Lett.* **82,** 3596 (2003).
26. Day, P. K., LeDuc, H. G., Mazin, B. A., Vayonakis, A. & Zmuidzinas, J. A broadband superconducting detector suitable for use in large arrays. *Nature* **425,** 817–821 (2003).
27. Lehnert, K. *et al.* Measurement of the excited-state lifetime of a microelectronic circuit. *Phys. Rev. Lett.* **90,** 027002 (2003).

28. Nogues, G. *et al.* Seeing a single photon without destroying it. *Nature* **400,** 239–242 (1999).
29. Schuster, D. I. *et al.* AC-Stark shift and dephasing of a superconducting qubit strongly coupled to a cavity field. Preprint at http://www.arXiv.org/cond-mat/0408367 (2004).
30. Rau, I., Johansson, G. & Shnirman, A. Cavity QED in superconducting circuits: susceptibility at elevated temperatures. Preprint at http://www.arXiv.org/cond-mat/0403257 (2004).

Acknowledgements We thank J. Teufel, B. Turek and J. Wyatt for their contributions to the project and are grateful to P. Day, D. DeMille, M. Devoret, S. Weinreb and J. Zmuidzinas for numerous conversations. This work was supported in part by the National Security Agency and Advanced Research and Development Activity under the Army Research Office, the NSF, the David and Lucile Packard Foundation, the W. M. Keck Foundation, and the Natural Science and Engineering Research Council of Canada.

Competing interests statement The authors declare that they have no competing financial interests.

Correspondence and requests for materials should be addressed to A. W. (andreas.wallraff@yale.edu).

Generation of ultraviolet entangled photons in a semiconductor

Keiichi Edamatsu[1,2], Goro Oohata[1,3], Ryosuke Shimizu[2] & Tadashi Itoh[4,2]

[1]*Research Institute of Electrical Communication, Tohoku University, Sendai 980-8577, Japan*
[2]*CREST, Japan Science and Technology Agency (JST), Japan*
[3]*ERATO Semiconductor Spintronics Project, JST, Japan*
[4]*Graduate School of Engineering Science, Osaka University, Toyonaka 560-8531, Japan*

Entanglement is one of the key features of quantum information and communications technology. The method that has been used most frequently to generate highly entangled pairs of photons[1,2] is parametric down-conversion. Short-wavelength entangled photons are desirable for generating further entanglement between three or four photons, but it is difficult to use parametric down-conversion to generate suitably energetic entangled photon pairs. One method that is expected to be applicable for the generation of such photons[3] is resonant hyper-parametric scattering (RHPS): a pair of entangled photons is generated in a semiconductor via an electronically resonant third-order nonlinear optical process. Semiconductor-based sources of entangled photons would also be advantageous for practical quantum technologies, but attempts to generate entangled photons in semiconductors have not yet been successful[4,5]. Here we report experimental evidence for the generation of ultraviolet entangled photon pairs by means of biexciton resonant RHPS in a single crystal of the semiconductor CuCl. We anticipate that our results will open the way to the generation of entangled photons by current injection, analogous to current-driven single photon sources[6,7].

The material we used in this study was copper chloride (CuCl) single crystal. Because CuCl has a large bandgap (~3.4 eV), it is suitable for generating photon pairs in the short wavelength region near ultraviolet. Furthermore, the material has large binding energies for the exciton (~200 meV) and biexciton (~30 meV). These characteristics have made CuCl one of the most thoroughly investigated materials on the physics of excitons and biexcitons (ref. 8 and references therein). In particular, the 'giant oscillator strength' in the two-photon excitation of the biexciton results in a large increase in RHPS efficiency, which is advantageous for our experiment. In fact the RHPS in CuCl has been observed since the 1970s (refs 8, 9 and ref. 10 and references therein). Figure 1a schematically shows the RHPS process in resonance to the biexciton state. The two pump (parent) photons (frequency ω_i) resonantly create the biexciton, and are converted into the two scattered (daughter) photons (ω_s, $\omega_{s'}$). The biexciton state (Γ_1) created in this process has zero angular momentum ($J = 0$), so we expected the polarizations of the daughter photons to be entangled so that their total angular momentum is also zero. With this expectation in mind, we note that polarization correlation between two classical pump beams has been known since the early 1980s (ref. 11). In practice, instead of the oversimplified picture in Fig. 1a, we must consider the exciton-polariton picture; the RHPS obeys the phase-matching condition that takes into account the polariton dispersion relation[8]. The RHPS in this case is also called two-photon resonant polariton scattering or spontaneous hyper-Raman scattering. In this process, shown in Fig. 1b, the biexciton is created from a pair of parent photons (polaritons, more accurately). The sum of the parent photons' energies matches the biexciton energy. The biexciton progressively coherently decays into two polaritons, the sum of whose photon energies, as well as the sum of momenta, is conserved as that of the biexciton. Although the RHPS in CuCl has been known for decades, the possibility of generating entangled photons by this process was theoretically pointed out only lately[12]. In addition, a large parametric gain via the biexcitonic resonance in CuCl was reported recently[13]. Similar stimulated parametric scattering of polaritons has also been observed in semiconductor microcavities, even at high temperatures[14].

In the present experiment, we used a vapour-phase-grown thin single crystal of CuCl. Figure 2 presents the schematic drawing of our experimental set-up and Fig. 3 shows the spectrum of light emitted from the sample. The large peak at the downward arrow in Fig. 3 is the Rayleigh scattered light of the pump beam that was tuned to the two-photon excitation resonance of the biexciton. The two peaks indicated by LEP and HEP (lower and higher energy polaritons) on either side of the pump beam originate from the RHPS. The RHPS is very efficient (a few orders of magnitude higher than that of typical parametric down-conversion): We got of the order of 10^{10} photons s^{-1} sr^{-1} by using pump light of ~2 mW. A pair of photons, one from LEP and the other from HEP, is emitted into different directions according to the phase-matching condition, so we placed two optical fibres at appropriate positions and led each photon within the pair into two independent monochromators followed by two photomultipliers (PMTs). A time-interval analyser recorded the time interval (τ) between the detected

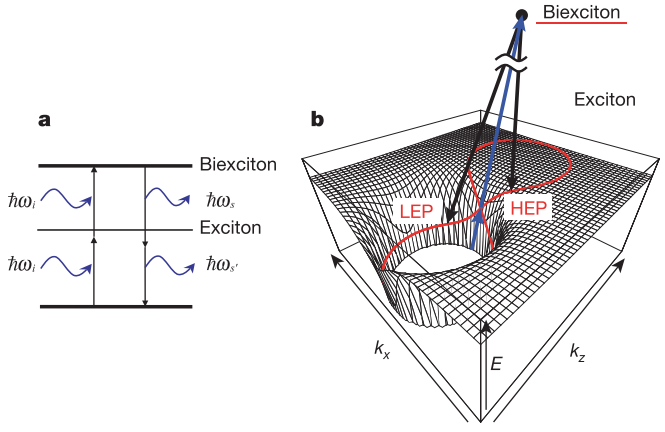

Figure 1 Schematic diagram of the resonant hyper-parametric scattering (RHPS) via biexciton. **a**, Two pump (parent) photons of frequency ω_i are converted to the two scattered (daughter) photons (ω_s, $\omega_{s'}$). **b**, The polariton dispersion drawn in two dimensions of momentum space. The biexciton decays into two polaritons that satisfy the phase-matching condition so that both energy and momentum are conserved. The red curve on the polariton-dispersion surface indicates the states on which the phase-matching condition can be satisfied.

ac Stark Shift and Dephasing of a Superconducting Qubit Strongly Coupled to a Cavity Field

D. I. Schuster, A. Wallraff, A. Blais, L. Frunzio, R.-S. Huang,* J. Majer, S. M. Girvin, and R. J. Schoelkopf

Departments of Applied Physics and Physics, Yale University, New Haven, Connecticut 06520, USA

(Received 16 August 2004; published 30 March 2005)

We have performed spectroscopy of a superconducting charge qubit coupled nonresonantly to a single mode of an on-chip resonator. The strong coupling induces a large ac Stark shift in the energy levels of both the qubit and the resonator. The dispersive shift of the resonator frequency is used to nondestructively determine the qubit state. Photon shot noise in the measurement field induces qubit level fluctuations leading to dephasing which is characteristic for the measurement backaction. A crossover in line shape with measurement power is observed and theoretically explained. For weak measurement a long intrinsic dephasing time of $T_2 > 200$ ns of the qubit is found.

DOI: 10.1103/PhysRevLett.94.123602 PACS numbers: 42.50.Pq, 32.60.+i, 42.50.Lc, 85.35.Gv

The investigation of strong coupling between a single quantum two-level system and a single photon, as first realized in atomic cavity quantum electrodynamics (CQED) [1], is not only at the forefront of research in quantum optics and atomic physics [2] but also has great prospects in the realm of quantum information processing [3] where realizing entanglement between qubits and photons is essential for quantum communication. Recently, it has been proposed [4] and demonstrated for the first time in a solid state system that strong coupling CQED [5,6] can be realized in superconducting quantum circuits [7]. Following these results, strong coupling has also been achieved in a second solid state system, namely, semiconducting quantum dots embedded in microcavities [8,9]. In this Letter we demonstrate the use of *nonresonant (dispersive)* strong coupling between a Cooper pair box (CPB) [10] and a coherent microwave field in a high quality transmission line resonator to measure the quantum mechanical state of the Cooper pair box in a quantum nondemolition (QND) scheme [4,11,12]. The interaction between the Cooper pair box and the measurement field containing n photons on average gives rise to a large ac Stark shift of the qubit energy levels, analogous to the one observed in CQED [13], demonstrated here for the first time in superconducting qubits. As a consequence of the strong coupling, quantum fluctuations in n induce a broadening of the transition linewidth, which represents the backaction of the measurement on the qubit.

In our circuit QED architecture [4] [see Fig. 1(a)] a split Cooper pair box [10], modeled by the two-level Hamiltonian $H_a = -1/2(E_{\rm el}\sigma_x + E_{\rm J}\sigma_z)$ [14], is coupled capacitively to the electromagnetic field of a full wave ($l = \lambda$) transmission line resonator, described by a harmonic oscillator Hamiltonian $H_{\rm r} = \hbar\omega_{\rm r}(a^\dagger a + 1/2)$. In the Cooper pair box, the energy difference $E_a = \hbar\omega_{\rm a} = (E_{\rm el}^2 + E_{\rm J}^2)^{1/2}$ between the ground state $|\downarrow\rangle$ and the first excited state $|\uparrow\rangle$ [see Fig. 1(b)], is determined by its electrostatic energy $E_{\rm el} = 4E_{\rm C}(1 - n_{\rm g})$ and its Josephson coupling energy $E_{\rm J} = E_{\rm J,max}\cos(\pi\Phi_{\rm b})$. Here, $E_{\rm C} = e^2/2C_\Sigma \approx 5$ GHz is the charging energy given by the total box capacitance C_Σ, $n_{\rm g} = C_g^\star V_{\rm g}/e$ is the gate charge controlled by the gate voltage V_g applied through a gate with effective capacitance $C_g^\star$, and $E_{\rm J,max} \approx 8$ GHz is the maximum Josephson coupling energy of the two junctions which is modulated by applying a flux bias $\Phi_{\rm b} = \Phi/\Phi_0$ to the loop of the split box [see Fig. 1(a)]. $\Phi_0 = 2e/h$ is the magnetic flux quantum. Near its resonance frequency $\omega_r = 1/\sqrt{LC} \approx 2\pi$ 6 GHz, the resonator is accurately modeled as a harmonic oscillator with lumped inductance L and capacitance C.

In the presence of strong mutual coupling between the qubit and the resonator [5], their *dressed* excitation ener-

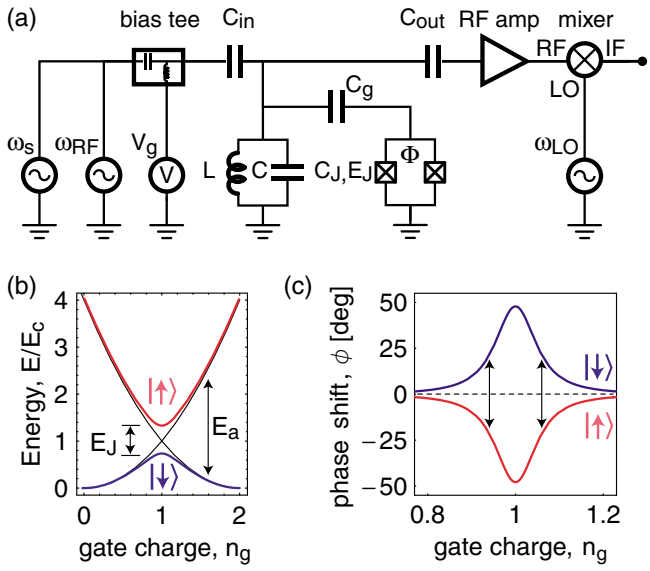

FIG. 1 (color online). (a) Simplified circuit diagram of measurement setup. The phase ϕ and amplitude T of a microwave at $\omega_{\rm rf}$ transmitted through the resonator, amplified, and mixed down to an intermediate frequency $\omega_{\rm IF} = \omega_{\rm rf} - \omega_{\rm LO}$ using a local oscillator at $\omega_{\rm LO}$ is measured. An additional spectroscopy microwave at $\omega_{\rm s}$ is applied to the input port of the resonator. (b) Ground $|\downarrow\rangle$ and excited $|\uparrow\rangle$ state energy levels of CPB vs gate charge n_g. (c) Calculated phase shift ϕ in ground and excited states vs n_g for $\Delta_{\rm a,r}/2\pi = 100$ MHz.

gies $\tilde{\omega}_a$ and $\tilde{\omega}_r$, are modified from their bare values ω_a and ω_r. For large detuning $\Delta_{a,r} = \omega_a - \omega_r$ the dressed energy levels are determined by the Hamiltonian [4]

$$H \approx \hbar\left(\omega_r + \frac{g^2}{\Delta_{a,r}}\sigma_z\right)a^\dagger a + \frac{1}{2}\hbar\left(\omega_a + \frac{g^2}{\Delta_{a,r}}\right)\sigma_z, \qquad (1)$$

where $g/2\pi \approx 5.8$ MHz is the coupling strength between a single photon and the qubit [5]. In this nonresonant case, the dressed resonator frequency $\tilde{\omega}_r = \omega_r \pm g^2/\Delta_{a,r}$ depends on the qubit state $\sigma_z = \pm 1$ and the detuning $\Delta_{a,r}$. The qubit state can thus be inferred from the phase shift ϕ that a probe microwave transmitted through the resonator at frequency ω_{rf} experiences because of the interaction with the qubit [4,5]. In Fig. 1(c), the expected phase shift $\phi = \pm\tan^{-1}(2g^2/\kappa\Delta_{a,r})$, where $\kappa = \omega_r/Q$ is the decay rate of photons from the resonator with quality factor $Q \approx 10^4$, is plotted versus gate charge n_g. ϕ is maximum at $n_g = 1$ where the detuning $\Delta_{a,r}$ is smallest and falls off as the detuning is increased with increasing n_g. Moreover, ϕ has opposite signs in the ground $|\downarrow\rangle$ and excited $|\uparrow\rangle$ states of the CPB.

Qubit state transitions can be driven by applying an additional microwave of frequency ω_s, detuning $\Delta_{s,a} = \omega_s - \tilde{\omega}_a$, and power P_s to the input port of the resonator [see Fig. 1(a)]. On resonance ($\Delta_{s,a} = 0$) and for a continuous (cw) large amplitude spectroscopy drive, the qubit transition saturates and the populations in the excited and the ground states approach 1/2. In this case, the measured phase shift of the probe beam at ω_{rf} is expected to saturate at $\phi = 0$ [see Fig. 1(c)]. By sweeping the spectroscopy frequency ω_s and the gate charge n_g and *continuously* measuring ϕ, we have mapped out the energy level separation $\tilde{\omega}_a$ of the qubit (see Fig. 2). In the lower panel of Fig. 2(a), the measured phase shift ϕ is shown for the nonresonant case, where $\omega_s < \tilde{\omega}_a$ for all values of gate charge n_g. The measured phase shift is, as expected, a continuous curve similar to the one shown in Fig. 1(c). In the middle panel of Fig. 2(a), the spectroscopy microwave at $\nu_s = \omega_s/2\pi = 6.15$ GHz is in resonance with the qubit at $n_g = 1$, populating the excited state and thus inducing a dip in the measured phase shift ϕ around $n_g = 1$, as expected. Note that, as predicted [4], our measurement scheme has the advantage of being most sensitive at charge degeneracy, a bias point where traditional electrometry, using a radio frequency single electron transistor [15], for example, is unable to distinguish the qubit states.

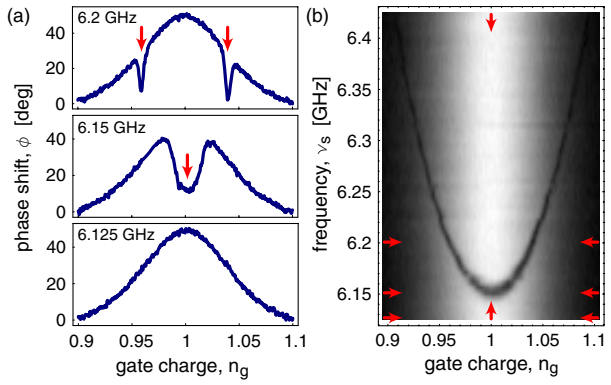

FIG. 2 (color online). (a) Probe microwave phase shift ϕ vs gate charge n_g at spectroscopy frequency $\nu_s = 6.125$ GHz (lower panel), 6.15 GHz (middle panel), and 6.2 GHz (upper panel). (b) Density plot of ϕ vs n_g and ν_s; white (black) corresponds to large (small) phase shift. Horizontal arrows indicate line cuts shown in (a); vertical arrows indicate line cuts shown in Fig. 4(a). Measurements in (a) and (b) were performed populating the resonator with $n \sim 25$ photons on average.

When ν_s is increased to higher values, resonance with the qubit occurs for two values of n_g situated symmetrically around $n_g = 1$, leading to two symmetric dips in ϕ [see upper panel of Fig. 2(a)]. From the $[n_g, \nu_s]$ positions of the spectroscopic lines in the measured phase ϕ, the Josephson energy $E_J = 6.2$ GHz and the charging energy $E_C = 4.8$ GHz are determined in a fit using the full qubit Hamiltonian beyond the two-level approximation [14] [see density plot of ϕ vs n_g and ν_s in Fig. 2(b)]. In this experiment the flux bias Φ_b has been chosen to result in a minimum detuning of about $\Delta_{a,r}/2\pi \approx 100$ MHz at $n_g = 1$. The tunability of E_J (i.e., the detuning at charge degeneracy) has been demonstrated previously [5]. It is also worth noting that the spectroscopy frequency ω_s typically remains strongly detuned ($\Delta_{s,r} = \omega_s - \omega_r > 2\pi 100$ MHz) from the resonator, such that a large fraction of the spectroscopy photons are reflected at the input port and only a small number n_s, determined by the Lorentzian line shape of the resonator, populates the resonator.

Various other radio or microwave frequency qubit readout schemes have been developed recently [15–17]. In a related experiment, the level separation of a split Cooper pair box coupled *inductively* to a *low frequency, moderate* Q tank circuit has been determined spectroscopically [18].

The width and the saturation level of the spectroscopic lines discussed above depend sensitively on the power P_s of the spectroscopic drive. Both quantities are related to the excited state population

$$P_\uparrow = 1 - P_\downarrow = \frac{1}{2}\frac{n_s\omega_{vac}^2 T_1 T_2}{1 + (T_2\Delta_{s,a})^2 + n_s\omega_{vac}^2 T_1 T_2}, \qquad (2)$$

found from the Bloch equations in steady state [19], where $\omega_{vac} = 2g$ is the vacuum Rabi frequency, n_s the average number of spectroscopy photons in the resonator, T_1 the relaxation time, and T_2 the dephasing time of the qubit. We have extracted the transition linewidth and saturation from spectroscopy frequency scans for different drive powers P_s with the qubit biased at charge degeneracy ($n_g = 1$). We observe that the spectroscopic lines have a Lorentzian line shape with width and depth in accordance with Eq. (2). The

half width at half maximum (HWHM) of the line is found to follow the expected power dependence $2\pi\delta\nu_{\mathrm{HWHM}} = 1/T_2' = (1/T_2^2 + n_s\omega_{\mathrm{vac}}^2 T_1/T_2)^{1/2}$ [19], where the input microwave power P_s is proportional to $n_s\omega_{\mathrm{vac}}^2$ [see Fig. 3(a)]. In the low power limit ($n_s\omega_{\mathrm{vac}}^2 \to 0$), the unbroadened linewidth is found to be small, $\delta\nu_{\mathrm{HWHM}} \approx$ 750 kHz, corresponding to a long dephasing time of $T_2 >$ 200 ns at $n_g = 1$, where the qubit is only second order sensitive to charge fluctuations limiting the dephasing time in this sample. At a larger drive, the width increases proportionally to the drive amplitude. The depth of the spectroscopic dip at resonance ($\Delta_{s,a} = 0$) reflects the probability of the qubit to be in the excited state $P_\uparrow$ and depends on P_s as predicted by Eq. (2) [see Fig. 3(b)]. At low drive the population increases linearly with P_s and then approaches 0.5 for large P_s. From time resolved measurements (data not shown), T_1 is found to be on the order of a few microseconds, a value which is much shorter than that expected for radiative decay of the qubit in the cavity [4], indicating the existence of other, possibly nonradiative decay channels.

In the above we have demonstrated that the strong coupling of the qubit to the radiation field modifies the resonator transition frequency in a way that can be exploited to measure the qubit state. Correspondingly, the resonator acts back onto the qubit through their mutual strong coupling. Regrouping the terms of the Hamiltonian in Eq. (1) one sees that the *dressed* qubit level separation is given by $\tilde{\omega}_a = \omega_a + 2\,ng^2/\Delta_{a,r} + g^2/\Delta_{a,r}$, where we note that the resonator gives rise to an ac Stark shift of the qubit levels of $\pm ng^2/\Delta_{a,r}$, proportional to the intraresonator photon number $n = \langle a^\dagger a\rangle$, as well as a Lamb shift $\pm g^2/2\Delta_{a,r}$, due to the coupling to the vacuum fluctuations. The ac Stark shift is measured spectroscopically at $n_g = 1$ for fixed power P_s by varying the probe beam power P_{rf} which changes the average measurement photon number n in the resonator (see Fig. 4). We observe that the qubit level separation $\tilde{\nu}_a = \tilde{\omega}_a/2\pi$ is linear in P_{rf} [see Fig. 5(a)], i.e., that the ac Stark shift $\nu_{ac} = 2ng^2/2\pi\Delta_{a,r}$ is linear in the photon number n, as expected. In the limit of $P_{rf} \to 0$ ($n \to 0$), the bare qubit level separation $\omega_a + g^2/\Delta_{a,r} = 2\pi$ 6.15 GHz is determined, where $g^2/\Delta_{a,r}$ is the small Lamb shift which cannot be separated from ω_a in our current experiments. Knowing the coupling constant g from an independent measurement of the vacuum Rabi mode splitting [5] and $\Delta_{a,r}$ from spectroscopic measurements in the $n \to 0$ limit, the dependence of the intraresonator photon number n on the input power P_{rf} is determined from the measured ac Stark shift ν_{ac}. We find that an input microwave power of $P_{rf} = -29$ dBm corresponds to $n = 1$ which is consistent with an intended attenuation of approximately 105 dB in the input coaxial line. The ac Stark shift of the qubit at this particular detuning is a remarkable 0.6 MHz per photon in the cavity and is comparable to the linewidth. Using this method, the intraresonator photon number was calibrated to a precision of $\sim \pm 1$ dB for the vacuum Rabi mode splitting measurements presented in Ref. [5].

Quantum fluctuations (photon shot noise) δn around the average photon number n of the coherent field populating the resonator give rise to random fluctuations in the qubit transition frequency due to the ac Stark shift. This leads to measurement-induced dephasing, and thus to a broadening of the qubit linewidth (see Figs. 4 and 5). This is the measurement backaction and can be understood quantitatively by considering the relative phase $\varphi(t) = 2g^2/\Delta_{a,r}\int_0^t dt'\delta n(t')$ accumulated in time between the ground and the excited states of the qubit. Following Ref. [4], the measurement-induced phase decay of the qubit is then characterized by

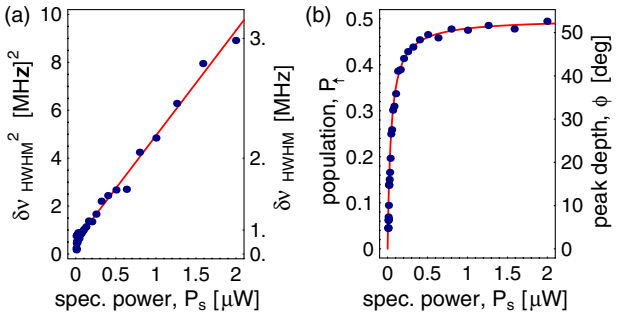

FIG. 3 (color online). (a) Measured qubit linewidth $\delta\nu_{\mathrm{HWHM}}$ vs input spectroscopy power P_s (solid circles) with fit (solid line). Probe beam power P_{rf} is adjusted such that $n < 1$. (b) Measured peak depth ϕ and excited state population probability $P_\uparrow$ on resonance $\Delta_{s,a} = 0$ vs P_s (solid circles) with fit (solid line).

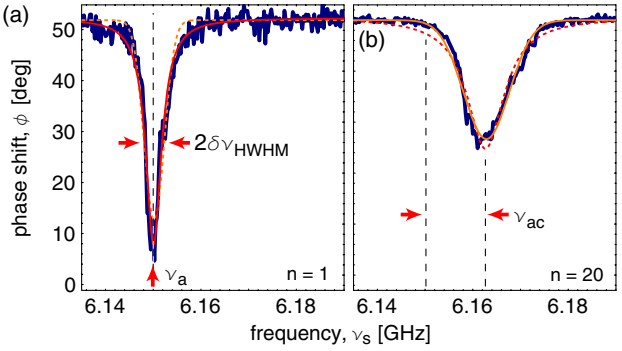

FIG. 4 (color online). Measured spectroscopic lines (wide lines with noise) at (a) intraresonator photon number $n \approx 1$ ($P_{rf} = -30$ dBm) with fit to Lorentzian line shape (solid line) and at (b) $n \approx 20$ ($P_{rf} = -16$ dBm) with fit to Gaussian line shape (solid line). Dashed lines are best fits to (a) Gaussian or (b) Lorentzian line shapes, respectively. The qubit transition frequency ν_a at low P_{rf}, the half width half maximum $\delta\nu_{\mathrm{HWHM}}$, and the ac Stark shift ν_{ac} of the lines are indicated.

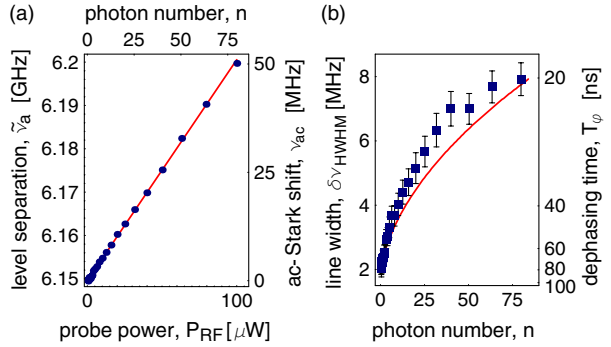

FIG. 5 (color online). (a) Measured qubit level separation $\tilde{\nu}_a$ and fit (solid line) vs input microwave probe power P_{rf}. The ac Stark shift ν_{ac} and the intraresonator photon number n extracted from the fit are also indicated. (b) Measurement broadened qubit linewidth $\delta\nu_{HWHM}$ vs n. Error bars are reflecting estimated systematic uncertainties in the extracted linewidth. The corresponding total dephasing time $T_\varphi = 1/2\pi\delta\nu_{HWHM}$ is also indicated. The solid line is obtained from Eq. (4) with a spectroscopy power broadened $T_2' \approx 80$ ns.

$$\langle e^{i\varphi(t)}\rangle = \exp\Big[-\frac{2g^4}{\Delta_{a,r}^2}\iint_0^t dt_1 dt_2 \langle \delta n(t_1)\delta n(t_2)\rangle\Big], \quad (3)$$

where the fluctuations δn are assumed to be Gaussian. In the above expression, the photon correlation function $\langle \delta n(t)\delta n(0)\rangle = n\exp(-\kappa|t|/2)$ of the coherent probe beam in the resonator is governed by the cavity decay rate κ and physically represents the white photon shot noise filtered by the cavity response. The spectroscopic line shape $S(\omega)$ is obtained from the Fourier transform of $\langle\exp[i\varphi(t)]\rangle e^{-t/T_2'}$, where $1/T_2'$ takes into account dephasing mechanisms independent of the measurement

$$S(\omega) = \frac{1}{\pi}\sum_{j=0}^{\infty}\frac{(-4\chi)^j}{j!}\frac{1/T_2' + 2\kappa\chi + j\kappa/2}{(\omega-\tilde{\omega}_a)^2 + (\frac{1}{T_2'} + 2\kappa\chi + \frac{j\kappa}{2})^2}. \quad (4)$$

The form of the line shape depends on the dimensionless parameter $\chi = n\theta_0^2$, where $\theta_0 = 2g^2/\kappa\Delta_{a,r}$ is the transmission phase shift describing the strength of the measurement. For small χ the measurement rate is slow compared to κ and the phase diffuses in a random walk $\langle\varphi(t)^2\rangle \sim 4\theta_0^2 n\kappa t$, leading to a homogeneously broadened Lorentzian line of HWHM of $2\theta_0^2 n\kappa + 1/T_2'$. For large χ, i.e., strong measurement, the measurement rate exceeds κ leading to a qubit transition frequency which depends on the instantaneous value of the cavity photon number and hence to an inhomogeneously broadened Gaussian line [see Fig. 4(b)], whose variance is simply $\sqrt{n}$ multiplied by the Stark shift per photon. The full crossover from intrinsic Lorentzian line shape with width $\propto n$ at small n to Gaussian line shape with width $\propto \sqrt{n}$ at large n as described by Eq. (4) with no adjustable parameters is in good agreement with the measured dependence of the linewidth on n [see Fig. 5(b)]. The slightly increased measured linewidth could be attributed to fluctuations (e.g., charge noise) activated at high photon numbers and to the nonlinearity of the ac Stark shift above the critical photon number [4]. We note that this effect is not seen in Fig. 4(a) because of compensation by the change of the cavity pull at large n from the zero-photon limit g^2/Δ.

In our experiments we have demonstrated that the strong coupling of a Cooper pair box to a nonresonant microwave field in an on-chip cavity gives rise to a large qubit dependent shift in the excitation energy of the resonator. The ac Stark effect shifts the qubit level separation by about one linewidth per photon at 2% detuning, and the backaction of the fluctuations in the field gives rise to a large broadening of the qubit line. Good agreement of the line shape with theory indicates that the dispersive measurement is QND, as expected.

We thank M. Devoret and I. Chiorescu for discussions. This work was supported in part by NSA and ARDA under ARO Contract No. DAAD19-02-1-0045, and the NSF under Grants No. ITR-0325580 and No. DMR-0342157, the David and Lucile Packard Foundation, the W. M. Keck Foundation, and the NSERC of Canada.

*Also at Ames Laboratory, Iowa State University, Ames, IA 50011, USA.

[1] H. Mabuchi and A. Doherty, Science **298**, 1372 (2002).
[2] D. Walls and G. Milburn, *Quantum Optics* (Spinger-Verlag, Berlin, 1994).
[3] M. A. Nielsen and I. L. Chuang, *Quantum Computation and Quantum Information* (Cambridge University Press, Cambridge, U.K., 2000).
[4] A. Blais *et al.*, Phys. Rev. A **69**, 062320 (2004).
[5] A. Wallraff *et al.*, Nature (London) **431**, 162 (2004).
[6] I. Chiorescu *et al.*, Nature (London) **431**, 159 (2004).
[7] Y. Nakamura, Y. A. Pashkin, and J. S. Tsai, Nature (London) **398**, 786 (1999); D. Vion *et al.*, Science **296**, 886 (2002); J. M. Martinis, S. Nam, J. Aumentado, and C. Urbina, Phys. Rev. Lett. **89**, 117901 (2002); Y. Yu *et al.*, Science **296**, 889 (2002); I. Chiorescu, Y. Nakmura, C. J. P. M. Harmans, and J. E. Mooij, Science **299**, 1869 (2003); T. Yamamoto *et al.*, Nature (London) **425**, 941 (2003).
[8] T. Yoshie *et al.*, Nature (London) **432**, 200 (2004).
[9] J. P. Reithmaier *et al.*, Nature (London) **432**, 197 (2004).
[10] V. Bouchiat *et al.*, Phys. Scr. **T76**, 165 (1998).
[11] P. Grangier, J. A. Levenson, and J.-P. Poziat, Nature (London) **396**, 537 (1998).
[12] G. Nogues *et al.*, Nature (London) **400**, 239 (1999).
[13] P. Brune *et al.*, Phys. Rev. Lett. **72**, 3339 (1994).
[14] Y. Makhlin, G. Schön, and A. Shnirman, Rev. Mod. Phys. **73**, 357 (2001).
[15] K. Lehnert *et al.*, Phys. Rev. Lett. **90**, 027002 (2003).
[16] A. Lupascu *et al.*, Phys. Rev. Lett. **93**, 177006 (2004).
[17] I. Siddiqi *et al.*, Phys. Rev. Lett. **93**, 207002 (2004).
[18] D. Born *et al.*, Phys. Rev. B **70**, 180501 (2004).
[19] A. Abragam, *The Principles of Nuclear Magnetism* (Oxford University Press, Oxford, 1961).

Approaching Unit Visibility for Control of a Superconducting Qubit with Dispersive Readout

A. Wallraff, D. I. Schuster, A. Blais, L. Frunzio, J. Majer, M. H. Devoret, S. M. Girvin, and R. J. Schoelkopf

Departments of Applied Physics and Physics, Yale University, New Haven, Connecticut 06520, USA

(Received 27 February 2005; published 1 August 2005)

In a Rabi oscillation experiment with a superconducting qubit we show that a visibility in the qubit excited state population of more than 95% can be attained. We perform a dispersive measurement of the qubit state by coupling the qubit nonresonantly to a transmission line resonator and probing the resonator transmission spectrum. The measurement process is well characterized and quantitatively understood. In a measurement of Ramsey fringes, the qubit coherence time is larger than 500 ns.

DOI: 10.1103/PhysRevLett.95.060501 PACS numbers: 03.67.Pp, 42.50.Pq, 85.35.Gv

One of the most promising solid-state architectures for the realization of a quantum information processor [1] is based on superconducting electrical circuits [2]. A variety of such circuits acting as qubits [1], the basic carriers of quantum information in a quantum computer, have been created and their coherent control has been demonstrated [3–8]. Recent experiments have realized controlled coupling between different qubits [9–13] and also first two-qubit quantum logic gates [14].

An outstanding question for superconducting qubits, and in fact for all solid-state implementations of quantum information processors, is whether the qubits are sufficiently well isolated to allow long coherence times and high-fidelity preparation and control of their quantum states. This question is complicated by inevitable imperfections in the measurement. A canonical example is a Rabi oscillation experiment, where the experimenter records the oscillations of a meter's response as a function of pulse length to infer the qubit's excited state population immediately after the pulse. The measurement contrast (e.g., the amplitude of the meter's measured swing relative to its maximum value) is reduced in general by both errors in the qubit preparation and readout, and sets a lower limit on the visibility of oscillations in the qubit population. Most experiments with superconducting qubits to date have reported only the measurement contrast, implying only a lower limit on the visibility in the range of 10%–50% [3–8,14].

A full understanding of the measurement process is required to extract the qubit population from the meter's output. The qubit control is then characterized by the visibility, defined as the maximum qubit population difference observed in a Rabi oscillation or Ramsey fringe experiment. It is essential to demonstrate that a qubit can be controlled without inducing undesired leakage to other qubit states or entanglement with the environment. Some experiments [15] observe a substantial reduction of the visibility due to entanglement with spurious environmental fluctuators [16]. In the few experiments in which the contrast has been characterized, it was close to the expected value [17,18], which implies that high visibility should be achievable with superconducting qubits.

In this Letter, we report results on time-domain control of the quantum state of a superconducting qubit, where the qubit state is determined using a dispersive microwave measurement in a circuit quantum electrodynamics (QED) architecture [19]. This novel technique has shown good agreement with predictions in steady-state experiments [20]. Here, we observe the measurement response, both during and after qubit state manipulation, which is in quantitative agreement with the theoretical model of the system, allowing us to separate the contributions of the qubit and the readout to the observed contrast. The observed contrast of 85% and a visibility of greater than 95% for Rabi oscillations demonstrates that high accuracy control is possible in superconducting qubits.

In our circuit QED architecture [19], a Cooper pair box [21], acting as a two level system with ground $|\downarrow\rangle$ and excited states $|\uparrow\rangle$ and level separation $E_a = \hbar\omega_a = \sqrt{E_{el}^2 + E_J^2}$ is coupled capacitively to a single mode of the electromagnetic field of a transmission line resonator with resonance frequency ω_r; see Fig. 1(a). As demonstrated for this system, the electrostatic energy E_{el} and the Josephson energy E_J of the split Cooper pair box can be controlled *in situ* by a gate voltage V_g and magnetic flux Φ [20,22]; see Fig. 1(a). In the resonant ($\omega_a = \omega_r$) strong coupling regime a single excitation is exchanged coherently between the Cooper pair box and the resonator at a rate g/π, also called the vacuum Rabi frequency [22]. In the nonresonant regime ($|\Delta| = |\omega_a - \omega_r| > g$) the capacitive interaction gives rise to a dispersive shift $(g^2/\Delta)\sigma_z$ in the resonance frequency of the cavity which depends on the qubit state σ_z, the coupling g, and the detuning Δ [19,20]. We have suggested that this shift in resonance frequency can be used to perform a quantum nondemolition (QND) measurement of the qubit state [19]. With this technique we have recently measured the ground state response and the excitation spectrum of a Cooper pair box [20,22].

In the experiments presented here, we coherently control the quantum state of a Cooper pair box in the resonator by applying microwave pulses of frequency ω_s, which are resonant or nearly resonant with the qubit transition frequency $\omega_a/2\pi \approx 4.3$ GHz, to the input port C_{in} of the resonator; see Fig. 1(a). Even though ω_s is strongly de-

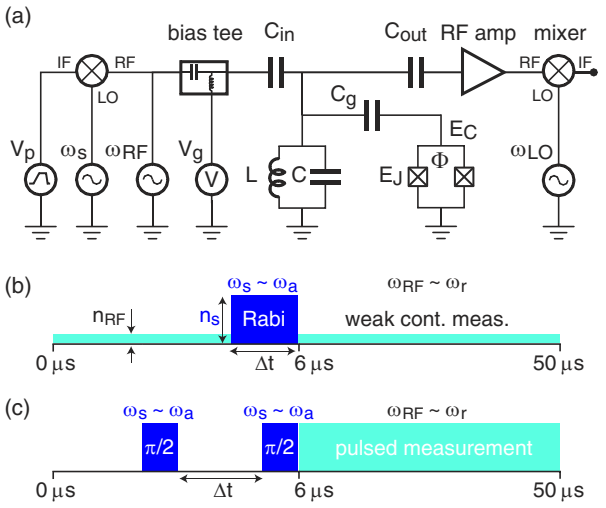

FIG. 1 (color online). (a) Simplified circuit diagram of measurement setup. A Cooper pair box with charging energy E_C and Josephson energy E_J is coupled through capacitor C_g to a transmission line resonator, modeled as parallel combination of an inductor L and a capacitor C. Its state is determined in a phase sensitive heterodyne measurement of a microwave transmitted at frequency ω_{RF} through the circuit, amplified and mixed with a local oscillator at frequency ω_{LO}. The Cooper pair box level separation is controlled by the gate voltage V_g and flux Φ. Its state is coherently manipulated using microwaves at frequency ω_s with pulse shapes determined by V_p [8]. (b) Measurement sequence for Rabi oscillations with Rabi pulse length Δt, pulse frequency ω_s, and amplitude $\propto \sqrt{n_s}$ with continuous measurement at frequency ω_{RF} and amplitude $\propto \sqrt{n_{RF}}$. (c) Sequence for Ramsey fringe experiment with two $\pi/2$ pulses at ω_s separated by a delay Δt and followed by a pulsed measurement.

tuned from the resonator frequency ω_r, the resonator can be populated with n_s drive photons which induce Rabi oscillations in the qubit at a frequency of $\nu_{Rabi} = \sqrt{n_s}g/\pi$. Simultaneously, we perform a continuous dispersive measurement of the qubit state by determining both the phase and the amplitude of a coherent microwave beam transmitted through the resonator at frequency ω_{RF} which is resonant or nearly resonant with the resonator frequency $\omega_r/2\pi \approx 5.4$ GHz [19,22]. The phase shift $\phi = \tan^{-1}(2g^2/\kappa\Delta)\sigma_z$ is the response of our meter from which we determine the qubit population. For the measurement, we chose a resonator that has a quality factor of $Q \sim 0.7 \times 10^4$ corresponding to a photon decay rate of $\kappa/2\pi = 0.73$ MHz. The resonator is populated with $n \sim 1$ measurement photons on average, where n is calibrated using the ac-Stark shift [20]. All experiments are performed in a dilution refrigerator at a temperature of 20 mK. The charging energy of the box is $E_C = e^2/2C \approx h\ 5.2$ GHz. Details on the device fabrication can be found in Ref. [23].

We initially determine the maximum swing of the meter in a calibration measurement by first maximizing the detuning Δ to minimize the interaction ($g^2/\Delta \to 0$) which defines $\phi = 0$. We prepare the Cooper pair box in the ground state $|\downarrow\rangle$ by relaxation, the thermal population of excited states being negligible. The box is biased at charge degeneracy ($E_{el} = 0$), where its energy is to first-order insensitive to charge noise [4]. Using flux bias, the detuning is adjusted to $\Delta/2\pi \approx -1.1$ GHz corresponding to a maximum in the Josephson coupling energy of $E_J/h \approx 4.3$ GHz $< \omega_r/2\pi$. In this case we measure a minimum meter response of $\phi_{|\downarrow\rangle} = -35.3$ deg corresponding to a coupling strength of $g/2\pi = 17$ MHz. Saturating the qubit transition by applying a long microwave pulse which incoherently mixes the ground and excited states such that the occupation probabilities are $P_{|\downarrow\rangle} = P_{|\uparrow\rangle} = 1/2$, the measured phase shift is found to be $\phi = 0$, as expected [20]. From these measurements, the predicted phase shift induced by a fully polarized qubit ($P_{|\uparrow\rangle} = 1$) would be $\phi_{|\uparrow\rangle} = 35.3$ deg. Thus, the maximum swing of the meter is bounded by $\phi_{|\uparrow\rangle} - \phi_{|\downarrow\rangle}$.

In our measurement of Rabi oscillations, a short microwave pulse of length Δt is applied to the qubit in its ground state with a repetition rate of 20 kHz while the measurement response ϕ is continuously monitored and digitally averaged 5×10^4 times; see Fig. 1(b). The signal to noise ratio (SNR) in the averaged value of ϕ in an integration time of 100 ns is approximately 25, see Fig. 2, corresponding to a SNR of 0.1 in a single shot. For the present setup the single shot readout fidelity for the qubit state integrated over the relaxation time ($T_1 \sim 7\ \mu$s) is approximately 30% [24]. Either a readout amplifier with lower noise temperature or a larger signal power would potentially allow a high-fidelity single shot measurement of the qubit state in this setup.

The time dependence of the averaged value of ϕ in response to a π pulse of duration $\Delta t \sim 16$ ns applied to the qubit is shown in Fig. 2(a). Before the start of the pulse the measured phase shift is $\phi_{|\downarrow\rangle} \approx -35.3$ deg corresponding to the qubit being in the ground state. Because of the state change of the qubit induced by the pulse, the resonator frequency is pulled by $2g^2/\Delta$ and, thus, the measured phase shift is seen to rise exponentially towards $\phi_{|\uparrow\rangle}$ with the resonator amplitude response time $2/\kappa \approx 400$ ns, i.e., twice the photon life time. After the π pulse, the qubit excited state decays exponentially with its energy relaxation time $T_1 \sim 7.3\ \mu$s, as extracted from the decay in the measured phase shift; see Fig. 2(a). As a result, the maximum measured response ϕ_{max} does not reach the full value of $\phi_{|\uparrow\rangle}$. In general, the measurement contrast $C = (\phi_{max} - \phi_{min})/(\phi_{|\uparrow\rangle} - \phi_{|\downarrow\rangle})$ will be reduced in any qubit readout for which the qubit lifetime is not infinitely longer than the measurement response time. Additionally, in non-QND measurements the contrast is reduced even further due to mixing of the qubit states induced by the interaction with the measurement apparatus. In our QND measurement presented here, the qubit lifetime is about 15 times the response time of the measurement, allowing us to reach a high maximum contrast of $C \sim 85\%$ in the bare measurement response ϕ.

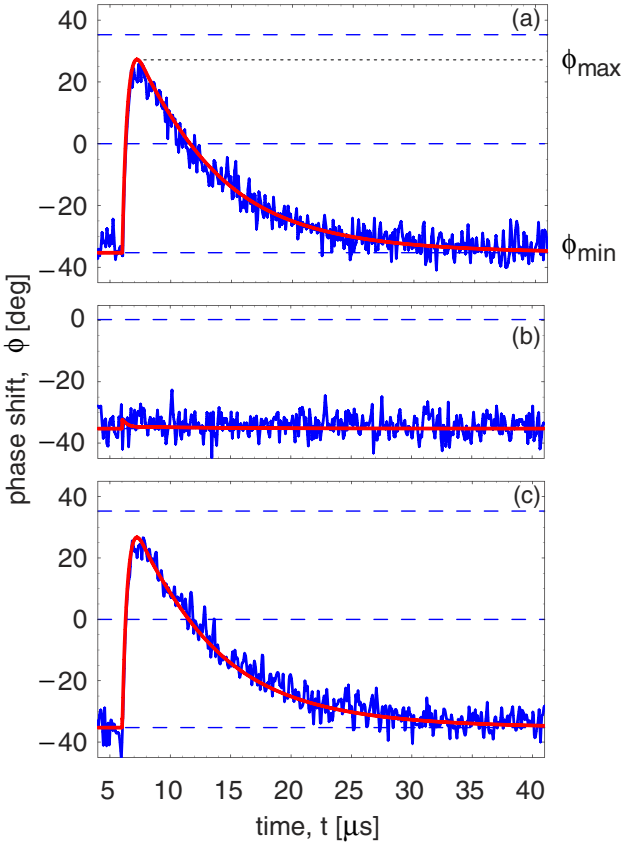

FIG. 2 (color online). Measurement response ϕ (blue lines) and theoretical prediction (red lines) vs time. At $t = 6$ μs (a) a π pulse, (b) a 2π pulse, and (c) a 3π pulse is applied to the qubit. In each panel the dashed lines correspond to the expected measurement response in the ground state $\phi_{|\downarrow\rangle}$, in the saturated state $\phi = 0$, and in the excited state $\phi_{|\uparrow\rangle}$.

In Figs. 2(b) and 2(c), the measured response ϕ of the meter to a 2π and a 3π pulse acting on the qubit is shown. As expected, no phase shift is observable for the 2π pulse since the response time of the resonator is much longer than the duration $\Delta t = 32$ ns of the pulse. In agreement with the expectations for this QND scheme, the measurement does not excite the qubit, i.e., $\phi_{\min} = \phi_{\max} = \phi_{|\downarrow\rangle}$. The response to the 3π pulse is virtually indistinguishable from the one to the π pulse, as expected for the long coherence and energy relaxation times of the qubit. In the 2D density plot Fig. 3, Rabi oscillations are clearly observed in the phase shift acquired versus measurement time t and Rabi pulse length Δt.

The observed measurement response ϕ is in excellent agreement with theoretical predictions, see red lines in Fig. 2, demonstrating a good understanding of the measurement process. The temporal response $\phi(t) = \arg\{i\langle a(t)\rangle\}$ of the cavity field a is calculated by deriving and solving Bloch-type equations of motion for the cavity and qubit operators [25] using the Jaynes-Cummings Hamiltonian in the dispersive regime [19,20] as the starting

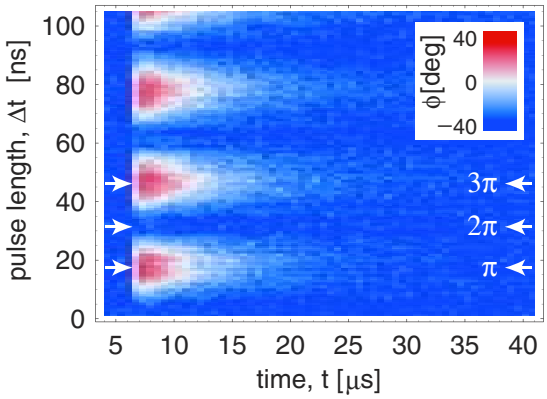

FIG. 3 (color online). Color density plot of phase shift ϕ (see inset for scale) versus measurement time t and Rabi pulse length Δt. Data shown in Fig. 2 are slices through this data set at the indicated pulse lengths.

point. A semiclassical factorization approximation is done to truncate the resulting infinite set of equations to a finite set (e.g., $\langle a^\dagger a\sigma_z\rangle \sim \langle a^\dagger a\rangle\langle\sigma_z\rangle$; all lower order products are kept). This amounts to neglecting higher order correlations between qubit and field which is a valid approximation in the present experiment. The calculations accurately model the exponential rise in the observed phase shift on the time scale of the resonator response time due to a state change of the qubit. They also accurately capture the reduced maximum response $\phi_{\max}$ due to the exponential decay of the qubit. Overall, excellent agreement in the temporal response of the measurement is found over the full range of qubit and measurement time scales with no adjustable parameters; see Fig. 2.

The visibility of the excited state population $P_{|\uparrow\rangle}$ in the Rabi oscillations is extracted from the time dependent measurement response ϕ for each Rabi pulse length Δt. We find $P_{|\uparrow\rangle}$ by calculating the normalized dot product between the measured response ϕ and the predicted response taking into account the systematics of the measurement. This amounts to comparing the area under a measured response curve to the theoretically predicted area; see Fig. 2. The averaged response of all measurements taken over a window in time extending from the start of the Rabi pulse out to several qubit decay times T_1 is used to extract $P_{|\uparrow\rangle}$. This maximizes the signal to noise ratio in the extracted Rabi oscillations.

The extracted qubit population $P_{|\uparrow\rangle}$ is plotted versus Δt in Fig. 4(a). We observe a visibility of $95 \pm 6\%$ in the Rabi oscillations with error margins determined from the residuals of the experimental $P_{|\uparrow\rangle}$ with respect to the predicted values. Thus, in a measurement of Rabi oscillations in a superconducting qubit, a visibility in the population of the qubit excited state that approaches unity is observed for the first time. Moreover, the decay in the Rabi oscillation amplitude out to pulse lengths of 100 ns is very small and consistent with the long T_1 and T_2 times of this charge

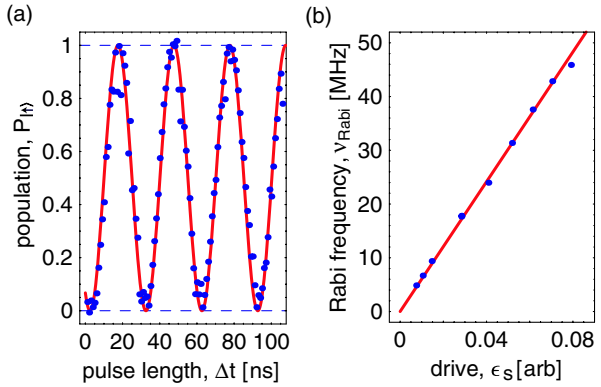

FIG. 4 (color online). (a) Rabi oscillations in the qubit population $P_{|\uparrow\rangle}$ vs Rabi pulse length Δt (blue dots) and fit with unit visibility (red line). (b) Measured Rabi frequency ν_{Rabi} vs pulse amplitude ϵ_s (blue dots) and linear fit.

qubit; see Fig. 4(a) and Ramsey experiment discussed below. We have also verified the expected linear scaling of the Rabi frequency ν_{Rabi} with the pulse amplitude $\epsilon_s \propto \sqrt{n_s}$; see Fig. 4(b).

We have determined the coherence time of the Cooper pair box from a Ramsey fringe experiment at charge degeneracy using $\pi/2$ pulses of 20 ns duration; see Fig. 1(c). To avoid dephasing induced by a weak continuous measurement beam [20] we switch on the measurement beam only after the end of the second $\pi/2$ pulse. The resulting Ramsey fringes oscillating at the detuning frequency $\delta_{a,s} = \omega_a - \omega_s \sim 6$ MHz decay with a long coherence time of $T_2 \sim 500$ ns; see Fig. 5(a). The corresponding qubit phase quality factor of $Q_\varphi = T_2\omega_a/2 \sim 6500$ is

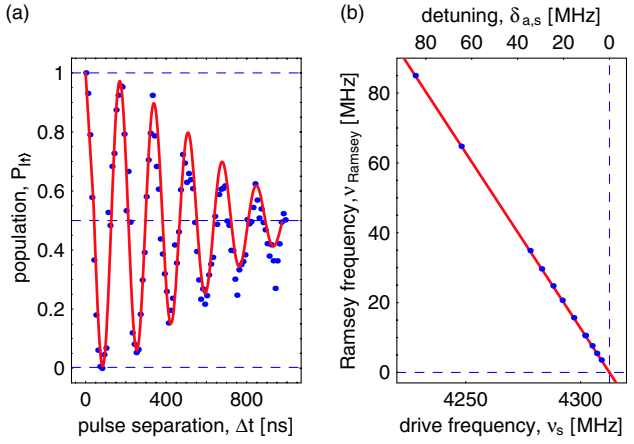

FIG. 5 (color online). (a) Measured Ramsey fringes (blue dots) observed in the qubit population $P_{|\uparrow\rangle}$ vs pulse separation Δt using the pulse sequence shown in Fig. 1(b) and fit of data to sinusoid with Gaussian envelope (red line). (b) Measured dependence of Ramsey frequency ν_{Ramsey} on detuning $\delta_{a,s}$ of drive frequency (blue dots) and linear fit (red line).

similar to the best values measured so far in qubits biased at an optimal point [4]. The Ramsey frequency is shown to depend linearly on the detuning $\delta_{a,s}$, as expected; see Fig. 5(b). We note that a measurement of the Ramsey frequency is an accurate time resolved method to determine the qubit transition frequency $\omega_a = \omega_s + 2\pi\nu_{\mathrm{Ramsey}}$.

In conclusion, performing Rabi and Ramsey experiments we have observed high visibility in the oscillations of state population of a superconducting qubit. The temporal response and the backaction of the readout are quantitatively understood and well characterized. Our charge qubit, which is embedded in a well-controlled electromagnetic environment, has T_1 and T_2 times among the longest realized so far in superconducting systems. The simplicity and level of control possible in this circuit QED architecture makes it an attractive candidate for superconducting quantum computation.

We thank Jay Gambetta for discussions. This work was supported in part by NSA and ARDA under ARO Contract No. DAAD19-02-1-0045, and the NSF under Grants No. ITR-0325580 and No. DMR-0342157, the David and Lucile Packard Foundation, the W. M. Keck Foundation, and the NSERC of Canada.

[1] M. A. Nielsen and I. L. Chuang, *Quantum Computation and Quantum Information* (Cambridge University Press, Cambridge, 2000).
[2] M. H. Devoret, A. Wallraff, and J. M. Martinis, cond-mat/0411174.
[3] Y. Nakamura, Y. A. Pashkin, and J. S. Tsai, Nature (London) **398**, 786 (1999).
[4] D. Vion *et al.*, Science **296**, 886 (2002).
[5] J. M. Martinis *et al.*, Phys. Rev. Lett. **89**, 117901 (2002).
[6] Y. Yu *et al.*, Science **296**, 889 (2002).
[7] I. Chiorescu *et al.*, Science **299**, 1869 (2003).
[8] E. Collin *et al.*, Phys. Rev. Lett. **93**, 157005 (2004).
[9] A. J. Berkley *et al.*, Science **300**, 1548 (2003).
[10] Y. A. Pashkin *et al.*, Nature (London) **421**, 823 (2003).
[11] J. B. Majer *et al.*, Phys. Rev. Lett. **94**, 090501 (2005).
[12] I. Chiorescu *et al.*, Nature (London) **431**, 159 (2004).
[13] R. McDermott *et al.*, Science **307**, 1299 (2005).
[14] T. Yamamoto *et al.*, Nature (London) **425**, 941 (2003).
[15] R. Simmonds *et al.*, Phys. Rev. Lett. **93**, 077003 (2004).
[16] F. Meier and D. Loss, Phys. Rev. B **71**, 094519 (2005).
[17] T. Duty *et al.*, Phys. Rev. B **69**, 140503 (2004).
[18] O. Astafiev *et al.*, Phys. Rev. B **69**, 180507 (2004).
[19] A. Blais *et al.*, Phys. Rev. A **69**, 062320 (2004).
[20] D. I. Schuster *et al.*, Phys. Rev. Lett. **94**, 123602 (2005).
[21] V. Bouchiat *et al.*, Phys. Scr. **t76**, 165 (1998).
[22] A. Wallraff *et al.*, Nature (London) **431**, 162 (2004).
[23] L. Frunzio *et al.*, IEEE Trans. Appl. Supercond. **15**, 860 (2005).
[24] D. I. Schuster *et al.* (unpublished).
[25] A. Blais *et al.* (unpublished).

Backaction Effects of a SSET Measuring a Qubit Spectroscopy and Ground State Measurement

Benjamin Turek, Johannes Majer, Aashish Clerk, Steve Girvin, Andreas Wallraff, Kevin Bladh, David Gunnarsson, Tim Duty, Per Delsing, and Robert Schoelkopf

***Abstract*—We investigate the backaction of superconducting single-electron transistor (SSET) continuously measuring a Cooper-pair box. Due to the minimized backaction of the SSET, we observe a $2e$ periodic Coulomb staircase according to the two-level system Hamiltonian of the Cooper-pair box. We demonstrate that we can control the quantum broadening of the ground state in-situ. We perform spectroscopy measurements and demonstrate that we have full control over the Cooper-pair box Hamiltonian. The ability to reduce the backaction is a necessary condition to use the SSET as a quantum state readout for the CPB as a qubit.**

***Index Terms*—Quantum computing, superconducting devices.**

I. Introduction

An interesting question in solid-state quantum computation is how to measure a qubit and how the measurement process influences the qubit. Recently there has been considerable experimental progress using superconducting circuits to realize the qubit and the meter that measures the qubit. Many of the these devices are based on the single-Cooper-pair box [1], [2]. Coherent oscillations in such a Cooper-pair box have been observed [3]–[5] as well as Rabi oscillations [6] and Ramsey oscillation [7]. Despite these encouraging results, the measuring device and the influence of the measurement on the qubit are not yet completely understood.

In this article we report measurements where the Cooper-pair box is measured using a superconducting single-electron transistor (SSET). The SSET can be operated such that it continuously and weakly measures the charge of the Cooper-pair box. However, it also couples noise to the Cooper-pair box. This effect is called backaction and influences the states of the box in different ways. One can divide this influence in four categories, in order of decreasing severity, as follows:

First, the SSET can create nonequilibrium quasiparticles in the box. Therefore the states of the box are not described by Cooper-pair tunneling alone, and the box is no longer a simple two-level system. Quasiparticle poisoning is often [5], [8], [9], but not always [2], [4] observed in SSET measurements of the box, but its origin is not well understood. Second, even if there are no quasiparticles present, the SSET can excite the qubit. Now the box is still described by a two-level Hamiltonian, however the system does not stay in the ground state but is in a mixture of ground and excited state. Third, SSET's backaction can cause increased relaxation. After the box has been brought to the first excited state, the noise of the SSET can destroy the state of the box by extracting energy and bringing the system back to the ground state. The fourth category is the dephasing caused by the measurement process [10]. By the fundamental laws of quantum mechanics, measuring a system perturbs its state, and specifically destroys the phase of a superposition. Therefore this form of backaction is the fundamental limit.

The purpose of this article is to investigate the first two manifestations of backaction and to demonstrate that we were able to reduce them to observe the box in the $2e$-periodic ground state. Furthermore, we show that the box obeys a simple spin-1/2 Hamiltonian in which both terms can be controlled in-situ. We perform continuous-wave spectroscopy on the box, measuring the energy level separation and the avoided crossing of the charge states. We find that the quantum broadening of the Coulomb staircase is consistent with the level repulsion observed in spectroscopy.

II. The Cooper-Pair Box

The Cooper-pair box consists of a superconducting island which is connected to a superconducting lead via a Josephson junction (Fig. 1). Another gate lead allows one to change the electrostatic potential of the island with the application of a voltage V_{gb} through the capacitance C_{gb}. The state of the island is described by the number of Cooper-pairs on the island. Because the Josephson energy E_J is smaller than four times the charging energy $E_c = e^2/2C_\Sigma$, one has to consider only two charging states. The Cooper-pair box is described by the following Hamiltonian

$$\hat{H} = \frac{E_{el}}{2}\hat{\sigma}_z + \frac{E_J}{2}\hat{\sigma}_x \quad E_{el} = 4E_c(n_{gb} - 1) \tag{1}$$

where σ_z and σ_x are the Pauli matrices. n_{gb} is the number of electrons induced by the gate electrode $n_{gb} = C_{gb}V_{gb}/e$. The Josephson junction consists of two junctions in parallel, forming a SQUID loop [2] (see Fig. 1). The effective Josephson coupling E_J of these two junctions can be tuned with the magnetic flux Φ through the loop: $E_J = E_J^{\max}|\cos(\pi\Phi/\Phi_0)|$. Here $\Phi_0 = h/2e$ is the superconducting flux quantum. Therefore the split Cooper-pair box is described by the two-level Hamiltonian (1), where both terms can be controlled during the experiment.

Manuscript received October 4, 2004. This work was supported in part by the National Security Agency and Advanced Research and Development Activity under the Army Research Office, the NSF, the David and Lucile Packard Foundation, and the W. M. Keck Foundation.

B. Turek, J. Majer, A. Clerk, S. Girvin, A. Wallraff, and R. Schoelkopf are with the Department of Applied Physics and Physics, Yale University, New Haven, CT 06511 USA (e-mail: johannes.majer@yale.edu).

K. Bladh, D. Gunnarsson, T. Duty and P. Delsing are with the Microtechnology Center at Chalmers MC2, Department of Microelectronics and Nanoscience, Chalmers University of Technology and Göteborg University, SE-412 96, Göteborg, Sweden.

Digital Object Identifier 10.1109/TASC.2005.850096

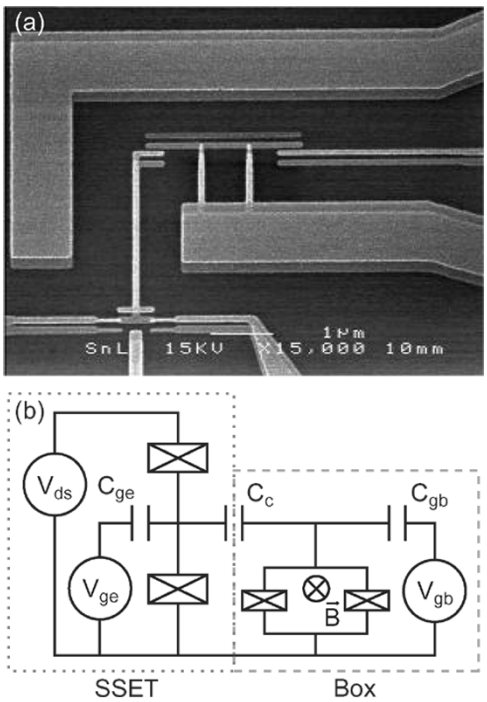

Fig. 1. (a) A scanning electron micrograph (SEM) of the device. The device is fabricated using shadow evaporation technique [11]. (b) The circuit diagram for the Cooper-pair box coupled with C_C to the superconducting-single-electron transistor.

The states and the energy levels of the system can by found by diagonalizing the Hamiltonian (1). The energy difference between the ground state and the excited state is given by

$$\Delta E = \sqrt{E_J^2 + (4E_c)^2(n_{gb} - 1)^2} \tag{2}$$

Far away from the degeneracy point ($|n_{gb} - 1| \gg 0$) the eigenstates are given by pure charge states. However in the vicinity of the degeneracy point ($|n_{gb} - 1| \approx E_J/4E_c$) the eigenstates are superpositions of charge states and the energy levels show an avoided crossing.

The charge of the box in the ground state is given by the expectation value of the charge operator $\hat{q} = e(1 + \hat{\sigma}_z)$ in the ground state:

$$\langle q \rangle_{\substack{\text{ground} \\ \text{state}}} = e\left(1 + \frac{n_{gb} - 1}{\sqrt{\left(\frac{E_J}{4E_c}\right)^2 + (n_{gb} - 1)^2}}\right) \tag{3}$$

Without any Josephson coupling ($E_J = 0$) the box charge versus applied gate voltage (i.e. Coulomb staircase) is just a simple step function, which is 0 for $n_{gb} < 1$ and 2 for $n_{gb} > 1$. However with a finite Josephson energy E_J, a superposition of charge states exists in the region where $E_J \approx E_{el}$ and therefore the step becomes broadened. The larger the value of E_J gets, the broader the step function. The charge of the box in the excited state is given by $\langle q \rangle_{\text{excited state}} = 2e - \langle q \rangle_{\text{ground state}}$.

III. Measurements

The sample was measured in a dilution refrigerator at 13 mK. This thermal energy is far less than the relevant energy scales

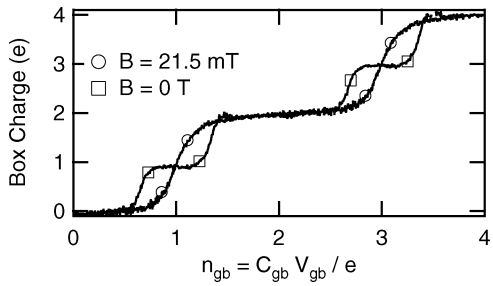

Fig. 2. The Coulomb staircase, i.e. box charge versus induced gate charge n_{gb}, without (square symbols) and with (circular symbols) magnetic field applied. The magnetic field affects the superconducting gap and removes the quasiparticle poisoning.

of either the SSET or the box. The charge of the box is measured with a SSET placed nearby (Fig. 1). Via the capacitor C_C, a small fraction ($C_C/C_\Sigma = 2.5\%$) of the charge of the box island couples to the SSET island. The SSET is operated as an radio-frequency single-electron transistor (RF-SET) [12], which is an outstanding electrometer. The sensitivity of the electrometer as well as the backaction noise [13] depend strongly on the operation point of the SSET, which can be tuned with the drain-source voltage V_{DS} and the SSET gate voltage V_{ge}.

First we biased the SSET on the gap rise. The measured box charge as a function of the applied gate voltage V_{gb}, is completely $1e$ periodic, similar to the observations by Männik *et al.* [9]. At this bias point ($V_{ds} = 4\Delta/e \approx 1$ mV), the current through the SSET breaks many pairs in the drain and source lead of the SSET, though the power dissipated is only 1–10 pW. This apparently induces nonequilibrium quasiparticles in the box, though there is no direct connection between them and the mechanism is not known. This backaction noise is of the first kind as described above.

We then bias the SSET on the double Josephson quasiparticle process (DJQP) [13], [14], which occurs at lower SSET drain-source voltage. Fig. 2 shows with square symbols the measured Coulomb staircase. The Coulomb staircase is $2e$-periodic, however at odd number of electrons an intermediate step occurs due to quasiparticle poisoning. However after applying a magnetic field of 20 mT perpendicular to the substrate, the small step disappears (Fig. 2 circular symbols). The Coulomb staircase follows exactly the theoretical prediction (3). Applying a magnetic field lowers the superconducting gap in the aluminum, and could reduce the gap in the larger leads more than in the thin island [15]. The quasiparticle states in the leads would have a lower energy than on the island and therefore the quasiparticles can not tunnel on the island and poison the Coulomb staircase, as observed in SSET's [16]. A similar method has been used by Duty *et al.* [4] where a large magnetic field parallel to the device is applied. In contrast to previous experiments by Lehnert *et al.* [8] the box measured here has a smaller charging energy and therefore the quasiparticle states are more separated. In conclusion, using the optimal bias point of the SSET, applying a magnetic field and reducing the charging energy of the box allows us to measure a full Coulomb staircase that is not quasiparticle poisoned. Hence, we can avoid the backaction of the first category.

We measured the Coulomb staircase as function of the applied magnetic field (Fig. 3). One observes that the Coulomb

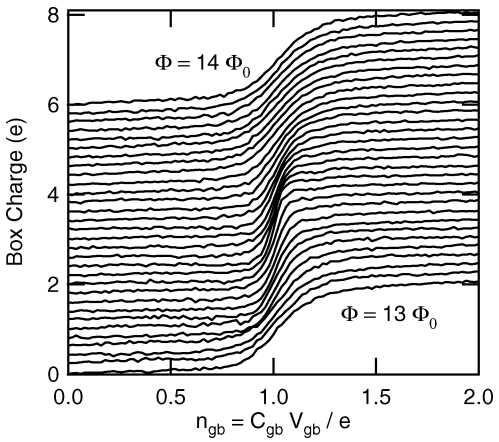

Fig. 3. Coulomb staircase for different magnetic field values. The staircase is periodically broadened and sharpened as a function of the applied flux. For integer flux quanta, i.e. large E_J, the staircase is maximally broadened and for half integer flux quanta, i.e. small E_J, step-like. Note: 13 Φ_0 correspond to 27 mT.

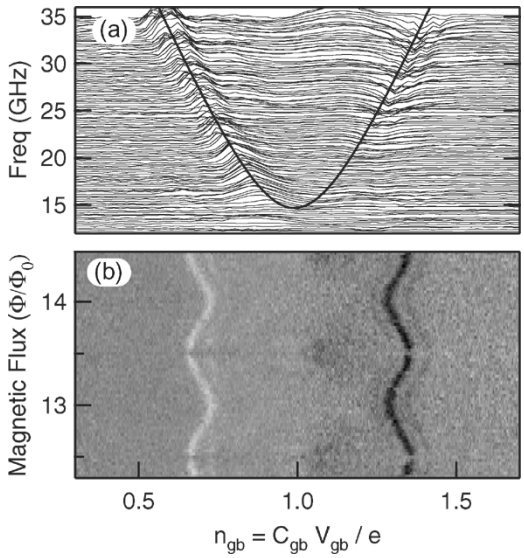

Fig. 4. Microwave spectroscopy results. Obtained by measuring the Coulomb staircase with microwaves applied and subtracting the staircase without microwaves. (a) Spectroscopy versus microwave frequency. From the fit with the hyperbola (Eq. (2)) we obtain $E_J = 14.9$ GHz and $E_c = 18.9$ GHz. (b) Spectroscopy versus magnetic field. A microwave signal with a frequency of 25 GHz is applied. The peak and dip oscillate as a function of the applied flux. For integer flux quanta, i.e. large E_J, the avoided energy level crossing is large and the resonances move inwards, toward the degeneracy point ($n_{gb} = 1$). Note: each plot is 10 hours of data without any offset charge jump.

staircase periodically sharpens and broadens. The period is consistent with the number of flux quanta in the split box junction. At integer flux quanta the Josephson energy is maximal and the Coulomb staircase is maximally broadened. At half integer flux, the Josephson energy is suppressed and the Coulomb staircase approaches a step-like function. We fit the theoretical expression (3) to the staircases, which allows us to extract the energy ratio between Josephson and charging energy $(E_J/4E_c)$. This ratio as a function of magnetic field is plotted in Fig. 5.

The shape of the Coulomb staircase in Fig. 3 is not generic. In order to observe these curves the SSET has to be biased slightly below the DJQP resonance. At this bias point theory [13] predicts that the backaction noise is primarily relaxing the box, i.e. there is backaction noise of the third category, but no backaction of the second kind. The box is therefore forced into the ground state by the noise of the SSET.

To observe the excited state and the energy spectrum of the box, we perform spectroscopy by applying a continuous microwave signal to the gate of the Cooper-pair box. When the microwave energy $h\nu$ (where h is Planck's constant) matches the energy difference between the ground and excited state, the microwaves induce a transition from the ground state to the excited state. The system can be put in a mixture of ground and excited state at two discrete points in gate charge where the excitation is resonant. This microwave response appears as an extra peak and dip in the Coulomb staircase. We measured the Coulomb staircase with and without microwave signal and subtracted them to separate out the microwave induced response. Fig. 4(a) shows the microwave peak and dip as a function of the applied microwave frequency. The position of peak and dip follow the expected hyperbolic behavior with an avoided crossing of about 15 GHz. By fitting the positions with the expression for the energy level difference (2) we can extract the Josephson energy $E_J = 14.9$ GHz and the charging energy $E_c = 18.9$ GHz. This measurement was performed at integer flux quanta applied and therefore maximal E_J. One observes that the peak and dip height disappear toward the degeneracy point. This is due to the fact that the eigenstates are superposition of charge states and the difference of the box charge between the ground state and the excited state becomes small and disappears at the degeneracy point. The fact that our Coulomb staircase is not quasiparticle poisoned is very important, because it allows us to observe the spectroscopy signal down to the degeneracy point.

We also performed spectroscopy for a constant frequency of 25 GHz and varying magnetic fields (Fig. 4(b)). One observes that the peak and dip positions oscillate periodically with the applied the flux. As the E_J becomes larger, the avoided crossing is larger and therefore the energy levels are more rounded. Hence the position, where the microwave frequency is in resonance with the energy level difference, moves toward the degeneracy point $(n_{gb} = 1)$. One can also observe that the signal disappears at the positions where E_J is minimal (i.e. half integer flux quanta). When E_J is zero, the eigenstates are pure charge states. Our microwave excitation is applied to the gate and is therefore a charge excitation. Since only a perpendicular component can induce transitions between states, the microwave signal is not able to drive the transition.

The spectroscopically obtained values of E_J and E_c versus magnetic field are shown in Fig. 5 (empty symbols) and can be compared with the values derived from the ground state. One observes that the two curves, obtained in completely different measurements, agree very well. This confirms that the measured Coulomb staircase is indeed the ground state of the two-level system and that the broadening is only due to quantum fluctuations. Hence we demonstrate that the Cooper-pair box is not affected by backaction of the second category. One observes a small discrepancy of the two measurements at low values of E_J. This is possibly due to $1/f$ charge noise which additionally broadens the step.

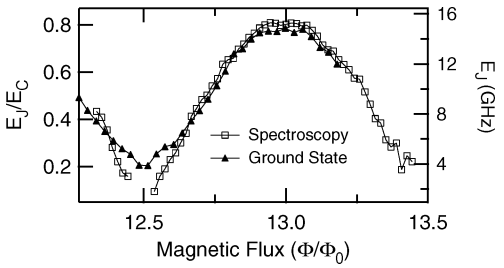

Fig. 5. Energy ratio E_J/E_c versus magnetic field, obtained from the broadening of the ground state (solid symbols) and from the spectroscopy (open symbols).

IV. Conclusion

In these experiments we demonstrate that we are able to eliminate the two most severe forms of backaction on the Cooper-pair box: The backaction that creates nonequilibrium quasiparticles on the Cooper-pair box and the backaction noise that excites the box from the ground to the excited state. With biasing the SSET at the optimal position and applying a small field, we are able to observe the ground state of the Cooper-pair box without quasiparticle poisoning. Spectroscopy and ground state measurements demonstrate that the Cooper-pair box is behaving according to the simple two-level Hamiltonian (1) and that we are able to control both terms in-situ. The good agreement between spectroscopy and ground state results shows that we are indeed observing the ground state of the system.

However, as discussed above, the SSET may still be relaxing the box, i.e. backaction of the third category. Further measurements will address the backaction induced contribution to the relaxation.

Acknowledgment

The authors would like to thank M. H. Devoret, D. Esteve, K. Lehnert, L. Frunzio, and J. Teufel for useful discussions.

References

[1] M. Büttiker, "Zero-current potential drop across small-capacitance Josephson junctions," *Phys. Rev. B*, vol. 36, pp. 3548–3555, 1987.
[2] V. Bouchiat, D. Vion, P. Joyez, D. Esteve, and M. H. Devoret, "Quantum coherence with a single Cooper pair," *Phys. Scr.*, vol. T76, pp. 165–170, 1998.
[3] Y. Nakamura, Y. A. Pashkin, and J. S. Tsai, "Coherent control of macroscopic quantum states in a single-Cooper-pair box," *Nature*, vol. 398, pp. 786–788, 1999.
[4] T. Duty, D. Gunnarsson, K. Bladh, and P. Delsing, "Coherent dynamics of a Josephson charge qubit," *Phys. Rev. B*, vol. 69, p. 140 503(R), 2004.
[5] A. Guillaume, J. F. Schneiderman, P. Delsing, H. M. Bozler, and P. M. Echternach, "Free evolution of superposition states in a single Cooper pair box," *Phys. Rev. B*, vol. 69, p. 132 504, 2004.
[6] Y. Nakamura, Y. A. Pashkin, and J. S. Tsai, "Rabi oscillations in a Josephson-junction charge two-level system," *Phys. Rev. Lett.*, vol. 87, p. 246 601, 2001.
[7] D. Vion, A. Aassime, A. Cottet, P. Joyez, H. Pothier, C. Urbina, D. Esteve, and M. H. Devoret, "Manipulating the quantum state of an electrical circuit," *Science*, vol. 296, pp. 886–889, 2002.
[8] K. W. Lehnert, K. Bladh, L. F. Spietz, D. Gunnarsson, D. I. Schuster, P. Delsing, and R. J. Schoelkopf, "Measurement of the excited-state lifetime of a microelectronic circuit," *Phys. Rev. Lett.*, vol. 90, p. 027 002, 2003.
[9] J. Männik and J. E. Lukens, "Effect of measurement on the periodicity of the Colomb staircase of a superconducting box," *Phys. Rev. Lett.*, vol. 92, p. 057 004, 2004.
[10] M. H. Devoret and R. J. Schoelkopf, "Amplifying quantum signals with the single-electron transistor," *Nature*, vol. 406, pp. 1039–1046, 2000.
[11] G. J. Dolan, "Offset masks for lift-off photoprocessing," *Appl. Phys. Lett.*, vol. 31, p. 337, 1977.
[12] R. J. Schoelkopf, P. Wahlgren, A. A. Koshevnikov, P. Delsing, and D. E. Prober, "The radio-frequency single-electron transistor (RF-SET): a fast and ultrasensitive electrometer," *Science*, vol. 280, pp. 1238–1242, 1998.
[13] A. A. Clerk, S. M. Girvin, A. K. Nguyen, and A. D. Stone, "Resonant Cooper-pair tunneling: quantum noise and measurement characteristics," *Phys. Rev. Lett.*, vol. 89, p. 176 804, 2002.
[14] S. Pohlen, "The Superconducting Single Electron Transistor," Ph.D. thesis, Harvard, 1999.
[15] A. Anthore, H. Pothier, and D. Esteve, "Density of states in a superconductor carrying a supercurrent," *Phys. Rev. Lett.*, vol. 90, p. 127 001, 2003.
[16] J. Aumentado, M. W. Keller, J. M. Martinis, and M. H. Devoret, "Nonequilibrium quasiparticles and 2e periodicity in single-Cooper-pair transistors," *Phys. Rev. Lett.*, vol. 92, p. 066 802, 2004.

Fabrication and Characterization of Superconducting Circuit QED Devices for Quantum Computation

Luigi Frunzio, Andreas Wallraff, David Schuster, Johannes Majer, and Robert Schoelkopf

***Abstract*—We present fabrication and characterization procedures of devices for circuit quantum electrodynamics (cQED). We have made 3-GHz cavities with quality factors in the range 10^4–10^6, which allow access to the strong coupling regime of cQED. The cavities are transmission line resonators made by photolithography. They are coupled to the input and output ports via gap capacitors. An Al-based Cooper pair box is made by e-beam lithography and Dolan bridge double-angle evaporation in superconducting resonators with high quality factor. An important issue is to characterize the quality factor of the resonators. We present an RF-characterization of superconducting resonators as a function of temperature and magnetic field. We have realized different versions of the system with different box-cavity couplings by using different dielectrics and by changing the box geometry. Moreover, the cQED approach can be used as a diagnostic tool of qubit internal losses.**

***Index Terms*—Distributed parameter circuits, Q factor, scattering parameters measurement, superconducting cavity resonators.**

I. Introduction

We have recently demonstrated that a superconducting quantum two-level system can be strongly coupled to a single microwave photon [1], [2]. The strong coupling between a quantum solid state circuit and an individual photon, analogous to atomic cavity quantum electrodynamics (CQED) [3], has previously been envisaged by many authors, see [4] and references therein. Our circuit quantum electrodynamics architecture [4], in which a superconducting charge qubit, the Cooper pair box (CPB) [5], is coupled strongly to a coplanar transmission line resonator, has great prospects both for performing quantum optics experiments [6] in solids and for realizing elements for quantum information processing [7] with superconducting circuits [8]–[14] and also for other architectures [15], [16].

In developing these qubit-resonator systems, one key ingredient is to design and realize transmission line resonators with high internal quality factor, $Q_{\rm int}$, and with resonant frequency, ν_o, in the 5–15 GHz range to match the other energy scales of our device, and to be in the quantum regime ($h\nu_o \gg k_BT$) at $T = 30$ mK. On the other hand, the resonator is loaded with input and output capacitances and we need a loaded quality factor $Q_L \approx 10^4$ in order to obtain reasonably fast rate of measurement, $\kappa = \nu_o/Q_L \approx 1$ MHz.

In fabricating the transmission line resonator, we opted for a coplanar waveguide (CPW) for many different reasons. First, a CPW has a simple layer structure with no need for deposited insulators. Second, it has a balanced structure with a relatively easy planar connection to the CPB. Third, a CPW has a ν_o that is relatively insensitive to kinetic inductance and dominated by geometrical distributed inductance. Last but not the least, CPW-based structures, made by Al thin film deposited on sapphire, have been recently shown [17] to allow very high Q's (order of 10^6).

We decided to fabricate on passivated Si wafers because this is the substrate on which we had previously developed the qubit fabrication. We also decided to try as material for the resonators both Al, for easy compatibility with the qubit process, and Nb, because its higher critical temperature allows testing of resonators at higher temperatures.

In Section II, we present design consideration for devices for circuit quantum electrodynamics (cQED). We will show that we can engineer Q with different coupling of the resonator to the input and output ports and that the internal losses can be made negligible at the designed Q [1], [2]. Section III introduces the fabrication procedures for both the resonator and the CPB. Sections IV–VI present an RF-characterization of the superconducting transmission line resonators versus temperature and magnetic field.

II. Circuit Design

A picture of a 10×3 mm^2 chip containing a 3-GHz superconducting Nb CPW resonator is shown in Fig. 1(a). The length of the meandering resonator is $2l = 4$ mm. The center conductor is 10 μm wide, separated from the lateral ground planes extending to the edges of the chip by a 5 μm gap, resulting in a wave impedance of the coplanar waveguide of $Z = 50\ \Omega$ to match the impedance of conventional microwave components. The capacitance per unit length is $C_s \approx 0.13$ fF/μm^2 which gives a total resonator capacitance of $C = C_s l/2 = 1.6$ pF. The resonator is coupled by identical capacitors at each end (see solid line square in Fig. 1(a)) to an input and output feed line, fanning out to the edge of the chip and keeping the impedance constant. In Fig. 1(b) and (1d) are shown micrographs of two of the coupling capacitors with different geometries. The one in Fig. 1(b) consists of two 100-μm long and 4-μm wide fingers separated by a 2-μm gap. It has a capacitance, $C_{\kappa,b} \approx 6$ fF, larger than that in Fig. 1(d), which has a simpler geometry with a 4- μm gap and $C_{\kappa,d} \approx 0.3$ fF.

Manuscript received October 4, 2004. This work was supported in part by the National Security Agency (NSA) and Advanced Research and Development Activity (ARDA) under Army Research Office (ARO) Contract DAAD19-02-1-0045, the NSF ITR Program under Grant DMR-0325580, the NSF under Grant DMR-0342157, the David and Lucile Packard Foundation, and the W. M. Keck Foundation.

The authors are with the Department of Applied Physics, Yale University, New Haven, CT 06520 USA (e-mail: luigi.frunzio@yale.edu).

Digital Object Identifier 10.1109/TASC.2005.850084

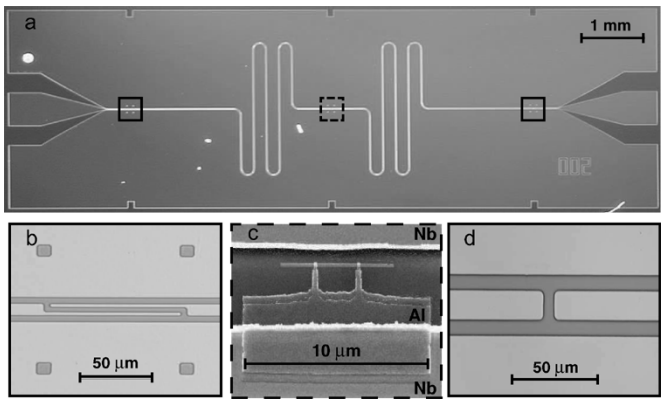

Fig. 1. Picture of a device for circuit QED. (a) The 3 GHz superconducting coplanar waveguide resonator is fabricated using optical lithography. The length of the meandering resonator is $l = 24$ mm. The center conductor is 10 μm wide, separated from the lateral ground planes extending to the edges of the chip by a 5 μm gap. The resonator is coupled by identical capacitors at each end (solid line squares) to input and output ports. (b) Micrograph of a coupling capacitance with two 100 μm long and 4 μm wide fingers separated by a 2 μm gap. (c) Scanning electron micrograph of a Cooper pair box fabricated onto the silicon substrate into the gap between the center conductor (top) and the ground plane(bottom) in the center of a resonator (dashed line square) using electron beam lithography and double angle evaporation of aluminum. (d) Micrograph of a coupling capacitance with a 4 μm gap.

The capacitive coupling to the input and output lines, together with the loading impedance, $R_L = 50\ \Omega$, are very important in determining the loaded quality factor Q_L, defined by

$$\frac{1}{Q_L} = \frac{1}{Q_{\rm int}} + \frac{1}{Q_{\rm ext}} \tag{1}$$

where the external quality factor is

$$Q_{\rm ext} = \frac{\omega C}{G_{\rm ext}} \tag{2}$$

with

$$G_{\rm ext} = \frac{2R_L C_\kappa^2 \omega^2}{1 + R_L^2 C_\kappa^2 \omega^2}. \tag{3}$$

There are two possible regimes for the resonator. It can be undercoupled when C_κ is small (like $C_{\kappa,d}$) and then $Q_L \approx Q_{\rm int}$. This is the regime in which it is possible to measure $Q_{\rm int}$. Otherwise, the resonator can be overcoupled when C_κ is large (like $C_{\kappa,b}$) and then $Q_L \approx Q_{\rm ext}$. It is then possible to engineer the Q_L to obtain fast measurement with κ much larger than the qubit decay rates [1], [2].

In Fig. 1(c) an electron micrograph of a Cooper pair box is shown. The CPB consists of a 7-μm long and 200-nm wide superconducting island parallel to the center conductor which is coupled via two 200 × 100 nm^2 size Josephson tunnel junctions to a much larger superconducting reservoir. The CPB is fabricated onto the silicon substrate [see dashed line square in Fig. 1(a)] in the gap between the center conductor (top) and the ground plane (bottom) at an antinode of the electric field in the resonator. The Josephson junctions are formed at the overlap between the island and the fingers extending from the reservoir, which is capacitively coupled to the ground plane. The CPB is a two-state system described by the Hamiltonian $H = -(E_{el}\sigma_x + E_J\sigma_z)/2$ where E_{el} is the electrostatic energy and $E_J = E_{J,max}\cos(\pi\Phi_b)$ is the Josephson energy. The overall energy scales of these terms, the charging energy E_{el} and the Josephson energy $E_{J,max}$, can be readily engineered during the fabrication by the choice of the total box capacitance and resistance respectively, and then further tuned *in situ* by electrical means. A flux bias $\Phi_b = \Phi/\Phi_o$, applied with an external coil to the loop of the box, controls E_J. We have demonstrated that changing the length of the CPB island and its distance to the center conductor and changing the dielectrics (removing the passivation step of the Si substrate), we can obtain stronger couplings of qubit and resonator as predicted by simple electrostatic calculations of the capacitances.

III. Device Fabrication

The pattern of 36 different Nb resonators is generated exposing a bilayer photoresist (600 nm LOR5A and 1.2 μm S1813) through a mask with traditional UV photolithography. Then a 200-nm thick Nb film is dc magnetron sputtered in Ar at 1.5 Pa with a rate of 1 nm/s in an UHV system with a base pressure of 20 μPa. The substrate is a 2″ 300-μm thick p-doped (Boron) (100) oriented Si wafer with resistivity $\rho > 1000\ \Omega$cm previously passivated by thermal wet oxidation with a 470-nm thick layer of SiO_2. A lift-off process in NMP followed by ultrasonic agitation completes the resonator fabrication.

Al resonators are fabricated on the same type of substrate depositing a 200-nm thick Al film by thermal evaporation at a rate of 1 nm/s in the same UHV system. Then the same mask is used to expose a single photoresist layer (1.2 μm S1813) and then realized by wet etching $(8:4:1:1 = H_3PO_4 : CH_3COOH : HNO_3 : H_2O)$ the metal.

In both cases, chips containing individual resonators are obtained by dicing the Si wafer. The CPB qubit [Fig. 1(c)] is then fabricated on an individual resonator by a simple Dolan bridge technique [18] exposing a bilayer resist (500 nm MMA-(8.5)MAA EL13 and 100 nm 950 K PMMA A3) by e-beam lithography and then e-beam evaporating Al (35 nm for the base and 70 nm for the top electrode) at a rate of 1 nm/s in a double-angle UHV system with a base pressure of 20 μPa. The junction barrier is realized with a 12 min thermal oxidation in a 400 Pa of O_2. A lift-off process in hot acetone and ultrasonic agitation complete the device. To couple the qubit reservoir to ground with a large capacitance, the base electrode is deposited with a little angle taking advantage of the shadow of the thicker Nb film to define the capacitor.

IV. Measurement Technique

The frequency dependence of the transmission through the resonators[1] was measured using a vector network analyzer. The equivalent circuit of the measurement setup is shown in the inset of Fig. 3. The sample was mounted on a PC board in a closed copper sample box (Fig. 2) equipped with blind mate SMP connectors that launch the microwaves onto the PC board CPW's. The sample was cooled to temperatures ranging from

[1]The transmission is measured in dB $= 10\log|V_2/V_1|^2$, where V_2 is the voltage measured at the input port of the analyzer and V_1 is the voltage applied at the output port of the analyzer.

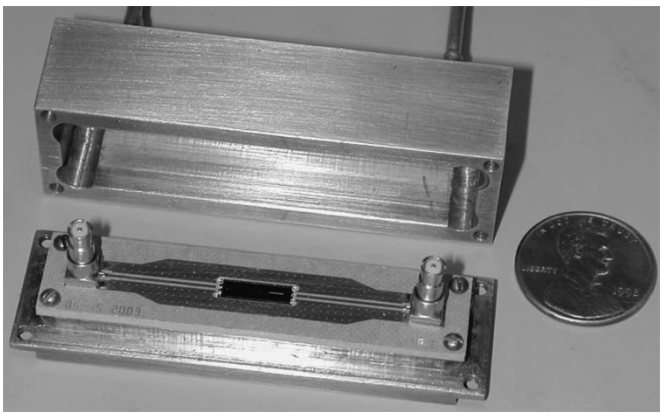

Fig. 2. Picture of the copper sample box containing a resonator mounted on the PC board.

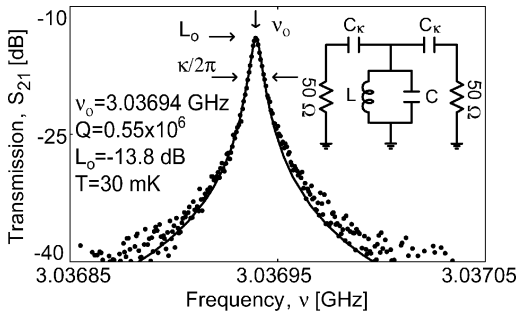

Fig. 3. Measured transmission power spectrum of an undercoupled resonator. The solid line is a fit to a Lorentzian line.

the critical temperature, T_c of the superconducting films down to $T = 30$ mK.

The transmission S_{21} through the resonator around its fundamental resonant frequency ν_o is shown in Fig. 3 at $T = 30$ mK. The curve was acquired using a -60 dBm input power[2] and a room temperature amplifier. The input power was lowered until no distortion of the resonance curve due to excessive input power could be observed. The network analyzer was response calibrated (S_{21}) up to the input and output ports of the cryostat and the absorption of the cabling in the cryostat was determined to be approximately -7 dB in a calibrated S_{11} and S_{22} reflection measurement. The quality factor of the resonator is determined by fitting a Lorentzian line to the measured power spectrum as shown by the solid line in Fig. 3. This is the power spectrum of an undercoupled resonator and from the fit we have extracted $\nu_o = 3.036\,94$ GHz. At this frequency the insertion loss is $L_o = -13$ dB. The quality factor is determined from the full width at half max of the fitted power spectrum and is found to be $Q_L \approx Q_{\rm int} = \nu_o/2\delta\nu_o = 2\pi\nu_o/\kappa = 0.55 \times 10^6$.

V. Temperature Dependence of Q and ν_o

In Fig. 4, we show the measured temperature dependence of the quality factor Q for an undercoupled resonator (solid dots) and an overcoupled one (open dots). The lines in Fig. 4 are generated by summing a $Q_{\rm int}$ that scales exponentially with the reduced temperature, T_c/T, in parallel with a constant $Q_{\rm ext}$. At

[2]The input power is in dBm where $-60\ {\rm dBm} = 20\log(1\ \mu{\rm W}/1\ {\rm mW})$.

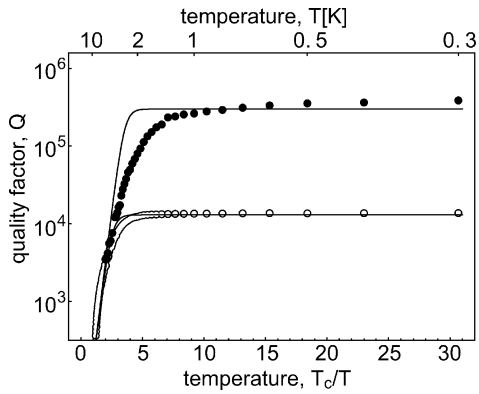

Fig. 4. Temperature dependence of the quality factor Q of two 3 GHz superconducting Nb coplanar waveguide resonators at their first harmonic resonant frequency (6 GHz). Solid dots are data collected on a undercoupled resonator and open dots are from an overcoupled one. The lines are generated by summing a $Q_{\rm int}$ that scales exponentially with the reduced temperature, T_c/T, in parallel with a constant $Q_{\rm ext}$.

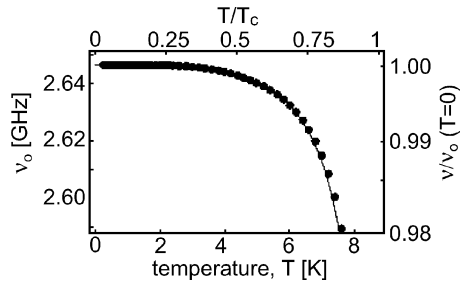

Fig. 5. Temperature dependence of the resonant frequency ν_o of a superconducting Nb coplanar waveguide resonator. Solid line is a fit to a kinetic inductance model.

low temperature, the coupling saturates the Q of the overcoupled resonator, while it seems that Q for the undercoupled one has still some weak temperature dependence whose nature is still unknown. We speculate that either vortices or losses in the dielectrics could limit the Q of this resonator but neither of these interpretations offer an easy understanding of the weak temperature dependence.

We have observed a shift of the resonant frequency ν_o with temperature as shown in Fig. 5, which can be understood in terms of the temperature dependent kinetic inductance of the resonator [17], [19]. ν_o is proportional to $1/\sqrt{L}$, where the total inductance of the resonator L is the sum of the temperature independent geometric inductance L_m and the temperature dependent kinetic inductance L_k. The kinetic inductance scales as $L_k \propto \lambda_L(T)^2$, where $\lambda_L(T)$ is the temperature dependent London penetration depth. The best fit in Fig. 4 was achieved for a ratio $L_k/L_m \approx 4\%$ and a critical temperature of $T_c \approx 8.75$ K, which we have independently measured on a test sample fabricated on the same wafer.

VI. Magnetic Field Dependence of Q

As explained in Section II, we need to apply a magnetic field perpendicular to the qubit loop in order to tune E_J. Then, we measured the quality factor of two resonators as a function of the magnetic field at $T = 300$ mK, as shown in Fig. 6. It is evident that the Nb film (upper part) is less sensitive to the applied

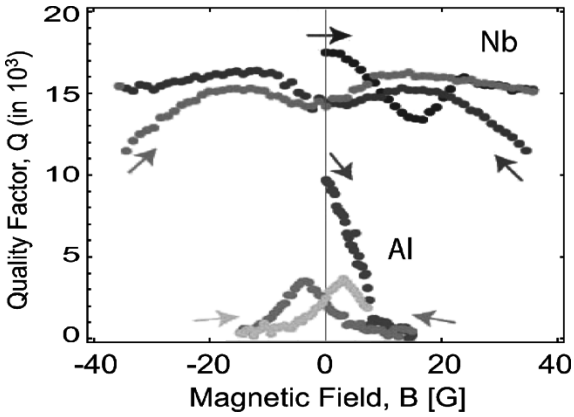

Fig. 6. Magnetic field dependence of the quality factor Q of two different superconducting coplanar waveguide resonators at $T = 300$ mK. In the upper part data refer to a Nb resonator, while in the lower part they refer to an Al resonator. Arrows indicate the direction in which the magnetic field was swept in both case starting from zero.

field than the Al film (lower part). In both cases there seems to be a reproducible and irreversible hysteretic behavior that can be reset by thermal cycling the sample. In our recent works [1], [2] we have observed a focusing effect on the magnetic field such that the effective field in the gap of the resonator was approximately two orders of magnitude larger than the applied magnetic field. We believe that the hysteretic phenomena could be in fact a result of vortices being trapped in the resonator film due to these large effective fields.

VII. Conclusion

In summary, we have designed and fabricated devices for realizing a circuit quantum electrodynamics architecture in which a qubit can be strongly coupled to a single microwave photon. We have shown that we can engineer Q with different coupling of the resonator to the input and output ports and that the internal losses can be made negligible at the designed Q. Indeed, we have achieved high $Q = 0.55 \times 10^6$ in the undercoupled CPW resonators and $Q \approx 10^4$ in the overcoupled ones, which allow fast measurement of the qubit.

To help determine the mechanism of the losses, one can fabricate resonators on different substrates [Si with different resistivity, sapphire, Si_3N_4)], or in different superconductors (Ta, Al). In fact, quality factor measurements in this type of resonant circuits serve as a sensitive probe of material losses in dielectrics and superconductors in the GHz frequency range at millikelvin temperatures. These presently unknown properties may in fact pose a serious limit for all superconducting qubits, though the large internal Q's already observed are highly encouraging. Better knowledge of the material losses, and techniques to characterize them, may be crucial not only for future improvements of circuit QED devices, but also for designing and realizing robust, long-lived superconducting qubits.

References

[1] A. Wallraff, D. Schuster, A. Blais, L. Frunzio, R.-S. Huang, J. Majer, S. Kumar, S. Girvin, and R. Schoelkopf, "Strong coupling of a single photon to a superconducting qubit using circuit quantum electrodynamics," *Nature*, vol. 431, pp. 162–167, 2004.

[2] D. Schuster, A. Wallraff, A. Blais, L. Frunzio, R.-S. Huang, J. Majer, S. M. Girvin, and R. J. Schoelkopf, "AC-Stark shift and dephasing of a superconducting quibit strongly coupled to a cavity field," *Phys. Rev. Lett.*, to be published.

[3] H. Mabuchi and A. Doherty, "Cavity quantum electrodynamics: Coherence in context," *Science*, vol. 298, pp. 1372–1377, 2002.

[4] A. Blais, R.-S. Huang, A. Wallraff, S. Girvin, and R. Schoelkopf, "Cavity quantum electrodynamics for superconducting electrical circuits: an architecture for quantum computation," *Phys. Rev. A*, vol. 69, p. 062 320, 2004.

[5] V. Bouchiat, D. Vion, P. Joyez, D. Esteve, and M. H. Devoret, "Quantum coherence with a single Cooper pair," *Physica Scripta*, vol. T76, pp. 165–170, 1998.

[6] D. Walls and G. Milburn, *Quantum Optics*. Berlin, Germany: Springer-Verlag, 1994.

[7] M. A. Nielsen and I. L. Chuang, *Quantum Computation and Quantum Information*. Cambridge, U.K.: Cambridge Univ. Press, 2000.

[8] Y. Nakamura, Y. A. Pashkin, and J. S. Tsai, "S. Coherent control of macroscopic quantum states in a single- Cooper-pair box," *Nature*, vol. 398, pp. 786–788, 1999.

[9] D. Vion, A. Aassime, A. Cottet, P. Joyez, H. Pothier, C. Urbina, D. Esteve, and M. H. Devoret, "Manipulating the quantum state of an electrical circuit," *Science*, vol. 296, pp. 886–889, 2002.

[10] J. M. Martinis, S. Nam, J. Aumentado, and C. Urbina, "Rabi oscillations in a large Josephson-junction qubit," *Phys. Rev. Lett.*, vol. 89, p. 117 901, 2002.

[11] Y. Yu, S. Han, X. Chu, S.-I. Chu, and Y. Wang, "Coherent temporal oscillations of macroscopic quantum states in a Josephson junction," *Science*, vol. 296, pp. 889–892, 2002.

[12] I. Chiorescu, Y. Nakmura, C. J. P. M. Harmans, and J. E. Mooij, "Coherent quantum dynamics of a superconducting flux qubit," *Science*, vol. 299, pp. 1869–1871, 2003.

[13] T. Yamamoto, Y. A. Pashkin, O. Astafiev, Y. Nakamura, and J. S. Tsai, "Demonstration of conditional gate operation using superconducting charge qubits," *Nature*, vol. 425, pp. 941–944, 2003.

[14] I. Chiorescu, P. Bertet, K. Semba, Y. Nakmura, C. J. P. M. Harmans, and J. E. Mooij, "Coherent dynamics of a flux qubit coupled to a harmonic oscillator," *Nature*, vol. 431, pp. 159–162, 2004.

[15] A. S. Srensen, C. H. van derWal, L. Childress, and M. D. Lukin, "Capacitive coupling of atomic systems to mesoscopic conductors," *Phys. Rev. Lett.*, vol. 92, p. 063 601, 2004.

[16] L. Tian, P. Rabl, R. Blatt, and P. Zoller, *Interfacing Quant. Opt. Solid State Qubits*, to be published.

[17] P. K. Day, H. G. LeDuc, B. A. Mazin, A. Vayonakis, and J. Zmuidzinas, "A broad-band superconducting detector suitable for use in large arrays," *Nature*, vol. 425, pp. 817–821, 2003.

[18] G. J. Dolan, "Offset masks for lift-off processing," *Appl. Phys, Lett.*, vol. 31, pp. 337–339, 1977.

[19] K. Yoshida, K. Watanabe, T. Kisu, and K. Enpuku, "Evaluation of magnetic penetration depth and surface resistance of superconducting thin films using coplanar waveguides," *IEEE Trans. Appl. Supercond.*, vol. 5, no. 2, pp. 1979–1982, Jun. 1995.

Theory of Microwave Parametric Down-Conversion and Squeezing Using Circuit QED

K. Moon[1,2] and S. M. Girvin[1]

[1]*Sloane Physics Laboratory, PO Box 208120, Yale University, New Haven, Connecticut 06520-8120, USA*
[2]*Department of Physics and Institute of Physics and Applied Physics, Yonsei University, Seoul 120-749, Korea*

(Received 1 June 2005; published 30 September 2005)

We study theoretically the parametric down-conversion and squeezing of microwaves using cavity quantum electrodynamics of a superconducting Cooper-pair box (CPB) qubit located inside a transmission line resonator. The nonlinear susceptibility χ_2 describing three-wave mixing can be tuned by dc gate voltage applied to the CPB and vanishes by symmetry at the charge degeneracy point. We show that the coherent coupling of different cavity modes through the qubit can generate a squeezed state. Based on parameters realized in recent successful circuit QED experiments, squeezing of 95% $\sim$ 13 dB below the vacuum noise level should be readily achievable.

DOI: 10.1103/PhysRevLett.95.140504 PACS numbers: 03.67.Lx, 42.50.Dv, 74.50.+r, 42.50.Pq

Squeezed states are a valuable tool to usefully manipulate the Heisenberg uncertainty principle by reducing the quantum fluctuations of a certain variable of interest at the expense of increased uncertainty for its conjugate variable. Using squeezed states one can perform very quiet measurements much below the vacuum noise level [1]. Squeezed states manifest the quantum coherent nature of light and provide a chance to beat the standard quantum limit by preferentially doing an experiment using the squeezed quadrature alone [2,3]. Squeezed states have been experimentally observed in a nonlinear optical cavity experiment [4,5]. Recently, the theory of squeezing in a high-Q cavity was considered [6]. Upon the injection of a high-energy photon, a nonlinear optical medium can coherently generate two photons, the sum of whose frequencies is equal to that of the high-energy photon via optical parametric down-conversion (PDC). If one injects low-energy photons instead, one may induce second harmonic generation, which also forms a squeezed state. In addition to this three-wave mixing, four-wave mixing can be used to generate squeezed states. In pioneering condensed matter experiments, the Josephson junction parametric amplifier was used in the microwave regime to produce $(47 \pm 8)\% \sim 3$ dB squeezing below the vacuum level [7–9] via degenerate four-wave mixing. There has been tremendous recent progress in realizing quantum optics physics in electrical circuits. It is now possible to experimentally reach the extreme strong coupling limit of cavity QED [10–12] and to see very strong microwave nonlinearities in high inductance small scale Josephson junctions whose Hamiltonian can be controlled with remarkable accuracy [13]. Coherent dynamics of a flux qubit coupled to a harmonic oscillator in a SQUID circuit has also been demonstrated [14].

Motivated by these experimental advances in ''circuit QED,'' we here study squeezing in a system consisting of a Cooper-pair box (CPB) located inside a high Q coplanar waveguide resonator. Two different discrete photon modes (fundamental and first harmonic) are coupled through the CPB as shown in Fig. 1 and squeezing occurs via three-wave mixing. Compared to the cavity QED of atomic physics, circuit QED has the advantages of infinite transit time of the ''atom'' (qubit) inside the cavity and much stronger coupling between qubit and photon. We emphasize that strong coupling means we only need a single ''atom.'' The circuit QED system recently successfully demonstrated strong coupling (vacuum Rabi splitting) between a single photon and a qubit in all solid-state system [11]. While this architecture offers a very quiet environment leading to excellent coherence of the qubit ($T_1 \sim 7\ \mu$s, $T_2^* \sim 500$ ns) [12], the solid-state environment still leads to qubit decay rates and dephasing rates much larger than those in corresponding atomic physics microwave cavity QED experiments [15]. Hence it is crucial to investigate these environmental effects on the efficiency of squeezing. Using both numerical and analytical calculations based on the currently available experimental parameters, we have estimated that the circuit QED system can readily produce about 95% squeezing, that is, 13 dB below the vacuum noise level.

We start with the following Hamiltonian to describe the coupled system of qubit and cavity photons for microwave circuit QED [10,11]: $H = H_0 + H_I$. The Hamiltonian H_0 is given by

$$H_0 = \frac{E_{01}}{2}\sigma_z + \hbar\omega_1 a_1^\dagger a_1 + \hbar\omega_2 a_2^\dagger a_2, \qquad (1)$$

where $E_{01} = \sqrt{E_J^2 + E_{\mathrm{el}}^2}$, E_J is the Josephson coupling

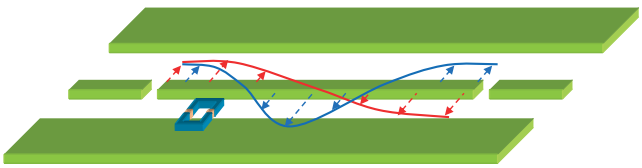

FIG. 1 (color). The schematic diagram for the circuit QED coupled to a Cooper-pair box located at one edge of the cavity. The red and blue lines represent the fundamental and the second harmonic cavity modes, respectively. The change of CPB position from the edge will vary the coupling strengths g_1 and g_2.

energy, $E_{\rm el}=4E_C(1-2N_g)$, E_c the charging energy, N_g the gate charge, and ω_1 the angular frequency of the fundamental resonator mode and $\omega_2=2\omega_1$ is the first harmonic frequency. The coupling Hamiltonian H_I can be written

$$H_I=-[g_1(a_1^\dagger+a_1)+g_2(a_2^\dagger+a_2)]\times[1-2N_g+\sin\theta\sigma_x-\cos\theta\sigma_z], \quad (2)$$

where g_i represents the coupling strength between the qubit and the ith cavity photon mode, and $\theta=\tan^{-1}(E_J/E_{\rm el})$. At the charge degeneracy point (CDP), that is, $N_g=1/2$, H_I reduces to the Jaynes-Cummings Hamitonian, since $\cos\theta\cong-(4E_C/E_J)(1-2N_g)=0$ and $\sin\theta=1$. One can see that away from the CDP, we have couplings other than the Jaynes-Cummings term, whose strength linearly increases with the deviation. Because the only relevant cavity frequencies will be the fundamental and first harmonic, we expect degenerate PDC to occur in our system, where a single high-energy photon coherently generates two photons, each with half the frequency. We emphasize that this is degenerate PDC because the cavity only has discrete modes. In order to achieve squeezing via PDC in circuit QED, the system should be able to convert a single ω_2 photon into two ω_1 photons, which requires a term of the form $a_1^\dagger a_1^\dagger a_2$ in the effective Hamiltonian. This will result from the third order processes in terms of H_I, which will be in general negligible since $g_1^2g_2/\omega_1^3\ll 1$ in typical experiments [11]. However, we can resonantly enhance the process by tuning either ω_1 or ω_2 close to E_{01}. We have chosen the case $\omega_2\cong E_{01}$.

We first apply the following unitary transformation U_1 to the Hamiltonian H

$$U_1=\exp\Big[\sum_{i=1,2}\frac{g_i}{\omega_i}(a_i-a_i^\dagger)(1-2N_g-\cos\theta\sigma_z)\Big]. \quad (3)$$

This corresponds to shifting the centers of the harmonic oscillator coordinates $X_i=a_i+a_i^\dagger$ by $(2g_i/\omega_i)(1-2N_g-\cos\theta\sigma_z)$. Subsequently, we apply the unitary transformation

$$U_2=\exp\Big[\frac{g_1\sin\theta}{2(E_{01}-\omega_1)}(a_1^\dagger\sigma^- - a_1\sigma^+)\Big]. \quad (4)$$

Upon application of these two unitary transformations, we obtain, after perturbative expansion in g_1 and g_2, the following Hamiltonian: $H_{\rm eff}=U_2U_1HU_1^\dagger U_2^\dagger=H_0+H'$ for $E_{01}\cong\omega_2$,

$$H'=-\frac{1}{2}g_2\sin\theta(a_2^\dagger\sigma^- + a_2\sigma^+)+\frac{g_1^2\sin2\theta}{2\omega_1}(a_1^\dagger a_1^\dagger\sigma^- + a_1a_1\sigma^+). \quad (5)$$

We define the energy detuning between the cavity photon frequency ω_2 and the qubit energy splitting E_{01} to be $\Delta\equiv E_{01}-\omega_2$ and consider the case $g_2\ll\Delta\ll\omega_1$. It is this Hamiltonian which we will study numerically. However, to develop an analytical understanding, we can apply the following additional unitary transformation U_3

$$U_3=\exp\Big[\frac{g_2\sin\theta}{2\Delta}(a_2^\dagger\sigma^- - a_2\sigma^+)\Big]. \quad (6)$$

Finally, we obtain the following low-energy effective Hamiltonian through $\hat H_{\rm eff}=U_3H_{\rm eff}U_3^\dagger$,

$$\hat H_{\rm eff}=H_0+\frac{g_2^2\sin^2\theta}{2\Delta}[1+\sigma_z(2n_2+1)]+\frac{\zeta}{2}(a_1^\dagger a_1^\dagger a_2+a_1a_1a_2^\dagger)\sigma_z, \quad (7)$$

where the second term on the right represents the Lamb and light shifts of the qubit splitting frequency and $\zeta=(2g_1^2g_2\sin\theta\sin2\theta/\Delta\omega_1)$. The third term is the desired squeezing term. $\hat H_{\rm eff}$ is exactly the standard Hamiltonian for degenerate optical PDC including the Lamb shift [3]. Note that the squeezing operator couples to the qubit state σ_z and the phase of the squeezed quadrature will shift by $\pi/2$ if the qubit is placed in the excited state.

In deriving the above result, we have neglected the effect of cavity damping $\sum_{i=1,2}\sqrt{\kappa_i}\int_{-\infty}^{\infty}d\omega a_ib_\omega^\dagger$, where b_ω represents the continuum modes outside the cavity and κ_i the cavity loss rates. Unitary transformation of the damping terms leads to radiative atom damping [10] and two-photon decay terms [16] such as $(\sqrt{\kappa_2}\zeta/2\Delta)\int_{-\infty}^{\infty}d\omega a_1a_1b_\omega^\dagger$. The two-photon decay rate is much smaller than the cavity loss κ_2 by a factor of $(\zeta/\Delta)^2/2$, and hence we will neglect it. Similarly the radiative atom damping term is smaller than the intrinsic atom decay rate and we will neglect it. In the limit of weak pumping, down-converted pairs of photons are produced incoherently at a rate $\bar n_2(\zeta/\kappa_1)^2$ given by Fermi's golden rule with $\bar n_2$ the average number of pump photons.

To understand the squeezing produced by strong pumping, one needs to consider the substantial deexcitation rate γ from the excited state of solid-state qubits. Furthermore, the qubit dephasing rate γ_φ is typically at least 1 order of magnitude greater than γ. For charge qubits, optimal phase coherence occurs at the charge degeneracy point [17] where (it happens that) the symmetry prevents the three-wave mixing which we require for PDC. Hence it is crucial to take into account these effects to obtain a realistic estimate of squeezing. For a deviation of 10% from the charge degeneracy point, coherence times of $T_2\sim 200$ ns have been demonstrated [17]. We start with the Hamiltonian $\tilde H_I$ obtained via the unitary transformation U_1U_2 in Eq. (5), which is defined in the rotating wave frame of ω_2,

$$\tilde H_I=\frac{\Delta}{2}\sigma_z+g_2\sin\theta|\alpha_p|\sigma_y+\frac{\Gamma}{4}(a_1^\dagger a_1^\dagger\sigma^- + a_1a_1\sigma^+). \quad (8)$$

Here $\Gamma=2g_1^2\sin2\theta/\omega_1$ and we have taken the pump to be classical: $\langle a_2\rangle=\alpha_p=i|\alpha_p|$.

Following the standard quantum theory of damping, we investigate the coupled system of qubit and cavity plus the reservoir. After integrating out the reservoir degrees of freedom and using the Markov approximation, one obtains

the master equation [3] for the reduced density matrix ρ of the qubit plus cavity system,

$$\frac{d\rho}{dt} = -i[\tilde{H}_I, \rho] + \kappa_1\left[a_1\rho a_1^\dagger - \frac{1}{2}a_1^\dagger a_1\rho - \frac{1}{2}\rho a_1^\dagger a_1\right] + \frac{\gamma}{4}\left[\sigma^-\rho\sigma^\dagger - \frac{1}{2}\sigma^\dagger\sigma^-\rho - \frac{1}{2}\rho\sigma^\dagger\sigma^-\right] + \frac{\gamma_\varphi}{2}[\sigma_z\rho\sigma_z - \rho]. \quad (9)$$

Using the quantum regression theorem [3], the variances $V(\omega)$ (homodyne spectrum) of quadrature $X_1 = a + a^\dagger$ and $X_2 = (a - a^\dagger)/i$ for the *output* cavity photon mode are given by

$$V(\omega) = 1 \pm \kappa_1 \int_{-\infty}^{\infty} d\tau e^{-i\omega\tau}\,\mathrm{Tr}\{(a_1 \pm a_1^\dagger) \times e^{\mathcal{L}\tau}(a_1\rho_{ss} \pm \rho_{ss}a_1^\dagger)\}, \quad (10)$$

where $\mathcal{L}$ is the Liouvillean operator, ρ_{ss} the density matrix at the steady state, and the $(+)$ and $(-)$ signs correspond to X_1 and X_2 quadratures, respectively. We have numerically calculated the $V(\omega)$ of quadrature X_1 and X_2 based on an exact diagonalization study in the Hilbert space of size $2N \times 2N$ corresponding to the two possible spin states and the number of photons being restricted to less than N. We have chosen the following conservative set of experimental parameters: $\omega_1/2\pi = 3$ GHz, $T_1 = 2$ μs, $T_2 = 100$ ns, $Q = 5 \times 10^5$, $g_2/2\pi = 18$ MHz, $E_C/E_J \cong 1$, and $\sin\theta \cong 1$ near the CDP, where $T_2 = \gamma_\perp^{-1}$, $\gamma_\perp = \gamma_\varphi + \gamma/2$, and $\Delta/\omega_1 \cong 0.05$ [11]. In Fig. 2, we have plotted $V(\omega)$ as a function of ω for $\Delta = 2.6 \times 10^4$, $\Gamma = 5$, $N = 10$, and $g_2|\alpha_p| = 2827$ in units of $\kappa_1 = \omega_1/Q$. We find that the maximum squeezing is obtained at $\omega = 0$ as expected. The frequency width of the squeezing spectrum is controlled by the cavity width κ_1. The variable Γ is tunable by varying the qubit gate voltage. It is experimentally observed that the dephasing time T_2 decreases very rapidly, as the qubit is detuned from the CDP [17]. Hence we will restrict the relative deviations from the CDP to be small $|2N_g - 1| \leq 0.1$, where $T_2 \geq 100$ ns. This restriction yields a maximum value of $\Gamma \cong (8g_2^2/\omega_1)(E_C/E_J)(1 - 2N_g) \sim 0.53$ MHz. In Fig. 3, $V(\omega = 0)$ is plotted as a function Γ for $N = 10, 12, 15, 20$. We have checked that $\Delta X_1 \Delta X_2$ satisfies the minimum uncertainty bounds and closely approaches the minimum uncertainty condition. The maximum output squeezing is obtained by extrapolation of the numerical results for finite N to $N = \infty$ yielding $V(\omega = 0) = 0.05$, that is, -13 dB, as shown in the inset of Fig. 3.

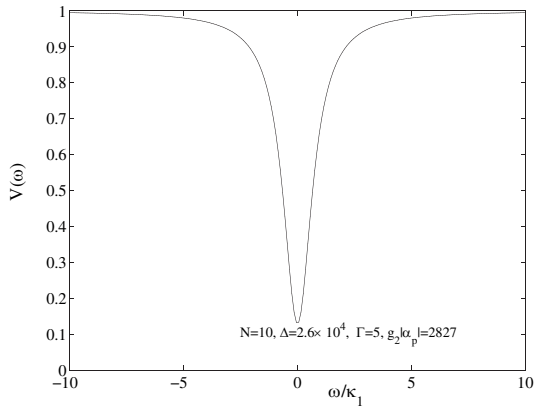

FIG. 2. The quadrature variance $V(\omega)$ for X_1 is plotted as a function of ω for $N = 10$, $\Delta = 2.6 \times 10^4$, $\Gamma = 5$, $g_2|\alpha_p| = 2827$ in units of κ_1. The maximum squeezing is obtained at $\omega = 0$.

We have performed extensive simulations by varying the sets of parameters. Increasing Δ consistently improves the squeezing because it reduces the effect of dephasing of the qubit. We can analytically study the effect of finite qubit decay time and dephasing on the squeezing as follows. Based on perturbative analysis, we have demonstrated that the PDC rate is given by $(g_2\Gamma\sin\theta/\Delta)\sigma_z$ as shown in Eq. (7). When concerned with the spin dynamics of the qubit alone, we may neglect the coupling term between cavity photon and the qubit, which is much smaller than the other terms in Eq. (8). By neglecting the coupling, we obtain the following steady state solution for the spin polarization $\langle\sigma_z\rangle$: $\langle\sigma_z\rangle = -\gamma(\gamma_\perp^2 + \Delta^2)/[4g_2^2|\alpha_p|^2\sin^2\theta\gamma_\perp + \gamma(\gamma_\perp^2 + \Delta^2)]$. In the absence of pump photons, ($|\alpha_p| = 0$), the qubit correctly decays down to the ground state, that is $\langle\sigma_z\rangle = -1$. For large detuning, the finite pump only slightly quenches the spin polarization.

Because of the quenching of qubit spin, the effective PDC parameter χ_2 is given by the following formula

$$\chi_2 = \frac{g_2\sin\theta|\alpha_p|\Gamma}{\Delta}\,\frac{\gamma_\perp^2 + \Delta^2}{4g_2^2|\alpha_p|^2\sin^2\theta(\gamma_\perp/\gamma) + \gamma_\perp^2 + \Delta^2}. \quad (11)$$

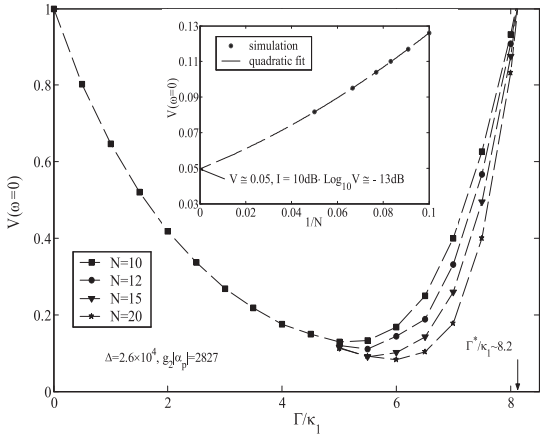

FIG. 3. The quadrature variance $V(\omega = 0)$ for X_1 is plotted as a function of Γ for several different values of $N = 10, 12, 15, 20$. The minimum value of $V(\omega = 0)$ decreases with the increase of the maximum photon number N. The critical value of Γ is about 8.2 in units of κ_1. In the inset, the maximum output squeezing for several values of N is plotted with respect to $1/N$. By extrapolation to $N = \infty$, we obtain the $V_{\min}(\omega = 0) = 0.05$, that is, -13 dB.

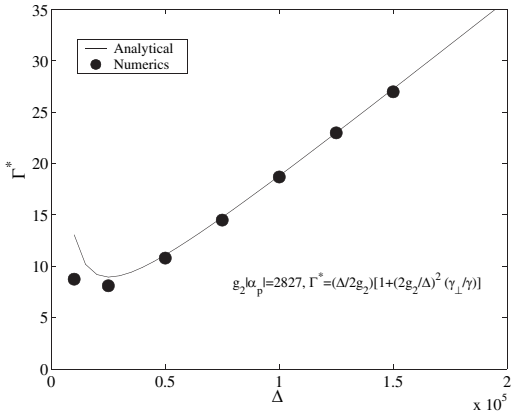

FIG. 4. The critical value Γ^* is plotted as a function of Δ. The dotted line represents the result from the analytical formula and the filled circles from the numerical simulation. Here Γ^* and Δ are in units of κ_1.

Maximum squeezing is achieved near the critical point $\chi_2 \cong \kappa_1/2$ [3], which leads to the optimal value of Γ for $\Delta \gg \gamma_\perp$

$$\Gamma^* = \frac{\kappa_1}{2x}[1 + 4(\gamma_\perp/\gamma)x^2], \tag{12}$$

where $x = g_2 \sin\theta|\alpha_p|/\Delta$. In Fig. 4, Γ^* is plotted as a function of Δ. The dotted line represents the result from the analytical formula of Eq. (12) which shows excellent agreement with the numerical simulation (filled circles). By differentiating with respect to x, one can obtain the minimum value of Γ^* required to achieve the maximum squeezing: $\Gamma^*_{\min} = 2\kappa_1(\gamma_\perp/\gamma)^{1/2}$ for $x^* = (\gamma/4\gamma_\perp)^{1/2}$. Since the value of the Γ/κ_1 can reach as large as 13.3 for the chosen set of parameters, it is well above $\Gamma^*_{\min}/\kappa_1 = 2(\gamma_\perp/\gamma)^{1/2} \cong 8.9$. Hence the maximum squeezing can be realized with the chosen experimental parameters. The validity of perturbation theory in g_2 [10] imposes the following constraint on the product of the pump amplitude and the coupling, $g_2|\alpha_p| < (\Delta/2\sin\theta)$. We note that one can control the values of g_1 and g_2 independently by shifting the position of the qubit within the cavity. When the CPB is located at $1/4$ of the resonator length from the left edge, g_2 vanishes as shown in Fig. 1. Hence by placing the CPB slightly left of the above position, the pump amplitude can always be made large enough for the classical approximation to be valid.

In summary, we have studied degenerate parametric down-conversion and squeezing in circuit QED, where a superconducting Cooper-pair box (CPB) qubit is located inside a transmission line resonator. We have shown that away from the charge degeneracy point, the coherent coupling of different cavity modes through the qubit can generate a squeezed state via three-wave mixing. We have investigated the effect of the finite qubit lifetime and dephasing on squeezing, which will be crucial especially for the qubit away from the charge degeneracy point. By performing both the numerical and analytical calculations, we have demonstrated that the squeezing of about 13 dB below the vacuum noise level can be obtained for the currently available experimental parameters.

We thank A. Blais and J. Gambetta for valuable discussions and guidance in the quantum optics simulations. This work was supported in part by the National Security Agency (NSA) and Advanced Research and Development Activity (ARDA) under Army Research Office (ARO) Contracts No. DAAD19-02-1-0045 and No. ARDA-ARO W911NF-05-1-0365, and by NSF ITR-0325580, NSF DMR-0342157, and the Keck Foundation. K. M. wishes to acknowledge the financial support of the LG Yonam Foundation and the National Program for Tera-Level Nanodevices of the Korea Ministry of Science and Technology as one of the 21 Century Frontier Programs.

[1] Q. A. Turchette, N. Ph. Georgiades, C. J. Hood, H. J. Kimble, and A. S. Parkins, Phys. Rev. A **58**, 4056 (1998).
[2] P. D. Drummond, in *Quantum Squeezing*, edited by P. D. Drummond and Z. Ficek (Springer, New York, 2003), pp. 100–139.
[3] D. F. Walls and G. J. Milburn, *Quantum Optics* (Springer, New York, 1994).
[4] R. E. Slusher *et al.*, Phys. Rev. Lett. **55**, 2409 (1985).
[5] L. A. Wu *et al.*, Phys. Rev. Lett. **57**, 2520 (1986).
[6] N. G. de Almeida, R. M. Serra, C. J. Villas-Bôas, and M. H. Y. Moussa, Phys. Rev. A **69**, 035802 (2004), and references therein.
[7] B. Yurke, J. Opt. Soc. Am. B **4**, 1551 (1987).
[8] B. Yurke, P. G. Kaminsky, R. E. Miller, E. A. Whittaker, A. D. Smith, A. H. Silver, and R. W. Simon, Phys. Rev. Lett. **60**, 764 (1988).
[9] R. Movshovich, B. Yurke, P. G. Kaminsky, A. D. Smith, A. H. Silver R. W. Simon, and M. V. Schneider, Phys. Rev. Lett. **65**, 1419 (1990).
[10] A. Blais, R. S. Huang, A. Wallraff, S. M. Girvin, and R. J. Schoelkopf, Phys. Rev. A **69**, 062320 (2004).
[11] A. Wallraff, D. I. Schuster, A. Blais, L. Frunzio, R.-S. Huang, J. Majer, S. Kumar, S. M. Girvin, and R. J. Schoelkopf, Nature (London) **431**, 162 (2004).
[12] D. I. Schuster, A. Wallraff, A. Blais, L. Frunzio, R.-S. Huang, J. Majer, S. M. Girvin, and R. J. Schoelkopf, Phys. Rev. Lett. **94**, 123602 (2005).
[13] I. Siddiqi, R. Vijay, F. Pierre, C. M. Wilson, M. Metcalfe, C. Rigetti, L. Frunzio, and M. H. Devoret, Phys. Rev. Lett. **93**, 207002 (2004); I. Siddiqi, R. Vijay, F. Pierre, C. M. Wilson, L. Frunzio, M. Metcalfe, C. Rigetti, R. J. Schoelkopf, M. H. Devoret, D. Vion, and D. Esteve, Phys. Rev. Lett. **94**, 027005 (2005).
[14] I. Chiorescu, P. Bertet, K. Semba, Y. Nakamura, C. J. P. M. Harmans, and J. E. Mooij, Nature (London) **431**, 159 (2004).
[15] J. Raimond, M. Brune, and S. Haroche, Rev. Mod. Phys. **73**, 565 (2001).
[16] B. Yurke and E. Buks, quant-ph/0505018.
[17] D. Vion, A. Aassime, A. Cottet, P. Joyez, H. Pothier, C. Urbina, D. Esteve, and M. H. Devoret, Science **296**, 886 (2002); Fortschr. Phys. **51**, 462 (2003).

Quantum-limited measurement and information in mesoscopic detectors

A. A. Clerk, S. M. Girvin, and A. D. Stone
Departments of Applied Physics and Physics, Yale University, New Haven, Connecticut 06511
(Received 4 November 2002; published 28 April 2003)

We formulate general conditions necessary for a linear-response detector to reach the quantum limit of measurement efficiency, where the measurement-induced dephasing rate takes its minimum possible value. These conditions are applicable to both noninteracting and interacting systems. We assess the status of these requirements in an arbitrary noninteracting scattering-based detector, identifying the symmetries of the scattering matrix needed to reach the quantum limit. We show that these conditions are necessary to prevent the existence of information in the detector that is not extracted in the measurement process.

DOI: 10.1103/PhysRevB.67.165324 PACS number(s): 73.23.−b, 03.65.Ta

I. INTRODUCTION

Issues of quantum measurement in mesoscopic systems have recently garnered considerable interest, both because of their relevance to attempts at quantum computation[1] and quantum-limited amplifiers.[2] A general consequence of any quantum measurement is that it must induce decoherence in the system variable conjugate to that being measured. This basic fact naturally leads to the issue of measurement efficiency: what conditions must a particular detector satisfy so that it induces the *absolute minimum* amount of dephasing required by quantum mechanics? This minimum dephasing rate is identical to the measurement rate $\Gamma_{\rm meas}$, the rate at which information is extracted during the measurement process; thus, the measurement efficiency ratio $\chi \leqslant 1$ is defined by $\chi = \Gamma_{\rm meas}/\Gamma_\varphi$, where Γ_φ is the measurement-induced dephasing rate. Besides being of great conceptual interest, near-ideal measurement schemes are necessary to detect signatures of coherent qubit oscillations in the output noise of a detector,[3,4] and are essential if one wishes to construct a quantum-limited amplifier (i.e., an amplifier whose noise energy is the minimum allowed by quantum mechanics).[2] While the question of measurement efficiency has received attention in the context of general measurement theory,[5] it is only recently that it has been considered in the context of solid-state detectors. Averin[3] has considered the status of the quantum limit in a number of solid-state detectors, while recently Pilgram and Büttiker[6] considered the quantum limit for a system in which a mesoscopic conductor acts as a detector.

In this paper, we formulate general conditions that are needed for an arbitrary detector in the linear-response regime to reach the quantum limit of detection, where $\chi = 1$. These general conditions are valid for both interacting and noninteracting systems, and can be given a direct physical interpretation. We also discuss the quantum limit in terms of a simple concept from quantum information theory, the accessible information. To make these considerations more concrete, we apply them to a mesoscopic scattering detector similar to that considered in Ref. 6, identifying precise conditions and symmetries needed to reach the quantum limit. We find that the required symmetries are most easily understood if one considers the scattering detector in terms of information; these symmetries are not the same as those usually considered in mesoscopic systems. For example, we find that time-reversal symmetry is not necessary for reaching the quantum limit. We also find that, surprisingly, an adiabatic point-contact[7] system remains a quantum-limited detector even for voltages large enough that several channels contribute to transport and that the energy dependence of scattering is important; previous studies[8–10] have only shown that the quantum limit is achieved in the small voltage regime. Our results for the mesoscopic scattering detector are complementary to those obtained in Ref. 6.

II. GENERAL CONDITIONS

A. Model and derivation of the quantum limit

We start by considering a generic system consisting of a qubit (i.e. a two-level system described as a spin $\frac{1}{2}$) coupled to an arbitrary detector. The system Hamiltonian is $H = H_{\rm qubit} + H_{\rm detector} + H_{\rm int}$, where $H_{\rm qubit} = -\frac{1}{2}\Omega\sigma_z$, $H_{\rm int} = A\sigma_z Q$, and we leave $H_{\rm detector}$ unspecified. Q is the detector "input" operator that couples to the qubit, while A characterizes the strength of the qubit-detector coupling. Mixing effects, where the detector causes transitions in the qubit, are neglected by taking $[H_{\rm int}, H_{\rm qubit}] = 0$; such effects always cause a deviation from the quantum limit. We work in the weak-coupling regime ($A \to 0$), and can thus use the linear-response theory to describe the output of detector. Taking I to be the detector observable that is measured (i.e., the "output" operator), one has to lowest order in A,

$$\langle I(t)\rangle = \langle I(t)\rangle_{\rho_0} + A\lambda\langle\hat{\sigma}_z(t)\rangle_{\rho_Q}, \tag{1}$$

where the zero-frequency linear-response coefficient (or "forward gain") λ is given by

$$\lambda \equiv \frac{-i}{\hbar}\int_0^\infty d\tau \langle [I(\tau), Q(0)]\rangle_{\rho_0} \tag{2}$$

$$= \frac{2}{\hbar}{\rm Im}\int_0^\infty d\tau \langle I(\tau)Q(0)\rangle_{\rho_0}. \tag{3}$$

Here, ρ_0 is the initial density matrix of the detector and ρ_Q is the initial density matrix of the qubit. We have assumed that the qubit splitting frequency Ω is much smaller than the rate that characterizes the detector, which allows us to approxi-

mate the detector's response to the qubit as instantaneous. Alternatively, one can restrict attention to the case where the qubit is in a σ_z eigenstate, and thus $\langle \sigma_z(t) \rangle$ is time independent. The operators on the right-hand side (RHS) in the above equation evolve in the Heisenberg picture generated by $H_0 = H_{\rm qubit} + H_{\rm detector}$.

Next, we connect the detector noise in the output operator I and input operator Q to, respectively, the measurement rate $\Gamma_{\rm meas}$ and the dephasing rate Γ_φ. Defining the fluctuating part of an operator A as $\tilde{A} = A - \langle A \rangle_{\rho_0}$, the required zero-frequency noise correlators are given by,

$$S_I = 2\int_{-\infty}^{+\infty} dt \langle \tilde{I}(t)\tilde{I}(0)\rangle_{\rho_0} = 4\pi\hbar \sum_{i,f} P_i \delta(E_i - E_f)|\tilde{I}_{if}|^2, \tag{4a}$$

$$S_Q = 2\int_{-\infty}^{+\infty} dt \langle \tilde{Q}(t)\tilde{Q}(0)\rangle_{\rho_0} = 4\pi\hbar \sum_{i,f} P_i \delta(E_i - E_f)|\tilde{Q}_{if}|^2, \tag{4b}$$

$$S_{IQ} = 2\int_{-\infty}^{+\infty} dt \langle \tilde{I}(t)\tilde{Q}(0)\rangle_{\rho_0} = 4\pi\hbar \sum_{i,f} P_i \delta(E_i - E_f)(\tilde{I}_{if})(\tilde{Q}_{fi}). \tag{4c}$$

Here, we use the short hand $O_{if} = \langle i|O|f\rangle$, where $|i\rangle$, $|f\rangle$ are eigenstates of $H_{\rm detector}$ with energies E_i, E_f. The probability P_i is defined as $\langle i|\rho_0|i\rangle$; we assume that ρ_0 is diagonal in the basis of eigenstates. Taking the detector noise to be Gaussian, the standard expressions for the dephasing rate Γ_φ and measurement rate $\Gamma_{\rm meas}$ are given by[1]

$$\Gamma_\varphi = \frac{A^2}{\hbar^2} S_Q, \quad \Gamma_{\rm meas} = \frac{A^2 \lambda^2}{S_I}. \tag{5}$$

We briefly review the origin of Eqs. (5). The dephasing rate describes the measurement-induced decay of the off-diagonal elements of the qubit density matrix. It can be derived by looking at the decay at long times of the phase correlator $V(t) = \langle \sigma_+(t)\sigma_-(0)\rangle$, where σ_+ (σ_-) is the spin raising (lowering) operator:

$$V(t) = \left\langle \exp\left[-i\int_0^t dt' (\Omega + 2AQ(t')/\hbar) \right] \right\rangle \simeq e^{-i\tilde{\Omega}t} \exp\left(\frac{-2A^2}{\hbar^2} \int_0^t dt_1 \int_0^t dt_2 \langle \tilde{Q}(t_1)\tilde{Q}(t_2)\rangle \right) \tag{6}$$

$$\rightarrow e^{-i\tilde{\Omega}t} e^{-\Gamma_\varphi t}. \tag{7}$$

Here, $\tilde{\Omega} = \Omega + 2A\langle Q \rangle_{\rho_0}/\hbar$.

The measurement rate describes how long the measurement must be on before the signal associated with the two qubit states can be distinguished from the noise in I. The quantity of interest is the time integral of the detector output, $m(t) = \int_0^t dt' I(t')$. One needs that the distributions of $m(t)$ corresponding to the two different qubit states [i.e., $p(m(t)|\uparrow)$ and $p(m(t)|\downarrow)$] be statistically distinguishable. Assuming Gaussian distributions, distinguishability is defined as

$$\langle m(t)\rangle_\uparrow - \langle m(t)\rangle_\downarrow \geq \sqrt{2}[\sigma_\uparrow(t) + \sigma_\downarrow(t)], \tag{8}$$

where σ denotes the variance of the distribution and the $\sqrt{2}$ factor is included in order to make the final upper bound on χ unity. Using Eq. (1) for $\langle I(t)\rangle$, and letting $\tau_{\rm meas} = 1/\Gamma_{\rm meas}$, the condition becomes

$$2A\lambda\tau_{\rm meas} \geq 2\sqrt{2}\sqrt{\left(\frac{1}{2}S_{II}\right)\tau_{\rm meas}}, \tag{9}$$

which directly yields the expression in Eq. (5) for $\Gamma_{\rm meas}$. Note that we have taken $\sigma_\uparrow = \sigma_\downarrow$ in the last step; this is sufficient to obtain the leading-order-in-A expression for $\Gamma_{\rm meas}$.

To relate Γ_φ and $\Gamma_{\rm meas}$, we first note that the right-hand sides of Eqs. (4a)–(4c) implicitly define an inner product (i.e., interpret the matrix elements $\{\tilde{I}_{if}\}$ and $\{\tilde{Q}_{if}\}$ as defining vectors). The Schwartz inequality then immediately yields

$$S_I S_Q \geq |S_{IQ}|^2 = \hbar^2(\lambda - \lambda')^2 + (\mathrm{Re}\, S_{IQ})^2, \tag{10}$$

where we have introduced the reciprocal response coefficient (or "backwards gain") λ':

$$\lambda' \equiv \frac{2}{\hbar}\mathrm{Im}\int_0^\infty d\tau \langle \hat{Q}(\tau)\hat{I}(0)\rangle_{\rho_0}. \tag{11}$$

λ' would describe the response of $\langle Q(t)\rangle$ to a perturbation that couples to the operator I. Note that as λ and λ' are defined in terms of commutators, we may substitute $I \rightarrow \tilde{I}$ and $Q \rightarrow \tilde{Q}$ in their definitions. General stability considerations lead to the condition $\lambda\lambda' \leq 0$. Using Eqs. (5), we thus have

$$\frac{\Gamma_{\rm meas}}{\Gamma_\varphi} = \frac{\hbar^2\lambda^2}{S_Q S_I} \leq \frac{\hbar^2\lambda^2}{\hbar^2(\lambda - \lambda')^2 + (\mathrm{Re}S_{IQ})^2} \leq 1. \tag{12}$$

The best one can do is measure the qubit as quickly as one dephases it.[11] Note that this derivation only requires the validity of linear-response and the weak-coupling approximations which give rise to Eqs. (5); very little is specified of the detector. Similar derivations of the quantum limit are presented in Refs. 3 and 5.

The inequality in Eq. (12) is in many ways intuitively reasonable. Both dephasing and measurement involve entangling the state of the qubit with states in the detector. In principle, there may be degrees of freedom in the detector which become entangled with the qubit *without* providing any detectable information in a measurement of $\langle I\rangle$; any such entanglement would lead to $\Gamma_\varphi > \Gamma_{\rm meas}$. More precisely, imagine that when the measurement is initially turned on, the system is in a product state:

$$|\psi(t=0)\rangle = \frac{1}{\sqrt{2}}(|\uparrow\rangle + |\downarrow\rangle) \otimes |D\rangle, \tag{13}$$

where $|D\rangle$ is the initial state of the detector, and $|\uparrow\rangle$, $|\downarrow\rangle$ denote qubit σ_z eigenstates. At some later time t, the state of the system may be written as

$$|\psi(t)\rangle = \frac{1}{\sqrt{2}}(|\uparrow\rangle\otimes|D_\uparrow(t)\rangle + |\downarrow\rangle\otimes|D_\downarrow(t)\rangle). \tag{14}$$

To say that we have measured the state of the system implies that the states $|D_\uparrow(t)\rangle$ and $|D_\downarrow(t)\rangle$ are distinguishable; to say that the qubit has been dephased only implies that the detector states $|D_\uparrow(t)\rangle$ and $|D_\downarrow(t)\rangle$ are orthogonal. While distinguishability implies orthogonality, the opposite is not true; thus, in general, $\Gamma_\varphi > \Gamma_{\rm meas}$. Note that, in this formulation, the dephasing rate will be related to the overlap between the two detector states:

$$|\langle D_\uparrow(t)|D_\downarrow(t)\rangle| \simeq e^{-\Gamma_\varphi t}. \tag{15}$$

B. Necessary conditions for reaching the quantum limit

We have thus seen that on a heuristic level, reaching the quantum limit requires that the detector have no ''extraneous'' degrees of freedom which couple to the qubit. Equivalently, all information on the state of the qubit residing in the detector should be accessible in the measurement of $\langle I\rangle$. The virtue of the derivation presented in the preceding section is that these statements can be given a precise meaning. One sees that three conditions are necessary to reach the quantum limit: (i) the Schwartz inequality in Eq. (10) must be optimized, (ii) the cross-correlator $\mathrm{Re}\, S_{IQ}$ must vanish, and (iii) the backwards gain λ' must vanish. Conditions (i) and (ii) can be succinctly reexpressed as a single condition, leading to the following necessary and sufficient requirements:

$$\{\forall \;\; i,f|P_i\neq 0, E_f = E_i\}, \quad \langle f|\tilde{I}|i\rangle = i\mathcal{C}\langle f|\tilde{Q}|i\rangle, \tag{16}$$

$$\lambda' \equiv \frac{2}{\hbar}\mathrm{Im}\int_0^\infty d\tau \langle \hat{Q}(\tau)\hat{I}(0)\rangle_{\rho_0} = 0. \tag{17}$$

Here, $\mathcal{C}$ is a real number that is independent of the detector eigenstates $|i\rangle$ and $|f\rangle$.[12] Equations (16) and (17) are central results of this paper. The first of these equations expresses the fact that to reach the quantum limit, there must be a close similarity between the detector's input and output operators—as far as the zero-frequency noise correlators are concerned, *the operators I and Q must be proportional to one another*. This required similarity between the detector input and output is a formal expression of the intuitive idea that a quantum-limited detector has no ''extraneous'' internal degrees of freedom. The second condition, Eq. (17), expresses the fact that a quantum-limited detector must have a strong intrinsic directionality that discriminates between the input and output. The output operator is influenced by behavior at the input, but not vice versa. This requirement is consistent with our tacit assumption that the quantity $\langle I\rangle$ can be measured without problems. To measure I, one needs to introduce a coupling in the Hamiltonian to I; the vanishing of λ' implies that this additional coupling will not contribute to $\langle Q(t)\rangle$, and thus cannot further dephase the qubit [cf. Eq. (6)].

On a technical level, Eq. (16) follows from the optimization of the Schwartz inequality and the requirement that $\mathrm{Re}\, S_{IQ}=0$ [i.e. conditions (i) and (ii) above]. The vanishing of λ' [Eq. (17)] can be interpreted in terms of causality. To see this, we first introduce the frequency-dependent cross-correlator $S_{IQ}(E)$:

$$\begin{aligned} S_{IQ}(E) &= 2\int_{-\infty}^{\infty} dt \langle \tilde{I}(t)\tilde{Q}(0)\rangle_{\rho_0} e^{iEt/\hbar} \\ &= 4\pi\hbar \sum_{i,f\neq i} P_i \delta(E+E_i-E_f)\tilde{I}_{if}\tilde{Q}_{fi}. \end{aligned} \tag{18}$$

We may use this to write

$$\lambda(\lambda') = \frac{1}{2\hbar}\left(+(-)\mathrm{Im}\,[S_{IQ}(0)] - \frac{1}{\pi}P\int_{-\infty}^{\infty} dE \frac{\mathrm{Re}\,[S_{IQ}(E)]}{E}\right). \tag{19}$$

If $\lambda'=0$, it follows from the above that at $E=0$, the imaginary part of $S_{IQ}(E)$ coincides with the Hilbert transform of the real part of $S_{IQ}(E)$:

$$\mathrm{Im}\,[S_{IQ}(E)]\Big|_{E=0} = \left(-\frac{1}{\pi}P\int_{-\infty}^{\infty} dE' \frac{\mathrm{Re}\,[S_{IQ}(E')]}{E'-E}\right)\Bigg|_{E=0}. \tag{20}$$

If this held for all E, it would follow from the Titchmarsh theorem[13] that $S_{IQ}(t) = \langle \tilde{I}(t)\tilde{Q}(0)\rangle_{\rho_0}$ is causal: it would vanish for $t<0$. This would clearly be sufficient to satisfy Eq. (17). More generally, the vanishing of λ' only requires the weaker zero-frequency causality condition in Eq. (20).

C. The quantum limit and information theory

We close this section by formalizing the connection between the quantum limit and information. A deviation from the quantum limit (i.e., $\chi<1$) implies the existence in the detector of ''missing information'' regarding the state of the qubit, information that is not revealed in the measurement of $\langle I\rangle$. The dephasing rate thus corresponds to what the measurement rate would be *if* we could make use of all the available information. This notion can be quantified by borrowing a concept from quantum information theory, the accessible information.[14–17] To define this, note first that if we choose a specific detector quantity (or set of quantities) Y to measure (described by, e.g., a set of commuting observables), we can think of our system as a noisy classical communication channel. The two possible inputs to the channel are the qubit states $|\uparrow\rangle$ and $|\downarrow\rangle$; interaction with the detector for a time t then leads to two corresponding detector states $|D_\uparrow(t)\rangle$ and $|D_\downarrow(t)\rangle$ [c.f. Eq. (14)].[18] Finally, the outputs from the channel are the outcomes of the measurement of Y. The ''noise'' here is a result of the intrinsic uncertainties of Y in the states

$|D_\uparrow(t)\rangle$ and $|D_\downarrow(t)\rangle$; the output will thus be described by the conditional probability distributions $p(y|\uparrow)$ and $p(y|\downarrow)$, which are determined by these states, where y represents possible outcomes of the measurement. Letting $\overline{p}(y) = [p(y|\uparrow)+p(y|\downarrow)]/2$, the mutual information R of this channel is[19]

$$R[Y] = H[\overline{p}(y)] - \frac{1}{2}(H[p(y|\uparrow)] + H[p(y|\downarrow)]), \quad (21)$$

where $H[p(y)]$ is the Shannon information entropy associated with the distribution p:

$$H[p(y)] = -\sum_{y_i} p(y_i)\ln[p(y_i)]. \quad (22)$$

Note that we have chosen to equally weight our two inputs to the channel. Assuming that this choice is optimal, Shannon's noisy channel coding theorem implies that $R[Y]$ is the maximum rate at which messages can be reliably transmitted down the channel by modulating the state of the qubit and making measurements of Y.[19] Alternatively, $R[Y]$ may be considered as being related to a generalized measurement rate describing the chosen measurement Y. For example, if the distributions $p(y(t)|\uparrow)$ and $p(y(t)|\downarrow)$ are Gaussian, one finds that at small times (i.e., before the two distributions are well separated)

$$R[Y]_{\text{Gaussian}} = \frac{1}{8}\frac{(\langle y(t)\rangle_\uparrow - \langle y(t)\rangle_\downarrow)^2}{\sigma_\uparrow(t)\sigma_\downarrow(t)}. \quad (23)$$

This corresponds to our definition of the measurement rate, cf. Eqs. (8) and (9). We thus have a new way to interpret the measurement rate Γ_{meas}: given that one is monitoring $\langle I\rangle$, Γ_{meas} represents the maximum rate at which information can be sent to the detector by modulating the qubit.

The quantum-mechanical accessible information $\mathcal{I}$ is now defined by maximizing the mutual information $R[Y]$ over all possible measurement schemes Y. Remarkably, for the case considered here (where the detector is described by a pure state), it can be calculated exactly;[14] a simplified proof is presented in Appendix A, where we also demonstrate that there are several possible optimal measurement schemes. Letting $|\langle D_\uparrow(t)|D_\downarrow(t)\rangle|^2 = \cos^2(\alpha(t))$, we have

$$\mathcal{I} = \max_{\{Y\}} R = \frac{1}{2}\{[1+\sin\alpha(t)]\ln[1+\sin\alpha(t)] + [1-\sin\alpha(t)]\ln[1-\sin\alpha(t)]\}. \quad (24)$$

This expression corresponds to having equally weighted our two input states, as we did in Eq. (21); one can check that this choice maximizes $\mathcal{I}$. At small times ($\Gamma_\varphi t \ll 1$), comparison against Eq. (15) yields $\alpha(t)\to 0$, and we have

$$\mathcal{I} \simeq \alpha(t)^2 = \Gamma_\varphi t. \quad (25)$$

As expected, the growth of the accessible information is determined by the dephasing rate. Achieving $\chi = 1$ thus implies that the rate that we actually obtain information, Γ_{meas}, coincides with the growth of the total accessible information.

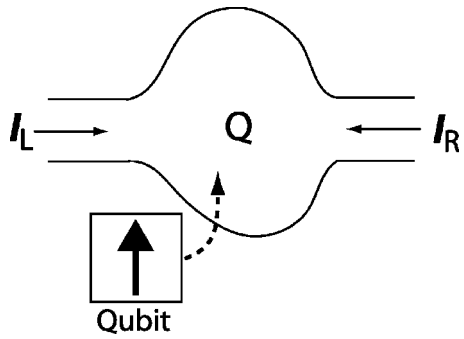

FIG. 1. Schematic diagram of the mesoscopic scattering detector, in which the current through a phase coherent scattering region is used to detect the qubit. Q denotes the charge in the scattering region, while I_R (I_L) is the current in the right (left) contact.

Thus, there is no ''missing'' information in the detector. We can also think of Eqs. (24) and (25) as providing an alternate route for deriving the quantum-limit inequality $\Gamma_\varphi \geqslant \Gamma_{\text{meas}}$, i.e.,

$$R[Y] \simeq \Gamma_{\text{meas}} t \leqslant \mathcal{I} \simeq \Gamma_\varphi t. \quad (26)$$

The utility of thinking about back-action effects and the quantum limit in terms of information will become clear in the following section, where we discuss the mesoscopic scattering detector. Note also that the relation between information and state disturbance has been studied in a slightly different context by Fuchs *et al.*[15]

III. MESOSCOPIC SCATTERING DETECTOR

To make the preceding discussion more concrete, we now consider the status of the quantum limit in a slightly less general detector setup, the mesoscopic scattering detector considered in Ref. 6. We determine the conditions needed to reach the quantum limit of detection by directly applying the general conditions derived in the preceding section, namely the proportionality condition in Eq. (16) and the causality condition in Eq. (17). This is in contrast to Ref. 6, which developed conditions needed for the quantum limit by directly calculating Γ_φ and Γ_{meas}. We explicitly show that the violation of Eq. (16) implies the existence of unused information in the detector, information that is not extracted in the measurement process.

The detector here is a two terminal scattering region (see Fig. 1) characterized by a scattering matrix s. Taking the contact to both the right and left reservoirs to have N propagating transverse modes, s will have dimension $2N$. The output operator of the detector I is simply the current through the region; the state of the qubit alters $\langle I\rangle$ by modulating the potential in the scattering region. Note that while we focus on the limit of a weak coupling between the qubit and detector, so that the linear-response approach of the preceding section is valid, we do not assume that the voltage is small enough that $\langle I\rangle \propto V$.[20] The mesoscopic scattering detector describes the setup used in two recent ''which path'' experiments.[21,22] These experiments used a quantum point contact to detect the presence of an extra electron in a nearby

quantum dot. As the dot was imbedded in an Aharanov-Bohm ring, the dephasing induced by the measurement could be studied directly.

We start by considering the simplest situation, also considered in Ref. 6, where the state of the qubit provides a uniform potential change in the scattering region. In this case, the input operator Q is the *total* charge in the scattering region. Unlike Ref. 6, we do not explicitly consider the effects of screening here. Within the random-phase approximation, consideration of such effects allows an explicit calculation of the qubit-detector coupling strength A, but does not result in any other changes over a noninteracting approach. In the weak-coupling regime, the particular value of A does not affect the approach to the quantum limit.

Letting $a^{\dagger}_{\alpha n}(E)$ represent the creation operator for an incident wave in contact $\alpha=L,R$, transverse mode n, and at energy E, the detector current operator for contact α takes the form;[23]

$$I_{\alpha}=\frac{e}{h}\int dE\int dE' \times\sum_{\beta,\gamma=L,R}\sum_{n,m=1}^{N}[a^{\dagger}_{\beta n}(E)A_{\beta n,\gamma m}(\alpha;E,E')a_{\gamma m}(E')], \tag{27}$$

$$A_{\beta n,\gamma m}(\alpha;E,E')=\delta_{\beta\gamma}\delta_{\alpha\beta}\delta_{nm}-\{[s_{\alpha\beta}(E)]^{\dagger}s_{\alpha\gamma}(E')\}_{nm}. \tag{28}$$

A positive current corresponds to a current incident on the scattering region; note that throughout this section, we neglect electron spin for simplicity. The total charge Q in the scattering region may be defined in terms of the total current incident on the scattering region—in the Heisenberg picture, $\partial_t Q(t)=I_L(t)+I_R(t)$. One obtains

$$Q=e\int dE\int dE'\sum_{\beta,\gamma=L,R}[a^{\dagger}_{\beta n}(E)\mathcal{N}_{\beta n,\gamma m}(E,E')a_{\gamma m}(E')], \tag{29}$$

$$\mathcal{N}(E,E+\hbar\omega)=\frac{1}{2\pi i}\left[s^{\dagger}(E)\frac{s(E+\hbar\omega)-s(E)}{\hbar\omega}\right]. \tag{30}$$

In the limit where $\omega\to 0$, $\mathcal{N}(E,E+\hbar\omega)$ reduces to the well-known Wigner-Smith delay-time matrix

$$\mathcal{N}(E)=\frac{1}{2\pi i}\left[s^{\dagger}(E)\frac{d}{dE}s(E)\right]. \tag{31}$$

Finally, the assumption that the qubit couples to the total charge in the scattering region is equivalent to assuming that the potential it creates is smooth in the WKB sense. We can use the fact that the sensitivity of the scattering matrix s to a global change of potential in the scattering region is the same as its sensitivity to energy. Thus, the linear-response coefficient λ has the form

$$\lambda=-\frac{e^2}{h}\int_{\mu_R}^{\mu_L}d\varepsilon\frac{d}{d\varepsilon}[\mathrm{tr}\, s^{\dagger}_{LR}(\varepsilon)s_{LR}(\varepsilon)] =-\frac{e^2}{h}\int_{\mu_R}^{\mu_L}d\varepsilon\sum_j\frac{dT_j(\varepsilon)}{d\varepsilon}, \tag{32}$$

where the T_j are the transmission eigenvalues of the system. Without loss of generality, we have assumed that our detector is biased such that the chemical potential of the left reservoir is greater than that of the right reservoir: $\mu_L-\mu_R=e|V|$; we also consider the limit of zero temperature.

A. Single-channel case

Given these definitions, we can now turn to Eqs. (16) and (17) and ask what is required of the scattering matrix s in order to reach the quantum limit. We first focus on the case $N=1$, where there is a single propagating mode in both contacts. The scattering matrix s is thus 2×2, and may be written as

$$s(E)=\begin{pmatrix} s_{LL} & s_{LR}\\ s_{RL} & s_{RR}\end{pmatrix}=\begin{pmatrix} \sqrt{R}e^{i\beta} & \sqrt{T}e^{i\varphi'}\\ \sqrt{T}e^{i\varphi} & -\sqrt{R}e^{i(\varphi+\varphi'-\beta)}\end{pmatrix}, \tag{33}$$

where $R=1-T$. At zero temperature, the detector is described by a single many-body state $|i\rangle$ in which all incident states in lead α with $E<\mu_\alpha$ are occupied and all other incident states are unoccupied:

$$|i\rangle=[\Pi_{E_L\leq\mu_L}a^{\dagger}_L(E_L)][\Pi_{E_R\leq\mu_R}a^{\dagger}_R(E_R)]|\mathrm{vac}\rangle. \tag{34}$$

First, we consider the causality condition in Eq. (17) which requires that the backwards gain λ' vanishes. As we know the initial state of the detector and have explicit expressions for I and Q, we can directly evaluate the function $S_{IQ}(E)$ appearing in Eq. (18) in terms of s. A direct calculation can be performed to show that

$$\int_{-\infty}^{\infty}dE\frac{\mathrm{Re}\,[S_{IQ}(E)]}{E}=\int_{-\infty}^{\infty}dE\frac{\mathrm{Re}\,[F(E)]}{E}, \tag{35}$$

$$\mathrm{Im}\,[S_{IQ}(0)]=\mathrm{Im}\,[F(0)], \tag{36}$$

where, letting $t\equiv s_{RL}$,the function $F(E)$ is defined as:

$$F(E)=-i\frac{e^2}{2\pi}\int_{\mu_R}^{\mu_L}dE' t^*(E')\left(\frac{t(E'+E)-t(E')}{E}\right). \tag{37}$$

Note that Eqs. (35) and (36) are independent of whether I is taken to be I_L , I_R , or a linear combination of the two. Now, causality dictates that the scattering matrix s is analytic in the upper half complex plane, and thus so is the function $F(E)$. The real and imaginary parts of F are thus related by a Hilbert transform, and Eqs. (20), (35), and (36) imply that $\lambda'=0$ for the scattering detector *irrespective of the choice of s*. Thus, the causality properties of the scattering matrix s ensure that one of the conditions necessary for reaching the quantum limit is always satisfied. Note that substituting these

expressions for $S_{IQ}(E)$ in Eq. (19) does indeed yield the expected form of λ [Eq. (32)]. It is also useful to note that gauge invariance can be used to directly establish[24] $\lambda' = 0$. The essence of the argument is that a coupling to the current [i.e., $H_{\rm int} = A\sigma_z I(x=0)$] is equivalent to introducing a local vector potential. The gauge transformation that removes this term will only modify the transmission phases in the scattering matrix s (i.e., ϕ and ϕ') in an energy-independent manner. Using Eq. (29), one can check that $\langle Q \rangle$ is independent of energy-independent phase changes; thus $\lambda' = 0$.

Next, we turn to the condition given in Eq. (16), which requires a certain proportionality between $\tilde{I}$ and $\tilde{Q}$ in order to reach the quantum limit. Given the state $|i\rangle$ that describes the detector [Eq. (34)], the only matrix elements of I and Q which contribute to the zero frequency noise correlators [cf. Eqs. (4)], involve energy-conserving transitions where a scattering state incident from the left reservoir is destroyed, while a scattering state incident from the right reservoir is created. Since these transitions require an occupied initial state and an unoccupied final state, they can only occur in the energy interval $\mu_R < E < \mu_L$. We are thus interested in the coefficients of the operators $a_R^\dagger(E)a_L(E)$ appearing in the expansion of I and Q in this energy interval. The proportionality requirement of Eq. (16) thus results in a necessary condition on $s(\varepsilon)$:

$$\forall E \epsilon [\mu_R, \mu_L], \quad [s_{LR}]^*(E) s_{LL}(E) = i\mathcal{C}\mathcal{N}_{RL}(E), \quad (38)$$

where $\mathcal{C}$ is a real, energy-independent constant. Using Eq. (33), the imaginary and real parts of the above condition become

$$\forall \quad E \epsilon [\mu_R, \mu_L], \quad \frac{d}{dE}[\beta(E) - \phi(E)] = 0, \quad (39)$$

$$\frac{\frac{dT}{dE}(E)}{T(E)[1-T(E)]} = -\frac{4\pi}{\mathcal{C}}. \quad (40)$$

Similar conditions for reaching the quantum limit for this version of the scattering detector were first developed in Ref. 6 by directly calculating $\Gamma_{\rm meas}$ and Γ_φ [note that there is a sign error in Eq. (7) of Ref. 6 which must be corrected to obtain our Eq. (39)].[25] The fulfilling of these conditions does not correspond to symmetries usually considered in mesoscopic systems; for example, as we will show, the presence of time-reversal symmetry is not a necessary requirement. Instead, the conditions of Eqs. (39) and (40) correspond directly to the requirement that there be no missing information in the detector, information that is not revealed in the measurement of $\langle I \rangle$. We demonstrate this explicitly in what follows.

1. Phase condition

The first condition [Eq. (39)] for reaching the quantum limit requires that the difference between transmission and reflection phases in the scattering matrix be constant in the energy interval defined by the voltage. If this condition holds, changing the state of the qubit will not modulate this phase difference. Equation (39) thus constrains information—it ensures that the detector does not extract additional information about the qubit that resides in the relative phase between transmission and reflection. Such information is clearly not revealed in the measurement of $\langle I \rangle$, and would necessarily lead to additional dephasing over and above the measurement rate. In principle, this additional information could be extracted by performing an interference experiment. To be more specific, note that the cross correlator S_{IQ} [c.f. Eq. (4c)] is given by

$$S_{IQ} = i\hbar\lambda + \frac{e^2}{\pi}\int_{\mu_R}^{\mu_L} dE' \left(T(1-T)\frac{d}{dE}(\beta - \varphi) \right). \quad (41)$$

By definition, the imaginary part of this correlator determines the linear-response coefficient λ [cf. Eq. (3)] associated with measuring $\langle I \rangle$. In contrast, the *real* part of this correlator may be interpreted as the linear-response coefficient associated with a measurement where one interferes reflected and transmitted electrons; the factor of $T(1-T)$ corresponds to the fact that the magnitude of this signal will be proportional to the amplitude of both the reflected and transmitted beams. More explicitly, consider the Hermitian operator $I_{\rm mod}$, defined by

$$I_{\rm mod} = \frac{e}{\hbar}\int_{\mu_R}^{\mu_L} dE [i a_R^\dagger(E) A_{RL}(L;E,E) a_L(E) + \text{H.c.}]. \quad (42)$$

If one were to now measure $I_{\rm mod}$, the corresponding linear response coefficient $\lambda_{\rm mod}$ is precisely the real part of S_{IQ} [this can be seen by comparing Eqs. (42) and (27)]. The fact that additional information on the state of the qubit is available in the expectation $\langle I_{\rm mod} \rangle$ implies that the qubit is entangling with the detector faster than the measurement rate associated with $\langle I \rangle$. This remains true even if one does not explicitly extract this information, as was demonstrated recently in the experiment of Sprinzak *et. al.*[22]

Stepping back, we see that the general condition $\text{Re}\, S_{IQ} = 0$ [i.e., the required factor of i on the RHS of Eq. (16)] needed to reach the quantum limit directly corresponds to the requirement of no missing information discussed in the preceding section. In general, a nonvanishing $\text{Re}\, S_{IQ}$ implies that additional information about the qubit's state could be obtained by simultaneously measuring another quantity in addition to I (e.g., in our case, the quantity $I_{\rm mod}$).

Note that in the scattering detector, the symmetry required to ensure that Eq. (39) holds (i.e., that the phases β and ϕ coincide) is not one that is usually considered in mesoscopic systems. In particular, *the presence of time-reversal symmetry is not necessary to fulfilling the condition of Eq. (39)*; time-reversal symmetry only implies that $\varphi = \varphi'$, and specifies nothing on the relation between φ and β. However, as pointed out in Ref. 6, a *sufficient* condition for achieving Eq. (39) is that one has parity symmetry, that is *both* time-reversal symmetry and left-right inversion symmetry (the latter condition implies that the two reflection phases in s are identical).[26] Note that this is not a necessary condition. We see that the required symmetry here is best understood as being related to information.

2. Transmission condition

We now turn to the second condition [Eq. (40)] needed to have the scattering detector reach the quantum limit, a condition that constrains the energy dependence of the transmission probability T. This condition arises from the requirement that the proportionality between I and Q needed for the quantum limit must hold over the entire energy interval defined by the voltage. In general, energy averaging causes a departure from the quantum limit—over sufficiently large intervals, the operators I and Q look less and less like one another. Like Eq. (39), Eq. (40) can also be interpreted as a requirement of no missing information. Here, the requirement is that energy averaging does not result in the loss of information about the qubit that is encoded in the energy dependence of T. While such information is not obtained in the measurement of $\langle I\rangle$ [which involves energy averaging, cf. Eq. (32)], it could be obtained if one measured the entire function $\langle I(V)\rangle$ for $0\leqslant|V|\leqslant\mu_L-\mu_R$. As discussed, the presence of any missing information necessarily implies a departure from the quantum limit.

Interestingly enough, Eq. (40) may be understood completely classically, even though it formally results from requiring the proportionality of two quantum operators. To do so, we calculate the classical information capacity R [cf. Eq. (21)] corresponding to two different possible measurements. First, imagine we measure the integrated current $m=\int_0^t dt' I(t')$, and assume the probability distributions $p(m|\uparrow)$ and $p(m|\downarrow)$ are Gaussian. For weak coupling, one finds for the capacity:

$$R_{\rm avg}=\Gamma_{\rm meas}t=\frac{t}{2h}\frac{\left(eA\int_{\mu_R}^{\mu_L}d\varepsilon\frac{dT(\varepsilon)}{d\varepsilon}\right)^2}{\int_{\mu_R}^{\mu_L}d\varepsilon T(\varepsilon)[1-T(\varepsilon)]} \tag{43}$$

$$\simeq\frac{(\delta\varepsilon)t}{2h}\frac{\left(eA\sum_j\frac{dT(\varepsilon_j)}{d\varepsilon}\right)^2}{\sum_j T(\varepsilon_j)[1-T(\varepsilon_j)]}. \tag{44}$$

In the last line, we have discretized the energy integrals, i.e., partitioned the interval $[\mu_R,\mu_L]$ into equal segments of length $\delta\varepsilon$. If we now imagine we could measure each $m_j=\int_0^t I_j(t)$, where $I_j(t)$ is the contribution to the current from the jth energy interval, a similar calculation reveals

$$R_{\rm tot}=\frac{(\delta\varepsilon)t}{2h}\sum_j\frac{\left(eA\frac{dT(\varepsilon_j)}{d\varepsilon}\right)^2}{T(\varepsilon_j)[1-T(\varepsilon_j)]}. \tag{45}$$

One can easily check that $R_{\rm tot}\geqslant R_{\rm avg}$; this corresponds to the additional information that is generally available in the energy dependence of T. A necessary and sufficient condition for ensuring $R_{\rm tot}=R_{\rm avg}$ is precisely the condition in Eq. (40). On a purely classical level, this condition ensures that no information is lost when one averages over energy.

How can the problems generally posed by energy averaging be avoided? One possible solution would be to use voltages small enough that the scattering matrix s can be approximated as being linear in energy, that is $eV(dT/dE)\ll 1$ (this is the approach of Ref. 6). However, as the linear-response coefficient λ is given by the energy derivative of the transmission [cf. Eq. (32)], such a small voltage would imply both a small signal and essentially no gain. The change in current induced by the qubit, $\Delta I=\pm A\lambda$, would be much smaller than the current associated with the coupling voltage A:

$$\lambda\simeq\frac{e^2}{h}\left(\frac{dT}{dE}e|V|\right)\ll\frac{e^2}{h}, \tag{46}$$

$$\Gamma_{\rm meas}\propto\left(\frac{dT}{dE}eV\right)^2\left(\frac{A}{eV}\right)\frac{A}{h}\ll\frac{A}{h}. \tag{47}$$

Even though this smallness of λ does not theoretically affect the approach to the quantum limit, it does severely limit the detector's practical value—for very slow measurement rates, environmental effects on the qubit will become dominant over back-action effects.

If we now consider finite voltages and fully energy-dependent scattering, Eq. (40) tells us the condition under which energy averaging the transmission does not impede reaching the quantum limit. The solution to Eq. (40) has the form

$$T(E)=\frac{1}{1+e^{4\pi(E-E_0)/\mathcal{C}}}. \tag{48}$$

This form for $T(E)$ implies that there is no extra information in the energy dependence of T which is lost upon energy averaging. Amusingly, Eq. (40) corresponds *exactly* to the energy-dependent transmission of one channel of an adiabatic quantum point contact.[7] The constant E_0 represents the threshold energy of the channel (i.e., the transverse mode), and the constant $\mathcal{C}$ is given by

$$\mathcal{C}=-\frac{2\sqrt{2}\hbar v_F}{\sqrt{dR}}, \tag{49}$$

where d is the transverse width of the constriction at its center and R is the radius of curvature of the transverse confining potential at the constriction center.

B. Multichannel case

We now consider the situation where there are N channels in each of the two contacts leading to the reservoirs. It is useful to write s in terms of its N transmission eigenvalues $T_j(E)$ using the standard polar decomposition:[27]

$$s(E)=\begin{pmatrix}s_{LL}&s_{LR}\\ s_{RL}&s_{RR}\end{pmatrix}=\begin{pmatrix}U&\\ &V\end{pmatrix}\begin{pmatrix}\sqrt{R}&\sqrt{T}\\ \sqrt{T}&-\sqrt{R}\end{pmatrix}\begin{pmatrix}U'&\\ &V'\end{pmatrix}. \tag{50}$$

Here, U,U',V,V' are $N\times N$ energy-dependent unitary matrices, and $\sqrt{R}$ and $\sqrt{T}$ are diagonal matrices having entries $\sqrt{1-T_j(E)}$ and $\sqrt{T_j(E)}$, respectively.

In the multichannel case, the backwards gain λ' again vanishes irrespective of the details of s as a result of the analytic properties of s. The relevant question then to ask is what conditions must be satisfied by $s(E)$ so that the proportionality between I and Q required to reach the quantum limit [i.e., Eq. (16)] is achieved. As in the single-channel case, the relevant matrix elements of I and Q involve destroying a scattering state incident from the left and creating an equal-energy state describing an incident wave from the right; the additional complication now is that these transitions could result in a change of transverse mode. One thus needs to examine the coefficients of the operator products $a^{\dagger}_{Rn}(E)a_{Lm}(E)$ appearing in the expansion of I and Q, in the energy interval $[\mu_R,\mu_L]$. The proportionality condition of Eq. (16) again yields the requirement that Eq. (38) holds for all energies in this interval; now, however, both the right- and left-hand sides of this equation are $N\times N$ matrices:

$$\forall E\epsilon[\mu_R,\mu_L],[s_{LR}(E)]^{\dagger}s_{LL}(E)=i\mathcal{C}\mathcal{N}_{RL}(E). \quad (51)$$

Here, $\mathcal{C}$ is again an energy-independent real number. Using the polar decomposition, one can derive from Eq. (51) two necessary matrix conditions that must hold for all energies in the interval defined by the voltage:

$$\sqrt{T(E)}\phi_U(E)\sqrt{R(E)}-\sqrt{R(E)}\phi_V(E)\sqrt{T(E)}=0, \quad (52)$$

$$\frac{\frac{dT}{dE}(E)}{T(E)[1-T(E)]}=-\frac{4\pi}{\mathcal{C}}\times\hat{1}. \quad (53)$$

These conditions are the multichannel analogs of Eqs. (39) and (40). $\hat{1}$ denotes the $N\times N$ unit matrix, and we have introduced the generalized "phase-derivative" Hermitian matrices ϕ_U and ϕ_V

$$\phi_U(\varepsilon)=-iU^{\dagger}(\varepsilon)\left[\frac{d}{dE}U(\varepsilon)\right], \quad (54)$$

$$\phi_V(\varepsilon)=-iV^{\dagger}(\varepsilon)\left[\frac{d}{dE}V(\varepsilon)\right]. \quad (55)$$

These matrices play the role of the energy derivatives of the phases β and ϕ in the single-channel case. Note the evident asymmetry in Eq. (52): the polar decomposition matrices U and V enter, but the matrices U' and V' do not. We comment on this in what follows.

1. Phase and channel mixing conditions

The first requirement [Eq. (52)] places a stringent requirement on the scattering matrix s. Like the corresponding requirement for the single-channel system, it ensures that there is no additional information on the state of the qubit available in measurable changes of scattering phases. Again, *time-reversal symmetry is not necessary* to have this condition hold, as time-reversal symmetry only ensures $U=U'$ and $V=V'$. However, unlike the single-channel case, even the presence of parity symmetry (i.e., the combination of both time-reversal symmetry and left-right inversion symmetry) is *not sufficient* to guarantee that Eq. (52) is satisfied. The presence of parity symmetry would indeed ensure $\phi_U=\phi_V$, but as, in general, $[\sqrt{T},\phi_U]$ and $[\sqrt{R},\phi_U]\neq 0$, this is not enough. In addition to having $\phi_U=\phi_V$, one also generally needs either that ϕ_U is diagonal, meaning that the mode index (i.e., transverse momentum) is conserved during scattering, or that all the transmission eigenvalues T_j are identical. We thus see that if the transmissions fluctuate, mode mixing (e.g., the nonconservation of transverse energy) also prevents one from reaching the quantum limit of detection. This can be understood from the point of view of information. If ϕ_U and ϕ_V matrices are not purely diagonal, information about the qubit could be gained by looking at changes in how electrons incident in a given mode are partitioned into outgoing modes. Such changes would not be detectable if all channels had the same transmission. Note that the matrices U' and V' appearing in the polar decomposition of s [Eq. (50)] are irrelevant to reaching the quantum limit. As each transverse mode is equally populated with incoming waves in the state $|i\rangle$, there is no information associated with the preferred mode structure for incoming waves (i.e., the eigenvectors of U' and V').

2. Transmission condition

Consider now the condition imposed by Eq. (53), which constrains the form of the transmissions $T_j(\varepsilon)$ of the detector. Similar to the corresponding condition for the single-channel system, this requirement ensures that there is no additional information available in either the energy *or* the channel structure of the $\{T_j(\varepsilon)\}$ which is lost upon averaging. One obtains a necessary form for the transmissions, similar to what was found in Ref. 6:

$$T_j(E)=\frac{1}{1+e^{4\pi(E-E_j)/\mathcal{C}}}. \quad (56)$$

Note that different modes differ from one another only by their threshold energy E_j; the constant $\mathcal{C}$ is the same for each mode. Again, this form for the transmissions $\{T_j(\varepsilon)\}$ corresponds exactly to those expected for a multichannel adiabatic point contact.[7] The assumption of adiabaticity implies that transverse energy is conserved. Thus, if parity symmetry also holds, we reach the surprising conclusion that *a multichannel adiabatic point contact remains a quantum limited detector even if the voltage is large enough that several modes contribute to transport*. Previous studies have established that point-contact detectors reach the quantum limit in the limit of small voltages, where the energy dependence of scattering can be neglected.[8–10] We have shown here that in the adiabatic case, the quantum limit continues to hold even at voltages large enough that the energy dependence of scattering is important. This is significant from a practical standpoint—requiring small voltages limits the magnitude of the output current and thus, the overall scale of the measurement rate, making the detector more susceptible to environmental effects.

3. General expression for noise correlators

For completeness, we give explicit expressions for the noise correlators. Writing them in terms of energy dependent $N\times N$ matrix kernels (i.e., $S_X=\int_{\mu_R}^{\mu_L}d\varepsilon[\mathrm{tr}\,\hat{S}_X(\varepsilon)]$), we obtain

$$\hat{S}_I(\varepsilon)=\frac{2e^2}{h}T(1-T), \tag{57a}$$

$$\hat{S}_Q(\varepsilon)=\frac{e^2\hbar}{2\pi}\Bigg(\frac{(\partial_\varepsilon T)^2}{2T(1-T)}+2TR(\phi_U-\phi_V)^2 +2[\phi_U,\sqrt{TR}][\sqrt{TR},\phi_V]+[\phi_U,T][T,\phi_U] +[\phi_V,T][T,\phi_V]\Bigg), \tag{57b}$$

$$\hat{\lambda}(\varepsilon)=-\frac{e^2}{h}(\partial_\varepsilon T), \tag{57c}$$

$$\hat{S}_{IQ}(\varepsilon)=i\hbar\hat{\lambda}(\varepsilon)+\frac{e^2}{\pi}[TR(\phi_U-\phi_V)]. \tag{57d}$$

A similar expression for the charge noise S_Q of a mesoscopic conductor was first derived by Büttiker.[28] Unlike the expression for the current noise S_I, which can easily be understood in terms of partition noise, it would seem at first that there is no simple, heuristic way to interpret the expression for S_Q. However, if we invoke ideas of information, each term in Eq. (57b) acquires a simple meaning. The first term represents information associated with the energy dependence of the transmissions; the second represents information associated with the energy dependence of phase differences; and the last three terms represent information associated with the partitioning of electrons into different modes. In general, using Eqs. (5) and (25), we may *define* the charge noise in terms of the accessible information $\mathcal{I}$ in the coupled conductor plus qubit system:

$$S_Q=\lim_{A\to 0}\lim_{t\to 0}\frac{\hbar^2}{A^2}\frac{d}{dt}\mathcal{I}(t). \tag{58}$$

While this last expression may seem purely tautological, it is clear that the various contributions to Eq. (57b) for the charge noise are best understood in terms of information. Note that the accessible information $\mathcal{I}$ could be obtained directly in the present system by calculating the overlap between the detector states corresponding to the two qubit states. Such a calculation would take the form of an orthogonality catastrophe calculation, similar to that presented in Ref. 29.

C. Local potential coupling

In the remaining part of this paper, we consider a more general version of the mesoscopic scattering detector, showing that the main results of the preceding section continue to hold. We relax the condition that the state of the qubit modulates a *uniform* potential in the scattering region, thus allowing for a wider class of input operators Q than that given in Eq. (29). In general, we may write

$$Q=e\int dEdE'\sum_{\beta,\gamma=L,R}[a^\dagger_{\beta n}(E)W_{\beta n,\gamma m}(E,E')a_{\gamma m}(E')], \tag{59}$$

where $W(E,E')$ is a $2N\times 2N$ Hermitian matrix having dimensions of inverse energy. The situation considered in the preceding section corresponds to choosing W to be $\mathcal{N}(E,E')$ [Eq. (30)], which at $E=E'$ is just the Wigner-Smith delay-time matrix. By comparing against the current operator I [cf. Eq. (27)], it is clear that the proportionality condition in Eq. (16) necessary for the quantum limit constrains the diagonal in energy, off diagonal in lead index part of the potential matrix W:

$$\forall E\epsilon[\mu_R,\mu_L],\quad [W(E,E)]_{RL}=i\frac{1}{\mathcal{C}}[s_{LR}]^\dagger(E)s_{LL}(E), \tag{60}$$

where $\mathcal{C}$ is a real constant. We thus see that the required proportionality between I and Q needed to reach the quantum limit at zero temperature leaves a large part of the potential matrix W undetermined (i.e., terms diagonal in the lead index and/or off diagonal in energy). We now show that by considering a form for W that is drastically different from $\mathcal{N}$, one can make it easier to reach the quantum limit and have a reasonable gain. In particular, one can work at small voltages without necessarily having a vanishing gain.

We specialize the discussion to a case that in many ways is the opposite of having global potential coupling. We take the scattering matrix s to be energy independent over the energy interval defined by the voltage, and take W to correspond to a local potential $W(E,E')=W$ over the energies of interest. In this case, the scattering matrix s will have one of two different energy-independent values depending on the state of the qubit:

$$s_\pm=s_0\pm eA(\Delta s), \tag{61}$$

where s_0 is the scattering matrix at zero coupling ($A=0$). The matrix W may be directly related to the change in the scattering matrix, Δs (see Appendix B for a derivation):

$$W=is_0^\dagger(\Delta s). \tag{62}$$

Note the similarity to the form of W in the global-potential coupling case (where $W=\mathcal{N}$); now, the energy derivative ds/dE has been replaced by the finite difference $\Delta s\equiv(s_+-s_-)/(2eA)$.

Turning to the conditions needed for the quantum limit, we find again that the causality properties of the scattering matrices $s_\pm$ ensure $\lambda'=0$ always. The remaining proportionality requirement of Eq. (16) places constraints on $s_\pm$. These have an analogous form to Eqs. (53) and (52), but now the energy derivative d/dE is replaced by the finite difference Δ (i.e., $\Delta X=(X[s_+]-X[s_-])/(2eA)$):

$$\frac{\Delta T}{T(1-T)}=\mathcal{C}\times\hat{1}, \tag{63}$$

$$\sqrt{T}\tilde{\phi}_U\sqrt{R}-\sqrt{R}\tilde{\phi}_V\sqrt{T}=0, \tag{64}$$

where $\tilde{\phi}_U=-iU^\dagger(\Delta U)$ and $\tilde{\phi}_V=-iV^\dagger(\Delta V)$. Importantly, *the above conditions do not involve any energy averaging*, as we have taken s and W to be energy independent. Nonetheless, there still is a nonvanishing gain λ determined by both the voltage and the ΔT_j:

$$\lambda=\frac{e^2V}{h}\sum_j \Delta T_j. \tag{65}$$

Thus, using a local coupling between the qubit and the scattering detector makes it easier to reach the quantum limit and have a sizeable gain—one can use voltages small enough that energy averaging is not a problem, while still having the qubit modulate the transmissions. Note that in the single-channel case, all that is needed for the quantum limit is that the state of the qubit should not change the difference between reflected and transmitted phases: $\Delta(\phi-\beta)=0$. Also note the various noise correlators are given by Eqs. (57), with the substitution $d/dE\to\Delta$.

IV. CONCLUSIONS

We have developed a general set of conditions that are needed for a detector in the linear-response regime to reach the quantum limit of detection. One needs both a restricted proportionality between the input and output operators of the detector [cf. Eq. (16)], and a causal relation between the output and input [cf. Eq. (17)]. Applying the concept of accessible information to the detector, one sees that deviations from the quantum limit imply the existence of missing information residing in the detector, information that is not being utilized. The general conditions in Eqs. (16) and (17) ensure the nonexistence of such information. Applying these concepts to the mesoscopic scattering detector, we find that these general conditions place restrictions on the form of the detector's scattering matrix. These restrictions do not involve symmetry properties usually considered in mesoscopic systems, but are rather best understood as following from the requirement of having no missing information. In the mesoscopic scattering detector, missing information may reside in the relative phase between transmission and reflection, in the energy or mode structure of the transmission probabilities, or in the partitioning of scattered electrons between different modes. Surprisingly, we find that an adiabatic point contact conforms to all the conditions needed for the quantum limit, even when the voltage is large enough that many modes are involved in transport, and the energy dependence of scattering is important.

ACKNOWLEDGMENTS

We thank M. Devoret for useful conversations. This work was partially supported by ARDA through the Army Research Office under Grant No. DAAD19-02-1-0045, by the NSF under Grants Nos. DMR-0084501 and DMR-0196503, and by the W. M. Keck Foundation.

APPENDIX A: ACCESSIBLE INFORMATION

In this appendix, we provide a simple proof of Eq. (24) for the accessible information $\mathcal{I}$. Given the two states $|D_\uparrow\rangle$ and $|D_\downarrow\rangle$, the goal is to maximize the classical mutual information R [defined in Eq. (21)] over all possible choices of measurements. A given choice of measurement Y corresponds to a choice of basis; the probability distributions $p(y_i|\uparrow)$ and $p(y_i|\downarrow)$ are determined by the elements of the corresponding states in this basis. Treating the $p(y_i|\sigma)$ as independent variables restricted to the interval $[0,1]$ and using Lagrange multipliers, we minimize R subject to the following constraints:

$$\sum_{i=1}^{N} p(y_i|\sigma)=1, \tag{A1}$$

$$\sum_{i=1}^{N}\sqrt{p(y_i|\uparrow)p(y_i|\downarrow)}=|\langle D_\uparrow|D_\downarrow\rangle|\equiv\cos\alpha. \tag{A2}$$

The second condition, in principle, need only be an inequality, with the left-hand side being greater than or equal to the right-hand side; however, it can be verified that the maximum value of R occurs when it is enforced as an equality. Also note that without loss of generality, we can choose the inner product appearing in Eq. (A2) to be real and positive, as R is independent of the relative phase between the states $|D_\sigma\rangle$. Finally, we have assumed to start that these states have at most N nonzero components in the chosen basis. Variation with respect to $p(y_i|\uparrow)$ yields the following condition:

$$\ln\frac{p(y_i|\uparrow)}{\bar{p}(y_i)}+2\lambda_\uparrow+\lambda\sqrt{\frac{p(y_i|\downarrow)}{p(y_i|\uparrow)}}=0, \tag{A3}$$

with a similar equation emerging from variation with respect to $p(y_i|\downarrow)$. λ, $\lambda_\uparrow$, and $\lambda_\downarrow$ are Lagrange multipliers; $\bar{p}(y_i)=[p(y_i|\uparrow)+p(y_i|\downarrow)]/2$ is the averaged distribution. Subtracting the $\uparrow$ and $\downarrow$ equations yields

$$\lambda=\frac{\sqrt{p(y_i|\downarrow)p(y_i|\uparrow)}}{p(y_i|\uparrow)-p(y_i|\downarrow)}\ln\frac{p(y_i|\uparrow)}{p(y_i|\downarrow)}=\frac{\sqrt{1-\beta_i^2}}{2\beta_i}\ln\frac{1+\beta_i}{1-\beta_i}, \tag{A4}$$

where we have defined β_i via

$$\beta_i=\frac{p(y_i|\uparrow)-p(y_i|\downarrow)}{\bar{p}(y_i)}. \tag{A5}$$

β_i may be thought of as the amount of information gained in a measurement, *given* that the outcome of the measurement is y_i. Now, Eq. (A4) must hold for each β_i $(i=1,\ldots,N)$; moreover, the function on the right-hand side is symmetric in β_i and monotone decreasing for $0\leqslant\beta_i\leqslant1$. It thus follows that for each i,

$$(\beta_i)^2=\text{constant}=\sin^2\alpha. \tag{A6}$$

The last equality follows from substitution into Eq. (A2). Further substitution into Eq. (21) for R yields the expression in Eq. (24); note that the averaged distribution $\overline{p(y_i)}$ and the relevant number of basis elements N do not appear in this expression. One can explicitly check that choosing any of the $p(y_i|\sigma)$ to be 0 or 1 results in a lower value of R; thus, Eq. (24) does indeed correspond to the maximum value of R and thus, by definition, to the accessible information $\mathcal{I}$. The condition (A6) required to optimize R implies that the amount of information gained via measurement is the same for each of the measurement outcomes y_i. Equivalently, each basis element in an optimal basis has the same information content associated with it. This is similar to requirements obtained to have the mesoscopic scattering detector reach the quantum limit; in that case, each channel and each energy were required to have the same information content [cf. Eq. (53)]. Note also that *there are several distinct choices of bases (i.e., measurement schemes) which optimize R*; this point was not made in Ref. 14. A particularly simple optimal basis can be constructed for $N=2$. In this basis, the nonzero components of the states $|D_\sigma\rangle$ are given by

$$|D_\uparrow\rangle=(\cos\theta,\sin\theta),\quad |D_\uparrow\rangle=(\sin\theta,\cos\theta), \tag{A7}$$

where $\theta=\pi/4+\alpha/2$. By definition, the state (1,0) leads to the measurement outcome y_1 with perfect certainty, while the state (0,1) leads to the measurement outcome y_2 with perfect certainty. In geometric terms, the optimal basis given here is one in which the angle between the two states $|D_\sigma\rangle$ is bisected by the vector (1,1).

More generally, consider the form of an optimal basis where $N=M$ (i.e., there are M possible outcomes when a measurement is made on the state $|D_\uparrow\rangle$ or $|D_\downarrow\rangle$). Taking M to be even for simplicity, and letting $|j\rangle$ denote the basis states, a possible optimal basis is one in which

$$\langle j|D_\uparrow\rangle=\sqrt{\frac{1+(-1)^j\sin\alpha}{M}}, \tag{A8}$$

$$\langle j|D_\downarrow\rangle=\sqrt{\frac{1-(-1)^j\sin\alpha}{M}}. \tag{A9}$$

The fact that there are many possible outcomes of a measurement does not degrade from the optimality of mutual information R, as the information associated with each measurement outcome is the same.

APPENDIX B: DERIVATION OF Δs

In this appendix, we provide a brief derivation of Eq. (62) which relates the coupling potential matrix W [cf. Eq. (59)] to the associated change in the scattering matrix, Δs. The latter quantity determines the noise correlators and gain of the local-potential coupling version of the mesoscopic scattering detector. Our approach is similar to that used in Ref. 30 to relate the scattering matrix of a quantum dot to its Hamiltonian.

In what follows, we assume (as in Sec. II B) that the potential matrix W and the zero-coupling scattering matrix s are independent of energy on the scales of interest. We start by writing the system Hamiltonian in terms of the scattering states of problem at zero coupling, assuming the qubit is frozen in the $\uparrow$ state:

$$H=\hbar v_F\sum_m\int dk\Big\{k\psi_m^\dagger(k)\psi_m(k) + (Ae)\sum_{m'}\int dk'[\psi_{m'}^\dagger(k')W_{m'm}\psi_m(k)]\Big\}. \tag{B1}$$

We have assumed a linear dispersion near the Fermi energy, with $\hbar k$ and $\hbar k'$ representing the deviation of the momentum from the Fermi momentum. We have also neglected the fact that the effective Fermi velocity is channel dependent (v_F drops out of all final expressions). The operator $\psi_m^\dagger(k)$ creates a scattering state incident in the lead and transverse mode indexed by m. For definiteness, we take our leads (both left and right) to be defined only on the half line $x<0$, and to be confined in the y and z directions. Further, we assume that the scattering region is situated on $x>0$. We may write the full electron field operator in terms of the $\psi_m(k)$ operators, using the zero-coupling scattering matrix s. Writing $\vec{x}=(x,y,z)$, we have:

$$\Psi(\vec{x})=\sum_m\int\frac{dk}{\sqrt{4\pi}}\psi_m(k)\Big[e^{i(k_F+k)x}\phi_m(y,z) + \sum_n e^{-i(k_F+k)x}\phi_n(y,z)s_{nm}\Big] \tag{B2}$$

$$=\frac{1}{\sqrt{2}}\sum_m\psi_m(-x)e^{ik_Fx}\phi_m(y,z) + \frac{1}{\sqrt{2}}\sum_{m,n}\psi_m(x)e^{-ik_Fx}\phi_n(y,z)s_{nm}. \tag{B3}$$

In the last line, we have introduced the operators $\psi_m(x)$, which are the Fourier transforms of the scattering state operators $\psi_m(k)$. Note again that this expression is only valid for $x<0$, as the leads are only defined on $x<0$. We thus see that for $x<0$, $\psi_m(x)$ describes an *outgoing* (i.e., left-moving) wave, while $\psi_m(-x)$ describes an *incoming* (i.e., right-moving) wave.

Next, we may express the system Hamiltonian in terms of the $\psi_m(x)$ operators. This in turn leads to an equivalent single-particle Schrödinger equation

$$E\tilde{\psi}_m(E,x)=\hbar v_F\Big[i\partial_x\tilde{\psi}_m(E,x)+Ae\,\delta(x)\sum_n W_{mn}\tilde{\psi}_n(E,x)\Big]. \tag{B4}$$

Here, $\tilde{\psi}_m(E,x)$ is a wave function that arises when the field operator $\psi_m(x)$ is expressed in terms of operators corresponding to the eigenmodes of the full Hamiltonian H. Given the relation of $\psi_m(x)$ to incoming and outgoing waves [cf. Eq. (B3)], we choose the following form for $\tilde{\psi}_m(x)$:

$$\tilde{\psi}_m(E,x)=\begin{cases} e^{-ikx}a_{\mathrm{in},m} & \text{if } x>0 \\ e^{-ikx}\sum_n s^{\dagger}_{mn}a_{\mathrm{out},n} & \text{if } x<0, \end{cases} \tag{B5}$$

where $E=\hbar v_F k$. Substituting this form into Eq. (B3), we see that the coefficients $a_{\mathrm{in},m}$ and $a_{\mathrm{out},m}$ do indeed correspond (respectively) to the amplitudes of incoming and outgoing waves.

Integrating Eq. (B4) from $x=0^-$ to $x=0^+$, interpreting $\tilde{\psi}(0)$ as $[\tilde{\psi}(0^+)+\tilde{\psi}(0^-)]/2$, and then using Eq. (B5), we find the following relation between the amplitude of incoming and outgoing waves:

$$a_{\mathrm{out},m}=\sum_{n,n'} s_{mn}\left[\frac{1-\frac{i}{2}Ae\hat{W}}{1+\frac{i}{2}Ae\hat{W}}\right]_{nn'} a_{\mathrm{in},n'} \tag{B6}$$

$$\equiv\sum_{n'}\left[s+Ae\Delta s\right]_{mn'}a_{\mathrm{in},n'}. \tag{B7}$$

In the last line, we indicate that this relation defines the new scattering matrix $s+Ae\Delta s$ that includes effects of the additional potential W. Expanding to lowest order in the dimensionless potential AeW, we find Eq. (62) as advertised.

[1] Y. Makhlin, Gerd Schon, and Alexander Shnirman, Phys. Rev. Lett. **85**, 4578 (2000); Rev. Mod. Phys. **73**, 357 (2001).

[2] M.H. Devoret and R.J. Schoelkopf, Nature (London) **406**, 1039 (2000).

[3] D.V. Averin, quant-ph/0008114 (unpublished); cond-mat/0004364 (unpublished).

[4] D.V. Averin and A.N. Korotkov, Phys. Rev. B **64**, 165310 (2002).

[5] V.B. Braginsky and F.Y. Khalili, *Quantum Measurement* (Cambridge University Press, Cambridge, 1992).

[6] S. Pilgram and M. Büttiker, Phys. Rev. Lett. **89**, 200401 (2002).

[7] L.I. Glazman, G.B. Lesovik, D.E. Khmelnitskii, and R.I. Shekhter, Pis'ma Zh. Eksp. Teor. Fiz. **48**, 218 (1988) [JETP Lett. **48**, 238 (1988)].

[8] S.A. Gurvitz, Phys. Rev. B **56**, 15 215 (1997).

[9] L. Stodolsky, Phys. Lett. B **60**, 5737 (1999).

[10] A.N. Korotkov and D.V. Averin, cond-mat/0002203 (unpublished).

[11] Note that in Ref. 2, the quantum limit is written as $\chi<2$. This results from using a definition of Γ_{meas} that is twice as large as the one used here.

[12] The proportionality condition expressed in Eq. (16) only involves a subset of matrix elements, and is thus not incompatible with the operators $\tilde{I}$ and $\tilde{Q}$ being Hermitian. In the case where the state $|f\rangle=|i\rangle$ in this equation, one simply needs that the corresponding matrix elements of $\tilde{I}$ and $\tilde{Q}$ vanish.

[13] E.C. Titchmarsh, *Introduction to the Theory of Fourier Integrals* (Oxford, University Press, Oxford, 1937).

[14] L.B. Levitin, in *Quantum Communication and Measurement*, edited by V.P. Belavkin, O. Hirota, and R.L. Hudson (Plenum Press, New York, 1995), p. 439.

[15] C.A. Fuchs, quant-ph/9601020 (unpublished); C.A. Fuchs and A. Peres, Phys. Rev. A **53**, 2038 (1996); C.A. Fuchs and K. Jacobs, *ibid.* **63**, 062305 (2001).

[16] M.A. Nielsen and I.L. Chuang, *Quantum Computation and Quantum Information* (Cambridge University Press, Cambridge, 2000).

[17] V. Vedral, Rev. Mod. Phys. **74**, 197 (2002).

[18] More generally, there will be two different detector density matrices $\rho_{D\uparrow},\rho_{D\downarrow}$ corresponding to the two qubit states; we consider the case of pure states for simplicity.

[19] See, e.g., T.M. Cover and J.A. Thomas, *Elements of Information Theory* (Wiley, New York, 1991).

[20] For simplicity, we do not consider self-consistency effects that can become important when the current is no longer linear with voltage, see, e.g., T. Christen and M. Büttiker, Europhys. Lett. **35**, 523 (1996).

[21] E. Buks, R. Schuster, M. Heiblum, D. Mahalu, and V. Umansky, Nature (London) **391**, 871 (1998).

[22] D. Sprinzak, E. Buks, M. Heiblum, and H. Shtrikman, Phys. Rev. Lett. **84**, 5820 (2000).

[23] Ya.M. Blanter and M. Büttiker, Phys. Rep. **336**, 1 (2000).

[24] L.S. Levitov, H. Lee, and G.B. Lesovik, J. Math. Phys. **37**, 4845 (1996).

[25] Note that our Eq. (40) has a constant on the right-hand side, while the corresponding equation in Ref. 6 [Eq. (12)] has an arbitrary energy-dependent function on the right-hand side. This difference results from the fact that Ref. 6 considers voltages so small that the effects of energy averaging can be neglected.

[26] Note that by left-right symmetry, we mean that the *scalar* potential $V(x,y,z)$ in the scattering region is a symmetric function of x, where x is the transport direction. One can still have an absence of time-reversal symmetry if, e.g., there is a vector potential in the scattering region.

[27] C.W.J. Beenakker, Rev. Mod. Phys. **69**, 731 (1997).

[28] M. Büttiker, H. Thomas, and A. Prêtre, Phys. Lett. A **180**, 364 (1993).

[29] I.L. Aleiner, N.S. Wingreen, and Y. Meir, Phys. Rev. Lett. **79**, 3740 (1997).

[30] I.L. Aleiner, P.W. Brouwer, and L.I. Glazman, Phys. Rep. **358**, 309 (2002).

Resonant Cooper-Pair Tunneling: Quantum Noise and Measurement Characteristics

A. A. Clerk, S. M. Girvin, A. K. Nguyen, and A. D. Stone

Department of Applied Physics and Physics, Yale University, New Haven, Connecticut, 06511

(Received 15 March 2002; published 8 October 2002)

We study the quantum charge noise and measurement properties of the *double* Cooper-pair resonance point in a superconducting single-electron transistor (SSET) coupled to a Josephson charge qubit. Using a density-matrix approach for the coupled system, we obtain a full description of the measurement backaction; for weak coupling, this is used to extract the quantum charge noise. Unlike the case of a nonsuperconducting SET, the backaction here can induce population inversion in the qubit. We find that the Cooper-pair resonance process allows for a much better measurement than a similar nonsuperconducting SET, and can approach the quantum limit of efficiency.

DOI: 10.1103/PhysRevLett.89.176804 PACS numbers: 73.21.-b, 73.40.Gk, 73.23.Hk

Among the many open issues related to solid state quantum computation, the question of how best to *measure* a solid state qubit remains a particularly interesting one. In the case where the qubit is a Cooper-pair box (i.e., a Josephson-junction single charge box), the standard choice for a readout device is the single-electron transistor (SET) [1–6]. An alternate and potentially more powerful approach is to use a *superconducting* single-electron transistor (SSET) biased at a point where the cyclic resonant tunneling of Cooper pairs dominates transport [7–12]. Such processes, known as Josephson quasiparticle (JQP) resonances, would appear to be an attractive choice for use in a measurement as their resonance structure implies an extremely high sensitivity. However, precisely because of their large gain, these processes may be expected to strongly alter the state of the qubit in a measurement. To assess the balance between these two opposing tendencies, a close examination of the physics of JQP tunneling is required.

In this paper, we focus on a *double* JQP process (DJQP) (see Fig. 1), which occurs at a lower SSET source-drain voltage than single JQP processes, and which has been used in a recent experiment [13]. We assess the potential of DJQP to act as a one-shot measurement of the state of a Cooper-pair box qubit. This involves characterizing both $\tau_{\rm meas}$, the time needed to discriminate the two qubit states in the measurement, and the backaction of the measurement on the qubit, which is described by a mixing rate $\Gamma_{\rm mix}$ and a dephasing rate $1/\tau_\varphi$. These quantities are intimately related to the noise properties of the SSET, which are of interest in themselves, given the novel nature of the DJQP process. $\tau_{\rm meas}$ is determined by the shot noise of the process, while $\Gamma_{\rm mix}$ and τ_φ are related to the charge noise on the SSET island. While the shot noise of a *single* JQP process has been analyzed recently [14], the quantum charge noise has not been addressed.

To describe the measurement process in our system, we employ a density-matrix description of the *fully coupled* SSET plus qubit system; this is similar to the approach taken by Makhlin *et al.* [4] for a SET, but extended to deal with Josephson tunneling. This approach is not limited by a requirement of weak coupling, as are standard approaches which perturbatively link $\Gamma_{\rm mix}$ to the transistor charge noise [5,6]; nonetheless, in the limit of weak coupling it can be used to calculate the quantum charge noise of the SSET. We find that the quantum (i.e., asymmetric in frequency) nature of the noise is particularly pronounced for the DJQP feature, leading to regimes where the SSET can strongly relax the qubit. Moreover, due to the resonant nature of Cooper-pair tunneling, there exist regimes where the SSET can cause a pronounced *population inversion* in the Cooper-pair box. For typical device parameters, we find that a far better single-shot measurement is possible using the DJQP process than with a comparable SET. Significantly, one can also approach the quantum limit of measurement efficiency [3,4], where $\tau_\varphi/\tau_{\rm meas} \uparrow 1$, in a regime which is both theoretically tractable *and* experimentally relevant.

Model.—The Hamiltonian of the coupled qubit plus SSET system is written as $\mathcal{H} = \mathcal{H}_S + \mathcal{H}_Q + \mathcal{H}_{\rm int}$. The qubit itself (or "box"), described by $\mathcal{H}_Q$, consists of a superconducting metal island in the Coulomb blockade regime where only two charge states are relevant. These can be regarded as the σ_z eigenstates of a fictitious spin 1/2. The island is attached via a tunnel junction to a bulk superconducting electrode, leading to the form

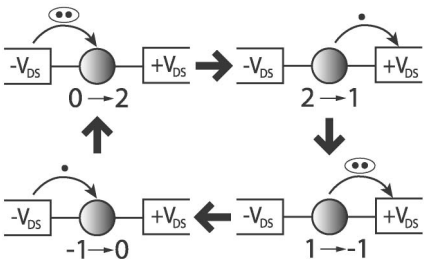

FIG. 1. Schematic showing the four steps of the double Josephson quasiparticle process which can occur in a superconducting single-electron transistor. Circles represent the central island of the SSET, while the rectangles are the electrodes. Numbers indicate the charge of the SSET island.

$$\mathcal{H}_Q = -\tfrac{1}{2}\{[4E_{CQ}(1-\mathcal{N}_Q)]\sigma_z + E_{JQ}\sigma_x\}, \quad (1)$$

where E_{CQ} is the charging energy of the box, E_{JQ} is the Josephson coupling energy of the box, and $\mathcal{N}_Q$ is the dimensionless gate voltage applied to the box. The SSET consists of a superconducting, Coulomb-blockaded island which is attached via tunnel junctions to two superconducting electrodes (Fig. 1). The SSET Hamiltonian $\mathcal{H}_S = H_K + H_C + H_V + H_T$ has a term H_K describing the kinetic energy of source, drain, and central island electrons, a term H_V which describes the work done by the voltage sources, and a tunneling term H_T. The charging term is $H_C = E_{CS}(n_S - \mathcal{N}_S)^2$, where E_{CS} is the SSET charging energy, n_S is the number of electrons on the central island, and $\mathcal{N}_S$ is the dimensionless gate voltage applied to the island. Finally, the qubit is capacitively coupled to the SSET: $H_{\rm int} = 2E_{CQ}\frac{C_C}{C_\Sigma}\sigma_z n_S \equiv E_{\rm int}\sigma_z n_S$. Here C_C is the cross capacitance between the box and the central island of the SSET, and C_Σ is the total capacitance of the SSET island. Note that we neglect the coupling of the qubit to its environment, as we are interested here in the intrinsic effect of the SSET on the qubit [15]. We also assume a SSET with identical tunnel junctions, whose dimensionless conductance g satisfies $g/(2\pi) \ll 1$.

The DJQP process occurs when the SSET gate voltage $\mathcal{N}_S$ and drain-source voltage $2V_{DS}$ are such that two Cooper-pair tunneling transitions (one in each junction) are resonant. We label these transitions as $n_s = 0 \to 2$ (left junction) and $n_s = 1 \to -1$ (right junction) (see Fig. 1). Resonance thus requires $eV_{DS} = E_{CS}$ and $\mathcal{N}_S = 1/2$. In addition, E_{CS}/Δ_S (where Δ_S is the superconducting gap of the SSET) must be chosen so that the quasiparticle transitions linking the two Cooper-pair resonances are energetically allowed (i.e., $n_S = 2 \to 1$ and $n_S = -1 \to 0$), whereas transitions which end the cycle (i.e., $n_S = 0 \to 1$) are not. We take $E_{CS} = \Delta_S$ to satisfy these conditions; this corresponds to the experiment of Ref. [13]. The two quasiparticle transitions which occur in the DJQP are characterized by a rate Γ, which is given by the usual expression for quasiparticle tunneling between two superconductors [16]. The effective Cooper-pair tunneling rate γ_J emerging from our description [i.e., Eq. (3) below] is given by [8]

$$\gamma_J(\delta) = \frac{E_{JS}^2\Gamma}{4[\delta^2 + (\Gamma/2)^2]}. \quad (2)$$

Here δ is the energy difference between the two charge states involved in tunneling, E_{JS} is the Josephson energy of the SSET, and we set $\hbar = 1$.

Calculation approach.—We consider the reduced density matrix ρ of the qubit plus SSET system obtained by tracing out the SSET fermionic degrees of freedom. The evolution of ρ is calculated perturbatively in the tunneling Hamiltonian H_T, keeping only the lowest order terms; this corresponds to the neglect of cotunneling processes, which is valid for small g and near the DJQP resonance. Using an interaction representation where only H_T (and not $H_{\rm int}$) is viewed as a perturbation, the equation of motion of ρ takes the standard form:

$$\frac{d}{dt}\rho(t) = -\int_{-\infty}^{t} dt' \langle [\mathcal{H}_T(t), [\mathcal{H}_T(t'), \rho(t') \otimes \rho_F]]\rangle. \quad (3)$$

The angular brackets denote the trace over SSET fermion degrees of freedom; as we work at zero temperature, ρ_F is the density matrix corresponding to the ground state of these degrees of freedom in the absence of tunneling.

To make further progress, we treat the Josephson coupling emerging from Eq. (3) as energy independent and given by the Ambegaokar-Baratoff value $E_{JS} = g\Delta_S/8$. We also use the smallness of g to neglect logarithmic renormalization terms, as was done in Ref. [4]. One can then solve for the time-independent solution of Eq. (3), which describes the state achieved by the system after all mixing and dephasing of the qubit by the SSET has occurred. To describe the dynamics of mixing (i.e., the relaxation of the qubit state populations to their stationary value), we also calculate the corresponding eigenmode of Eq. (3). A Markov approximation is made which involves replacing $\rho(t')$ by $\rho(t)$ on the right-hand side of Eq. (3). This approximation is justified as long as the time dependence of ρ in the mixing mode is weak compared to typical frequencies appearing in the correlators of Eq. (3), requiring here that $\Gamma_{\rm mix} \ll E_{CS}$ and $E_{JS} \ll E_{CS}$ [17].

Backaction.—We focus here primarily on the mixing effect of the measurement backaction; dephasing will be discussed more extensively in Ref. [17]. The mixing rate $\Gamma_{\rm mix} = \Gamma_{\rm rel} + \Gamma_{\rm exc}$ is set by the rates at which the measurement relaxes and excites the qubit. Let Ω denote the $\mathcal{N}_Q$-dependent energy difference between the two qubit states. For weak coupling ($E_{\rm int} \ll \Omega$), Fermi's golden rule relates $\Gamma_{\rm rel}$ and $\Gamma_{\rm exc}$ to the quantum charge noise of the SSET island $S_Q(\omega) = \int dt e^{-i\omega t}\langle n_S(t)n_S(0)\rangle$:

$$\Gamma_{\rm rel/exc} = E_{\rm int}^2\left(\frac{E_{JQ}}{\Omega}\right)^2 S_Q(\pm\Omega). \quad (4)$$

In our approach, these rates may be directly obtained by using the stationary solution (which gives the postmixing occupancies of the box eigenstates) and the mixing eigenvalue of Eq. (3). In the limit of weak coupling, one can then use Eq. (4) to extract $S_Q(\Omega)$. Our method for calculating the quantum noise, which uses the qubit as a spectrum analyzer, is physically intuitive and no more difficult to implement than standard approaches [6]; in addition, we are able to calculate $\Gamma_{\rm rel}$ and $\Gamma_{\rm exc}$ when the coupling is not weak, and Eq. (4) fails.

Figure 2 displays the quantum charge noise obtained at zero temperature, using SSET parameters which correspond to Ref. [13]. The solid curve in Fig. 2 is for the center of the DJQP resonance—$\mathcal{N}_S = 1/2$, $eV_{DS} = E_{CS}$. Note the sudden asymmetry that develops between

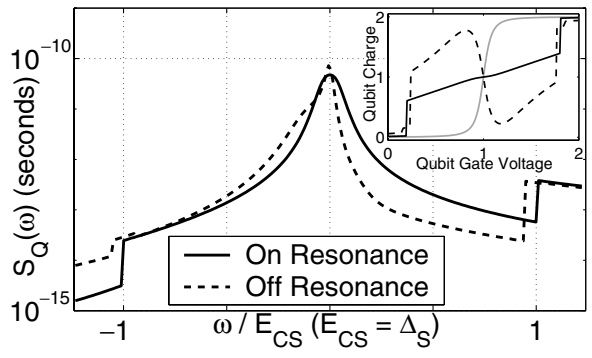

FIG. 2. Quantum charge noise associated with the DJQP process. The solid curve corresponds to $\mathcal{N}_S$, V_{DS} tuned to the center of the DJQP resonance; the dashed curve corresponds to moving eV_{DS} away from resonance by $+\Gamma/4$. We take $g = 0.5$ and $\Delta_S \simeq E_{CS} = 0.25$ meV in the SSET, corresponding to the device of Ref. [13]; this gives $E_{JS}/(h\Gamma) \simeq 0.04$. Inset: average qubit charge after mixing has occurred for weak coupling ($E_{\rm int}/E_{JQ} = 0.01$), as a function of qubit gate voltage $\mathcal{N}_Q$; see text for details. We take $E_{CQ} \simeq 77$ μeV and $E_{JQ} \simeq 27$ μeV. The frequency range probed by tuning $\mathcal{N}_Q$ matches the range of the main plot; the sharp steps in the average charge occur at $\Omega(\mathcal{N}_Q) \simeq E_{CS}$.

absorption [i.e., $S_Q(+|\omega|)$] and emission [i.e., $S_Q(-|\omega|)$] when $|\omega|$ increases beyond E_{CS}. These jumps correspond to the opening and closing of transport channels in the SSET, and their sharpness is a result of the singularity in the quasiparticle density of states. For example, as ω rises past E_{CS}, transitions which are normally forbidden in the DJQP cycle (i.e., $n_S = 0 \rightarrow 1$) suddenly become energetically allowed *if* they absorb energy from the qubit, causing a sudden increase in $S_Q(\omega)$.

The effect of the SSET quantum charge noise on the qubit is shown in the inset of Fig. 2, where the average qubit charge $\langle N_B \rangle \equiv 1 + \langle \sigma_z \rangle$ for $t \gg \tau_{\rm mix}$ is shown as a function of $\mathcal{N}_Q$. Changing $\mathcal{N}_Q$ tunes the qubit splitting frequency Ω, allowing one to probe the frequency dependence of the noise. The solid black curve corresponds to being at the center of the DJQP feature, and the grey curve corresponds to the unperturbed qubit ground state. The features in the quantum noise manifest themselves in $\langle N_B \rangle$, a quantity which is accessible in experiment.

Even more interesting is the situation when one tunes $\mathcal{N}_S$ or V_{DS} slightly off the DJQP resonance center. Unlike the case of a SET, where noise asymmetries are weak for $|\omega| \ll E_{CS}$ [6], there are strong features here that result from the resonant nature of Cooper-pair tunneling. By treating the mixing terms in Eq. (3) perturbatively, analytic expressions can be obtained for the quantum noise in this regime when $E_{JS} < \Gamma$ [in Ref. [13], $E_{JS}/(h\Gamma) \simeq 0.04$]. If one moves away from the DJQP center by tuning only V_{DS} (i.e., $\mathcal{N}_S = 1/2$, $eV_{DS} = E_{CS} + \delta_V/2$), we find ($|\omega| < E_{CS}$)

$$S_Q(\omega) = \gamma_J(\delta_V) \frac{[\gamma_J(\delta_V + \omega)/\gamma_J(\delta_V - \omega)]}{[4\gamma_J(\delta_V + \omega)\gamma_J(\delta_V - \omega)] + \omega^2}. \quad (5)$$

In the limit where $\omega \ll \Gamma/2$, Eq. (5) simply corresponds to classical telegraph noise (the SSET spends only appreciable time in the states $n_S = 0$ and $n_S = 1$). However, for finite δ_V and ω, Eq. (5) indicates that the noise develops a pronounced asymmetry, even though $|\omega| \ll E_C$. In particular, if $\delta_V > 0$, one has $S_Q(-|\omega|) > S_Q(+|\omega|)$, implying that *emission by the SSET exceeds absorption.* This behavior is shown by the dashed curves in Fig. 2, which correspond to $\mathcal{N}_S = 1/2$, $\delta_V = +\Gamma/4$. This effect is a direct consequence of the resonant nature of Cooper-pair tunneling—by emitting energy, *both* Cooper-pair tunneling processes in the DJQP cycle become more resonant, while absorbing energy pushes them even farther from resonance. The result is a population inversion in the qubit at zero temperature, which in turn leads to a striking, nonmonotonic dependence of qubit charge on $\mathcal{N}_Q$ (dashed curve in the inset of Fig. 2) [15]. Note that if one moves away from the center of the DJQP resonance by changing only the $\mathcal{N}_S$, no asymmetry in the noise results, as now emission (or absorption) moves one of the Cooper-pair transitions in the DJQP process farther *towards* resonance, while it moves the other transition farther *away* from resonance. Letting $\delta_V = 0$ and $\delta_{\mathcal{N}} = 4E_{CS}(\mathcal{N}_S - 1/2)$, we have for $E_{JS} < \Gamma$:

$$S_Q(\omega) = \gamma_J(\delta_{\mathcal{N}}) \frac{1 + \frac{(8\delta_{\mathcal{N}}\omega)^2}{\Gamma^2 E_{JS}^4/2} \gamma_J(\delta_{\mathcal{N}} - \omega)\gamma_J(\delta_{\mathcal{N}} + \omega)}{[4\gamma_J(\delta_{\mathcal{N}} + \omega)\gamma_J(\delta_{\mathcal{N}} - \omega)] + \omega^2}. \quad (6)$$

Measurement rate.—To determine the measurement time $\tau_{\rm meas}$, we extend our density-matrix description to also include m, the number of electrons that have tunneled through the left SSET junction [4,14]. We are thus able to calculate the distribution of tunneled electrons $P(m, t|i)$, where $i = \uparrow, \downarrow$ denotes the initial state of the qubit. $\tau_{\rm meas}$ is defined as the minimum time needed before the two distributions $P(m, t|\uparrow)$ and $P(m, t|\downarrow)$ are statistically distinguishable [4]:

$$\frac{1}{\tau_{\rm meas}} = \left(\frac{I_\uparrow - I_\downarrow}{\sqrt{2f_\uparrow I_\uparrow} + \sqrt{2f\downarrow I_\downarrow}} \right)^2. \quad (7)$$

Here $I_\uparrow$ and $I_\downarrow$ are the average SSET currents associated with the two qubit states, and $f_\uparrow$ and $f_\downarrow$ are the associated Fano factors which govern the zero-frequency shot noise in the current. In the absence of the qubit, the density-matrix equations for the SSET yield the following for the single Fano factor f:

$$f(\delta) = \frac{3}{2}\left[1 - \frac{1}{2} \frac{E_{JS}^2[3(\Gamma/2)^2 - \delta^2]}{([\Gamma/2]^2 + \delta^2 + E_{JS}^2/2)^2} \right], \quad (8)$$

where we take $eV_{DS} = E_{CS}$, $\delta = \delta_{\mathcal{N}} = 4E_{CS}(\mathcal{N}_S - 1/2)$. Equation (8) indicates that the effective charge of the carriers in the DJQP process is $3e/2$ in the limit where $\Gamma \gg E_{JS}$. In this limit, Cooper-pair tunneling is the rate-limiting step in the cycle; electrons effectively tunnel in clumps of e or $2e$, leading to an average charge of $3e/2$.

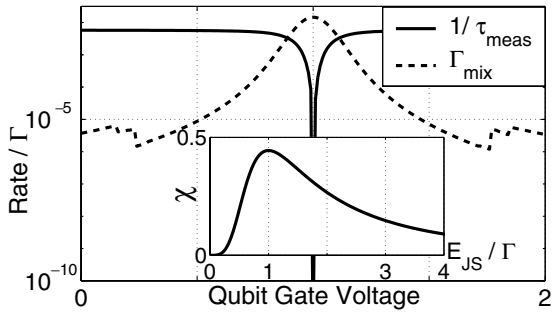

FIG. 3. $1/\tau_{\rm meas}$, $\Gamma_{\rm rel}$, and $\Gamma_{\rm exc}$ vs qubit gate voltage $\mathcal{N}_Q$ for a strongly coupled system, where $E_{\rm int}/E_{JQ} \simeq 0.3$ (i.e., $C_C/C_\Sigma = 0.05$). A good measurement is possible for a wide range of gate voltages. Inset: Heisenberg efficiency $\chi = \tau_\varphi/\tau_{\rm meas}$ at weak coupling, as a function of E_{JS}/Γ.

We consider $\tau_{\rm meas}$ in the limit of weak coupling ($E_{\rm int} \ll \Omega$) and weak mixing ($E_{JQ} \ll \Omega$). Taking $\delta_V = 0$ and $\delta\mathcal{N} = \Gamma/2$ for near optimal gain, and using Eqs. (6)–(8), we find that the intrinsic signal-to-noise ratio $(\tau_{\rm meas}\Gamma_{\rm mix})^{-1/2}$ of the measurement, in the relevant regime $E_{JS} < \Gamma$, is given by

$$(S/N)_{\rm DJQP} = \sqrt{\frac{4}{3}}|\cot\theta|\frac{\Omega}{\Gamma/2}. \tag{9}$$

Here $\cot\theta \equiv 4E_{CQ}(1 - \mathcal{N}_Q)/E_{JQ}$, and we take $\gamma_J(0) \ll \Omega < E_{CS}$. If a SET in the sequential-tunneling regime is used for the qubit measurement, it was found in Refs. [3,4] that the optimal S/N is given by ($\Omega < E_{CS}$)

$$(S/N)_{SET} = \lambda|\cot\theta|\sqrt{\left(\frac{\Omega}{eV_{DS}}\right)^2 + \frac{g^2}{\pi^2}}, \tag{10}$$

where λ is of order unity. As the quasiparticle transition rate $\Gamma \sim \frac{g}{2\pi}eV_{DS}$, we see that the S/N achieved using DJQP is parametrically larger (in $2\pi/g \gg 1$) than that obtained for the SET. This enhancement results largely from the narrow width of the DJQP feature—the energy scale over which the current changes (and thus the gain) is set by Γ rather than V_{DS}. The gain and S/N ratio of the SET could be improved by working in the cotunneling regime; however, this would result in a much larger $\tau_{\rm meas}$ ($\tau_{\rm meas} \propto g^{-2}$), making one more susceptible to unwanted environmental effects. In contrast, the DJQP feature has both a large gain *and* a short $\tau_{\rm meas}$ (i.e., $\tau_{\rm meas} \propto 1/g$). Shown in Fig. 3 as a function of $\mathcal{N}_Q$ are $\tau_{\rm meas}$, $\Gamma_{\rm rel}$, and $\Gamma_{\rm exc}$ for a strongly coupled device ($C_C/C_\Sigma = 0.05$), with all other parameters as listed in the caption of Fig. 2. We have taken $\delta_V = 0$ and $\delta\mathcal{N} = \Gamma/2$ for optimal gain. Figure 3 confirms that an excellent measurement is indeed possible, with $(S/N)^2 > 100$.

We have also studied the efficiency $\chi = \tau_\varphi/\tau_{\rm meas}$ of measurement using DJQP for a weak coupling ($E_{\rm int} \ll E_{JS}, \Gamma$) and $\Omega < E_{CS}$, where τ_φ is the measurement-induced dephasing time [17]. Unlike an SET in the sequential-tunneling regime, where $\chi \propto g^2$ is always much less than the quantum limit $\chi = 1$ [3,4], here χ is controlled by the ratio E_{JS}/Γ. As shown in the inset of Fig. 3, by tuning this ratio, χ *can be made to approach the quantum limit.* Here, for each value of E_{JS}/Γ, we have set V_{DS} and $\mathcal{N}_S$ to optimize the gain. Measurement using DJQP is able to reach a high efficiency when $E_{JS} \simeq \Gamma$ both because of the symmetry of the process and because of the coherent nature of Josephson tunneling; the large gain of the process is also important [17]. Clearly, the DJQP process allows for a far superior measurement of a Cooper-pair box qubit than a SET.

We thank M. Devoret, K. Lehnert, and R. Schoelkopf for useful discussions. This work was supported by the NSF under Grants No. DMR-0084501 and No. DMR-0196503, and by the Army Research Office under Grant No. ARO-43387-PH-QC.

[1] R. J. Schoelkopf *et al.*, Science **280**, 1238 (1998).
[2] A. N. Korotkov *et al.*, in *Single-Electron Tunneling and Mesoscopic Physics*, edited by H. Koch and H. Lubbig (Springer, Berlin, 1992).
[3] M. H. Devoret and R. J. Schoelkopf, Nature (London) **406**, 1039 (2000).
[4] Y. Makhlin *et al.*, Phys. Rev. Lett. **85**, 4578 (2000); Rev. Mod. Phys. **73**, 357 (2001).
[5] A. Aassime *et al.*, Phys. Rev. Lett. **86**, 3376 (2001).
[6] G. Johansson *et al.*, Phys. Rev. Lett. **88**, 046802 (2002).
[7] T. A. Fulton *et al.*, Phys. Rev. Lett. **63**, 1307 (1989).
[8] D.V. Averin and V.Ya. Aleshkin, JETP Lett. **50**, 367 (1989); Physica (Amsterdam) **165-166B**, 949 (1990).
[9] A. Maasen van den Brink *et al.*, Phys. Rev. Lett. **67**, 3030 (1991).
[10] Y. Nakamura *et al.*, Phys. Rev. B **53**, 8234 (1996).
[11] S. Pohlen, Ph.D. thesis, Harvard University, 1999 (unpublished).
[12] The use of only Cooper-pair tunneling in a modified SSET has been studied in A. B. Zorin, Phys. Rev. Lett. **76**, 4408 (1996); cond-mat/0112351. The use of quasiparticle-only processes in a SSET was studied in A. N. Korotkov, Appl. Phys. Lett. **69**, 2593 (1996).
[13] K. Lehnert *et al.* (to be published).
[14] M-S. Choi *et al.*, Phys. Rev. Lett. **87**, 116601 (2001).
[15] To observe the population inversion predicted here, environment-induced relaxation must be weak compared to the mixing from the measurement. For the devices of Ref. [13], the electromagnetic environment may be treated as a 50 Ω impedance whose voltage fluctuations cause relaxation; this leads to a relaxation rate of $\Gamma_{\rm envt} \sim 10^6$ Hz. The effect of $1/f$ noise is negligible given the large qubit splitting frequency. To have the measurement-induced mixing rates $\Gamma_{\rm rel/exc}$ [Eq. (4)] exceed $\Gamma_{\rm envt}$, a coupling strength $C_C/C_\Sigma \simeq 0.1$ is sufficient.
[16] See, e.g., M. Tinkham, *Introduction to Superconductivity* (McGraw-Hill, New York, 1996).
[17] τ_φ can be obtained in a manner analogous to that used in Ref. [4]. A full derivation and discussion will be presented in A. A. Clerk *et al.* (to be published).